Higgs-pair production via gluon fusion at NLO QCD in the Standard Model and Beyond

Thesis presented for the Degree of Doctor of Philosophy

Author:

Jonathan Ronca

Under the supervision of:

Francisco Campanario

VNIVERSITAT DE VALÈNCIA

Programa Oficial de Doctorado en Física

Instituto de Física Corpuscular, Departamento de Física Teórica
Universitat de València - Consejo Superior de Investigaciones Científicas

December 2020

Francisco Campanario Pallás, Investigador Ramón y Cajal del Departamento de Física Teórica de la Universidad de Valencia,

CERTIFICA que la presente memoria **"Higgs-pair production via gluon fusion at NLO QCD in Standard Model and Beyond"** ha sido realizada bajo su dirección, en el Departamento de Física Teórica de la Universidad de Valencia, por D. **Jonathan Ronca**, y constituye su Tesis Doctoral para optar al grado de Doctor en Física.

Y para que así conste, en cumplimiento de la legislación vigente, presenta ante la Facultad de Física de la Universidad de Valencia la referida memoria, y firma el presente certificado

en Burjassot, a 16 de Deciembre de 2020

Francisco Campanario Pallás

Abstract

The discovery of a neutral scalar boson compatible with the Standard Model Higgs boson in 2012 has opened the possibility of studying the Higgs potential. The current experimental uncertainties do not preclude this particle from belonging to models beyond the Standard. The study of the Higgs self-interactions is needed to clarify its nature.

The quartic Higgs self-coupling is out of reach from the experimental perspective. However, the future upgrade of the LHC and other colliders will open the possibility of investigating the trilinear Higgs self-coupling. A direct measurement of the trilinear Higgs coupling involves the Higgs-pair production channels. The dominant channel is the QCD induced gluon fusion with top-quark loops. A next-to-leading order calculation is mandatory to accomplish the demanded precision for a comparison with the experimental data.

The Feynman diagrams contributing to the cross section virtual corrections contain four-points two-loop Feynman integrals, which represent the nowadays bottleneck for many higher order corrections. Since an analytical calculation is not a viable strategy yet, a numerical approach is needed. A general numerical framework which includes both Standard Model and Two-Higgs-Doublets model is presented in this thesis. The crucial part of the calculation is the isolation and cancellation of the ultraviolet and infrared divergences coming from the (divergent) Feynman integrals. The ultraviolet divergences will be isolated through the endpoint subtraction, the infrared ones by a dedicated subtraction term coming from the heavy-quark limit calculation. The remaining part of the virtual amplitude can be computed by considering the single-Higgs production amplitude and the Higgs decay into a Z boson and a photon. The real corrections are calculated using public libraries for one-loop integral calculations. The outcome of this study is the differential cross section depending on the Higgs-pair invariant mass and its integral, namely the NLO Higgs-pair production via gluon fusion total cross section.

The top-mass effects at next-to-leading order introduce a significant deviation of the differential cross section from its heavy quark limit of more than 20% in the tail, which increases with the collider energy as well. This deviation at the level of the differential cross section is reflected in a decreasing of the total hadronic cross section of the 15%. The uncertainties related with the choice of the top-mass renormalisation scale and scheme are proven to be sizable. Such uncertainties are of the same order of the usual strong coupling renormalisation and factorization scale ones, bringing a strong impact on the estimation of the theoretical uncertainties.

Resumen

El descobriment l'any 2012 d'un bosó escalar i neutre compatible amb el bosó de Higgs del Model Estàndard ha obert la possibilitat d'estudiar el potencial de Higgs. Les actuals incerteses experimentals no exclouen que aquesta partcula puga pertànyer a models més enllà del Model Estàndard. L'estudi de les interaccions pròpies del Higgs seran necessàries per a clarificar la seua naturalesa.

L'acoblament quàrtic del Higgs amb ell mateix està fora de l'abast des d'una perspectiva experimental. Malgrat això, la futura actualització del LHC i altres collisionadors obriran la possibilitat d'investigar l'acoblament triple del Higgs amb ell mateix. Una mesura directa de l'acoblament triple del Higgs involucra canals de producció de parells de Higgs. El canal dominant és la fusió de gluons induïda per QCD amb bucles de quarks top. Un càlcul a segon ordre en teoria de pertorbacions és obligatori per complir amb les demandes de precisió per una comparació amb les dades experimentals.

Els diagrames de Feynman que contribueixen a la secció eficaç de les correccions virtuals inclouen integrals de Feynman de dos bucles i quatre punts, que hui en dia representa un coll de botella per moltes de les correccions d'ordre superior. Com que un càlcul analtic no és una estratègia viable encara, càlculs numèrics són necessaris. Un marc numèric general que inclou tant el Model Estàndard com models amb dos Higgs es presenta en aquesta tesi. La part crucial del càlcul és l'allament i cancellació de les divergències ultraviolades i infraroges que venen de les integrals de Feynman (divergents). Les divergències ultraviolades són allades utilitzant la sostracció de punt final, les infraroges per un terme de sostracció dedicat que ve d'un càlcul en el límit de quarks pesats. La part restant de l'amplitud virtual pot ser calculada considerent l'amplitud de producció d'un sol Higgs i el decament del Higgs en un bosó Z i un fotó. La correcció real ha sigut calculada utilitzant llibreries públiques per càlculs d'un bucle. El resultat d'aquest estudi és la secció diferencial depenent de la massa invariant del parell de Higgs i la seua integral, és a dir la secció eficaç total de producció de parrells de Higgs via fusió de gluons a NLO.

Els efectes deguts a la massa del top a segon ordre introdueixen desviacions importants de la secció eficaç diferencial comparada amb el límit de quarks pesats de més del 20% en la cola, incrementant-se amb l'energia del col·lisionador. La desviació al nivell de la secció eficaç es reflecteix en un decreixement de la secció hadrònica total del 15%. Les incerteses relacionades amb l'elecció de l'escala de renormalització a la massa del top i de l'esquema de renormalització han resultat ser considerables. Aquestes incerteses són del mateix ordre que les escales de renormalització i factorització usuals de la constant d'acoblament, tenint un fort impacte en l'estimació de les incerteses teòriques.

Contents

Introduction

The physics of the elementary particles is well described by the Standard Model (SM). The presence of the electroweak interaction prohibits terms which are quadratic with respect to the massive fields into the SM Lagrangian. Introducing such mass terms requires the so-called spontaneous symmetry breaking, which requires a scalar field with non-vanishing vacuum expactation value. As a reminder, the spontaneous symmetry breaking generate a neutral scalar boson, the Higgs boson [1–4]. Although it has been predicted in the '60s by theoretical arguments, in 2012 the LHC experiments ATLAS and CMS found a signal belonging to the resonance of a neutral particle of mass around 125 GeV [5, 6]; further analysis have confirmed that its spin, CP properties and coupling with the other particles are compatible with a SM Higgs boson [7, 8]. In order to definitively attest that this scalar neutral boson is the SM Higgs particle, its self-couplings have to be measured and compared with the phenomenlogical predictions of the SM.

Constraints coming from the Lorentz and gauge invariance, UV completeness and unitarity arguments set the scalar sector of a QFT model to have at most trilinear and quartic self-interactions with its scalar particle content. These terms constitute the Higgs potential, and its presence allows the spontaneous symmetry breaking. The present experimental uncertainties are unsufficient to set strong bounds on the Higgs self-couplings; the possibility of the detected boson to belong to an extended scalar sector of a more general model rather than the SM can not be discarded. Many Beyond the Standard Models (BSM) predict more complex scalar sectors with many Higgs bosons, and nothing prevent the eventuality that the LHC signal was referred to the detection of one particular Higgs boson of a BSM [9–11]. The quartic Higgs coupling is still out of reach at experimental level [12–16]; the trilinear Higgs self-coupling will be accessible in the next future, thanks to the high luminosity upgrade of the LHC or other future colliders [17–28]. An investigation of the Higgs potential can be done by considering direct observables coming from from the Higgs-pair production channels. However, the experimental determination of such processes is nonetheless complicated, because of the very small cross section related with the Higgs-pair production channels and its vast QCD background [23, 28–31]. This fact enlights the importance of a precise theoretical prediction of the cross section of the Higgs-pair production, for which higher order terms of the perturbative expansion with respect of the strong coupling are demanded.

The dominant process involving a Higgs-pair production is the QCD induced gluon fusion [30]. Since there is no mechanism that produces a direct gluon-Higgs interaction, the Feynman amplitude of this process already contains one-loop contributions at its leading order (LO). In addition, it has a strong electroweak and phase space suppression in comparison with the single-Higgs production channel. Therefore, to fullfil the demanded theoretical precision, the total cross section for this process requires a next-to-leading order (NLO) calculation, for which two-loop Feynman amplitude have to be taken into account.

Within the SM, the top-quark loops are responsible for more than the 99% of the total cross section caused by the presence of the Yukawa coupling, which is proportional to the top mass. Other models with an extended scalar sector, like the Two-Higgs-Doublets Model (2HDM), might have non-negligible contributions from the bottom quark, since the parameter space of such models permit enhancements on the their Yukawa couplings [10, 23]. This latter case will be consider in future projects.

The calculation of the Higgs-pair production via gluon fusion total cross section beyond the LO is very challenging: at NLO in the SM it involves four-points two-loops Feynman integrals, entering into the virtual corrections, and five-points one-loop Feynman integrals, which are the building block

of the real corrections. Besides the kinematic invariants of the process, two masses have to be taken into account, namely the top-quark and the Higgs boson mass. While for the one-loop contributions, there are well-grounded calculation techniques with a good degree of automation, for the two-loop Feynman diagrams involved in this process such standard has not been enstablished yet.

Along the past 25 years, great efforts have been made to study the higher order correction to the differential cross section of this process in specific kinematic regions [24, 32–46]. For low energies, the heavy top limit offers a very good approximation and an important simplification of the higher order amplitudes, since they will carry one less loop to each order. This approximation is known up to the third perturbative order (N^3LO) and provides a rough 120% increasing of the LO differential cross section. Mass refinements have been introduced up to the second perturbative order (NNLO) on the real corrections, leading to the so-called full-theory approximation, and as higher order terms into the top-quark mass expansion. The top-mass effects have an impact of the -20% with respect to the sole heavy top limit. Other regions that have been investigated are the $t\bar{t}$-production region, that contains the bulk of the total cross section, and the high-energy limit, for which recently analytical results have been produced. At NLO, all the analysis agree on a 20% mass effect with respect to the heavy top limit.

A complete NLO QCD Higgs-pair production via gluon fusion cross section is needed to obtain the exact top-mass effects occuring at the first perturbative order. A first calculation [47] has been carried out by applying the integration-by-parts identities [48, 49] of the amplitude, achieving its master integrals decomposition. The integration of the master integrals has been done numerically, exploiting the sector decomposition [50] and the contour deformation to perform the integration in the physical region. In order to successfully apply the amplitude reduction method, the top and Higgs masses had to be set respectively to $m_t = 173$ GeV and $m_H = 125$ GeV from the beginning of the calculation. This calculation represents the first NLO cross section with full top-mass dependence.

The aim of this thesis is to present an alternative calculation of the NLO Higgs-pair production via gluon fusion in a framework suitable for both the SM and the 2HDM. A final state with two Higgs bosons with different masses will be considered. The novelty introduced by the strategy here presented is the treatment of the masses as free parameters for the numerical integration. This feature allows the study of the uncertainties related to the choice of the renormalisation scheme and scale of the top-quark mass. The procedure can be summarize as follows: every diagram will firstly be projected into its form factors; on each integral contained in them, the Feynman parametrization will be applied together with a dedicated change of the integration variables that makes the endpoint subtraction of the ultraviolet (UV) divergences possible; the infrared (IR) divergences are subtracted at integrand level exploiting the universality of the IR structure in the ratio with respect to the LO amplitude, in the spirit of the Catani-Seymour subtraction method [51, 52]; the numerical instabilities due to the $t\bar{t}$-production threshold are avoided by giving to the top quark a small width; the finite part of the form factors treated in this way can be safely integrated over the Feynman parameter and the phase space. The renormalisation procedure and the introduction of the real corrections ensure the UV finiteness and the IR safety of the differential and total cross section. A method to restore the narrow width of the top quark is needed. The Richardson extrapolation method offers a way to combine results for different top-quark widths to extract the narrow width "limit". The outcome of this framework is the Higgs-pair production differential cross section. The integrated cross section will be found by using the Romberg's method, which combines the trapezoidal rule and the Richardson extrapolation in order to decrease its numerical uncertainties method.

Results for this procedure applyed to the NLO SM Higgs-pair production via gluon-fusion [53–55] will be discussed in detail in this thesis, presenting the differential cross section distributions and the total cross section for different centre-of-mass energies. There will be shown how the uncertainties related to the renormalisation and factorization scales together with the top-mass renormalisation scheme and scale uncertainties have a huge impact, leading to sizeable relative errors. At last, it will be discussed how a dynamical top-mass renormalisation scale choice is needed to control the top-mass effects at high energies. The possibility of choosing different top-quark masses is nowadays possible only with the method described in this thesis, and it will be discussed in details.

This thesis is structured as follows: Chapter 1 is devoted to define the theoretical background on

which this work is built, presenting the models under consideration, the basics of the phenomenological results regarding the Higgs boson, the general framework used for calculating a cross section involving QCD contributions, and the state-of-the-art of the Higgs-pair production via gluon fusion; Chapter 2 and 3 will describe in detail the LO and NLO cross section calculation respectively in the common framework suitable both for SM and 2HDM, with particular focus on the isolation of the UV and IR divergences from the virtual correction, the renormalisation of the UV divergences and the dedicated subtraction terms for the IR divergences, and the calculation of the real contributions; Chapter 4 shows the numerical setup employed to obtain the differential cross section distribution and the total cross section, presenting the Monte Carlo integration algorithm to evaluate numerically the form factors, the Richardson extrapolation method to extract the narrow width limit of the top-quark mass and the integration of the differential distribution through the trapezoidal method combined with the Richardson extrapolation; Chapter 5 will present the discussion of the results obtained by applying the procedure shown in the previous Chapters, with particular focus on the top-mass uncertainties, their impact on the NLO differential and integrated cross section and how to combine them together with the state-of-the-art predictions; at last, Chapter 7 will recap all the core arguments discussed in this thesis, present the conclusions and an outlook on the future perspective of this project.

Chapter 1

Theoretical background

1.1 The Standard Model

The Standard Model (SM) represents the most successful model describing the particle interactions. It has been built and tested along 60 years of data from collider experiments embedded into a quantum field theory framework. The discovery of a scalar particle compatible with an Higgs boson [1–6] represent the most recent success of the SM. It further provides a solid theoretical framework for a pleathora of phenomenological outcomes comparable with the experiment.

Theoretically speaking, it is a quantum field theory described by the Lorentz invariant Lagrangian $\mathcal{L}_{\text{SM}}$ symmetric with respect to the gauge group $SU(3)_C \otimes SU(2)_L \otimes U(1)_Y$. The $SU(3)_C$ Lie group is the representation of the strong interaction [56–63] between quarks mediated by the gluons; the associated charge is called *color charge*. The $SU(2)_L \otimes U(1)_Y$ product represents the electroweak interaction (EW) between leptons [64–66]; its associated conserved quantities are the weak isospin I and the hypercharge Y. As will be described later on, the spontaneous symmetry breaking $SU(2)_L \otimes U(1)_Y \to U(1)_{\text{EM}}$ will lead to the conservation of the *electric charge* $Q = I_3 + Y$, know as Gell-Mann-Nishijima formula [67, 68].

The Lagrangian $\mathcal{L}_{\text{SM}}$ can be written as

$$\mathcal{L}_{\text{SM}} = \mathcal{L}_{\text{G}} + \mathcal{L}_f, \tag{1.1}$$

where

$$\begin{gathered}
\mathcal{L}_{\text{G}} = -\frac{1}{4} \sum_{b}^{\{C,L,Y\}} \text{Tr}\left[F_b^{\mu\nu} F_{b,\mu\nu}\right], \qquad \mathcal{L}_f = \sum_q i\overline{\psi}_q \not{D} \psi_q + \sum_l i\overline{\psi}_l \not{D} \psi_l, \\
[D_\mu, D_\nu] = -i \sum_{b}^{\{C,L,Y\}} g_b T_b^a F_b^{a,\mu\nu}, \qquad D_\mu = \partial_\mu - i \sum_{b}^{\{C,L,Y\}} g_b T_b^a A_{b,\mu}^a \\
\psi_q = \begin{Bmatrix} u & c & t \\ d & s & b \end{Bmatrix}, \qquad \psi_l = \begin{Bmatrix} e & \mu & \tau \\ \nu_e & \nu_\mu & \nu_\tau \end{Bmatrix}.
\end{gathered} \tag{1.2}$$

The indices b runs over the gauge group, a is the index of the adjoint representation, $A_{b,\mu}^a$ are the fields that represents the boson which mediates the b interactions and g_b are the coupling constants. For each generator of the gauge group, a boson field have to be added.

The adjoint representation of the SM gauge group is characterized by

$$\begin{gathered}
T_C^a = \frac{\lambda^a}{2}, \qquad [T_C^a, T_C^b] = i f^{abc} T_C^c, \qquad a = \{1, \ldots, 8\}, \qquad A_C^{a,\mu} = G^{a,\mu} \\
T_L^i = \frac{\sigma^i}{2}, \qquad [T_L^i, T_L^j] = i\frac{\epsilon^{ijk}}{2}\sigma^k \qquad a = \{1, 2, 3\}, \qquad A_L^{i,\mu} = W^{i,\mu} \\
T_Y = \mathbb{1} Y, \qquad A_Y^\mu = B^\mu
\end{gathered} \tag{1.3}$$

where σ^i are the Pauli matrices and λ^a are the Gell-Mann matrices. There are 8 *gluons* $G^{a,\mu}$, and 4 elecroweak bosons $W^{i,\mu}$ and B^μ.

Quarks

$Q_L = \begin{pmatrix} u_L \\ d_L \end{pmatrix}, \begin{pmatrix} c_L \\ s_L \end{pmatrix}, \begin{pmatrix} t_L \\ b_L \end{pmatrix}$	$\in$	$\mathbf{3} \otimes \mathbf{2} \otimes \frac{1}{6}$
$u_R,\ c_R,\ t_R$	$\in$	$\mathbf{3} \otimes \mathbb{1} \otimes \frac{2}{3}$
$d_R,\ s_R,\ b_R$	$\in$	$\mathbf{3} \otimes \mathbb{1} \otimes -\frac{1}{3}$

Leptons

$L_L = \begin{pmatrix} \nu_{e,L} \\ e_L \end{pmatrix}, \begin{pmatrix} \nu_{\mu,L} \\ \mu_L \end{pmatrix}, \begin{pmatrix} \nu_{\tau,L} \\ \tau_L \end{pmatrix}$	$\in$	$\mathbb{1} \otimes \mathbf{2} \otimes -\frac{1}{2}$
$e_R,\ \nu_R,\ \tau_R$	$\in$	$\mathbb{1} \otimes \mathbb{1} \otimes -1$

Table 1.1: Matter content of the SM with the relative representation in the SM gauge group. The right-handed neutrinos are singlets w.r.t. the gauge transformation, hence they are not included within the Standard Model. Each weak isospin doublet have quantum isospin numbers $I = \frac{1}{2}$ and $I_3 = \pm\frac{1}{2}$.

The matter content is encoded into the spinors ψ_p. Each spinor have two chiral components labeled left-handed and right-handed. Strong interaction are not sensible to the chiral components, while EW interaction acts only on the left-handed components: fermions are organized in left-handed doublets and right-handed singlets under the EW gauge group. The fermions that form a triplet under $SU(3)_C$ are the *quarks*.

The physical EW boson are obtained by combining the $W^{i,\mu}$ and B^μ as follows:

$$\begin{pmatrix} A^\mu \\ Z^\mu \end{pmatrix} = \begin{pmatrix} \cos\theta_W & \sin\theta_W \\ -\sin\theta_W & \cos\theta_W \end{pmatrix} \begin{pmatrix} B^\mu \\ W^{3,\mu} \end{pmatrix}, \qquad W^{\mp,\mu} = \frac{1}{\sqrt{2}}(W^{1,\mu} \mp iW^{2,\mu}). \tag{1.4}$$

The field A^μ is the *photon* and with the *EW boson* Z^μ contributes to the neutral currents. The EW bosons $W^{\mp,\mu}$ lead to charged currents. The fermions which interact only via EW interaction are the *leptons*. The matter content that goes into the spinors ψ_p are depicted in Table 1.1.

Imposing the invariance under the SM gauge group requires all the fields in $\mathcal{L}_{\text{SM}}$ to be massless, since the EW gauge subgroup prohibits mass terms. Experimentally is known that the EW bosons have a large mass and, of course, fermions are massive too. Therefore, a mechanism that introduces a mass term into the SM Lagrangian is needed.

1.1.1 The Higgs mechanism

Scalars

$\Phi = \begin{pmatrix} \phi^+ \\ \phi^0 \end{pmatrix}$	$\in$	$\mathbb{1} \otimes \mathbf{2} \otimes \frac{1}{2}, \quad \langle\Phi\rangle = \frac{1}{\sqrt{2}} \begin{pmatrix} 0 \\ v \end{pmatrix}$

Table 1.2: Scalar sector of the SM. This complex doublet has isospin $I = \frac{1}{2}$.

The mass terms allowed into a Lagrangian which satisfies the Lorentz invariance is quadratic in the fields for which the mass is demanded. Unfortunately, the structure of a mass term violates the gauge symmetry. The problem has been solved by the *Higgs mechanism* [1–4], based on the *spontaneous symmetry breaking*.

The potential of a free complex scalar isospin doublet Φ which satisfies the renormalizability and the unitarity is

$$V_\Phi = \mu^2\Phi^+\Phi + \frac{\lambda}{2}|\Phi^+\Phi|^2, \tag{1.5}$$

where $\mu^2 < 0$ and $\lambda > 0$. The field Φ has a non-vanishing vacuum expectation value (VEV):

$$\langle\Phi\rangle = \frac{1}{\sqrt{2}} \begin{pmatrix} 0 \\ v \end{pmatrix}, \qquad v = \sqrt{-\frac{2\mu^2}{\lambda}} \approx 246 \text{ GeV}. \tag{1.6}$$

Notice that only a neutral scalar field can acquire a VEV because of the conservation of the electric charge. This VEV spontaneously breaks the symmetry:

$$SU(2)_L \otimes U(1)_Y \to U(1)_{\mathrm{EM}}, \tag{1.7}$$

that underlines the fact that electromagnetism is not broken.

Fixing the gauge of the field Φ to be the *unitary gauge*[1]:

$$\Phi(x) = \frac{1}{\sqrt{2}} \begin{pmatrix} 0 \\ v + H(x) \end{pmatrix}, \tag{1.8}$$

where $H(x)$ is the *physical Higgs* field. The unitary gauge make manifest the non-zero expectation value of Φ.

Embedding the Lagrangian $\mathcal{L}_\Phi$ into the Standard Model implies the replacement of $\partial^\mu \to D^\mu$, therefore:

$$\begin{aligned} \mathcal{L}_{\mathrm{H}} &= D^\mu \Phi^+ D_\mu \Phi - \mu^2 \Phi^+ \Phi - \frac{\lambda}{2} |\Phi^+ \Phi|^4, \\ D^\mu \Phi^+ D_\mu \Phi &\sim_{\langle \Phi \rangle} \frac{v^2}{8} \left[g_L^2 (W^{1,\mu} + iW^{2,\mu})(W^1_\mu - iW^2_\mu) + (g_L W^3_\mu - g_Y B_\mu)(g_L W^{3,\mu} - g_Y B^\mu) \right] \\ &= m_W^2 W^{+,\mu} W^-_\mu + m_Z^2 Z^\mu Z_\mu, \end{aligned} \tag{1.9}$$

where $g_L = \sqrt{g_L^2 + g_Y^2} \cos\theta_W$, and

$$m_W = \frac{g_L v}{2}, \quad m_Z = \frac{v}{2}\sqrt{g_L^2 + g_Y^2} = \frac{m_W}{\cos\theta_W}, \quad m_A = 0, \quad m_H = \sqrt{-\frac{\mu^2}{2}}. \tag{1.10}$$

The mass terms introduced by adding the scalar field $\Phi(x)$ does not break the EW gauge symmetry: three of the four degrees of freedom of $\Phi(x)$ have been eaten by the weak bosons and thus they acquire mass. Notice that the SM with spontaneous symmetry breaking is still gauge invariant, even though it is not immediately manifest [69, 70].

The interaction of the particles with the ground state of the Higgs make the particles acquire a mass term. For the fermion, the *Yukawa Lagrangian* offers the simplest way to introduce such mass term:

$$\begin{aligned} -\mathcal{L}_Y &= Y^d_{ij}\, \overline{Q}_{i,L} \Phi d_{j,R} + Y^u_{ij} \overline{Q}_{i,L} \Phi^c u_{j,R} + Y^l_{ij} \overline{L}_{i,L} \Phi l_{j,R} + h.c. \\ &\Downarrow \\ -\mathcal{L}_Y &\sim_{\langle \Phi \rangle} Y^d_{ij} \frac{v}{\sqrt{2}} \overline{d}_{i,L} d_{j,R} + Y^u_{ij} \frac{v}{\sqrt{2}} \overline{u}_{i,L} u_{j,R} + Y^l_{ij} \frac{v}{\sqrt{2}} \bar{l}_{i,L} l_{j,R} + h.c. \quad , \end{aligned} \tag{1.11}$$

where Φ^c is the charge conjugate of Φ, $Q_{i,L}$ and $L_{i,L}$ are the quark and lepton isospin doublet, the Y^k_{ij} are the *Yukawa couplings* and

$$m^k_{ij} = Y^k_{ij} \frac{v}{\sqrt{2}}, \tag{1.12}$$

are the mass matrices. Each of these mass matrices can be diagonalized by means of the CKM matrix, for the quark sector, [71, 72] and the PMNS [73, 74] matrix, for the lepton sector.

The Standard Model Lagrangian[2] is the sum of the massless $\mathcal{L}_{\mathrm{G}} + \mathcal{L}_{\mathrm{f}}$ and the Higgs and Yukawa Lagrangian

$$\mathcal{L}_{\mathrm{SM}} = \mathcal{L}_{\mathrm{G}} + \mathcal{L}_{\mathrm{f}} + \mathcal{L}_{\mathrm{H}} + \mathcal{L}_{\mathrm{Y}}. \tag{1.13}$$

The Feynman rules that this Lagrangian provides are depicted in Appendix I.

[1] It is based on the fact that a complex field $\phi(x)$ can be expressed into polar coordinates, obtaining two real fields $r(x)$ and $\Theta(x)$. A gauge transformation acts like a shift of $\Theta(x) \to \Theta'(x)$. Therefore, fixing the function $\Theta(x)$ is equivalent to perform a gauge transformation. In general, gauge symmetry ensures that a doublet can be rotated with a $SU(2)$ transformation that sets the first component to 0 and the second to be real.

[2] The actual SM Langragian contains additional terms related to the gauge fixing and the ghost Lagrangian. We did not discuss it in details since it is not the main focus of the discussion.

1.2 Two-Higgs-Doublets Model

The study of the scalar sector of the SM can be made experimentally by measuring the parameter ρ: for a model locally invariant under $SU(2)_L \otimes U(1)_Y$ with n multiplets with weak isospin $I^{(i)}$, hypercharge $Y_{(i)}$ and VEV v_i, the tree-level parameter ρ is

$$\rho = \frac{\sum_i^n [I^{(i)}(I^{(i)}+1) - Y_{(i)}^2] v_i}{2\sum_i^n Y_{(i)}^2 v_i}. \tag{1.14}$$

The experimental data [75] shows that ρ is compatible with 1, which is the case of the SM with its single complex doublet. However, this constraint does not exclude other possibilities, i.e. higher multiplets with zero VEVs or higher dimensional representations. The latter cases tend to introduce overcomplexities that are not the main focus of this thesis; we will consider the simplest extension of the SM scalar sector that leads the introduction of additional singlets and doublets.

An extended SM scalar sector is motivated by its presence in many other models, like supersypersymmetry [76] and the Peccei-Quinn model [77, 78], and it might explain the baryon asymmetry [79–81]. Further details can be found in the review of Ref. [10].

Scalars

$\Phi_1 = \begin{pmatrix} \phi_1^+ \\ \phi_1^0 \end{pmatrix}$	$\in$	$\mathbb{1} \otimes \mathbf{2} \otimes \frac{1}{2}$,	$\langle \Phi_1 \rangle = \frac{1}{\sqrt{2}} \begin{pmatrix} 0 \\ v_1 \end{pmatrix}$
$\Phi_2 = \begin{pmatrix} \phi_2^+ \\ \phi_2^0 \end{pmatrix}$	$\in$	$\mathbb{1} \otimes \mathbf{2} \otimes \frac{1}{2}$,	$\langle \Phi_2 \rangle = \frac{1}{\sqrt{2}} \begin{pmatrix} 0 \\ v_2 \end{pmatrix}$

Table 1.3: Scalar sector of the SM. This complex doublet has isospin $I = \frac{1}{2}$.

The model we are going to introduce is the *Two-Higgs-Doublets Model* (2HDM) [82], which consists in the extension of the scalar sector of the SM with one additional scalar doublet with a different non-vanishing VEV. This model respects the experimental constraint $\rho = 1$ and represent the most simple UV-complete model with an extended scalar sector.

The most general potential for the scalar content of the 2HDM that respects Lorentz invariance, SM gauge symmetry, unitarity and renormalizability is

$$\begin{aligned} V_{\text{2HDM}} = {} & \mu_{11}^2 \Phi_1^+ \Phi_1 - \mu_{12}^2 [\Phi_1^+ \Phi_2 + \Phi_2^+ \Phi_1] + \mu_{22}^2 \Phi_2^+ \Phi_2 + \frac{\lambda_1}{2} \left(\Phi_1^+ \Phi_1\right)^2 + \frac{\lambda_2}{2} \left(\Phi_2^+ \Phi_2\right)^2 + \\ & + \lambda_3 \Phi_1^+ \Phi_1 \Phi_2^+ \Phi_2 + \lambda_4 \Phi_1^+ \Phi_2 \Phi_2^+ \Phi_1 + \frac{\lambda_5}{2} \left[\left(\Phi_1^+ \Phi_2\right)^2 + \left(\Phi_2^+ \Phi_1\right)^2 \right]. \end{aligned} \tag{1.15}$$

where the details of the two Higgs doublets are depicted in Table 1.3. Imposing hermeticity and stability of the vacuums state, the following conditions can be imposed [83–86]:

$$\begin{gathered} \lambda_1 > 0, \qquad \lambda_2 > 0, \qquad \lambda_3 > -\sqrt{\lambda_1 \lambda_2}, \qquad \lambda_3 + \lambda_4 - |\lambda_5| > -\sqrt{\lambda_1 \lambda_2} \\ \lambda_1, \lambda_2, \lambda_3 \in \mathbb{R}, \end{gathered} \tag{1.16}$$

and the non-zero VEVs of the scalar doublets

$$\Phi_1 = \frac{1}{\sqrt{2}} \begin{pmatrix} 0 \\ v_1 \end{pmatrix}, \qquad \Phi_2 = \frac{1}{\sqrt{2}} \begin{pmatrix} 0 \\ v_2 \end{pmatrix}, \tag{1.17}$$

are constrained by $v_1^2 + v_2^2 = v$. Additional constraints on the 2HDM parameters can be set, like the unitarity contraints and experimental bounds [86–91].

Following the same steps presented for the SM case, it can be shown that after the spontaneous symmetry breaking $SU(2)_L \otimes U(1)_Y \to U(1)_{\rm EM}$, 3 d.o.f. of the two doublets are eaten by the massive bosons. However, instead of a single Higgs boson, there are five scalar Higgs bosons after the spontaneous symmetry breaking. Expressing the doublets in the unitary gauge:

$$\Phi_j = \begin{pmatrix} \phi_j^+ \\ \frac{1}{\sqrt{2}}(v_j + \rho_j + i\eta_j) \end{pmatrix}. \tag{1.18}$$

The mass terms with this new set of variables are

$$\begin{aligned} V_{\rm 2HDM}|_{\rm mass} = \; & [\mu_{12}^2 - (\lambda_4+\lambda_5)v_1v_2](\phi_1^-, \phi_2^-) M_\phi \begin{pmatrix} \phi_1^- \\ \phi_2^- \end{pmatrix} - (\rho_1, \rho_2) M_\rho \begin{pmatrix} \rho_1 \\ \rho_2 \end{pmatrix} \\ & + \left[\frac{\mu_{12}^2}{v_1 v_2} - 2\lambda_5 \right] (\eta_1, \eta_2) M_\eta \begin{pmatrix} \eta_1 \\ \eta_2 \end{pmatrix} \end{aligned} \tag{1.19}$$

$$M_\phi = \begin{pmatrix} \frac{v_2}{v_1} & -1 \\ -1 & \frac{v_1}{v_2} \end{pmatrix}, \qquad M_\eta = \begin{pmatrix} v_2^2 & -v_1v_2 \\ -v_1v_2 & v_1^2 \end{pmatrix}, \qquad M_\phi = v_1v_2 M_\eta$$

$$M_\rho = \begin{pmatrix} \mu_{12}^2 \frac{v_2}{v_1} + \lambda_1 v_1^2 & -\mu_{12}^2 + (\lambda_3+\lambda_4+\lambda_5)v_1v_2 \\ -\mu_{12}^2 + (\lambda_3+\lambda_4+\lambda_5)v_1v_2 & \mu_{12}^2 \frac{v_1}{v_2} + \lambda_2 v_2^2 \end{pmatrix}.$$

The two mass matrices M_ϕ and M_η have a zero eigenvalue. The corresponding particle is the Goldstone boson eaten by the charge EW bosons and the boson Z. Therefore, we are left with a charged boson H^+ (and its antiboson), a pseudoscalar A and two neutral scalar bosons H_1 and H_2.

The mass matrices can be diagonalized by means of two angles: α for the neutral scalar Higgs bosons and β for the charged and pseudoscalar ones. The latter is related to the doublets VEVs by

$$\tan\beta = \frac{v_2}{v_1}. \tag{1.20}$$

Assuming that there is no CP violation, both v_1 and v_2 can be assumed to be real [92]. Therefore, the physical fields of the 2HDM scalar sector are

$$\begin{aligned} H^\pm &= \phi_2^\pm \cos\beta - \phi_1^\pm \sin\beta, & m_\pm^2 &= \frac{(v_1^2+v_2^2)}{v_1v_2}\left[\mu_{12}^2 - (\lambda_4+\lambda_5)v_1v_2\right], \\ A &= \eta_2\cos\beta - \eta_1\sin\beta, & m_A^2 &= \frac{(v_1^2+v_2^2)}{v_1v_2}\left[\mu_{12}^2 - (\lambda_3+\lambda_4+\lambda_5)v_1v_2\right], \\ H_1 &= \rho_2\cos\alpha - \rho_1\sin\alpha, & m_{H_1}^2 &= \frac{1}{2}\left[{\rm Tr}\left[M_\rho\right] - \sqrt{{\rm Tr}\left[M_\rho\right]^2 - 4\det M_\rho}\right], \\ H_2 &= \rho_2\cos\alpha + \rho_1\sin\alpha, & m_{H_2}^2 &= \frac{1}{2}\left[{\rm Tr}\left[M_\rho\right] + \sqrt{{\rm Tr}\left[M_\rho\right]^2 - 4\det M_\rho}\right]. \end{aligned} \tag{1.21}$$

The new Yukawa interactions have to be included into the 2HDM Lagrangian. The Yukawa terms for the down-type quarks is

$$\begin{aligned} -\mathcal{L}_Y^d &= Y_{ij}^1\, \overline{Q}_{i,L}\Phi_1 d_{j,R} + Y_{ij}^2\, \overline{Q}_{i,L}\Phi_2 d_{j,R} + h.c. \\ &\Downarrow \\ -\mathcal{L}_Y^d &\sim_{\langle\Phi_1\rangle,\langle\Phi_2\rangle} \left(Y_{ij}^1 \frac{v_1}{\sqrt{2}} + Y_{ij}^2 \frac{v_2}{\sqrt{2}} \right) \overline{d}_{i,L} d_{j,R} + h.c. \end{aligned} \tag{1.22}$$

The relevant Feynman rules used in thesis are depicted in Appendix I.

In general, the two Yukawa matrices cannot be diagonalized simultaneously: this fact leads to tree-level flavour-changing neutral currents (FCNC), which have never been seen by the experiments. These kind of currents can be avoided by imposing additional symmetries. Moreover, the Paschos-Glashow-Weinberg (PGW) theorem [93] grants that tree level FCNC cannot occur if the fermions with same quantum numbers are coupled to the same Higgs doublet. To ensure the absence of tree level FCNC by means of the PGW theorem, there are many possibilities:

Type I: All fermions coupled to Φ_2 only;

Type II: Down-type quark and leptons coupled to Φ_1, up-type quark coupled to Φ_2;

Type X: Leptons coupled to Φ_1, quarks coupled to Φ_2;

Type Y: Down-type quark coupled to Φ_1, up-type quark and leptons. coupled to Φ_2

Another possibility is that the Yukawa couplings involving Φ_1 and Φ_2 are proportional in the flavour space [94–96].

Type I can be induced by imposing a $\mathbb{Z}_2$ symmetry on Φ_1, Type II by imposing an additional $\mathbb{Z}_2$-symmetry on $d_{j,R}$. Type I has been studied in the context of dark matter[97–103], in the particular case of the inert Φ_2 doublet with $v_2 = 0$. In addition, the latter model with $\lambda_5 \to 0$ is Peccei-Quinn symmetric. On the other hand, Type II is particularly relevant since it can be treated as the effective field theory at low-energy for the Minimal Supersymmetric Standard Model with all heavy supersymmetric partners [9, 104–106].

The 2HDM has a variety of interactions vertices and 5 additional particles, leading to a rich phenomenology involving CP conserving and violating sources [10]. This model has been employed in the study of various BSM investigations, like composite and little Higgs models [107–109], Naturalness [110] and the origin of the neutrino masses [98].

The 125 GeV resonance discovered in 2012 compatible with a Higgs boson candidate have set another strong constraints. The possibility that it was a signal of the pseudoscalar boson A has been studied in Ref. [111], but it was discarded by the data analysis [7, 8], as well as the chance that the detection was related with a neutral heavy scalar [112]. Therefore, the most reasonable scenario is that the signal detected at the LHC comes from either a SM Higgs boson H or a neutral scalar light Higgs H_2.

1.3 Higgs boson detection

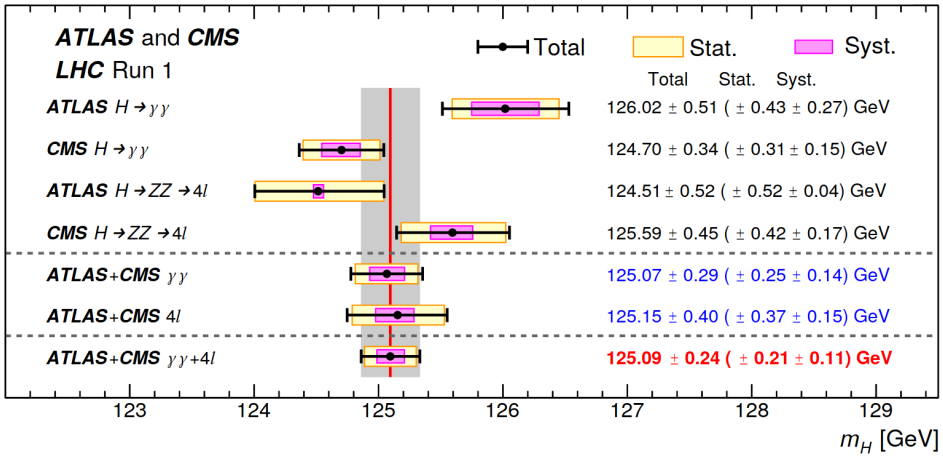

Figure 1.1: Higgs boson mass determination [113]. Combined analysis of ATLAS and CMS experiments

In 2012, the LHC experiments ATLAS [5] and CMS [6] announced the discovery of a neutral scalar boson compatible with the SM Higgs boson. The combined result of the experiments (Fig. 1.1) have fix its mass to $m_H = 125.09 \pm 0.24$ GeV [113]. It was the last unknown parameter of the SM, and it gives access to various phenomenological predictions.

The detection has been analyzed starting from two dataset recorded by ATLAS and CMS during the LHC Run 1, looking at the decays $H \to ZZ/WW \to 4l$, $H \to \gamma\gamma$, $H \to b\bar{b}$ and $H \to \tau^+\tau^-$. The two independent analysis agreed with a significant excess of events above the background, signal of the production of a neutral boson. Later on, the two datasets have been combined in a comprehensive study specific on the channels $H \to ZZ \to 4l$ and $H \to \gamma\gamma$, which gave the best mass resolution.

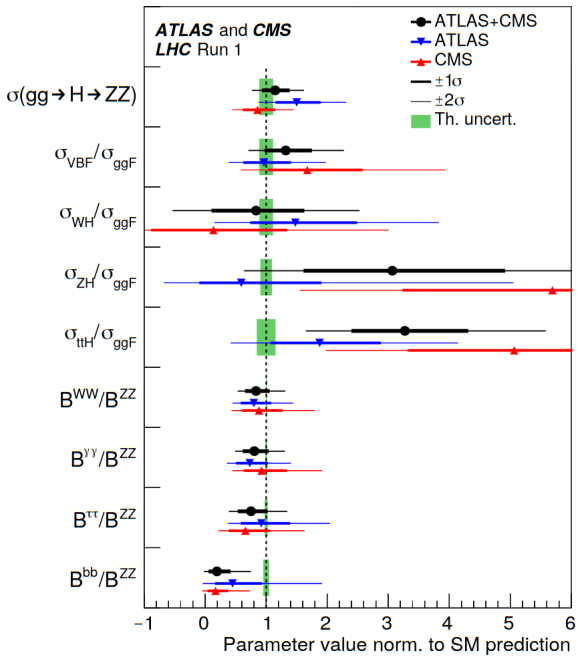

Figure 1.2: Best fit for the Higgs production and decay.

Knowing the Higgs mass, its production and decay can be study. A detailed analysis of the following production processes have been done: gluon fusion, vector boson fusion and associated production with a vector boson or a top-quark pair [113]. The decay rates, that this analysis has considered, are: $H \to ZZ, WW, \gamma\gamma, \tau\tau, bb$ and $\mu\mu$. The already mentioned dataset shows a compatibility with the production and decay of a SM Higgs (Fig. 1.2). Also, this analysis provided predictions on its couplings to vector bosons and fermions.

At last, the CP properties of this particle have been infered by the angular distribution of the leptonic decays, showing complete agreement with the hypothesis $J^p = 0^+$, once again compatible with the SM Higgs [7, 8].

However, the evidence of the existence of this Higgs boson does not exclude a priori the possibility of its belonging to an extended scalar sectors, since the 2HDM scalar sector has a particle compatible with the detected one [11, 23].

1.4 Higgs boson pair production

As it has been shown before, the data analysis have checked most of the quantities related with the Higgs boson, namely its mass, CP properties and coupling with other particles with great precision, and shows compatibility with the SM prediction. However, the Higgs self-coupling is not accessible with the present LHC dataset. The upcoming high luminosity upgrade of the LHC and other future colliders will give us access to the study of the Higgs self-coupling [17–28].

The self-couplings of Higgs bosons are allowed by the constraints imposed on the SM and 2HDM lagrangians, and they comes from the Higgs potential:

$$\begin{aligned} V_\Phi &= -\mu^2 H^2 - \frac{\mu^2}{v} H^3 - \frac{\mu^2}{4v^2} H^4 \\ &= \frac{m_H^2}{2} H^2 + \frac{\lambda_{3H}}{3!} H^3 + \frac{\lambda_{4H}}{4!} H^4 \\ \lambda_{3H} &= -\frac{3m_H^2}{v}, \qquad \lambda_{4H} = -\frac{3m_H^2}{v^2}. \end{aligned} \tag{1.23}$$

The parametrization of the 2HDM gives rise to more complex structures, but the trilinear-quartic

Higgs couplings can be written as follows (Appendix I)

$$V_{\text{2HDM}} = \sum_j \frac{m_{H_j}^2}{2} H_j^2 + \sum_{ijk} \frac{\lambda_{ijk}}{3!} H_i H_j H_k + \sum_{ijkl} \frac{\lambda_{ijkl}}{4!} H_i H_j H_k H_l$$
$$\lambda_{ijk} = -\frac{3c_{ijk}}{v}, \qquad \lambda_{ijkl} = -\frac{3c_{ijkl}}{v^2} \tag{1.24}$$

Exploring the Higgs self-coupling is crucial to fully reconstruct the shape of the Higgs potential with a non-zero VEV.

This is a very challenging measurement, since the Higgs-pair production is a strongly suppressed process. With respect to the Higgs production, it has a first suppression due to the phase space, that now has to take into account an additional final state heavy particle; moreover, it is a process of higher EW order, which give another suppression factor. In addition to all this suppressions, there are several irreducible background subprocesses which lead to the same final state but does not contain any Higgs self-coupling.

The quartic Higgs interaction is unreachable by the experiment due to the strong EW suppression [12–16]; the trilinear Higgs coupling instead will be accessible with the upgrade of the LHC, allowing the study of processes which involves the production of an off-shell Higgs boson that decays into two Higgs bosons [114]. These interaction may occur into the Higgs-pair production processes, which is the ingredient for a direct measurement of the trilinear Higgs coupling.

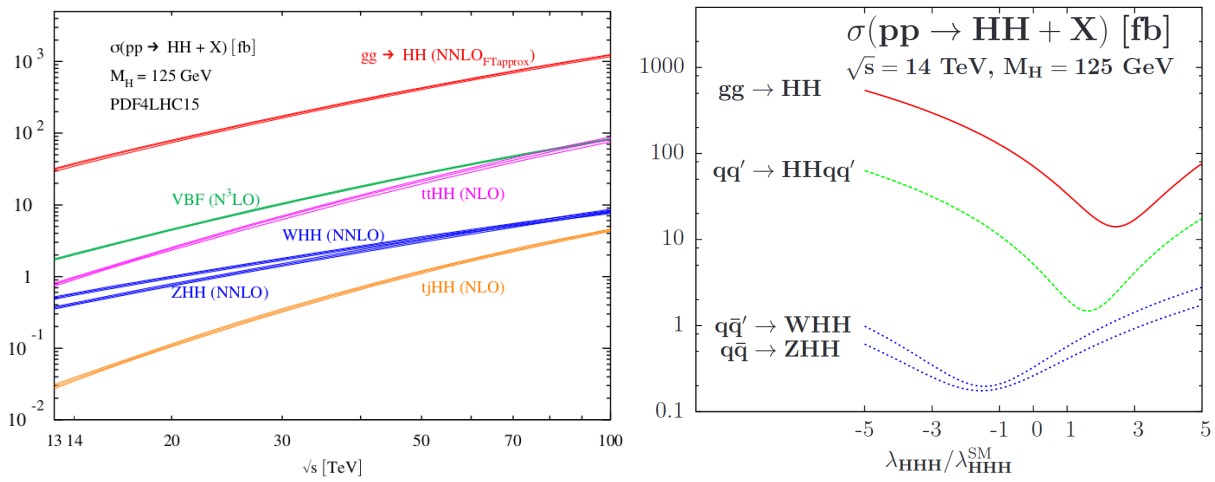

Figure 1.3: *Left plot: Cross section of the Higgs-pair production channels [30]. Right plot: sensitivity of the the Higgs-pair production channels with respect to the trilinear Higgs coupling [23].*

There are four channels contributing to the Higgs-pair production process: gluon fusion [115–118], vector-boson fusion [119–121], double Higgs-strahlung [117, 122] and associated production with heavy quarks [23, 123]. The gluon fusion is the dominant process (Figure 1.3), with a cross section of one order of magnitude higher with respect to the others. However, its cross section σ is still three order of magnitudes lower than the single-Higgs production [29]. In addition, for the gluon fusion channel, the relative uncertainties of its cross section are related to the relative uncertainties of the trilinear coupling in the ratio with the SM [23] with the following approximate relation

$$\frac{\Delta\sigma}{\sigma} \sim \frac{\Delta\lambda_{3\text{H}}}{\lambda_{3\text{H}}}. \tag{1.25}$$

These fact can be inferred by the negative slope of the red curve of Figure 1.3 (right plot), and it sets the importance of investigating the gluon fusion channel of the Higgs-pair production process with high theoretical accuracy. This can only be achieved by introducing higher order correction. Since gluon fusion is a QCD induced process, it is known that higher orders[3] in QCD may introduce very

[3] In the next section we will define to which order are we referring here.

large contributions to the total cross section: for single-Higgs production via gluon fusion, higher order terms introduced corrections of more than 60% [124–127].

Since the Higgs boson does not couple with the gluons directly, the gluon fusion channel is mediated by quark loops already at the lower order. The Yukawa couplings are proportional to the quark mass: this means that the main contribution to the cross section comes from the heaviest quark, namely the top quark; lighter quarks corrections are below the 1%. It has been proven that the Higgs-pair production via gluon fusion cross section behaves analogously to the single-Higgs production with respect to the perturbative order: higher order corrections are very large [32, 125]. The main reason for this is that additional QCD perturbative orders open more channels that sum to the latter ones.

The equivalent process in the 2HDM will be neutral scalar Higgs-pair production, where we allow the final state to be $H_i H_j$. If $i = j$ the process is very similar to the SM one, where the only difference lies into the Yukawa couplings to the top quark and the Higgs mass. The difference starts to be noticeable in the case where $i \neq j$, which involves two different Yukawa coupling and masses, making the actual calculation more complex. Moreover, it is important to notice that the Yukawa couplings, while in the SM are proportional only to the quark mass, in the 2HDM are proportional to $\tan\beta$ (or $\cot\beta$); this fact might strongly enhance such couplings and make the contributions of the lighter quarks in the loop relevant [10].

1.4.1 Measurement

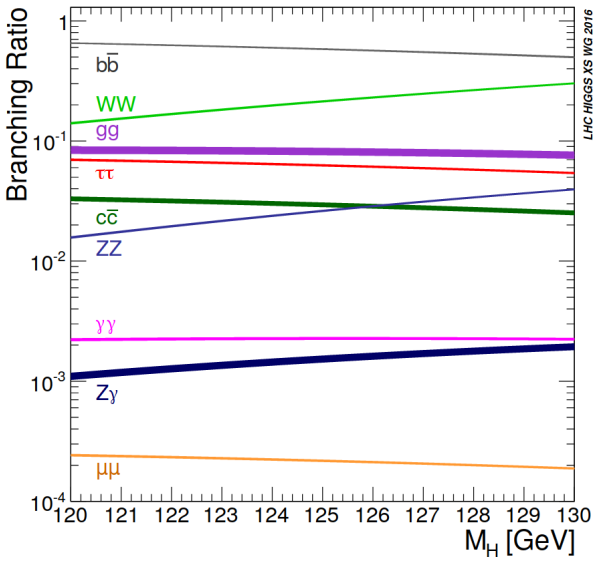

Figure 1.4: Branching ratios of the Higgs boson [128].

As shown in Fig 1.4, the Higgs mainly decays into a bottom quark pair [30]: hence it may be natural to search the $b\bar{b}b\bar{b}$ final state. However, this final state has a huge QCD background, that makes the extraction of the signal incredibly hard. A more reliable analysis can be done by considering more rare final state like $b\bar{b}\gamma\gamma$ and $b\bar{b}\tau\tau$ [28, 29].

The $b\bar{b}\gamma\gamma$ final state constitutes a promising candidate due to its clean signal, leading to a determination of the Higgs coupling with 40% uncertainty [23, 31]. The current bounds on the trilinear Higgs coupling come from CMS analysis of the $HH \to b\bar{b}\gamma\gamma$ channel, which have set $-8\lambda_{3H} < \lambda_{3H} < 15\lambda_{3H}$. With the forthcoming high luminosity LHC, ATLAS can decrese the bound to $-0.8\lambda_{3H} < \lambda_{3H} < 7.7\lambda_{3H}$ [114].

The process $b\bar{b}\tau\tau$ has a more complex background that makes the study of this channel harder, and is strongly dependent on the capability of reconstructing the τ pairs of the experiment. However, it has been proven that, in optimistic scenarios, it represent a valid final state candidate [23].

1.5 Cross section: an overview on the calculation

The perturbative QCD provides an ideal framework to calculate the cross section of the Higgs-pair production via gluon fusion. In this work, we will consider the production of two neutral scalar Higgs bosons, namely $pp \to H_1 H_2$.

The total cross section can be written as a perturbative series with respect to the strong coupling constant: this will provide the following expansion

$$\sigma(pp \to gg \to H_1 H_2) = \sigma_{\rm LO} + \Delta\sigma_{\rm NLO} + \cdots + \Delta\sigma_{\rm N^nLO} + O\left(\alpha_s^{2(n+1)}\right). \tag{1.26}$$

The QCD factorization theorems [129] set the condition under which high energy hadrons can be described as bound states of its constituents, quark and gluons, carrying a fraction of its total momentum. Hence, in proton-proton collision their constituents interact: we are interested in the case where a gluon carrying momentum $p_1 = x_1 P_1$ interacts with a gluon carrying momentum $p_2 = x_2 P_2$, with P_i the protons momenta. This represents a short distance interaction, that can be studied pertubatively and it is independent on the external hadron; short-distance interactions *factorize* from the long-distance one, which are encoded into the parton distribution functions (PDFs) [130]. These objects have a non-perturbative nature, and they take into account the structure of the hadrons. PDFs are interpreted as the probability that a parton inside a proton carry a certain fraction of the total momentum.

Starting from the Leading Order (LO) cross section, the factorization theorem states that

$$\sigma_{\rm LO}(pp \to gg \to H_1 H_2) = \int_0^1 dx_1 dx_2 f_g(x_1, \mu_F) f_g(x_2, \mu_F) \hat{\sigma}_{\rm LO}(g(p_1)g(p_2) \to H_1 H_2), \tag{1.27}$$

where $f_g(x_i, \mu_F)$ are the PDFs for the gluons, x_i is the fraction of the i proton momentum, μ_F is the *factorization scale* and $\hat{\sigma}$ is the partonic cross sections. μ_F is the scale down to which the factorization theorem holds. This expression can be written in a simpler way: at the LHC the scattering is studied in the center-of-mass frame of the colliding protons $\sqrt{s}$; the production of the two Higgs bosons starts above the production threshold $\hat{s} = (m_{H_1} + m_{H_2})^2$; putting together these consideration, the LO cross section becomes

$$\begin{gathered}\sigma_{\rm LO}(pp \to gg \to H_1 H_2) = \int_{\tau_0}^1 d\tau \frac{d\mathcal{L}^{gg}}{d\tau} \hat{\sigma}(\hat{s})|_{\hat{s}=\tau s}, \\ \frac{d\mathcal{L}^{gg}}{d\tau} = \int_\tau^1 \frac{dx}{x} f_g(x, \mu_F) f_g\left(\frac{\tau}{x}, \mu_F\right), \qquad \tau = \frac{\hat{s}}{s}, \qquad \tau_0 = \frac{(m_{H_1} + m_{H_2})^2}{s},\end{gathered} \tag{1.28}$$

where $\frac{d\mathcal{L}^{gg}}{d\tau}$ is the gluon luminosity.

The PDFs are determined by experimental fits of data obtained from deep inelastic scattering processes. The pure theoretical dependent part is the partonic cross section $\hat{\sigma}$. The perturbative QCD approach relates it with the square of the scattering amplitude integrated over the phase space at a fixed order:

$$\hat{\sigma}_{\rm LO}(\hat{s}) = \int d{\rm PS}_2 \overline{|\mathcal{M}_{\rm LO}|^2}, \tag{1.29}$$

where $d{\rm PS}_2$ is the phase space element and $\mathcal{M}_{\rm LO}$ is the scattering amplitude. The line over the square amplitude stands for the polarization average. The scattering amplitude, namely the sum of the Feynman diagrams [131], can be build from the knowledge of the Lagrangian, that introduce into the game a dependence on the theory.

Since in both the 2HDM and SM there are no interaction verteces between Higgs and gluons, the amplitude of $gg \to H_1 H_2$ is loop induced already at the LO. The bulk of the amplitude is carried by the top-quark loop, due to the Yukawa interaction that enhances the heavy quark contributions. This lead us to consider only the top loops. Notice that at LO[4], there is an additional threshold: $\hat{s} = 4m_t^2$. This corresponds to the $t\bar{t}$ production threshold.

[4]Of course, this threshold occurs at every perturbative order, but sbeyond LO, other thresholds arises. For the gluon rescattering diagrams at NLO, an additional threshold starts at $\sqrt{\hat{s}} = 0$ GeV, which leads to infrared singularities. This structure will be discussed in Chapter 3.

At Next-to-Leading Order (NLO), the calculation of two-loop amplitude is required; in addition, one-loop diagrams with one radiating parton have to be considered as well. The latter belong to three new QCD channels with different initial states: the quark-antiquark $q\bar{q}$, the quark-gluon qg and the gluon-gluon gg initial states. The NLO partonic cross section can be written as

$$\begin{aligned} \Delta\hat{\sigma}_{\text{NLO}} &= \Delta\hat{\sigma}_{\text{virt}} + \Delta\hat{\sigma}_{q\bar{q}} + \Delta\hat{\sigma}_{qg} + \Delta\hat{\sigma}_{gg} \\ \Delta\hat{\sigma}_{\text{virt}} &= \int d\text{PS}_2 \overline{|2\mathcal{M}^*_{\text{LO}}\mathcal{M}_{\text{virt}}|}, \\ \Delta\hat{\sigma}_{ij} &= \int d\text{PS}_3 \overline{|\mathcal{M}_{ij}|^2}, \end{aligned} \tag{1.30}$$

where $\mathcal{M}_{\text{virt}}$ is the *virtual amplitude* containing the two-loop diagrams, and $\mathcal{M}_{ij}$ are the contributions of the ij initial state, called *real corrections*.

1.5.1 Divergences and their treatment

In general, higher order corrections to an observable introduce divergences. This is a general feature of the perturbative expansion of a quantum field theory. The most recognizable source of divergences are the loop corrections, which are related to the integration over the so-called *loop momentum*. An example of divergent Feynman integral is the so-called *massless tadpole*:

$$\int_{\mathbb{M}} \frac{d^4k}{(2\pi)^4} \frac{1}{(k^2)^2}, \tag{1.31}$$

where k^μ is the loop momenta. Integrating over the time component and setting two cut-offs λ and Λ:

$$\int_{\mathbb{M}} \frac{d^4k}{(2\pi)^4} \frac{1}{(k^2)^2} \propto \int_\lambda^\Lambda \frac{d|\mathbf{k}|}{|\mathbf{k}|} = \log\frac{\Lambda}{\lambda}. \tag{1.32}$$

This integral is singular in both limits $\Lambda \to \infty$ and $\lambda \to 0$. The first is called *ultraviolet* (UV) *divergence*, arising at high values of the module of the loop momentum, and they comes purely from the loop integration. The latter is an *infrared* (IR) *divergence* , occuring in the small momentum region, and can occur even at tree level with the phase space integration. A typical loop source of infrared divergence comes from a massless propagator connecting two external propagator that becomes soft. However, a physical observable must be UV and IR finite: the divergences have to be isolated and canceled.

As we are interested in the NLO QCD corrections to Higgs-pair production, the treatment of the UV and IR divergences has to be discussed. The LO of the process we are considering, even though formed by one-loop diagrams, is screened from UV divergences because of the gauge invariance; in addition, since no massless propagators occur in the loops, IR divergences do not show up.

At NLO, UV and IR divergences appear. A *regularization scheme* is needed in order to isolate them. In this calculation, *dimensional regularization* is used [70]: the idea is to treat the amplitude as analytic function of the space-time dimension $d = 4 - 2\epsilon$:

$$\int_{\mathbb{M}} \frac{d^4k}{(2\pi)^4} \to (\mu^2)^{\frac{4-d}{2}} \int_{\mathbb{M}} \frac{d^dk}{(2\pi)^d} \tag{1.33}$$

where the *'t Hooft scale* μ has the role of preserving the mass dimensionality of the amplitude. The regularisation procedure makes the UV and IR divergences be poles in the ϵ analytic expansion around $\epsilon = 0$ (namely the 4-dimensions limit). At NLO, the analytic structure manifests poles up to second order.

The procedure of canceling the UV divergences is called *renormalisation*. Interpreting the fields, coupling and parameters of the Lagrangian to be *bare* quantities, they develop divergences at higher orders. In order to obtain physically meaningful predictions, they have to be expressed in terms of the physical quantities (i.e. the *renormalized* ones). Their higher order terms entering in the perturbative expansion are the *counterterms*. The choice of the counterterms fixes the *renormalisation scheme*.

The only constraint is that the counterterms have to cancel the UV poles coming from the NLO amplitude. The renormalisation scheme influences the finite part of the amplitude, which introduces a renormalisation scheme dependence order-by-order in the amplitude. However, this dependence completely disappears if the entire perturbation series is considered. More details on the specific renormalisation scheme we have chosen can be found in Chapter 3.

The IR divergences are treated in a different way. The Kinoshita-Lee-Nauenber (KLN) theorem [132, 133] ensure the IR safety of a sufficiently inclusive observable. The inclusiveness needed for the Higgs-pair production indicates that in addiction to the virtual amplitude, which has the same final state, additional contributions have to be considered: these are the real corrections. Since they develop soft and collinear divergences, they can be combined to the virtual contribution to obtain an IR safe observable.

Since the calculation will be performed numerically, the cancellation of the IR divergences is more involved, because it takes place between terms that are integrated over different final states: this would introduce strong numerical instabilities in the single integrations. There are different ways to overcome this issue, represented by different *subtraction techniques* [51, 52, 134–137]. They rely on the introduction of an auxiliary differential cross section $d\sigma_A$ with the same IR pole structure of the process. This term will be added and subtracted at the level of differential cross section in the following way:

$$\Delta\hat{\sigma}_{\rm NLO} = \int d{\rm PS}_2 \left[\overline{|2\mathcal{M}^*_{\rm LO}\mathcal{M}_{\rm virt}|} + \int dPS_1 d\sigma_A\right] + \int d{\rm PS}_3 \left[\overline{|\mathcal{M}_{q\bar{q}}|^2} + \overline{|\mathcal{M}_{qg}|^2} + \overline{|\mathcal{M}_{gg}|^2} - d\sigma_A\right] \tag{1.34}$$

Each separeted integral is now finite and the numerical integration will be stable. For this particular process, the auxiliary term has been build from the knowledge of the heavy-quark behaviour of the process. Further details will be presented in Chapter 3.

The last sources of divergences come from the collinear initial-state singularities, for which the KLN theorem does not hold, since one does not sum over the initial states. They can be absorbed by a renormalisation of the PDFs, meaning that the behaviour of the collinear emission of a parton by the initial state is a non-perturbative process that has been removed by the hard scattering.

1.6 Present status

The Higgs-pair production within the SM has been investigated in many approximations, valid for different phase space regions. There are three phase space region of interest: the low energy region ($\hat{s} \lesssim 4m_t^2$), the $t\bar{t}$ threshold region ($\hat{s} \approx 4m_t^2$) and the high energy region ($\hat{s} \gg 4m_t^2$). Moreover, two independent NLO SM Higgs-pair production with full top-mass dependence calculations are available in literature.

1.6.1 Low energy region

In the low energy region, the heavy top-quark limit (HTL) is valid. Many works have investigated this region up to N^{3}LO. The first result is the *Born-improved* NLO calculation [32]: it consists in the LO with full top-mass dependence calculation in addition with the HTL NLO contribution. In this way, virtual and real corrections can be built from the effective Higgs-gluon interaction arising from the integration of the top mass, leading to a one-loop virtual amplitude and a tree level real corrections. The differential K-factor, defined as

$$K = \frac{d\sigma_{\rm NLO}}{d\sigma_{\rm LO}}, \tag{1.35}$$

found in this approximation ranges between 1.9 and 2 with scale uncertainties of 20%.

A mass refinement of the Born-improved approximation leads to the *full-theory approximation* [24, 33], obtained by considering the mass dependent NLO real contributions. They consist in the inclusion of complete one-loop five points matrix elements, contribution to the real corrections. The introduction of these top-mass effects yields to a -10% with respect to the previous approximation and a decrease of the scale uncertainties of the 5%.

Going further in this direction, a NNLO Born-improved has been included in the previous calculations [34, 35]. This includes virtual two-loop effective amplitude and soft contributions with five and six points one-loop and tree level matrix elements. The inclusion of the HTL NNLO effects to the full-theory approximation leads to an increasing of the 20% of the K-factor. The scale uncertainties reduce to ±13%. The calculation including Next-to-Leading-Log (NNLL) decrease even more the scale uncertainties, achieving a ±11% [36, 37]. All the uncertainties have been estimated by varying the factorization and renormalisation scales a factor 2 up and down from $\sqrt{\hat{s}}/2$. Recently a complete HTL N^{3}LO calculation has been performed [38]. This refinements lead to an additional correction of the 3% to the NNLO cross section, and to scale uncertainties of about 2%.

A first attempt to include finite top-mass effects as terms of an expansion on the $1/m_t^2$ parameter has been done at NLO and NNLO. The NLO calculation considers the expansion of the integra*ls*, making use of the optical theorem and perfoming the $1/m_t^2$ expansion [39]. At NNLO level, genuine top-mass expansion terms are included into the integra*nds*, and the amplitude coefficients have been evaluated analytically. The most recent works in this direction have been included 8 expansion terms for the box and 5 for the triangle contributions, leading to a good convergence to higher Higgs-pair invariant mass values [40, 41]. The top-mass effects amount to about 10% at NLO and to 5% at NNLO. An N^{3}LO mass refinement have been introduced by the one-particle-reductible contributions, including diagrams involving two-loop effective verteces known from the previous expansion order.

1.6.2 Threshold region

Recently, in Refs. [42, 43], a method to incorporate the large non-analytic behaviour of the differential cross section around the threshold region into the HTL expansion of the NLO differential cross section has been proposed. This strategy rely on the Padé approximant ansatz, which reads

$$[n/m](\omega) = \frac{a_0 + a_1\omega + \cdots + a_n\omega^n}{1 + b_1\omega + \cdots + a_m\omega^m}, \qquad \frac{\hat{s}}{4m_t^2} = \frac{4\omega}{(1+\omega)^2}. \tag{1.36}$$

where the coefficients can be determined from the non-analytical part of the cross section for $\hat{s} \approx 4m_t^2$. This method can be adopted for the Higgs-pair production process within the 2HDM too, where the two final state Higgs particles may have different masses.

This method, applied to the SM, yields reliable results up to NNLO cross section for $\sqrt{\hat{s}} \lesssim 450$ GeV and provides a useful strategy to determine the top-mass effects at NNLO, currently far from a computationally viable full top-mass calculation.

1.6.3 High energy region

The high energy energy region can be explored by performing an expansion for $m_t^2 \ll s, |t|$ and $m_H = 0$. This approach has been explored at NLO SM in Refs. [44–46], where other refinements have been considered: 8 additional terms of the top mass $m_t^2/\hat{s}$ expansion, and 2 terms of the finite Higgs mass expansion $m_H^2/m_t^2 \approx 0.13$. The form factors obtained in such approximation are completely analytical, based on the master integral decomposition and their analytical evaluation. It is an extremely useful result that can be exploited in cross checks with full top-mass dependence form factors. The radius of the convergence of the expansion have been increased further by introducing Padé approximants for the master integrals.

The differential distribution obtained with this approach have been cross-checked with the full NLO calculation, resulting into a full agreement down to 500 GeV.

1.6.4 p_T expansion and full top-mass NLO contribution

A promising method has been investigated in Ref. [138] where an expansion in terms of small transverse momentum $p_{\mathrm{T}}^2 \sim 0$ has been performed. It has a very wide range of validity, that covers the low energy and threshold regions, arriving up to $\sqrt{\hat{s}} \lesssim 750$ GeV, giving an approximation at NLO SM better than per-mille.

At last, a NLO SM Higgs-pair production calculation with full top-mass dependence has been carried out in Refs. [47, 139]. The form factors have been decomposed in terms of the master integral by means of the IBP reduction and the differential cross section has been evaluated numerically, since not all the master integrals found were known analytically. The bottleneck of this calculation was represented by the IBP reduction. A simplification introduced to facilitate the integral reduction was fixing the numerical value for the ratio m_H/m_t. The masses have been fixed for $m_t = 173$ GeV and $m_H = 125$ GeV. The complete result leads to a NLO differential K-factor of 20-30% smaller w.r.t. the Born-improved method.

The other NLO SM Higgs-pair production via gluon fusion cross section calculation [53, 54] will be exhaustively discussed in Chapter 5 of this thesis, since it represents the major outcome of this work. As a remarkable difference from the first calculation, our work treats the top mass and the Higgs masses as independent variables: this allowed us to estimate the uncertainties related with the top-mass renormalisation scale and scheme [55].

1.7 Topic of this thesis

We present our NLO QCD Higgs-pair production via gluon fusion calculation with full top-mass dependence. Our procedure is meant to be as general as possible, including the possibility of applying it to all possible 2HDM Higgs-pair final states.

The main difference between the two models applied to the process in exam is the presence of Higgs bosons of different mass. This introduce more complexity in the calculation, since the two-loop Feynman integrals contributing to the form factors will depend on five mass scales and (two kinematic invariants, two Higgs bosons and the top-quark mass). In addition, they are two-loop integrals, for which no automated strategy have been developed so far.

However, building a general framework generalizing the SM calculation can be done revisiting the Feynman rules of the 2HDM and rescaling them with respect to the SM couplings. For the neutral scalar Higgs bosons, this rescaling turns into a simple factor, depending on the Higgs boson and the model type, in particular of the angles α and β. It can be represented schematically as

$$-i\frac{m_t}{v} \to -i\frac{m_t}{v}Y_j, \tag{1.37}$$

where j refers to the light Higgs H_1 or the heavy Higgs H_2. For the charged scalars $H^\pm$ and the pseudoscalar A, there is an additional γ^5, responsable of the eventual CP violation, which does not change the prescription we use:

$$-i\frac{m_t}{v} \to -\frac{m_t}{v}\gamma^5 Y_j. \tag{1.38}$$

The introduction of pseudoscalars requires a prescription to treat the γ^5, since we use dimensional regularisation and it is impossible to define a $d-$dimensional γ^5 [140]. In particular, it is not possible to have both

$$\{\gamma^5, \gamma^\mu\} = 0, \qquad \mu = \{1, \cdots, d\}, \tag{1.39}$$

and

$$\mathrm{Tr}\left[\gamma^5\gamma^\mu\gamma^\nu\gamma^\rho\gamma^\sigma\right] = 4!\epsilon^{\mu\nu\rho\sigma}. \tag{1.40}$$

A convenient choice for dealing with the AA final state is using the *naive dimensional regularization*: no definition of γ^5 will be set and both the relations in Eq. (1.39) and Eq. (1.40). The Dirac traces will be expressed in terms of δ and ϵ tensors pretending that they are four dimensionals, and at the end the result are interpreted in d dimensions. For mixed scalar-pseudoscalar cases, the presence of the ABJ anomaly [141, 142] makes the previous choice unconstistent. The proper way to treat the γ^5 has been proposed by 't Hooft and Veltmann [70], and systematized by Breitenlohner and Maison [143]. They define the $d-$dimension γ^5 from Eq. (1.40), leading to

$$\gamma^5 = \frac{1}{4!}\epsilon^{\mu\nu\rho\sigma}\gamma_\mu\gamma_\nu\gamma_\rho\gamma_\sigma, \tag{1.41}$$

and Eq. (1.39) to be

$$\begin{aligned} \{\gamma^5, \gamma^\mu\} &= 0, \qquad \mu = \{1, \cdots, 4\}, \\ [\gamma^5, \gamma^\mu] &= 0, \qquad \mu = \{5, \cdots, d\}, \end{aligned} \tag{1.42}$$

such that the axial term does not vanish.

Even if different Higgs-pair final states will lead to extremely variegate phenomenology, at the level of the calculation they can be treated within the same framework, as we will explain in details into Chapter 2 and 3. Moreover, since the charged scalar and the pseudoscalar Higgs bosons will introduce unnecessary complication into the calculation, we will restrain ourself in presenting the neutral scalars final state, meaning $gg \to H_1 H_2$ at partonic level.

Briefly, our strategy can be summarize as follows:

- Generate the LO and NLO amplitude;
- Perform the projection into form factors and the numerator algebra;
- Isolate the UV/IR divergences by means of the end-point subtraction;
- Take care of the IR divergences with a dedicated subtraction term;
- Renormalize the form factors to obtain UV finite virtual amplitude;
- Integrate over the phase space;
- Evaluate the square amplitude of the real corrections and integrate them over the phase space;
- IR singularities from virtual corrections cancels against the real corrections ones;
- Initial state singularities are absorbed from the PDFs.

All the integration involved in this calculation will be performed numerically, using a Monte Carlo integration. Its details will be discussed into Chapter 4. The phenomenology analysis will be presented in Chapter 5.

Chapter 2

Leading Order Cross Section

The LO cross section represents the first step of this calculation. Even though is not the main topic of this thesis, it is essential to consider the LO matrix elements not only to settle the framework, but as well because the NLO contribution is defined as the interference between the one-loop and two-loop form factors; moreover, the LO amplitude will take part to the renormalisation of the NLO amplitude and to the subtraction scheme for the IR divergences. It is a very old calculation [115], but it is nonetheless instructive to present the whole calculation together with its heavy quark limit.

In this Chapter, the complete LO Higgs-pair production cross section is presented. The analytical expression of the heavy quark limit amplitude will be presented, as well as the gluon-Higgs effective verteces [32]. At last, the LO form factors will be expressed in terms of scalar Feynman integrals after having applied the Passarino-Veltmann reduction [144]. It is important to underline that such integrals have to be known up to the order $O(\epsilon^2)$, as it is required by the NLO UV counterterms. The LO form factors will be implemented into a FORTRAN routine code, ready to be used in the context of the NLO calculation.

2.1 Preliminaries: Single-Higgs production with one off-shell gluon

The building block for our calculation is the single-Higgs production via gluon fusion amplitude:

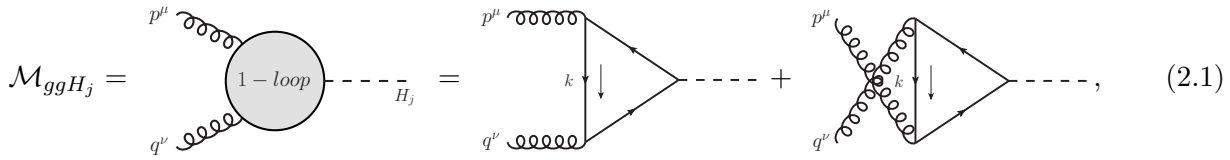

(2.1)

Considering the top-quark contribution only, the amplitude $\mathcal{M}_{ggH_j}$ can be written in terms of a single diagram:

$$\mathcal{M}_{ggH_j} = \epsilon_\mu(p)\epsilon_\nu(q)(1)\mathcal{M}^{\mu\nu,ab}_{ggH_j}(p,q), \tag{2.2}$$

where $\mathcal{M}^{\mu\nu,ab}_{ggH_j}(p,q)$ is the amputated amplitude. Let us stress that the first argument of $\mathcal{M}^{\mu\nu,ab}_{ggH_j}(p,q)$ is an on-shell momentum and the second is an off-shell one. The Feynman rules for this process are presented in Appendix I. The Casimir operator is $\mathrm{Tr}[T^aT^b] = \frac{1}{2}\delta^{ab}$. The SM rules can be recovered by setting $\lambda_{111} = m_H$ and $Y_1 = 1$, $\lambda_{ijk} = 0$ and $Y_j = 0$ for $i,j,k \geq 2$. At the end of this calculation, we will find an effective Feynman rule about the interaction between two gluons and a Higgs boson. With these rules, the gluon fusion amplitudes becomes

$$\begin{aligned}\mathcal{M}^{\mu\nu,ab}_{ggH_j}(p,q) = (-)(2)\frac{i}{(4\pi)^2}(4\pi\mu^2)^{2-\frac{d}{2}}\times \\ \int_k \mathrm{Tr}\left[(-ig_s\gamma_\mu T^a)\frac{i(\not{k}-\not{p}+m_t)}{(k-p)^2-m_t^2}\left(-i\frac{m_t}{v}Y_j\right)\frac{i(\not{k}+\not{q}+m_t)}{(k+q)^2-m_t^2}(-ig_s\gamma_\nu T^b)\frac{i(\not{k}+m_t)}{k^2-m_t^2}\right],\end{aligned} \tag{2.3}$$

where[1] $\int_k = \int \frac{d^dk}{i\pi^{\frac{d}{2}}}$ and the factor 2 comes from the exchange of the incoming gluons. Through simple algebra passages, and by considering the amputated diagram, it follows

$$\begin{aligned}\mathcal{M}^{\mu\nu,ab}_{ggH_j}(p,q) &= -iY_j\frac{m_t}{v}\frac{g_s^2}{(4\pi)^2}2\mathrm{Tr}[T^aT^b](4\pi\mu^2)^{2-\frac{d}{2}}\int_k \frac{\mathrm{Tr}\left[\gamma^\mu(\not{k}-\not{p}+m_t)(\not{k}+\not{q}+m_t)\gamma^\nu(\not{k}+m_t)\right]}{[k^2-m_t^2][(k-p)^2-m_t^2][(k+q)^2-m_t^2]}\\ &= -iY_j\left(\frac{\alpha_s m_t}{\pi v}\right)\delta^{ab}(4\pi\mu^2)^{2-\frac{d}{2}}\int_k\frac{\mathcal{N}^{\mu\nu}}{D_0D_1D_2},\\ \mathcal{N}^{\mu\nu} &= \frac{1}{4}\mathrm{Tr}[\gamma^\mu(\not{k}-\not{p}+m_t)(\not{k}+\not{q}+m_t)\gamma^\nu(\not{k}+m_t)].\end{aligned} \tag{2.4}$$

For later purposes, we consider the gluon with momenta q^μ to be off-shell, so that $q^2 \neq 0$, while $p^2 = 0$ and $(p+q)^2 = \hat{s}$. The Higgs boson is produced off-shell.

2.1.1 Projection onto the tensor basis: form factors

This rank-2 tensor can be written as

$$T^{\mu\nu}(p,q) = a_{00}g^{\mu\nu} + a_{pp}p^\mu p^\nu + a_{pq}p^\mu q^\nu + a_{qp}q^\mu p^\nu + a_{qq}q^\mu q^\nu, \tag{2.5}$$

and imposing the transversality of the external gluons:

$$\begin{cases} p_\mu T^{\mu\nu}(p,q) = 0 \\ q_\nu T^{\mu\nu}(p,q) = 0 \end{cases} \quad \text{such that} \quad \epsilon_h^\mu(p)p_\mu = 0, \quad \epsilon_h^\nu(q)q_\nu = 0 \quad \text{and} \quad p^2 = 0, \tag{2.6}$$

we find that

$$T^{\mu\nu}(p,q) = a_{00}\left(g^{\mu\nu} - \frac{q^\mu p^\nu}{(p\cdot q)}\right) = a_{00}T_1^{\mu\nu}. \tag{2.7}$$

Through $T_1^{\mu\nu}$, it is possible to define the projector

$$P^{\mu\nu} = \frac{T_1^{\mu\nu}}{(d-2)}, \tag{2.8}$$

such that the amplitude becomes

$$\begin{aligned}\mathcal{M}^{\mu\nu,ab}_{ggH_j}(p,q) &= -i\left(\frac{\alpha_s m_t}{\pi v}\right)Y_j\delta^{ab}\left(\frac{4\pi\mu^2}{m_t^2}\right)^\epsilon\Gamma(1+\epsilon)T_1^{\mu\nu}\mathcal{A}_1^{(0)},\\ \mathcal{A}_1^{(0)} &= C_\epsilon P_{\mu\nu}\int_k\frac{\mathcal{N}^{\mu\nu}}{D_0D_1D_2},\end{aligned} \tag{2.9}$$

where we introduce the form factor $\mathcal{A}_1^{(0)}$, and the normalization $C_\epsilon = \frac{(m_t^2)^{-\epsilon}}{\Gamma(1+\epsilon)}$.

Coming back to the expression of the amplitude, the numerator algebra yields:

$$P_{\mu\nu}\mathcal{N}^{\mu\nu} = \frac{m_t}{(d-2)}\left(-(d-5)k^2 + (d-1)m_t^2 - (d-2)(p\cdot q) - \frac{4(k\cdot p)(k\cdot q)}{p\cdot q}\right), \tag{2.10}$$

hence the form factor becomes

$$\begin{aligned}\mathcal{A}_1^{(0)} = C_\epsilon\frac{m_t}{(d-2)}\times\Bigg[&-(d-5)\int_k\frac{k^2}{D_0D_1D_2}\\ &+[(d-1)m_t^2-(d-2)(p\cdot q)]\int_k\frac{1}{D_0D_1D_2} - \frac{4}{(p\cdot q)}\int_k\frac{(k\cdot p)(k\cdot q)}{D_0D_1D_2}\Bigg].\end{aligned} \tag{2.11}$$

[1]Every loop contributes with the following factor: $\mu^{4-d}\int\frac{d^dk}{(2\pi)^d} = \frac{i}{(4\pi)^{d/2}}\mu^{4-d}\int\frac{d^dk}{i\pi^{d/2}} = \frac{i}{(4\pi)^2}(4\pi\mu^2)^{2-d/2}\int\frac{d^dk}{i\pi^{d/2}} = \frac{i}{(4\pi)^2}(4\pi\mu^2)^{2-d/2}\int_k$.

Using the Passarino-Veltmann reduction (see Appendix D), and defining the scalar integrals

$$B_0(0,\overline{m}_t^2) = \int_k \frac{1}{D_0 D_1}, \qquad B_0(q^2,\overline{m}_t^2) = \int_k \frac{1}{D_0 D_2}, \qquad B_0(m_{H_j}^2,\overline{m}_t^2) = \int_k \frac{1}{D_1 D_2}$$
$$C_0(0,q^2,m_{H_j}^2;\overline{m}_t^2) = \int_k \frac{1}{D_0 D_1 D_2} \tag{2.12}$$

we can express all the integrals appearing in Eq. (2.11) as scalar integrals:

$$\begin{aligned}\int_k \frac{k^2}{D_0 D_1 D_2} &= m_t^2 C_0(0,q^2,m_{H_j}^2;\overline{m}_t^2) + B_0(m_{H_j}^2,\overline{m}_t^2),\\ \int_k \frac{(k\cdot p)(k\cdot q)}{D_0 D_1 D_2} &= \frac{1}{4}\left[q^2 B_0(q^2;\overline{m}_t^2) - [q^2-(p\cdot q)]B_0(m_{H_j}^2;\overline{m}_t^2)\right],\end{aligned} \tag{2.13}$$

and replacing these integrals in the amplitude

$$\begin{aligned}\mathcal{A}_1^{(0)} = -\frac{C_\epsilon m_t}{(d-2)}\times\Bigg[&\frac{(d-4)(p\cdot q)-q^2}{(p\cdot q)}B_0(m_{H_j}^2,\overline{m}_t^2)\\ &+[(d-2)(p\cdot q)-4m_t^2]C_0(0,q^2,m_{H_j}^2;\overline{m}_t^2)+\frac{q^2}{(p\cdot q)}B_0(q^2;\overline{m}_t^2)\Bigg].\end{aligned} \tag{2.14}$$

2.1.2 Analytic amplitude of $gg^* \to H$

Let us replace the analytical value of the scalar integrals (see Appendix D):

$$\begin{aligned}B_0(m_{H_i}^2,\overline{m}_t^2) &= \frac{\Gamma(1+\epsilon)}{(m_t^2)^\epsilon}\left[\frac{1}{\epsilon}+2-2g(\tau_j)\right],\\ B_0(q^2,\overline{m}_t^2) &= \frac{\Gamma(1+\epsilon)}{(m_t^2)^\epsilon}\left[\frac{1}{\epsilon}+2-2g(\lambda)\right],\\ C_0(0,q^2,m_H^2;\overline{m}_t^2) &= \frac{\Gamma(1+\epsilon)}{(m_t^2)^{1+\epsilon}}\left[\frac{\tau\lambda}{2}\frac{f(\tau)-f(\lambda)}{\tau-\lambda}\right],\\ \tau = \frac{4m_t^2}{(p+q)^2} = \frac{4m_t^2}{\hat{s}}, &\qquad \lambda = \frac{4m_t^2}{q^2}, \qquad \epsilon = \frac{4-d}{2}.\end{aligned} \tag{2.15}$$

Hence, replacing these analytical values into the form factor $\mathcal{A}_1^{(0)}$, we arrive at the expression

$$\begin{aligned}\mathcal{A}_1^{(0)} &= -\frac{m_t}{2(1-\epsilon)}\Bigg\{-\frac{2\epsilon(p\cdot q)+q^2}{(p\cdot q)}\left(\frac{1}{\epsilon}+2-2g(\tau)\right)\\ &\quad+\left(\frac{(1-\epsilon)(p\cdot q)}{m_t^2}-2\right)\left[\tau\lambda\frac{f(\tau)-f(\lambda)}{\tau-\lambda}\right]+\frac{q^2}{(p\cdot q)}\left(\frac{1}{\epsilon}+2-2g(\lambda)\right)\Bigg\}\\ &= \frac{m_t}{(1-\epsilon)}\Bigg\{1-\frac{q^2}{(p\cdot q)}(g(\tau)-g(\lambda))-\left(\frac{(p\cdot q)}{2m_t^2}-1\right)\frac{\tau\lambda}{\tau-\lambda}(f(\tau)-f(\lambda))\\ &\quad+\epsilon\left[\frac{(p\cdot q)}{2m_t^2}\frac{\tau\lambda}{\tau-\lambda}(f(\tau)-f(\lambda))-2(g(\tau)-1)\right]\Bigg\}.\end{aligned} \tag{2.16}$$

Since the ϵ pole has been canceled through the calculation, this expression is finite. In the limit $\epsilon \to 0$, the form factor becomes:

$$\begin{aligned}\mathcal{A}_1^{(0)} &= m_t\left\{1-\frac{q^2}{(p\cdot q)}[g(\tau)-g(\lambda)]-\left[\frac{(p\cdot q)}{2m_t^2}-1\right]\frac{\tau\lambda}{\tau-\lambda}[f(\tau)-f(\lambda)]\right\}\\ &= 2m_t\left\{\frac{1}{2}+\frac{\tau}{\tau-\lambda}[g(\tau)-g(\lambda)]+\frac{1}{2}\left[1+\frac{\tau\lambda}{\tau-\lambda}\right][f(\tau)-f(\lambda)]\right\}.\end{aligned} \tag{2.17}$$

Using the identity:

$$2m_t = -\frac{(p\cdot q)}{m_t}\left(\frac{\tau\lambda}{\tau-\lambda}\right), \tag{2.18}$$

we can simplify the expression more, such that the form factor becomes

$$\begin{aligned}\mathcal{A}_1^{(0)} &= -\frac{(p\cdot q)}{m_t}\left\{\frac{\tau\lambda}{2(\tau-\lambda)}+\frac{\tau^2\lambda}{(\tau-\lambda)^2}\left[g(\tau)-g(\lambda)\right]+\frac{\tau^2\lambda^2}{2(\tau-\lambda)^2}[f(\tau)-f(\lambda)]+\frac{\tau\lambda}{2(\tau-\lambda)}[f(\tau)-f(\lambda)]\right\}\\ &= -\frac{(p\cdot q)}{m_t}\mathcal{I}(\tau,\lambda)\end{aligned} \tag{2.19}$$

and the total amplitude becomes

$$\begin{aligned}\mathcal{M}_{ggH_j}^{\mu\nu,ab}(p,q) &= -i\left(\frac{\alpha_s m_t}{\pi v}\right)Y_j\delta^{ab}\left(\frac{4\pi\mu^2}{m_t^2}\right)^{\epsilon}\Gamma(1+\epsilon)T_1^{\mu\nu}\mathcal{A}_1^{(0)}(p,q)\\ &= i\left(\frac{\alpha_s}{\pi v}\right)Y_j\delta^{ab}\left(\frac{4\pi\mu^2}{m_t^2}\right)^{\epsilon}\Gamma(1+\epsilon)\mathcal{I}(\tau,\lambda)\left[(p\cdot q)g^{\mu\nu}-q^\mu p^\nu\right].\end{aligned} \tag{2.20}$$

This form factor is independent on the neutral scalar Higgs boson taken into account: this fact will be useful later when we will build the amplitude for the Higgs-pair production matrix elements.

The heavy top-quark limit and the gluon in the on-shell limit will define a gluon-Higgs effective vertex. It can be done by taking the simultaneous limits $\lambda\to\infty$ and $\tau\to 0$. Since the off-shellness of the incoming gluon and the leading dependence on the top mass are encoded into the $\mathcal{I}(\tau,\lambda)$ factor, it will be the only term affected by this limit:

$$\mathcal{M}_{ggH_j}^{\mu\nu,ab}(p,q)\xrightarrow{\text{HTL}} -i\left(\frac{\alpha_s}{3\pi v}\right)Y_j\delta^{ab}\left(\frac{4\pi\mu^2}{m_t^2}\right)^{\epsilon}\Gamma(1+\epsilon)\left[(p\cdot q)g^{\mu\nu}-q^\mu p^\nu\right]. \tag{2.21}$$

2.2 Leading-order amplitude for H_1H_2 production

The LO amplitude for the Higgs-pair production channels gets contributions from one-loop diagrams. For the moment, we will only consider the case where the Higgs into the final state are CP-even; the

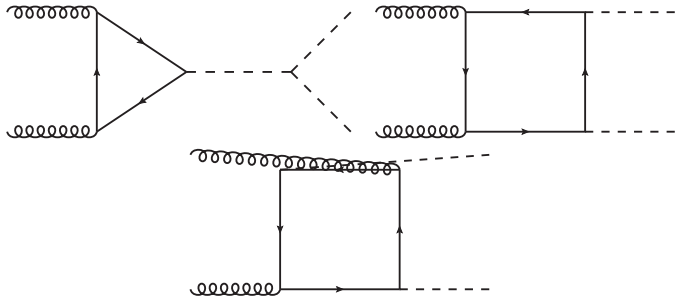

Figure 2.1: *Sample of the Feynman diagrams contributing to the LO.*

same calculation strategy can be exploited for the CP-odd Higgs final state.

The process under investigation is $gg\to H_1H_2$. The LO amplitude $\mathcal{M}_{LO}$ can be written as

$$\mathcal{M}_{\text{LO}} = \epsilon_\mu(p_1)\epsilon_\nu(p_2)(1)(1)(\mathcal{M}_\Delta^{\mu\nu,ab}+\mathcal{M}_\square^{\mu\nu,ab}), \tag{2.22}$$

where we have separated the two gauge-invariant subset of diagrams.

2.2.1 Triangle contribution

The triangle-like contribution $\mathcal{M}_\Delta^{\mu\nu}$ can be built by composing the $gg^*\to H_j$ matrix element with a tree-level factor as follows:

$$\begin{aligned}\mathcal{M}_\Delta^{\mu\nu,ab} &= \sum_j^3 \mathcal{M}_{ggH_j}^{\mu\nu,ab}(p_1,p_2)\Big|_{p_2^2=0}\left(\frac{i}{(p_1+p_2)^2-m_{H_j}^2-im_{H_j}\Gamma(m_{H_j}^2)}\right)\left(-i3\frac{\lambda_{j12}}{v}\right)\\ &= \widetilde{F}_\Delta^{(0)}T_1^{\mu\nu},\end{aligned} \tag{2.23}$$

where in the last step, we have defined the triangle form factor $F_\Delta^{(0)}$. Collecting all our expressions, we get

$$\begin{aligned}\widetilde{F}_\Delta^{(0)} &= \frac{i\alpha_s}{(4\pi)}\frac{m_t^2}{v^2}\delta^{ab}\left(\frac{4\pi\mu^2}{m_t^2}\right)^\epsilon \Gamma(1+\epsilon)\widetilde{\mathcal{A}}_1^{(0)},\\ \widetilde{\mathcal{A}}_1^{(0)} &= \sum_j^3 \left(\frac{6Y_j\lambda_{j12}}{\hat{s}-m_{H_j}^2-im_{H_j}\Gamma(m_{H_j}^2)}\right)\frac{\hat{s}}{m_t^2}\,\mathcal{I}(\tau,\infty)\,.\end{aligned} \tag{2.24}$$

The on-shell limit for the $gg^* \to H$ amplitude leads to the following expression:

$$\mathcal{I}(\tau,\infty) = \lim_{\lambda\to\infty}\mathcal{I}(\tau,\lambda) = -\frac{\tau}{2}\left[1-\tau f(\tau)+f(\tau)\right]. \tag{2.25}$$

Since the form factor $\widetilde{F}_\Delta^{(0)}$ has a factorizable dependence from the type of virtual Higgs boson which propagates from the top-loop. This lead to an important factorization:

$$\begin{aligned}\widetilde{F}_\Delta^{(0)} &= C_\Delta F_\Delta^{(0)},\\ C_\Delta &= \sum_j^3 \frac{6Y_j\lambda_{j12}}{\hat{s}-m_{H_j}^2-im_{H_j}\Gamma(m_{H_j}^2)}.\end{aligned} \tag{2.26}$$

The form factor $F_\Delta^{(0)}$ is common to the one of the LO QCD single-Higgs production. This factorization is extremely important: it will turn to be useful later since the same structure of $\widetilde{F}_\Delta^{(0)}$ holds at NLO. Single-Higgs production form factors are already known at NLO, and we can implement them into our calculation as a simple factor.

Heavy top limit

The HTL triangle amplitude can be built as a tree-level amplitude where the vertex contribution is replaced by the ggH_j effective vertex, found in the previous section, leading to

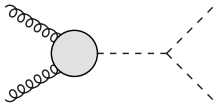

$$= -i\left(\frac{\alpha_s}{3\pi v^2}\right)\delta^{ab}\left(\frac{4\pi\mu^2}{m_t^2}\right)^\epsilon \Gamma(1+\epsilon)\frac{C_\Delta}{2}\left[(p\cdot q)g^{\mu\nu}-q^\mu p^\nu\right]. \tag{2.27}$$

2.2.2 Box diagrams

There are three box diagrams contributing at LO (Fig. 2.2). The corresponding ones with reversed fermion flow, due to the Furry's theorem, contributes with an additional factor 2.

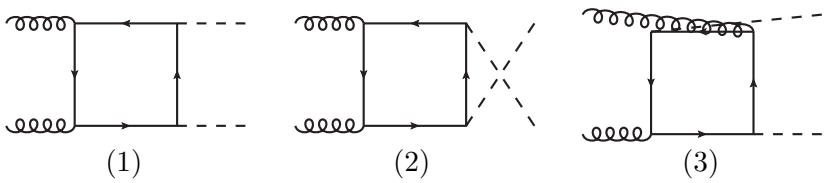

Figure 2.2: *LO box diagrams.*

To approach this calculation, a theoretical common framework can be useful. In general, each of these diagram can be expressed as follows:

$$\begin{aligned}\mathcal{M}_\Box^{\mu\nu,ab} &= -(-ig_s)^2\left(-i\frac{m_t}{v}\right)^2 Y_1Y_2(i)^4\mathrm{Tr}[T^aT^b]\frac{i}{(4\pi)^2}(4\pi\mu^2)^{2-\frac{d}{2}}\int_k \frac{N^{\mu\nu}(k,\mathbf{p})}{D_0D_1D_2D_3}\\ &= -\frac{i\alpha_s}{(4\pi)}\frac{m_t^2}{v^2}Y_1Y_2\mathrm{Tr}[T^aT^b](4\pi\mu^2)^\epsilon\int_k\frac{N^{\mu\nu}(k,\mathbf{p})}{D_0D_1D_2D_3},\end{aligned} \tag{2.28}$$

where $\mathbf{p} = \{p_1, p_2, p_3\}$ and k the loop momenta. Here there is a general tensor $N^{\mu\nu}$ depending on the momenta which is unique for each box diagram. The Feynman parametrization procedure allows one to write an integral of n denominators as a tadpole-like integral:

$$\begin{aligned}\frac{1}{D_0^{a_0}\cdots D_n^{a_n}} &= \frac{\Gamma(a_1+\cdots+a_n)}{\Gamma(a_1)\cdots\Gamma(a_n)}\int_0^1 dx_0 d\mathbf{x}\frac{x_0^{a_0-1}\cdots x_n^{a_n-1}\delta(1-\sum_j x_j)}{[D_0x_0+\cdots+D_nx_n]^{\sum_j a_j}} \\ &= \frac{\Gamma(a_1+\cdots+a_n)}{\Gamma(a_1)\cdots\Gamma(a_n)}\int_{\mathcal{C}} d\mathbf{x}\frac{(1-\sum_j x_j)^{a_0-1}\cdots x_n^{a_n-1}}{[D_0(1-\sum_j x_j)+\cdots+D_nx_n]^{\sum_j a_j}}\end{aligned}, \tag{2.29}$$

$$\mathcal{C} = \left\{\mathbf{x}=(x_1,\ldots,x_n)\in[0,1]^n \mid x_2 < 1-x_1 \wedge x_3 < 1-x_1-x_2 \wedge \cdots \wedge x_n < 1-\sum_{j=1}^{n-1} x_j\right\}.$$

Applying the Feynman parameterization to the box integral, the integrand takes the form:

$$\begin{aligned}\mathcal{M}_{\square}^{\mu\nu,ab} = -\frac{i\alpha_s}{(4\pi)}\frac{m_t^2}{v^2}Y_1Y_2\mathrm{Tr}[T^aT^b](4\pi\mu^2)^{2-\frac{d}{2}}\times \\ \times\,\Gamma(4)\int_{\mathcal{C}} d\mathbf{x}\int_k \frac{N^{\mu\nu}(k,\mathbf{p})}{[D_0(1-x_1-x_2-x_3)+D_1x_1+D_2x_2+D_3x_3]^4},\end{aligned} \tag{2.30}$$

where $\mathcal{C} = \{\mathbf{x}=(x_1,x_2,x_3)\in[0,1]\times[0,1]\times[0,1] \mid x_2 < 1-x_1 \wedge x_3 < 1-x_1-x_2\}$. All the internal lines are massive, and the Feynman parametrization yields a "tadpole-like" denominator

$$\begin{aligned}\mathcal{M}_{\square}^{\mu\nu,ab} &= -\frac{i\alpha_s}{(4\pi)}\frac{m_t^2}{v^2}Y_1Y_2\mathrm{Tr}[T^aT^b](4\pi\mu^2)^{2-\frac{d}{2}}\Gamma(4)\int_{\mathcal{C}} d\mathbf{x}\int_k \frac{N^{\mu\nu}(k,\mathbf{p})}{[k^2+2k\cdot q-M^2]^4} \\ q^\mu &= \sum_{i=1}^3 a_i(\mathbf{x})p_i^\mu, \qquad M^2 = m_t^2 - \sum_{i,j=1}^3 b_{ij}(\mathbf{x})(p_i\cdot p_j).\end{aligned} \tag{2.31}$$

Then, by shifting $k \to k-q$, it is possible to complete the square into the denominator:

$$\mathcal{M}_{\square}^{\mu\nu,ab} = -\frac{i\alpha_s}{(4\pi)}\frac{m_t^2}{v^2}Y_1Y_2\mathrm{Tr}[T^aT^b](4\pi\mu^2)^{2-\frac{d}{2}}\Gamma(4)\int_{\mathcal{C}} d\mathbf{x}\int_k \frac{N^{\mu\nu}(k-q,\mathbf{p})}{[k^2-q^2-M^2]^4}. \tag{2.32}$$

With this shift, the integrand becomes even with respect to k^μ; hence, odd powers of k^μ vanish after the integration.

The numerator $N^{\mu\nu}$ is a tensor of rank up to 4 in the loop momentum. We can replace rank-2 and rank-4 tensors with the following tensor structures

$$\begin{aligned}k^\mu k^\nu &\to \frac{k^2}{d}g^{\mu\nu}, \\ k^\mu k^\nu k^\rho k^\sigma &\to (k^2)^2\frac{g^{\mu\nu}g^{\rho\sigma}+g^{\mu\rho}g^{\nu\sigma}+g^{\mu\sigma}g^{\nu\rho}}{d(d+2)},\end{aligned} \tag{2.33}$$

since the tensors depending only on the loop momentum can not depend from any dimensionful quantities. Therefore, we can single out every $(2\alpha)-$rank factor:

$$\begin{aligned}\mathcal{M}_{\square}^{\mu\nu,ab} = -\frac{i\alpha_s}{(4\pi)}\frac{m_t^2}{v^2}Y_1Y_2\mathrm{Tr}[T^aT^b](4\pi\mu^2)^{2-\frac{d}{2}}\Gamma(4)\int_{\mathcal{C}} d\mathbf{x}\Bigg[A^{\mu\nu}(\mathbf{p},\mathbf{x})\int_k\frac{1}{[k^2-q^2-M^2]^4}+ \\ B^{\mu\nu}(\mathbf{p},\mathbf{x})\int_k\frac{k^2}{[k^2-q^2-M^2]^4}+ \\ C^{\mu\nu}(\mathbf{p},\mathbf{x})\int_k\frac{(k^2)^2}{[k^2-q^2-M^2]^4}\Bigg]\end{aligned} \tag{2.34}$$

The loop integrals can be now integrated. After a Wick rotation and the integration in $d-$dimensional spherical coordinates, we obtain the following close form

$$\int_k\frac{(k^2)^\alpha}{[k^2-q^2-M^2]^n} = (-1)^{(n-\alpha)}\frac{\Gamma(n-\alpha-\frac{d}{2})\Gamma(\alpha+\frac{d}{2})}{\Gamma(n)\Gamma(\frac{d}{2})}\frac{1}{[q^2+M^2]^{n-\alpha-\frac{d}{2}}}, \tag{2.35}$$

which brings the amplitude to have the following form

$$\begin{aligned}\mathcal{M}_{\Box}^{\mu\nu,ab} = -\frac{i\alpha_s}{(4\pi)}\frac{m_t^2}{v^2}Y_1Y_2\mathrm{Tr}[T^aT^b](4\pi\mu^2)^{2-\frac{d}{2}}\int_{\mathcal{C}} d\mathbf{x}\Bigg[\Gamma\left(4-\frac{d}{2}\right)\frac{A^{\mu\nu}(\mathbf{p},\mathbf{x})}{[q^2+M^2]^{4-\frac{d}{2}}}- \\ -\Gamma\left(3-\frac{d}{2}\right)\frac{d}{2}\frac{B^{\mu\nu}(\mathbf{p},\mathbf{x})}{[q^2+M^2]^{3-\frac{d}{2}}}+ \\ +\Gamma\left(2-\frac{d}{2}\right)\frac{d}{2}\left(1+\frac{d}{2}\right)\frac{C^{\mu\nu}(\mathbf{p},\mathbf{x})}{[q^2+M^2]^{2-\frac{d}{2}}}\Bigg].\end{aligned} \tag{2.36}$$

Using $\epsilon = \frac{4-d}{2}$ and extracting the dependence on the Gamma function, we obtain:

$$\begin{aligned}\mathcal{M}_{\Box}^{\mu\nu,ab} = -\frac{i\alpha_s}{(4\pi)}\frac{m_t^2}{v^2}Y_1Y_2\mathrm{Tr}[T^aT^b]\left(\frac{4\pi\mu^2}{m_t^2}\right)^{\epsilon}\Gamma(1+\epsilon)\int_{\mathcal{C}} d\mathbf{x}\Bigg[\frac{(1+\epsilon)}{(m_t^2)^2}\frac{A^{\mu\nu}(\mathbf{p},\mathbf{x})}{\left[\frac{q^2+M^2}{m_t^2}\right]^{2+\epsilon}}- \\ -\frac{(2-\epsilon)}{m_t^2}\frac{B^{\mu\nu}(\mathbf{p},\mathbf{x})}{\left[\frac{q^2+M^2}{m_t^2}\right]^{1+\epsilon}}+ \\ +\frac{(2-\epsilon)(3-\epsilon)}{\epsilon}\frac{C^{\mu\nu}(\mathbf{p},\mathbf{x})}{\left[\frac{q^2+M^2}{m_t^2}\right]^{\epsilon}}\Bigg]\end{aligned} \tag{2.37}$$

The denominators are now dimensionless, and they can be expressed as

$$\Delta(\mathbf{p},\mathbf{x}) = \frac{q^2+M^2}{m_t^2} = \frac{m_t^2+\sum_{ij}^3 a_ia_j(p_i\cdot p_j)-\sum_{ij}^3 b_{ij}(p_i\cdot p_j)}{m_t^2} = 1-\sum_{i,j=1}^{3} c_{ij}(\mathbf{x})\frac{p_i\cdot p_j}{m_t^2}. \tag{2.38}$$

A change of variables $g:\mathcal{C}\to[0,1]^3$ transforms the integration variables in the unit 3-cube[2]

$$\begin{aligned}\mathcal{M}_{\Box}^{\mu\nu,ab} = -\frac{i\alpha_s}{(4\pi)}\frac{m_t^2}{v^2}Y_1Y_2\mathrm{Tr}[T^aT^b]\left(\frac{4\pi\mu^2}{m_t^2}\right)^{\epsilon}\Gamma(1+\epsilon)\int_0^1 d\mathbf{x}\det[J(g)]\Bigg[\frac{(1+\epsilon)}{(m_t^2)^2}\frac{A^{\mu\nu}(\mathbf{p},\mathbf{x})}{\Delta^{2+\epsilon}}- \\ -\frac{(2-\epsilon)}{m_t^2}\frac{B^{\mu\nu}(\mathbf{p},\mathbf{x})}{\Delta^{1+\epsilon}}+ \\ +\frac{(2-\epsilon)(3-\epsilon)}{\epsilon}\frac{C^{\mu\nu}(\mathbf{p},\mathbf{x})}{\Delta^{\epsilon}}\Bigg].\end{aligned} \tag{2.39}$$

The integral is regular below the threshold $s = 4m_t^2$. The singular behaviour for $\epsilon = 0$ is proportional to the tensor $C^{\mu\nu}(\mathbf{p},\mathbf{x})$, coming from the rank-4 tensor integral:

$$\mathcal{M}_{\Box}^{\mu\nu,ab} \sim_{\epsilon^{-1}} -\frac{i\alpha_s}{(4\pi)}\frac{m_t^2}{v^2}Y_1Y_2\mathrm{Tr}[T^aT^b]\frac{6}{\epsilon}\int_0^1 d\mathbf{x}\det[J(g)]C^{\mu\nu}(\mathbf{p},\mathbf{x}). \tag{2.40}$$

Due to the renormalizability of the theory, this term has to vanish after the box sum. By only looking at the tensor structure:

$$\begin{aligned}2\mathrm{Tr}\left[\gamma^\mu \not{k}\not{k}\not{k}\gamma^\nu \not{k}\right] + \mathrm{Tr}\left[\not{k}\gamma^\mu \not{k}\not{k}\gamma^\nu \not{k}\right] &= 8k^2(2k^\mu k^\nu - k^2 g^{\mu\nu}) + 4(k^2)^2 g^{\mu\nu} \\ &\to 4(k^2)^2 g^{\mu\nu}\frac{4-d}{d} = (k^2)^2 C^{\mu\nu}(\mathbf{p},\mathbf{x}) \\ &\implies C^{\mu\nu}(\mathbf{p},\mathbf{x}) \propto \epsilon,\end{aligned} \tag{2.41}$$

where we neglected the presence of the denominator since they contribute like $1+O(\epsilon)$.

Hence, the single pole coefficient is zero, and the total amplitude is finite as expected.

[2]With a little abuse of notation, we use the same symbols $\mathbf{x}$ for the new variables: $\mathbf{x}\to\mathbf{X}=g(\mathbf{x})\equiv\mathbf{x}$

External momenta vs. internal momenta

Going towards the actual calculation, we start fixing our convention for the external legs (all incoming):

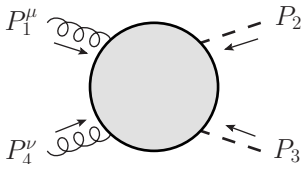

(2.42)

and a single way to identify the topology in terms of the "internal" momenta:

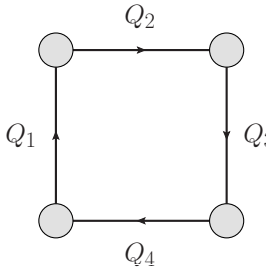

$$\sim \frac{1}{D_1 D_2 D_3 D_4}, \qquad \begin{cases} D_1 = (k+Q_1)^2 - m_t^2 \\ D_2 = (k+Q_2)^2 - m_t^2 \\ D_3 = (k+Q_3)^2 - m_t^2 \\ D_4 = (k+Q_4)^2 - m_t^2 \end{cases} . \tag{2.43}$$

Using momentum conservation, we can express the external momenta in terms of the internal

$$P_i = P_i(Q) = A_{ij} Q_j. \tag{2.44}$$

This is what we call *internal momenta convention*.

The kinematics is defined as follows:

$$\begin{aligned} P_1^2 = P_4^2 &= 0, \\ P_2^2 &= m_{H_1}^2, \\ P_3^2 &= m_{H_2}^2, \\ (P_1+P_4)^2 = (P_2+P_3)^2 &= \hat{s}, \\ (P_1+P_2)^2 = (P_3+P_4)^2 &= \hat{t}, \\ (P_1+P_3)^2 = (P_2+P_4)^2 &= \hat{u}, \\ P_4 &= -P_1 - P_2 - P_3, \end{aligned} \tag{2.45}$$

and the tensors defined with the external momenta become

$$\begin{aligned} T_1 &= g^{\mu\nu} - \frac{P_1^\nu P_4^\mu}{(P_1 \cdot P_4)}, \\ T_2 &= g^{\mu\nu} + \frac{(P_2^2) P_1^\nu P_4^\mu - 2(P_1 \cdot P_4) P_2^\nu P_4^\mu - 2(P_2 \cdot P_4) P_1^\nu P_2^\mu + 2(P_1 \cdot P_4) P_2^\nu P_2^\mu}{(P_1 \cdot P_4) p_T^2} \\ p_T^2 &= \frac{2(P_2 \cdot P_4)(P_1 \cdot P_2)}{(P_1 \cdot P_4)} - P_2^2. \end{aligned} \tag{2.46}$$

With this convention, we can express each of these diagrams in terms of the same integral, containing the shortest possible internal momenta. On the other hand, the invariants expressed in terms of the internal momenta can have an involved dependence on them, and some cancellation may not occur.

The *external momenta convention* is the most common, meaning that we express the internal momenta with respect to the external ones:

$$Q_i = Q_i(P) = A_{ij} P_j. \tag{2.47}$$

While the two conventions will lead to the same result (of course), at higher loop, the internal momenta convention might help the computation of the Feynman integrals with many propagators, leading to more compact integrals expressions suitable for numerical calculations.

2.2.3 Applying the procedure

Feynman parametrization

Consider the box diagram (1) in Figure (2.2), and let us adapt our conventions:

$$\begin{cases} Q_1 = p_4 \\ Q_2 = p_1 \\ Q_3 = p_2 \\ Q_4 = p_3 \end{cases} \implies \begin{cases} P_1 = p_1 - p_4 \\ P_2 = p_2 - p_1 \\ P_3 = p_3 - p_2 \\ P_4 = p_4 - p_1 \end{cases} \tag{2.48}$$

as it can be seen in Figure (2.3). The box diagram (2) can be found by crossing $t \leftrightarrow u$ ($P_2 \leftrightarrow P_3$) from the box (1).

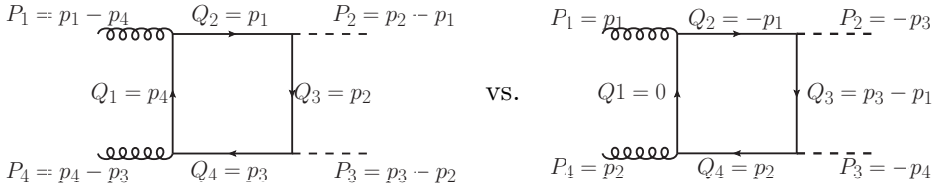

Figure 2.3: *Internal vs. external momenta convention.*

At one-loop, we can always shift the loop-momentum, such that we can absorb one of the internal momentum. This is equivalent to set one internal momentum to zero. We choose $p_4 = 0$, therefore

$$\begin{gathered} p_1^2 = p_3^2 = 0, \qquad p_2^2 = \hat{t}, \\ (p_1 \cdot p_2) = -\frac{\hat{t} - m_{H_1}^2}{2}, \quad (p_2 \cdot p_3) = -\frac{\hat{t} - m_{H_2}^2}{2}, \quad (p_1 \cdot p_3) = -\frac{\hat{s}}{2}. \end{gathered} \tag{2.49}$$

Instead of using the standard Feynman parametrization of the whole denominator, we can notice that if we parametrize only two propagators:

$$\frac{1}{D_0 D_1^n} = \int_0^1 dx \frac{x^{n-1}}{[D_0 x + D_1(1-x)]^{n+1}}, \tag{2.50}$$

the integration boundary already is the interval $[0, 1]$. Exploiting this relation, we can apply recursively this parametrization to avoid the explicit change of variables with maps the general boundaries into the unit 3-cube. Applying this knowledge to the planar box diagram, we obtain the following integral:

$$\begin{gathered} D_0' = D_0, \qquad D_{i+1}' = D_{i+1}(1 - x_i) + D_i' x_i \\ \implies \int_k \frac{1}{D_0 D_1 D_2 D_3} = \Gamma(4) \int_0^1 d\mathbf{x} (x_2 x_3^2) \int_k \frac{1}{[D_3']^4}. \end{gathered} \tag{2.51}$$

The D_3' is quadratic in the loop momenta, and it can be expressed in terms of the general variables defined in the previous section:

$$\begin{gathered} \det[J(g)] = x_2 x_3^2, \quad q_1^\mu = p_1^\mu x_1 x_2 x_3 + p_2^\mu x_3 (1 - x_2) + p_3^\mu (1 - x_3) \\ M_1^2 = m_t^2 - p_2^2 (1 - x_2) x_3, \end{gathered} \tag{2.52}$$

and

$$\Delta_1 = 1 - \frac{p_2^2}{m_t^2}(1 - x_2) x_3 + \frac{q_1^2}{m_t^2}. \tag{2.53}$$

Of course, this procedure is equivalent to the standard parametrization where a particular change of variable $g : \mathcal{C} \to [0, 1]^3$ with Jacobian $\det[J(g_1)] = x_2 x_3^2$ is performed: applying the parametrization to all four propagators, we arrive to the following structure

$$\begin{gathered} \det[J(g_1)] = x_2 x_3^2, \quad q_1^\mu = p_1^\mu x_1 x_2 x_3 + p_2^\mu x_2 (1 - x_1) + p_3^\mu (1 - x_2) \\ M_1^2 = m_t^2 - p_2^2 (1 - x_1) x_2, \end{gathered} \tag{2.54}$$

where we used the following transformation

$$g_1 : \mathcal{C} \to [0,1]^3, \quad g_1(\mathbf{x}) = \begin{pmatrix} x_2(1-x_1) \\ (1-x_2) \\ x_1 x_2 x_3 \end{pmatrix}, \quad \det\left[J(g_1)\right] = x_2^2 x_1. \tag{2.55}$$

Of course, it is exactly the previous transformation with the exchange of the variables names $x_1 \to x_2$, $x_2 \to x_3$ and $x_3 \to x_1$.

A simpler option will be using the external momenta conventions. This will brought the integrals in a more compact form:

$$\begin{cases} P_1 = p_1 \\ P_2 = -p_3 \\ P_3 = -p_4 \\ P_4 = p_2 \end{cases} \implies \begin{cases} Q_1 = 0 \\ Q_2 = -p_1 \\ Q_3 = p_3 - p_1 \\ Q_4 = p_2 \end{cases}, \tag{2.56}$$

$$\begin{gathered} p_1^2 = p_2^2 = 0, \quad p_3^2 = m_{H_1}^2, \quad p_4^2 = m_{H_2}^2 \\ p_1 \cdot p_2 = \frac{\hat{s}}{2}, \quad p_1 \cdot p_3 = -\frac{\hat{t} - m_{H_1}^2}{2}, \quad p_2 \cdot p_3 = -\frac{\hat{u} - m_{H_1}^2}{2}. \end{gathered}$$

A useful momenta will also be

$$2p_1 \cdot p_2 - 2p_1 \cdot p_3 - 2p_2 \cdot p_3 = m_{H_2}^2 - m_{H_1}^2. \tag{2.57}$$

The new momentum flow yields a different expression for the (same) integrals. Of course, the diagram is completely parameterization-independent, hence it will lead to the same final result.

We define the dimensionless variables:

$$\begin{gathered} \rho_s = \frac{\hat{s}}{m_t^2} = \frac{2(p_1 \cdot p_2)}{m_t^2}, \quad \rho_t = \frac{\hat{t}}{m_t^2} = \frac{p_3^2 - 2(p_1 \cdot p_3)}{m_t^2}, \\ \rho_u = \frac{\hat{u}}{m_t^2} = \frac{p_3^2 - 2(p_2 \cdot p_3)}{m_t^2}, \quad \rho_1 = \frac{m_{H_1}^2}{m_t^2} = \frac{p_3^2}{m_t^2}, \quad \rho_2 = \frac{m_{H_2}^2}{m_t^2} = \frac{p_4^2}{m_t^2} \\ \hat{\rho}_t = -\frac{2(p_1 \cdot p_3)}{m_t^2}, \quad \hat{\rho}_u = -\frac{2(p_2 \cdot p_3)}{m_t^2}. \end{gathered} \tag{2.58}$$

The general variables defined in the previous section in the external momenta convention are:

$$\begin{gathered} g_1 : \mathcal{C} \to [0,1]^3, \quad g_1(\mathbf{x}) = \begin{pmatrix} (1-x_1)(1-x_3) \\ x_1 x_2 \\ x_1(1-x_3) \end{pmatrix}, \quad \det[J(g_1)] = x_1(1-x_1), \\ q_1^\mu = -(1-x_1)p_1^\mu + x_1 x_2 p_2^\mu + (1-x_1)x_3 p_3^\mu, \\ M_1^2 = m_t^2 + (1-x_1)x_3 2(p_1 \cdot p_3) - (1-x_1)x_3 m_{H_1}^2, \\ \Delta_1 = 1 - (1-x_1)x_1 x_2 \rho_s - (1-x_1)x_1 x_3 \hat{\rho}_t - (1-x_1)x_1 x_2 x_3 \hat{\rho}_u - [1-(1-x_1)x_3](1-x_1)x_3 \rho_1 \end{gathered} \tag{2.59}$$

Numerator algebra

The Dirac algebra is needed to extract the tensor structure from the diagram. The numerator of the Feynman diagram is:

$$N_1^{\mu\nu} = \mathrm{Tr}\left[\gamma^\nu \left(\not{k} + m_t\right) \gamma^\mu \left(\not{k} - \not{p}_1 + m_t\right) \left(\not{k} + \not{p}_3 - \not{p}_1 + m_t\right) \left(\not{k} + \not{p}_2 + m_t\right)\right] \tag{2.60}$$

We are interested into the tensors $A^{\mu\nu}(\mathbf{p}, \mathbf{x})$, $B^{\mu\nu}(\mathbf{p}, \mathbf{x})$ and $C^{\mu\nu}(\mathbf{p}, \mathbf{x})$ defined into the previous section. Hence, after the evaluation of the Dirac trace, the shift of the loop-momentum and the integration over the odd powers of the integrating momentum, we obtain:

$$
\begin{aligned}
C_1^{\mu\nu} &= -\frac{4(d-2)g^{\mu\nu}}{d} \\
B_1^{\mu\nu} &= \frac{4g^{\mu\nu}}{d}\Big[6m_t^2 - 2d(p_1\cdot q_1) + d(p_2\cdot q_1) + d(p_3\cdot q_1) + (d-2)(p_1\cdot p_3) - d(p_2\cdot p_3) - \\
&\qquad - 2(d+1)q_1^2 + 2(p_2\cdot q_1) - 2(p_3\cdot q_1) + 2(p_1\cdot p_2) + 2(p_2\cdot p_3)\Big] - \\
&\quad - \frac{8p_2^\mu p_1^\nu}{d} + \left(4-\frac{8}{d}\right)p_2^\mu p_3^\nu + \left(\frac{8}{d}-4\right)p_3^\mu p_1^\nu - \frac{4(d+2)}{d}p_2^\mu q_1^\nu + \frac{16}{d}p_1^\nu q_1^\mu + \\
&\quad + \left(4-\frac{8}{d}\right)p_3^\nu q_1^\mu + \left(4-\frac{8}{d}\right)p_3^\mu q_1^\nu + \frac{8(d+4)}{d}q_1^\mu q_1^\nu \\
A_1^{\mu\nu} &= 4g^{\mu\nu}\Big[m_t^4 + 2m_t^2(p_1\cdot q_1) - m_t^2(p_2\cdot q_1) - m_t^2(p_3\cdot q_1) + (p_1\cdot p_2)\left(p_3\cdot q_1 - 2m_t^2\right) - \\
&\qquad - (p_1\cdot p_3)\left(m_t^2 + p_2\cdot q_1 - q_1^2\right) + m_t^2(p_2\cdot p_3) - (p_2\cdot p_3)(p_1\cdot q_1) + \\
&\qquad + 2(p_1\cdot q_1)(p_2\cdot q_1) + q_1^2(-2(p_1\cdot q_1) + p_2\cdot q_1 + p_3\cdot q_1 - p_2\cdot p_3) - (q_1^2)^2\Big] + \\
&\quad + p_2^\mu p_1^\nu\left(8m_t^2 - 4(p_3\cdot q_1)\right) - 4p_3^\mu q_1^\nu\left(m_t^2 - 2(p_1\cdot q_1) + p_1\cdot p_2 - q_1^2\right) + \\
&\quad + 4p_2^\mu q_1^\nu\left(m_t^2 - 2(p_1\cdot q_1) + p_1\cdot p_3 - q_1^2\right) + 4p_3^\mu p_1^\nu\left(m_t^2 + p_2\cdot q_1 - q_1^2\right) - \\
&\quad - 4p_3^\nu q_1^\mu\left(m_t^2 + 2(p_2\cdot q_1) + p_1\cdot p_2 - q_1^2\right) + 4p_2^\mu p_3^\nu\left(-m_t^2 + p_1\cdot q_1 + q_1^2\right) + \\
&\quad + 8q_1^\mu q_1^\nu\left(3m_t^2 + 2(p_1\cdot q_1) - 2(p_3\cdot q_1) - p_1\cdot p_3 + p_2\cdot p_3 + q_1^2\right) + 4(p_2\cdot p_3)p_1^\nu q_1^\mu.
\end{aligned}
\tag{2.61}
$$

Notice that these tensors do not depend on the four-vectors p_1^μ and p_2^ν, since they are contracted with the on-shell polarizations $\epsilon_\mu(p_1)$ and $\epsilon_\nu(p_2)$, which are orthogonal with respect to their momenta:

$$
\epsilon(p_j)\cdot p_j = 0. \tag{2.62}
$$

Moreover, after the calculation of the missing box diagram, the complete tensor coefficient $C^{\mu\nu}(\mathbf{p},\mathbf{x})$ will turn proportional to ϵ.

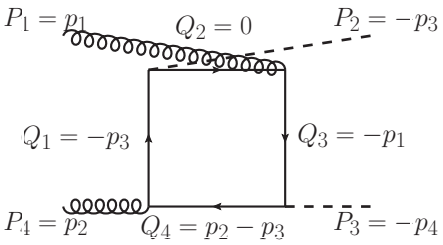

Figure 2.4: External momenta convention

Applying the same procedure for the box (3) (see Fig. (2.2)), the external momenta convention (Fig. (2.4)) yields

$$
\begin{cases} P_1 = p_1 \\ P_2 = -p_3 \\ P_3 = -p_4 \\ P_4 = p_2 \end{cases} \implies \begin{cases} Q_1 = -p_3 \\ Q_2 = 0 \\ Q_3 = -p_1 \\ Q_4 = p_2 - p_3 \end{cases} . \tag{2.63}
$$

The change of variables required with this setting is

$$
g_2 : \mathcal{C} \to [0,1]^3, \quad g_2(\mathbf{x}) = \begin{pmatrix} (1-x_1)(1-x_3) \\ x_1 x_2 \\ x_1(1-x_3) \end{pmatrix}, \quad \det[J(g_2)] = x_1(1-x_1), \tag{2.64}
$$

and completing the square, we obtain the shift q_2^μ and the tadpole-mass term Δ_2:

$$\begin{aligned} q_2^\mu &= -x_1x_2p_1^\mu + x_3(1-x_1)p_2^\mu - p_3^\mu(1-x_1) \\ M_2^2 &= m_t^2 + x_3(1-x_1)(2p_2\cdot p_3) - (1-x_1)m_{H_1}^2 \\ \Delta_2 &= 1 - x_1(1-x_1)[x_2\hat{\rho}_t + x_3\hat{\rho}_u + x_2x_3\rho_s + \rho_{H_1}]. \end{aligned} \tag{2.65}$$

Finally, the numerator algebra will provide the tensor coefficients needed by the master formula Eq. (2.39).

$$N_2^\mu = \mathrm{Tr}\left[\gamma^\nu(\not{k}-\not{p}_3+m_t)(\not{k}+m_t)\gamma^\mu(\not{k}-\not{p}_1+m_t)(\not{k}+\not{p}_2-\not{p}_3+m_t)\right] \tag{2.66}$$

$$\begin{aligned} C_2^{\mu\nu} &= 4g^{\mu\nu} \\ B_2^{\mu\nu} &= \frac{4g^{\mu\nu}}{d}\Big[-2\left[(d-4)m^2 + p_2\cdot q_3 - 2(p_3\cdot q_3) + p_3^2 - p_2\cdot p_3 - 2q_3^2\right] + (d+2)(p_1\cdot q_3) + \\ &\quad + d\left(-p_2\cdot q_3 + 2\left(p_3\cdot q_3 + q_3^2\right) + p_3^2 - (p_2\cdot p_3)\right) - d(p_1\cdot p_2) + 4(p_1\cdot p_3)\Big] + \\ &\quad + \left(4-\frac{8}{d}\right)p_2^\mu p_3^\nu - \frac{16}{d}p_3^\mu p_1^\nu + \left(\frac{16}{d}-8\right)p_3^\mu p_3^\nu + \left(\frac{8}{d}+4\right)p_2^\mu q_3^\nu - \frac{4(d+2)}{d}p_1^\nu q_3^\mu + \\ &\quad + \frac{8(d+2)}{d}p_3^\nu q_3^\mu - \frac{8(d+2)}{d}p_3^\mu q_3^\nu + 4p_2^\mu p_1^\nu \\ A_2^{\mu\nu} &= 4g^{\mu\nu}\Big[m_t^4 + m_t^2(p_2\cdot q_3) - 2m_t^2(p_3\cdot q_3) - q_3^2\left(2m_t^2 + p_2\cdot q_3 - 2(p_3\cdot q_3) - p_3^2 + p_2\cdot p_3\right) - \\ &\quad - (p_1\cdot p_2)\left(m_t^2 + p_3\cdot q_3 + q_3^2\right) + (p_1\cdot q_3)\left(-m_t^2 + 2(p_3\cdot q_3) + p_3^2 - p_2\cdot p_3 + q_3^2\right) - \\ &\quad - m_t^2p_3^2 + m_t^2(p_2\cdot p_3) + (p_1\cdot p_3)(p_2\cdot q_3) + (q_3^2)^2\Big] + \\ &\quad + 8q_3^\mu q_3^\nu\left(4m_t^2 - p_3^2 + p_1\cdot p_3 + p_2\cdot p_3\right) + 4p_3^\mu q_3^\nu\left(2m_t^2 - 2(p_1\cdot q_3) + p_1\cdot p_2 - 2q_3^2\right) - \\ &\quad - 4p_2^\mu q_3^\nu\left(m_t^2 + p_1\cdot p_3 - q_3^2\right) + 8p_3^\mu p_3^\nu\left(m_t^2 - p_1\cdot q_3 - q_3^2\right) + 4p_2^\mu p_1^\nu\left(m_t^2 + p_3\cdot q_3 + q_3^2\right) + \\ &\quad + 4p_1^\nu q_3^\mu\left(m_t^2 - 2(p_3\cdot q_3) - p_3^2 + p_2\cdot p_3 - q_3^2\right) + 4p_2^\mu p_3^\nu\left(-m_t^2 + p_1\cdot q_3 + q_3^2\right) + \\ &\quad + p_3^\nu q_3^\mu\left[8\left(3m_t^2 - p_2\cdot q_3 + 2(p_3\cdot q_3) + p_1\cdot p_3 + q_3^2\right) - 4(p_1\cdot p_2)\right] - 4p_3^\mu p_1^\nu(p_2\cdot q_3). \end{aligned} \tag{2.67}$$

Summing the diagrams

The box-like contribution to the leading order cross section is the sum of the box diagrams considered in the previous subsection:

$$\mathcal{M}_\Box^{\mu\nu,ab} = 2\left(\quad +\quad +\quad\right), \tag{2.68}$$

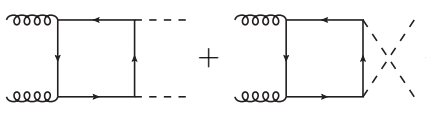

which lead to the following d-dimensional tensor-structure:

$$\begin{aligned} \mathcal{M}_\Box^{\mu\nu,ab} &= -2\frac{i\alpha_s}{(4\pi)}\frac{m_t^2}{v^2}Y_1Y_2\mathrm{Tr}[T^aT^b]\left(\frac{4\pi\mu^2}{m_t^2}\right)^\epsilon\Gamma(1+\epsilon)\times \\ &\times \int_0^1 d\mathbf{x}\Bigg\{\det[J(g_1)]\left[\frac{(1+\epsilon)}{(m_t^2)^2}\frac{A_1^{\mu\nu}}{\Delta_1^{2+\epsilon}} - \frac{(2-\epsilon)}{m_t^2}\frac{B_1^{\mu\nu}}{\Delta_1^{1+\epsilon}} + \frac{(2-\epsilon)(3-\epsilon)}{\epsilon}\frac{C_1^{\mu\nu}}{\Delta_1^\epsilon}\right] + \\ &\quad \det[J(g_1)]\left[\frac{(1+\epsilon)}{(m_t^2)^2}\frac{A_1^{\mu\nu}}{\Delta_1^{2+\epsilon}} - \frac{(2-\epsilon)}{m_t^2}\frac{B_1^{\mu\nu}}{\Delta_1^{1+\epsilon}} + \frac{(2-\epsilon)(3-\epsilon)}{\epsilon}\frac{C_1^{\mu\nu}}{\Delta_1^\epsilon}\right]\Bigg|_{t\leftrightarrow u} + \\ &\quad \det[J(g_2)]\left[\frac{(1+\epsilon)}{(m_t^2)^2}\frac{A_2^{\mu\nu}}{\Delta_2^{2+\epsilon}} - \frac{(2-\epsilon)}{m_t^2}\frac{B_2^{\mu\nu}}{\Delta_2^{1+\epsilon}} + \frac{(2-\epsilon)(3-\epsilon)}{\epsilon}\frac{C_2^{\mu\nu}}{\Delta_2^\epsilon}\right]\Bigg\}. \end{aligned} \tag{2.69}$$

A first check on its finiteness is needed, such that the ϵ-expansion may lead to a meaningful physical quantity. The ϵ divergent part is proportional to the tensor $C^{\mu\nu}(\mathbf{p},\mathbf{x})$:

$$\begin{aligned}\mathcal{M}_{\square}^{\mu\nu,ab}|_{A,B=0} = -2\frac{i\alpha_s}{(4\pi)}\frac{m_t^2}{v^2}Y_1Y_2\mathrm{Tr}[T^aT^b]\left(\frac{4\pi\mu^2}{m_t^2}\right)^{\epsilon}\Gamma(1+\epsilon)\times \\ \int_0^1 d\mathbf{x}\det[J(g)]\frac{(2-\epsilon)(3-\epsilon)}{\epsilon}\left\{\frac{C_1^{\mu\nu}}{\Delta_1^{\epsilon}}+\frac{C_1^{\mu\nu}}{\Delta_1^{\epsilon}}\Big|_{t\leftrightarrow u}+\frac{C_2^{\mu\nu}}{\Delta_2^{\epsilon}}\right\}.\end{aligned} \tag{2.70}$$

since $g_1 = g_2 = g$, as noticeable from the calculation of the single diagrams. The expansion of the integrand up to its finite term yields:

$$\begin{aligned}\mathcal{M}_{\square}^{\mu\nu,ab}|_{A,B=0} &\propto g^{\mu\nu}\int_0^1 d\mathbf{x}\det[J(g)]\left(\frac{6}{\epsilon}-5+\epsilon\right)\times \\ &\times\left\{-\frac{4(1-\epsilon)}{2-\epsilon}[2-\epsilon\log(\Delta_1\widetilde{\Delta}_1)+O(\epsilon^2)]+4[1-\epsilon\log(\Delta_2)+O(\epsilon^2)]\right\} \\ &= g^{\mu\nu}\int_0^1 d\mathbf{x}\det[J(g)]\left(\frac{6}{\epsilon}-5+\epsilon\right)\times \\ &\times\left\{-2(1-\epsilon)\left(1+\frac{\epsilon}{2}\right)[2-\epsilon\log(\Delta_1\widetilde{\Delta}_1)]+4[1-\epsilon\log(\Delta_2)]+O(\epsilon^2)\right\} \\ &= g^{\mu\nu}\int_0^1 d\mathbf{x}\det[J(g)]\left(\frac{6}{\epsilon}-5+\epsilon\right)2\epsilon\left[1+\log\left(\frac{\Delta_1\widetilde{\Delta}_1}{\Delta_2^2}\right)\right]+O(\epsilon^2) \\ &= g^{\mu\nu}\int_0^1 d\mathbf{x}\det[J(g)]\left(\frac{6}{\epsilon}-5+\epsilon\right)\left[2\epsilon\left(1+\log\left(\frac{\Delta_1\widetilde{\Delta}_1}{\Delta_2^2}\right)\right)+O(\epsilon^2)\right] \\ &= 12g^{\mu\nu}\int_0^1 d\mathbf{x}\det[J(g)]\left[1+\log\left(\frac{\Delta_1\widetilde{\Delta}_1}{\Delta_2^2}\right)\right]+O(\epsilon),\end{aligned} \tag{2.71}$$

which is finite in ϵ, as expected. Here, $\widetilde{\Delta}_1 = \Delta_1|_{t\leftrightarrow u}$ and from now on, the tilde variables will denote the switch $t \leftrightarrow u$, which implies $p_3 \to p_1 + p_2 - p_3$.

Hence, since the contributions proportional to $A^{\mu\nu}(\mathbf{p},\mathbf{x})$ and $B^{\mu\nu}(\mathbf{p},\mathbf{x})$ are already finite in ϵ, the complete expansion will be finite, and it reads:

$$\begin{aligned}\mathcal{M}_{\square}^{\mu\nu,ab} = -2\frac{i\alpha_s}{(4\pi)}\frac{m_t^2}{v^2}Y_1Y_2\mathrm{Tr}[T^aT^b]\left(\frac{4\pi\mu^2}{m_t^2}\right)^{\epsilon}\Gamma(1+\epsilon)\times \\ \times\int_0^1 d\mathbf{x}\det[J(g)]\left\{12g^{\mu\nu}\left[1+\log\left(\frac{\Delta_1\widetilde{\Delta}_1}{\Delta_2}\right)\right]+\frac{1}{(m_t^2)^2}\left(\frac{A_1^{\mu\nu}}{\Delta_1^2}+\frac{\widetilde{A}_1^{\mu\nu}}{\widetilde{\Delta}_1^2}+\frac{A_2^{\mu\nu}}{\Delta_2^2}\right)\Big|_{\epsilon=0}+ \\ -\frac{2}{m_t^2}\left(\frac{B_1^{\mu\nu}}{\Delta_1}+\frac{\widetilde{B}_1^{\mu\nu}}{\widetilde{\Delta}_1}+\frac{B_2^{\mu\nu}}{\Delta_2}\right)\Big|_{\epsilon=0}\right\}+O(\epsilon).\end{aligned} \tag{2.72}$$

We first present the case where the top-quark mass is considered to be heavy ($m_t \to \infty$), which can be solved analytically. Later, we show how a numerical approach for the LO amplitude can be exploited.

Heavy top limit

The heavy top limit $m_t \to \infty$ provide us a first analytical expression to handle. Before writing explicitely the top-mass expansion of tadpole masses and tensors, we can express these expansions symbolically:

$$\begin{aligned}\frac{1}{\Delta_i} &\sim_{m_t\to\infty} 1+\frac{\delta_i}{m_t^2}+O\left(\frac{1}{m_t^4}\right), \\ A_i^{\mu\nu} &\sim_{m_t\to\infty} a_{i,(-2)}^{\mu\nu}m_t^4+a_{i,(-1)}^{\mu\nu}m_t^2+O(1), \\ B_i^{\mu\nu} &\sim_{m_t\to\infty} b_{i,(-1)}^{\mu\nu}m_t^2+b_{i,(0)}^{\mu\nu}+O\left(\frac{1}{m_t^2}\right).\end{aligned} \tag{2.73}$$

Therefore, the Eq. (2.72) reads:

$$\begin{aligned}
\mathcal{M}_{\square}^{\mu\nu,ab} = &-2\frac{i\alpha_s}{(4\pi)}\frac{m_t^2}{v^2}Y_1Y_2\mathrm{Tr}[T^aT^b]\left(\frac{4\pi\mu^2}{m_t^2}\right)^{\epsilon}\Gamma(1+\epsilon)\times \\
&\times\int_0^1 d\mathbf{x}\det[J(g)]\Bigg\{12g^{\mu\nu}\left[1+\frac{2\delta_2-\delta_1-\widetilde{\delta}_1}{m_t^2}+O\left(\frac{1}{m_t^4}\right)\right]+ \\
&+\frac{1}{(m_t^2)^2}\Bigg(\left[a^{\mu\nu}_{1,(-2)}+\widetilde{a}^{\mu\nu}_{1,(-2)}+a^{\mu\nu}_{2,(-2)}\right]m_t^4+ \\
&+\Big[a^{\mu\nu}_{1,(-1)}+\widetilde{a}^{\mu\nu}_{1,(-1)}+a^{\mu\nu}_{2,(-1)}+ \\
&+2a^{\mu\nu}_{1,(-2)}\delta_1+2\widetilde{a}^{\mu\nu}_{1,(-2)}\widetilde{\delta}_1+2a^{\mu\nu}_{2,(-2)}\delta_2\Big]m_t^2+O(1)\Bigg)- \\
&-\frac{2}{m_t^2}\Bigg(\left[b^{\mu\nu}_{1,(-1)}+\widetilde{b}^{\mu\nu}_{1,(-1)}+b^{\mu\nu}_{2,(-1)}\right]m_t^2+ \\
&+\Big[b^{\mu\nu}_{1,(0)}+\widetilde{b}^{\mu\nu}_{1,(0)}+b^{\mu\nu}_{2,(0)}+ \\
&+\widetilde{b}^{\mu\nu}_{1,(-1)}\widetilde{\delta}_1+b^{\mu\nu}_{1,(-1)}\delta_1+b^{\mu\nu}_{2,(-1)}\delta_2\Big]+O\left(\frac{1}{m_t^2}\right)\Bigg)\Bigg\}+O(\epsilon)= \\
= &-2\frac{i\alpha_s}{(4\pi)}\frac{m_t^2}{v^2}Y_1Y_2\mathrm{Tr}[T^aT^b]\left(\frac{4\pi\mu^2}{m_t^2}\right)^{\epsilon}\Gamma(1+\epsilon)\times \\
&\times\int_0^1 d\mathbf{x}\det[J(g)]\Bigg\{12g^{\mu\nu}+\left[a^{\mu\nu}_{1,(-2)}+\widetilde{a}^{\mu\nu}_{1,(-2)}+a^{\mu\nu}_{2,(-2)}\right]- \\
&-2\left[b^{\mu\nu}_{1,(-1)}+\widetilde{b}^{\mu\nu}_{1,(-1)}+b^{\mu\nu}_{1,(-1)}\right]+ \\
&+\frac{1}{(m_t^2)}\Bigg(12g^{\mu\nu}(2\delta_2-\delta_1-\widetilde{\delta}_1)+ \\
&+\Big[a^{\mu\nu}_{1,(-1)}+\widetilde{a}^{\mu\nu}_{1,(-1)}+a^{\mu\nu}_{2,(-1)}+ \\
&+2a^{\mu\nu}_{1,(-2)}\delta_1+2\widetilde{a}^{\mu\nu}_{1,(-2)}\widetilde{\delta}_1+2a^{\mu\nu}_{2,(-2)}\delta_2\Big] \\
&-2\Big[b^{\mu\nu}_{1,(0)}+\widetilde{b}^{\mu\nu}_{1,(0)}+b^{\mu\nu}_{2,(0)}+ \\
&+\widetilde{b}^{\mu\nu}_{1,(-1)}\widetilde{\delta}_1+b^{\mu\nu}_{1,(-1)}\delta_1+b^{\mu\nu}_{2,(-1)}\delta_2\Big]\Bigg)\Bigg\}+O\left(\epsilon,\frac{1}{m_t^2}\right).
\end{aligned} \tag{2.74}$$

Since the Yukawas verteces contributes with an m_t^2, the integrand has to scale with $\frac{1}{m_t^2}$ to ensure the finiteness of the heavy top-quark limit. The implication of this is that the sum of the leading term of each expanded quantity has to vanish:

$$12g^{\mu\nu}+\left[a^{\mu\nu}_{1,(-2)}+\widetilde{a}^{\mu\nu}_{1,(-2)}+a^{\mu\nu}_{2,(-2)}\right]-2\left[b^{\mu\nu}_{1,(-1)}+\widetilde{b}^{\mu\nu}_{1,(-1)}+b^{\mu\nu}_{1,(-1)}\right]=0. \tag{2.75}$$

From the explicit mass expansion, we obtain

$$\begin{aligned}
a^{\mu\nu}_{1,(-2)}=\widetilde{a}^{\mu\nu}_{1,(-2)}=a^{\mu\nu}_{2,(-2)}=4g^{\mu\nu} \\
b^{\mu\nu}_{1,(-1)}=\widetilde{b}^{\mu\nu}_{1,(-1)}=6g^{\mu\nu},\qquad b^{\mu\nu}_{2,(-1)}=0,
\end{aligned} \tag{2.76}$$

which satisfies the Eq. (2.75). Hence:

$$\begin{aligned}\mathcal{M}_{\Box}^{\mu\nu,ab} = -2\frac{i\alpha_s}{(4\pi)}\frac{Y_1Y_2}{v^2}\mathrm{Tr}[T^aT^b]\left(\frac{4\pi\mu^2}{m_t^2}\right)^{\epsilon}\Gamma(1+\epsilon)\times \\ \times\int_0^1 d\mathbf{x}\det[J(g)]\Big\{16g^{\mu\nu}(2\delta_2-\delta_1-\widetilde{\delta}_1)+ \\ +\Big[a_{1,(-1)}^{\mu\nu}+\widetilde{a}_{1,(-1)}^{\mu\nu}+a_{2,(-1)}^{\mu\nu}\Big] \\ -2\Big[b_{1,(0)}^{\mu\nu}+\widetilde{b}_{1,(0)}^{\mu\nu}+b_{2,(0)}^{\mu\nu}\Big]\Big\}+O\left(\epsilon,\frac{1}{m_t^2}\right).\end{aligned} \tag{2.77}$$

The explicit expressions for the subleading terms needed are:

$$\begin{aligned}b_{1,(0)}^{\mu\nu} &= 2g^{\mu\nu}\Big[-4(p_1\cdot q_1)+3(p_2\cdot q_1)+(p_3\cdot q_1)+(p_1\cdot p_2)- \\ &\quad +(p_1\cdot p_3)-(p_2\cdot p_3)-5q_1^2\Big]- \\ &\quad -2p_2^\mu p_1^\nu+2p_2^\mu p_3^\nu-2p_3^\mu p_1^\nu-6p_2^\mu q_1^\nu+ \\ &\quad +4p_1^\nu q_1^\mu+2p_3^\nu q_1^\mu+2p_3^\mu q_1^\nu+16q_1^\mu q_1^\nu, \\ b_{2,(0)}^{\mu\nu} &= 2g^{\mu\nu}\Big[3(p_1\cdot q_3)-3(p_2\cdot q_3)+6\left(p_3\cdot q_3+q_3^2\right)+ \\ &\quad +p_3^2-2(p_1\cdot p_2)+2(p_1\cdot p_3)-p_2\cdot p_3\Big]+ \\ &\quad +4p_2^\mu p_1^\nu+2p_2^\mu p_3^\nu-4p_3^\mu p_1^\nu-4p_3^\mu p_3^\nu+ \\ &\quad +6p_2^\mu q_3^\nu-6p_1^\nu q_3^\mu+12p_3^\nu q_3^\mu-12p_3^\mu q_3^\nu, \\ a_{1,(-1)}^{\mu\nu} &= -4g^{\mu\nu}\Big[-2(p_1\cdot q_1)+p_2\cdot q_1+p_3\cdot q_1+ \\ &\quad +2(p_1\cdot p_2)+p_1\cdot p_3-p_2\cdot p_3\Big]+ \\ &\quad +8p_2^\mu p_1^\nu-4p_2^\mu p_3^\nu+4p_3^\mu p_1^\nu+4p_2^\mu q_1^\nu- \\ &\quad -4p_3^\nu q_1^\mu-4p_3^\mu q_1^\nu+24q_1^\mu q_1^\nu, \\ a_{2,(-1)}^{\mu\nu} &= -4g^{\mu\nu}\Big[(p_1\cdot q_3)-(p_2\cdot q_3)+2\left(p_3\cdot q_3+q_3^2\right)+ \\ &\quad +p_3^2+p_1\cdot p_2-p_2\cdot p_3\Big]+ \\ &\quad +4p_2^\mu p_1^\nu-4p_2^\mu p_3^\nu+8p_3^\mu p_3^\nu-4p_2^\mu q_3^\nu+ \\ &\quad +4p_1^\nu q_3^\mu+24p_3^\nu q_3^\mu+8p_3^\mu q_3^\nu+32q_3^\mu q_3^\nu.\end{aligned} \tag{2.78}$$

The complete analytical expression for the heavy top-quark limit is obtained by integrating w.r.t. the Feynman parameters (x_1, x_2, x_3). After doing this, the final expression is very compact:

$$\begin{aligned}\mathcal{M}_{\Box}^{\mu\nu,ab} &= -2\frac{i\alpha_s}{(4\pi)}\frac{Y_1Y_2}{v^2}\mathrm{Tr}[T^aT^b]\left(\frac{4\pi\mu^2}{m_t^2}\right)^{\epsilon}\Gamma(1+\epsilon)\frac{4}{3}\Big[p_2^\mu p_1^\nu-(p_1\cdot p_2)g^{\mu\nu}\Big] \\ &= i\frac{\alpha_s}{3\pi v^2}Y_1Y_2\delta^{ab}C_\epsilon\Big[(p_1\cdot p_2)g^{\mu\nu}-p_2^\mu p_1^\nu\Big].\end{aligned} \tag{2.79}$$

This last result can also be interpreted as a ggH_iH_j effective vertex for the low-energy lagrangian:

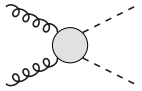

$$= i\frac{\alpha_s}{3\pi v^2}Y_1Y_2\delta^{ab}\left(\frac{4\pi\mu^2}{m_t^2}\right)^{\epsilon}\Gamma(1+\epsilon)\Big[(p_1\cdot p_2)g^{\mu\nu}-p_2^\mu p_1^\nu\Big]. \tag{2.80}$$

2.2.4 LO amplitude in the Heavy top limit

The sum of Eq. (2.27) and Eq. (2.80) leads to the HTL LO amplitude. It has a very simple expression:

$$\begin{aligned}\mathcal{M}_{\mathrm{LO}}^{\mathrm{HTL}} &= -i\frac{\alpha_s}{3\pi v^2}\delta^{ab}\sqrt{\kappa}\left(\frac{4\pi\mu^2}{m_t^2}\right)^{\epsilon}\Gamma(1+\epsilon)\Big[(p_1\cdot p_2)g^{\mu\nu}-p_2^\mu p_1^\nu\Big], \\ \sqrt{\kappa} &= \sum_j\left(\frac{3Y_j\lambda_{j12}}{\hat{s}-m_{H_j}^2+im_{H_j}\Gamma(m_{H_j}^2)}\right)-Y_1Y_2,\end{aligned} \tag{2.81}$$

where the factor κ encodes the explicit dependence on the parameters of the model.

The averaged square amplitude will depends only on the Higgs-pair invariant mass $\sqrt{\hat{s}}$, and it takes the following form:

$$\frac{1}{256}\sum_{\text{pol}}\overline{|\mathcal{M}_{\text{LO}}|^2} = \frac{\alpha_s^2}{(4\pi)^2 v^4}\frac{\kappa}{64}\frac{4}{9}\hat{s}^2. \tag{2.82}$$

This result is in complete agreement with the literature [32, 115].

2.3 Projecting onto the Lorentz structure

The necessity of knowing ϵ-expansion terms up to the second order leads to consider a different strategy for the finite top-mass calculation.

Following the same spirit of the calculation of the $gg^* \to H$ amplitude, we can infer the Lorentz structure behind the process and project the amplitude onto them. The form factors thus generated can be expressed in terms of scalar integrals by means of the Passarino-Veltmann decomposition [144].

A process involving two gluons and two scalar particles can be decomposed following the tensor structure

$$T^{\mu\nu} = a_{00}g^{\mu\nu} + \sum_{i,j=1}^{3} a_{ij}p_i^\mu p_j^\nu. \tag{2.83}$$

A relation between the coefficients a_{ij} can be found by imposing the transversality of the on-shell gluons and the Ward identities (Appendix B):

$$\begin{aligned} p_{1,\mu}\epsilon^\mu(p_1) = p_{2,\nu}\epsilon^\nu(p_1) = 0, \\ p_{1,\mu}T^{\mu\nu} = p_{2,\nu}T^{\mu\nu} = 0. \end{aligned} \tag{2.84}$$

These conditions will fix the tensor structure to be generated by two tensors $T_1^{\mu\nu}$ and $T_2^{\mu\nu}$:

$$\begin{aligned} T_1^{\mu\nu} &= g^{\mu\nu} - \frac{p_2^\mu p_1^\nu}{p_1\cdot p_2}, \\ T_2^{\mu\nu} &= g^{\mu\nu} + \frac{p_3^2 p_2^\mu p_1^\nu - 2(p_2\cdot p_3)p_1^\mu p_3^\nu - 2(p_1\cdot p_3)p_2^\mu p_3^\nu + 2(p_1\cdot p_2)p_3^\mu p_3^\nu}{(p_1\cdot p_2)p_T^2} \\ p_T^2 &= \frac{2(p_1\cdot p_3)(p_2\cdot p_3)}{(p_1\cdot p_2)} - p_3^2, \end{aligned} \tag{2.85}$$

which are orthogonal in $d = 4$. However, in d-dimensions the contraction over the tensor indices is

$$T_i^{\mu\nu}T_{i,\mu\nu} = d-2, \qquad T_{1,\mu\nu}T_2^{\mu\nu} = d-4 \tag{2.86}$$

The projectors $P_i^{\mu\nu}$ on a tensor $T_i^{\mu\nu}$ can be found by imposing the following conditions:

$$P_i^{\mu\nu}T_{j,\mu\nu} = \delta_{ij} \quad \Longrightarrow \quad \begin{cases} P_1 = \frac{(d-2)T_1^{\mu\nu} - (d-4)T_2^{\mu\nu}}{4(d-3)} \\ P_2 = \frac{(d-2)T_2^{\mu\nu} - (d-4)T_1^{\mu\nu}}{4(d-3)} \end{cases} \tag{2.87}$$

The expression of the complete LO amplitude of Eq. (2.22) projected into form factors is:

$$\begin{aligned} \mathcal{M}_{LO} &= \epsilon_\mu(p_1)\epsilon_\nu(p_2)(1)(1)(\mathcal{M}_\Delta^{\mu\nu,ab} + \mathcal{M}_\square^{\mu\nu,ab}) \\ &= \epsilon_\mu(p_1)\epsilon_\nu(p_2)\left[\left(F_\Delta^{(0)} + F_1^{(0)}\right)T_1^{\mu\nu} + F_2^{(0)}T_2^{\mu\nu}\right], \end{aligned} \tag{2.88}$$

which can be expressed in terms of scalar integrals. The Passarino-Veltmann decomposition for the

triangles will lead to:

$$\begin{aligned} F_{\Delta}^{(0)} &= -(-ig_s)^2(i)^4\left(2\mathrm{Tr}\left[T^aT^b\right]\right)\frac{i}{(4\pi)^2}\left(\frac{4\pi\mu^2}{m_t^2}\right)^{\epsilon}\Gamma(1+\epsilon)\times \\ &\qquad\times\sum_j^3\left(-iY_j\frac{m_t}{v}\right)\left(-i3\frac{\lambda_{j12}}{v}\right)\left(\frac{1}{\hat{s}-m_{H_j}^2-im_{H_j}\Gamma(m_{H_j}^2)}\right)(m_t\mathcal{A}_{\Delta}^{(0)}) \\ &= -\frac{i\alpha_s}{(4\pi)}\frac{m_t^2}{v^2}\delta^{ab}\left(\frac{4\pi\mu^2}{m_t^2}\right)^{\epsilon}\Gamma(1+\epsilon)\left[\sum_j^3\left(\frac{3Y_j\lambda_{j12}}{\hat{s}-m_{H_j}^2-im_{H_j}\Gamma(m_{H_j}^2)}\right)\right]\mathcal{A}_{\Delta}^{(0)}, \\ &= -\frac{i\alpha_s}{(4\pi)}\frac{m_t^2}{v^2}\delta^{ab}\left(\frac{4\pi\mu^2}{m_t^2}\right)^{\epsilon}\Gamma(1+\epsilon)C_{\Delta}\mathcal{A}_{\Delta}^{(0)}, \end{aligned} \tag{2.89}$$

$$\mathcal{A}_{\Delta}^{(0)} = P_1^{\mu\nu}\int_k\frac{\mathcal{N}_{\mu\nu}}{\mathcal{D}}, \qquad \lambda_3 = \sum_j^3\frac{3Y_j\lambda_{j12}}{\hat{s}-m_{H_j}^2-im_{H_j}\Gamma(m_{H_j}^2)}$$

where the explicit expression for $\mathcal{A}_{\Delta}^{(0)}$ is

$$\mathcal{A}_{\Delta}^{(0)} = 4C_{\epsilon}\left[\frac{(d-4)}{(d-2)}B_0(\hat{s},\overline{m}_t^2) - \left(\frac{4m_t^2}{d-2}-\frac{\hat{s}}{2}\right)C_0(0,0,\hat{s},\overline{m}_t^2)\right]. \tag{2.90}$$

where

$$C_{\epsilon} = \frac{m_t^{-\epsilon}}{\Gamma(1+\epsilon)}. \tag{2.91}$$

The Passarino-Veltmann decomposition for the box form factor lead to a more complex expressions:

$$\begin{aligned} F_j^{(0)} &= -(-ig_s)^2(i)^4\left(2\mathrm{Tr}\left[T^aT^b\right]\right)\frac{i}{(4\pi)^2}\left(\frac{4\pi\mu^2}{m_t^2}\right)^{\epsilon}\Gamma(1+\epsilon)\left(-i\frac{m_t}{v}\right)^2Y_1Y_2\mathcal{A}_j^{(0)} \\ &= -\frac{i\alpha_s}{(4\pi)}\frac{m_t^2}{v^2}Y_1Y_2\delta^{ab}\left(\frac{4\pi\mu^2}{m_t^2}\right)^{\epsilon}\Gamma(1+\epsilon)\mathcal{A}_j^{(0)}, \\ \mathcal{A}_j^{(0)} &= \sum_{l=1}^3 P_j^{\mu\nu}\int_k\frac{\mathcal{N}_{jl,\mu\nu}}{\mathcal{D}_{jl}}, \quad j\in(1,2), \end{aligned} \tag{2.92}$$

where the index j runs over the three independent box diagrams (Figure 2.2).

$$
\begin{aligned}
\mathcal{A}_1^{(0)} = -\Bigg\{ & 4\frac{(d-4)}{(d-2)} B_0(\hat{s},\overline{m}_t^2) - \frac{1}{2(d-3)(m_{H_1}^2 m_{H_2}^2 - \hat{t}\hat{u})} \Bigg[\\
& \frac{C_0\left(0,0,\hat{s},\overline{m}_t^2\right)}{(d-2)} \left[8m_t^2 4(d-3)(m_{H_1}^2 m_{H_2}^2 - t\hat{u}) + (d-4)(d-2)\hat{s}(\hat{t}+\hat{u})(\hat{t}+\hat{u}-8m_t^2)\right] + \\
& + C_0\left(0,m_{H_1}^2,\hat{t},\overline{m}_t^2\right) \frac{\left(\hat{t}-m_{H_1}^2\right)}{\hat{s}} \Big[(d-2)(m_{H_1}^2 m_{H_2}^2 - \hat{t}\hat{u})(m_{H_1}^2 + m_{H_2}^2 - 8m_t^2) + \\
& \qquad + \hat{s}(d-4)(\hat{t}^2 - 8m_t^2 t + m_{H_1}^2 m_{H_2}^2)\Big] + \\
& + C_0\left(0,m_{H_1}^2,\hat{u},\overline{m}_t^2\right) \frac{\left(\hat{u}-m_{H_1}^2\right)}{\hat{s}} \Big[(d-2)(m_{H_1}^2 m_{H_2}^2 - \hat{t}\hat{u})(m_{H_1}^2 + m_{H_2}^2 - 8m_t^2) + \\
& \qquad + \hat{s}(d-4)(\hat{u}^2 - 8m_t^2 \hat{u} + m_{H_1}^2 m_{H_2}^2)\Big] + \\
& + C_0\left(0,\hat{t},m_{H_2}^2,\overline{m}_t^2\right) \frac{\left(\hat{t}-m_{H_2}^2\right)}{\hat{s}} \Big[(d-2)(m_{H_1}^2 m_{H_2}^2 - \hat{t}\hat{u})(m_{H_1}^2 + m_{H_2}^2 - 8m_t^2) + \\
& \qquad + \hat{s}(d-4)(\hat{t}^2 - 8m_t^2 t + m_{H_1}^2 m_{H_2}^2)\Big] + \\
& + C_0\left(0,\hat{u},m_{H_2}^2,\overline{m}_t^2\right) \frac{\left(\hat{u}-m_{H_2}^2\right)}{\hat{s}} \Big[(d-2)(m_{H_1}^2 m_{H_2}^2 - \hat{t}\hat{u})(m_{H_1}^2 + m_{H_2}^2 - 8m_t^2) + \\
& \qquad + \hat{s}(d-4)(\hat{u}^2 - 8m_t^2 \hat{u} + m_{H_1}^2 m_{H_2}^2)\Big] + \\
& - C_0\left(\hat{s},m_{H_1}^2,m_{H_2}^2,\overline{m}_t^2\right)(d-4)\left(\hat{t}+\hat{u}-8m_t^2\right)\left((\hat{t}+\hat{u})^2 - 4m_{H_1}^2 m_{H_2}^2\right) + \\
& - D_0\left(0,0,m_{H_1}^2,m_{H_2}^2,\hat{s},\hat{t},\overline{m}_t^2\right)\Big[4m_t^2[2(d-3)\hat{s}+\hat{t}+\hat{u}-8m_t^2](m_{H_1}^2 m_{H_2}^2 - \hat{t}\hat{u}) + \\
& \qquad + (d-4)\hat{s}t^2(\hat{t}+\hat{u}-8m_t^2)\Big] + \\
& - D_0\left(0,0,m_{H_1}^2,m_{H_2}^2,\hat{s},\hat{u},\overline{m}_t^2\right)\Big[4m_t^2[2(d-3)\hat{s}+\hat{t}+\hat{u}-8m_t^2](m_{H_1}^2 m_{H_2}^2 - \hat{t}\hat{u}) + \\
& \qquad + (d-4)\hat{s}\hat{u}^2(\hat{t}+\hat{u}-8m_t^2)\Big] + \\
& - D_0\left(0,m_{H_1}^2,0,m_{H_2}^2,\hat{t},\hat{u},\overline{m}_t^2\right)\Big[4m_t^2\left(2(d-3)\hat{s}+\hat{t}+\hat{u}-8m_t^2\right)\left(m_{H_1}^2 m_{H_2}^2 - \hat{t}\hat{u}\right) - \\
& \qquad - (d-2)\left(\frac{m_{H_1}^2 + m_{H_2}^2 - 8m_t^2}{\hat{s}}\right)\left(m_{H_1}^2 m_{H_2}^2 - \hat{t}\hat{u}\right)^2 - \\
& \qquad - (d-4)\left(m_{H_1}^2 m_{H_2}^2 - \hat{t}\hat{u}\right)^2\Big]\Bigg]\Bigg\},
\end{aligned}
\tag{2.93}
$$

$$
\begin{aligned}
\mathcal{A}_2^{(0)} = &-\frac{1}{2(d-3)(m_{H_1}^2 m_{H_2}^2 - \hat{t}\hat{u})}\Bigg\{ \\
&- C_0\left(0,0,\hat{s},\overline{m}_t^2\right)\hat{s}\left[4(d-3)(m_{H_1}^2 m_{H_2}^2 - \hat{t}\hat{u}) + (d-2)(\hat{t}+\hat{u})(\hat{t}+\hat{u}-8m_t^2)\right] + \\
&- C_0\left(0,m_{H_1}^2,\hat{t},\overline{m}_t^2\right)\frac{\left(\hat{t}-m_{H_1}^2\right)}{\hat{s}}\Big[(d-4)(m_{H_1}^2 m_{H_2}^2 - \hat{t}\hat{u})(m_{H_1}^2 + m_{H_2}^2 - 8m_t^2) + \\
&\qquad + \hat{s}(d-2)(\hat{t}^2 - 8m_t^2\hat{t} + m_{H_1}^2 m_{H_2}^2)\Big] + \\
&- C_0\left(0,m_{H_1}^2,\hat{u},\overline{m}_t^2\right)\frac{\left(\hat{u}-m_{H_1}^2\right)}{\hat{s}}\Big[(d-4)(m_{H_1}^2 m_{H_2}^2 - \hat{t}\hat{u})(m_{H_1}^2 + m_{H_2}^2 - 8m_t^2) - \\
&\qquad + \hat{s}(d-2)(\hat{u}^2 - 8m_t^2\hat{u} + m_{H_1}^2 m_{H_2}^2)\Big] + \\
&- C_0\left(0,\hat{t},m_{H_2}^2,\overline{m}_t^2\right)\frac{\left(\hat{t}-m_{H_2}^2\right)}{\hat{s}}\Big[(d-4)(m_{H_1}^2 m_{H_2}^2 - \hat{t}\hat{u})(m_{H_1}^2 + m_{H_2}^2 - 8m_t^2) + \\
&\qquad + \hat{s}(d-2)(\hat{t}^2 - 8m_t^2\hat{t} + m_{H_1}^2 m_{H_2}^2)\Big] + \\
&- C_0\left(0,\hat{u},m_{H_2}^2,\overline{m}_t^2\right)\frac{\left(\hat{u}-m_{H_2}^2\right)}{\hat{s}}\Big[(d-4)(m_{H_1}^2 m_{H_2}^2 - \hat{t}\hat{u})(m_{H_1}^2 + m_{H_2}^2 - 8m_t^2) - \\
&\qquad + \hat{s}(d-2)(\hat{u}^2 - 8m_t^2\hat{u} + m_{H_1}^2 m_{H_2}^2)\Big] + \\
&+ C_0\left(\hat{s},m_{H_1}^2,m_{H_2}^2,\overline{m}_t^2\right)(4-d)\left(\hat{t}+\hat{u}-8m_t^2\right)\left[(\hat{t}+\hat{u})^2 - 4(m_{H_1}^2 m_{H_2}^2 - \hat{t}\hat{u})\right] + \\
&+ D_0\left(0,0,m_{H_1}^2,m_{H_2}^2,\hat{s},\hat{t},\overline{m}_t^2\right)\Big[-4m_t^2(\hat{t}+\hat{u}-8m_t^2)(m_{H_1}^2 m_{H_2}^2 - \hat{t}\hat{u}) + \\
&\qquad + (d-4)\hat{s}\hat{t}(m_{H_1}^2 m_{H_2}^2 - \hat{t}\hat{u}) + \\
&\qquad + (d-2)\hat{s}\hat{t}(\hat{t}^2 - 8m_t^2\hat{t} + m_{H_1}^2 m_{H_2})\Big] \\
&- D_0\left(0,0,m_{H_1}^2,m_{H_2}^2,\hat{s},\hat{u},\overline{m}_t^2\right)\Big[-4m_t^2(\hat{t}+\hat{u}-8m_t^2)(m_{H_1}^2 m_{H_2}^2 - \hat{t}\hat{u}) + \\
&\qquad + (d-4)\hat{s}\hat{u}(m_{H_1}^2 m_{H_2}^2 - \hat{t}\hat{u}) + \\
&\qquad + (d-2)\hat{s}\hat{u}(\hat{u}^2 - 8m_t^2\hat{u} + m_{H_1}^2 m_{H_2})\Big] \\
&- D_0\left(0,m_{H_1}^2,0,m_{H_2}^2,\hat{t},\hat{u},\overline{m}_t^2\right)\left(\hat{t}+\hat{u}-8m_t^2\right)\left[(d-4)\frac{(m_{H_1}^2 m_{H_2}^2 - \hat{t}\hat{u})}{\hat{s}} + 4m_t^2\right]\Bigg\}.
\end{aligned}
\tag{2.94}
$$

These expressions are finite in the physical limit $d \to 4$. Details on the notation of these integrals can be found in Appendix E. It is important to keep the d dependence since the counterterms needed to renormalize the UV divergences at NLO develope second order poles, for which terms of the LO form factors up to $O(\epsilon^2)$ are needed.

2.4 Leading-Order Cross section

As anticipated in the previous chapter, the total LO cross section is obtained by integrating the partonic cross section along with the gluon luminosity:

$$
\begin{aligned}
\sigma_{LO}(pp \to gg \to H_1 H_2) &= \int_{\tau_0}^1 d\tau\, \frac{d\mathcal{L}_{gg}}{d\tau}\, \hat{\sigma}_{\rm LO}(\hat{s}=\tau s), \qquad \tau_0 = \frac{(m_{H_1}+m_{H_2})^2}{s} \\
\frac{d\mathcal{L}_{gg}}{d\tau} &= \int_\tau^1 \frac{dx}{x} f_g\left(x,\mu_F\right) f_g\left(\frac{\tau}{x},\mu_F\right).
\end{aligned}
\tag{2.95}
$$

The explicit partonic cross section can be found by squaring Eq. (2.88), summing over the polarization vectors and integrating over the phase space:

$$
\begin{aligned}
\hat{\sigma}_{LO}(\hat{s}) &= C_{\rm flux} C_{\rm sym} \int d{\rm PS}_2 \overline{|\mathcal{M}_{\rm LO}|^2} \\
&= C_{\rm flux} C_{\rm sym} C_{\rm av} \int d{\rm PS}_2 \left[\left|F_\Delta^{(0)} + F_1^{(0)}\right|^2 + \left|F_2^{(0)}\right|^2\right],
\end{aligned}
\tag{2.96}
$$

where C_{av} takes into account the polarization average. More details on the phase space integration can be found in Appendix C. Here, $C_{sym} = 1$, since no identical particles lie in the final state, and $C_{\text{flux}} = \frac{1}{2\hat{s}}$.

$$\begin{aligned}\hat{\sigma}_{LO}(\hat{s}) &= \frac{1}{(2\hat{s})(256)} \int d\text{PS}_2 \left[\left| F_\Delta^{(0)} + F_1^{(0)} \right|^2 + \left| F_2^{(0)} \right|^2 \right] \\ &= \frac{\alpha_s^2}{(4\pi)^2} \frac{G_F^2 m_t^4}{512\pi\hat{s}^2} \int_{t^-}^{t^+} d\hat{t} \left[\left| C_\Delta \mathcal{A}_\Delta^{(0)} + Y_1 Y_2 \mathcal{A}_1^{(0)} \right|^2 + \left| Y_1 Y_2 \mathcal{A}_2^{(0)} \right|^2 \right].\end{aligned} \tag{2.97}$$

The partonic transferred momentum square $\hat{t}$ is related to the scattering angle θ in the following way:

$$\begin{gathered}\hat{t} = -\frac{\hat{s}}{2}(1 - \Sigma - \beta\cos\theta), \qquad \beta = \sqrt{1 - 2\Sigma + \Delta^2} \\ \Sigma = \frac{m_{H_1}^2 + m_{H_2}^2}{\hat{s}}, \qquad \Delta = \frac{m_{H_2}^2 - m_{H_1}^2}{\hat{s}} \\ \hat{t}^\pm = -\frac{\hat{s}}{2}(1 - \Sigma \mp \beta)\end{gathered} \tag{2.98}$$

The LO cross section has been extensively studied in the past decades [115–117], providing a total cross section of the order of $\sigma_{\text{LO}} \approx 10$ fb at $\sqrt{s} = 14$ TeV. As we will see later, the NLO contributions are significant: HTL NLO is known to increase the total cross section of around a factor 2. Finite top-mass effects will decrease those contributions, as discussed in this thesis in Chapter 5.

Chapter 3

NLO Cross Section

In this section, we describe in detail the complete calculation for the virtual cross section $\Delta\hat{\sigma}_{\text{virt}}$ and real cross section $\Delta\hat{\sigma}_{\text{real}}$ for the NLO Higgs-pair production via gluon fusion process. All the diagrams under investigation are represented in Appendix H.

The virtual amplitude is made of two-loop Feynman diagrams, and it gets contributions from three classes of diagrams: box diagrams, one-particle-reducible diagrams and triangle diagrams. The 47 box diagrams are grouped into six topologies: topology 1 consists into top-quark propagators self-energy corrections to the LO boxes; topologies 2 and 3 are the vertex corrections to the LO boxes, containing abelian and non-abelian corrections respectively; topology 4 and 5 are respectively the planar and non-planar double-boxes; topology 6 are the genuine IR divergent two-loop boxes, both planar and non-planar. The one-particle reducible diagrams can be constructed from the QCD Higgs production via gluon fusion process where an external gluon is off-shell. For this amplitude, the analytical expression has been found in Chapter 2. The triangle diagrams are the ones that contain the trilinear Higgs coupling: they represent the diagrams carrying the signal of the detection of a Higgs-pair final state produced by a Higgs-decay, while the other virtual amplitudes represent an irreducible background. The 24 triangle diagrams can be grouped in the same way shown for the boxes: 6 top-quark propagator self-energies corrections to the LO triangle diagrams; 10 vertex corrections to the LO triangle diagrams, both abelian and non-abelian; 4 non-planar triangles and 4 genuine IR contributions. It is important to notice that the number of triangle diagrams of the 2HDM is doubled with respect to the SM, since the off-shell Higgs can be either light (H_1) of heavy (H_2).

The real contribution is made of 43 one-loop diagram where and additional parton is emitted in the final state. There are three channels that contribute to the real cross section: $q\bar{q} \to H_1H_2g$, $qg \to H_1H_2q$ and $gg \to H_1H_2g$. Most of the diagrams of the real amplitude can be build from the LO amplitude where one external gluon is put off-shell. This feature will be relevant in the integration over the phase space, where such subprocess can be integrated separately from the whole process explicitely. The latter channel contains contribution from pentagon diagrams.

The calculation of the box diagrams represents the most challenging part of this thesis, and a dedicated strategy to approach this part of the virtual amplitude will be presented.

3.1 Virtual contributions

Following the same form factor decomposition exploited to calculate the LO diagrams, we can conveniently project the amplitude on the Lorentz structure.

$$\begin{aligned}\mathcal{M}_{\text{NLO}} &= \epsilon_\mu(p_1)\epsilon_\nu(p_2)(1)(1)(\mathcal{M}_\Delta^{\mu\nu,ab} + \mathcal{M}_\square^{\mu\nu,ab}) \\ &= \epsilon_\mu(p_1)\epsilon_\nu(p_2)\left[\left(F_\Delta^{(1)} + F_1^{(1)}\right)T_1^{\mu\nu} + F_2^{(1)}T_2^{\mu\nu}\right]\end{aligned} \tag{3.1}$$

We are interested in the form factors $F_j^{(1)}$ and $F_\Delta^{(1)}$, that represent the core of the square amplitude: the interference of these form factor with the LO ones are the NLO virtual contributions needed for the partonic cross section.

We start considering the form factor $F_\Delta^{(1)}$, which gets contribution from the 12 triangle diagrams. They represent a gauge invariant subset of diagrams which contain the triple Higgs coupling, and the QCD corrections are completely localized into the single off-shell Higgs production, whose contribution is already known in literature to be a global factor multiplying the LO form factor. This last observation tremendously simplifies the estimation of this form factor: $F_\Delta^{(1)}$ is completely determined by the LO form factor $F_\Delta^{(0)}$ and a scalar factor $C(\hat{s})$ that has been implemented in specific routines like `HIGLU` [145]. Therefore, the triangle form factors can be expressed as:

$$F_\Delta^{(1)} = F_\Delta^{(0)} \left[1 + \frac{\alpha_s}{(4\pi)} C(\hat{s})\right]. \tag{3.2}$$

The form factors $F_1^{(1)}$ and $F_2^{(1)}$ get contributions from the double Yukawa gauge subset of diagrams, which constitute the background process for the trilinear Higgs coupling. They constitute an extremely relevant part of the cross section since they are proportional to the top-mass. We can start the calculation factorizing the common factor that occur in each contribution:

$$\begin{aligned} F_j^{(1)} &= -(-ig_s)^4 \left(\frac{i}{(4\pi)^2}\right)^2 \left(-i\frac{m_t}{v}\right)^2 Y_1 Y_2 \left(\frac{4\pi\mu^2}{m_t^2}\right)^{4-d} \Gamma^2(1+\epsilon)\delta^{ab}\mathcal{A}_j^{(1)} \\ &= -\frac{\alpha_s^2}{(4\pi)^2}\frac{m_t^2}{v^2}\delta^{ab} Y_1 Y_2 \left(\frac{4\pi\mu^2}{m_t^2}\right)^{2\epsilon} \frac{\Gamma(1-\epsilon)\Gamma(1+\epsilon)}{\Gamma(1-2\epsilon)}\mathcal{A}_j^{(1)}, \\ \mathcal{A}_j^{(1)} &= C_\epsilon^2 \sum_{l=1}^{N_{\text{diags}}} K_l^{\text{col}} P_j^{\mu\nu} \int_k \frac{\mathcal{N}_{jl,\mu\nu}}{\mathcal{D}_{jl}} = C_\epsilon^2 \sum_{l=1}^{N_{\text{diags}}} K_l^{\text{col}} \widetilde{\mathcal{A}}_{jl}^{(1)}, \quad i \in (1,2). \end{aligned} \tag{3.3}$$

The minus is related to the presence of closed fermion loops in each diagram; the δ^{ab} is a common factor that comes from the color algebra, and the additional factor due to color algebra is encoded into K_j^{col}; at last, the Yukawas coupling represent a global factor. We also used the substitution:

$$\Gamma^2(1+\epsilon) \simeq \frac{\Gamma(1-\epsilon)\Gamma(1+\epsilon)}{\Gamma(1-2\epsilon)} + O(\epsilon^3). \tag{3.4}$$

With this setup, we have completely factorized out the common factors in the form factors $F_j^{(1)}$, and the two-loop contributions lie into $\widetilde{\mathcal{A}}_{jl}^{(1)}$. For simplicity, when we refer to the form factors of single diagrams, we will have in mind $\widetilde{\mathcal{A}}_{jl}^{(1)}$, with diagram number l.

3.1.1 One-particle reducible diagrams

There are eight one-particle-reducible diagrams which contribute both to $F_1^{(1)}$ and $F_2^{(1)}$. These diagrams can be absorbed into a single contribution and its crossing.

The one-particle-reducible diagram under investigation can be evaluated by exploiting the one-loop $gg^* \to H_j$ diagram. Since it is easier to express this contribution starting from the amplitude, we will extract the form factors from the following form:

$\mathcal{M}_{\text{1-PR}} =$ 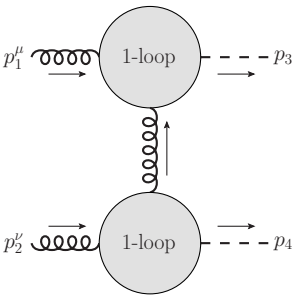

$= \mathcal{M}_{ggH_1}^{\mu\rho,ac}(p_1, p_3 - p_1) \frac{-i\delta^{cd} g_{\rho\sigma}}{(p_3-p_1)^2} \mathcal{M}_{ggH_2}^{\nu\sigma,bd}(p_2, p_1 - p_3).$ (3.5)

Since we already know the analytical expression of the LO QCD single-Higgs production via gluon fusion amplitude, we can use it to infer the form factor of $\mathcal{M}_{1\text{-PR}}$. To simplify the expression, we can make use of the kinematic variables and the momentum conservation:

$$\begin{aligned}\mathcal{M}_{1\text{-PR}} &= -\frac{i\alpha_s^2}{(4\pi)^2}\frac{m_t^2}{v^2}Y_1Y_2\delta^{ab}\frac{16\mathcal{I}(\tau_1,\lambda_t)\mathcal{I}(\tau_2,\lambda_t)}{m_t^2(p_1-p_3)^2}\left[(p_1\cdot q_{31})g^{\mu\sigma}-q_{31}^{\mu}p_1^{\sigma}\right]\left[p_2\cdot q_{31}g^{\nu}{}_{\sigma}-q_{31}^{\nu}p_{2,\sigma}\right]\\ &= -\frac{i\alpha_s^2}{(4\pi)^2}\frac{m_t^2}{v^2}Y_1Y_2\delta^{ab}\frac{16\mathcal{I}(\tau_1,\lambda_t)\mathcal{I}(\tau_2,\lambda_t)}{m_t^2(p_1-p_3)^2}\left[(p_1\cdot p_3)g^{\mu\sigma}-p_3^{\mu}p_1^{\sigma}\right]\left[(p_2\cdot p_4)g^{\nu}{}_{\sigma}-p_4^{\nu}p_{2,\sigma}\right]\\ &= -\frac{i\alpha_s^2}{(4\pi)^2}\frac{m_t^2}{v^2}Y_1Y_2\delta^{ab}\frac{16\mathcal{I}(\tau_1,\lambda_t)\mathcal{I}(\tau_2,\lambda_t)}{m_t^2(p_1-p_3)^2}M^{\mu\nu}, \qquad \text{with}\end{aligned} \tag{3.6}$$

$$M^{\mu\nu} = \left[(p_1\cdot p_3)(p_2\cdot p_4)g^{\mu\nu}-(p_2\cdot p_4)p_3^{\mu}p_1^{\nu}-(p_1\cdot p_3)p_4^{\nu}p_2^{\mu}+(p_1\cdot p_2)p_4^{\nu}p_3^{\mu}\right],$$

where we exploited momentum conservation $p_1+p_2=p_3+p_4$ to obtain a more compact expression.

Note that $\mathcal{I}(\tau_2,\lambda)$ is the function that contains the loop-integrals, and it is already finite: the projection of $\mathcal{M}_{1\text{-PR}}$ onto the Lorentz tensors can be performed in $d=4$. The explicit expressions for the tensors have been shown in Eq. (2.85). Then, we have

$$P_j^{\mu\nu} = \frac{1}{2}T_j^{\mu\nu}. \tag{3.7}$$

The projection of $M_{\mu\nu}$ onto the tensor $T_1\mu\nu$ yields

$$\begin{aligned}P_1^{\mu\nu}M_{\mu\nu} &= \frac{1}{2}\left[(p_1\cdot p_3)(p_2\cdot p_4)+(p_1\cdot p_2)(p_3\cdot p_4)-(p_1\cdot p_4)(p_2\cdot p_3)\right]\\ &= -\frac{1}{2}(p_1-p_3)^2(p_1\cdot p_2),\end{aligned} \tag{3.8}$$

and, recalling structure of the amplitude given in Eq. (3.3), the first form factor for the one-particle-reducible graphs is:

$$\widetilde{\mathcal{A}}_{1,1\text{PR}}^{(1)} = -i\left[4\mathcal{I}(\tau_1,\lambda_t)\mathcal{I}(\tau_2,\lambda_t)+4\mathcal{I}(\tau_1,\lambda_u)\mathcal{I}(\tau_2,\lambda_u)\right]\rho_s, \tag{3.9}$$

where we have taken into account the $\hat{t}\to\hat{u}$ crossed diagram as well.

The second projection of $M_{\mu\nu}$ gives us:

$$\begin{aligned}P_2^{\mu\nu}M_{\mu\nu} &= \frac{1}{2}\left[(p_1\cdot p_3)(p_2\cdot p_4)-(p_1\cdot p_2)(p_3\cdot p_4)+(p_1\cdot p_4)(p_2\cdot p_3)\right]\\ &= -\frac{1}{2}p_T^2(p_1\cdot p_2)\end{aligned} \tag{3.10}$$

and the second form factor is:

$$\widetilde{\mathcal{A}}_{2,1\text{PR}}^{(1)} = -i\left[4\mathcal{I}(\tau_1,\lambda_t)\mathcal{I}(\tau_2,\lambda_t)\left(\frac{\rho_t\rho_u-\rho_1\rho_2}{\rho_t}\right)+4\mathcal{I}(\tau_1,\lambda_u)\mathcal{I}(\tau_2,\lambda_u)\left(\frac{\rho_t\rho_u-\rho_1\rho_2}{\rho_u}\right)\right]. \tag{3.11}$$

These form factors represent the total contribution of the one-particle-reducible diagrams, which is known analytically.

3.1.2 Two-loop box diagrams

The two-loop box diagrams represent the challenging part of this calculation. It involves two-loop diagrams with five scale parameters. Since a reduction strategy is prohibitive for such process, we will approach the calculation with the same spirit we have presented the LO amplitude. In order to show the calculation algorithm we have used, we present its application on two spefic boxes.

Consider the Box 15 (Fig. 3.1). We fix the external momenta convention and a specific change of variables for the Feynman parameters suited on this particular diagram[1]. Of course, Box 15

[1]It is possible to extend this setup for the whole set of diagrams belonging to the same topology, by mixing the internal and external momenta approaches. We can fix a routing for the whole topology and modify the external momenta according to it.

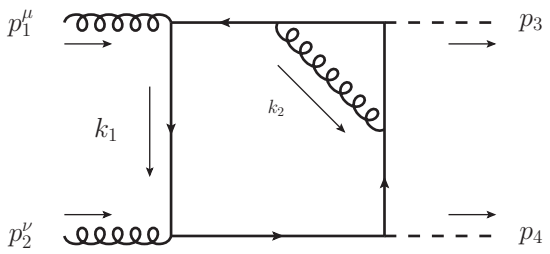

Figure 3.1: *External momenta convention for Box 15.*

contributes both to $F_1^{(1)}$ and $F_2^{(1)}$, but the approach is unified for both projections. The explicit expression for the j-th form factor contribution of Box 15 is:

$$\begin{aligned}
\widetilde{\mathcal{A}}_{j,15} &= (i)^6(-i)I_{j,15} \\
&= iI_{j,15}, \\
I_{j,15} = P_j^{\mu\nu}\int_{k_1,k_2}\frac{1}{k_2^2}\mathrm{Tr}[&\Delta_t(k_1)\gamma_\mu\Delta_t(k_1-p_1)\gamma^\sigma\Delta_t(k_1+k_2-p_1)\Delta_t(k_1+k_2-p_1+p_3)\times \\
&\times\gamma_\sigma\Delta_t(k_1-p_1+p_3)\Delta_t(k_1+p_2)\gamma_\nu], \\
\Delta_t(q) &= \frac{(\not{q}+m_t)}{q^2-m_t^2}
\end{aligned} \tag{3.12}$$

From now on, we will call $I_{j,15}$ as form factor, since it differs from $\hat{\mathcal{A}}_{j,15}^{(1)}$ only by a constant term.

The $I_{j,15}$ has the usual structure of a Feynman integral, but this time we cannot apply a reduction algorithm, since the complexity of the process with the full top-mass dependence makes the reduction a prohibitive task. At the state-of-the-art, the IBP reduction has been made possible by considering the Standard Model Higgs-pair production with fixed ratio between top and Higgs mass. Our aim is to keep the full-m_t dependence along the whole calculation. Hence we follow a numerical strategy, following the same procedure we have done in Section (2.2.2).

After expanding the numerator of Eq. (3.12), it can be written as:

$$I_{j,15} = \int_{k_1,k_2}\frac{N_{j,15}(k_1,k_2)}{D_1D_2D_3D_4D_5D_6D_7} \tag{3.13}$$

where

$$\begin{aligned}
D_1 &= k_1^2 - m_t^2, & D_5 &= (k_1-p_1)^2 - m_t^2, \\
D_2 &= (k_1+k_2-p_1+p_3)^2 - m_t^2, & D_6 &= (k_1+p_2)^2 - m_t^2, \\
D_3 &= (k_1+k_2-p_1)^2 - m_t^2, & D_7 &= k_2^2. \\
D_4 &= (k_1-p_1+p_3)^2 - m_t^2,
\end{aligned} \tag{3.14}$$

The Feynman parametrization of $I_{13}^{\mu\nu}$ have to be applied on each subset of propagator depending

on k_1 and k_2 subsequentially. The quantities defined in

$$I_{j,15} = \Gamma(6) \int_{k_2} \frac{1}{D_7} \int_0^1 d\mathbf{x}_5 \det[J(g_{15})] \int_{k_1} \frac{N_{j,15}(k_1 - q_{15,1}, k_2)}{(k_1^2 - q_{15,1}^2 - M_{15,1}^2)^6},$$

$$g_{15} : \mathcal{C} \to [0,1]^5, \quad g_{15}(\mathbf{x}) = \begin{pmatrix} x_2(1-x_1) \\ (1-x_1)(1-x_2) \\ x_1(1-x_3)x_4 \\ x_1(1-x_3)(1-x_4) \\ x_1 x_3 x_5 \end{pmatrix}, \quad \det[J(g_{15})] = x_1^3(1-x_1)x_3(1-x_3),$$

$$\begin{aligned} q_{15,1} &= (1-x_1)k_2 - (1-x_1x_3)p_1 + p_2 x_1 x_3 x_5 + [(1-x_1)x_2 + x_1(1-x_3)x_4]p_3, \\ M_{15,1}^2 &= m_t^2 + 2(1-x_1)(k_2 \cdot p_1) - 2(1-x_1)x_2(k_2 \cdot p_3) - k_2^2(1-x_1) + \\ &\quad - \hat{t}[(1-x_1)x_2 + x_1(1-x_3)x_4], \end{aligned}$$

$$\begin{aligned} q_{15,1}^2 + M_{15,1}^2 = m_t^2 &- k_2^2(1-x_1)x_1 + 2x_1(1-x_1)k_2 \cdot \{x_3 p_1 - x_3 x_5 p_2 + [x_2 - (1-x_3)x_4]p_3\} - \\ &- \hat{t} x_1 x_3 [(1-x_1)x_2 + x_1(1-x_3)x_4] - \hat{u} x_1 x_3 x_5 [(1-x_1)x_2 + x_1(1-x_3)x_4] - \\ &- s x_1 x_3 x_5 (1 - x_1 x_3) - m_{H_1}^2 [(1-x_1)x_2 + x_1(1-x_3)x_4][1 - (1-x_1)x_2 - x_1(1-x_3)x_4]. \end{aligned} \tag{3.15}$$

The integration over k_1 involves rank-6 tensors, and the following identities are needed for factorizing the tensor structures of solely loop momenta:

$$\begin{aligned} \int_k \frac{k^\mu k^\nu (k^2)^\alpha}{k^2 - M^2} &= \frac{g^{\mu\nu}}{d} \int_k \frac{(k^2)^{\alpha+1}}{k^2 - M^2}, \\ \int_k \frac{k^\mu k^\nu k^\rho k^\sigma (k^2)^\alpha}{k^2 - M^2} &= \frac{g^{\mu\nu}g^{\rho\sigma} + g^{\mu\rho}g^{\nu\sigma} + g^{\mu\sigma}g^{\nu\rho}}{d(d+2)} \int_k \frac{(k^2)^{\alpha+2}}{k^2 - M^2}. \end{aligned} \tag{3.16}$$

The general rank-α tadpole integral has the analytical solution written in Eq. (2.35), and it allows to express the integral in terms of a sum of its rank terms:

$$I_{j,15} = \sum_{\alpha=0}^{3} (-1)^{(6-\alpha)} \frac{\Gamma(6 - \alpha - \frac{d}{2})\Gamma(\alpha + \frac{d}{2})}{\Gamma(\frac{d}{2})} \int_0^1 d\mathbf{x}_5 \det[J(g_{15})] \int_{k_2} \frac{\widetilde{B}_{j,15}^{(\alpha)}(k_2)}{\left(q_{15,1}^2 + M_{15,1}^2\right)^{6-\alpha-\frac{d}{2}} D_7} \tag{3.17}$$

The integral must be parametrize one additional time. Before applying the parametrization, the denominators have to be slightly rearranged, such that they assume the desired form:

$$q_{15,1}^2 + M_{15,1}^2 = -x_1(1-x_1)D_8. \tag{3.18}$$

Hence, the integral we are considering is

$$\int_{k_2} \frac{\widetilde{B}_{j,15}^{(\alpha)}(k_2)}{D_7 D_8^{6-\alpha-\frac{d}{2}}} = \frac{\Gamma(7 - \alpha - \frac{d}{2})}{\Gamma(6 - \alpha - \frac{d}{2})} \int_0^1 dx_6 \int_{k_2} \frac{x_6^{5-\alpha-\frac{d}{2}} \widetilde{B}_{j,15}^{(\alpha)}(k_2)}{(k_2 - q_{15,2}^2 - M_{15,2}^2)^{7-\alpha-\frac{d}{2}}}, \tag{3.19}$$

where

$$g : \mathcal{C} \to [0,1], \quad g(x_6) = \mathbb{1}, \quad \det[J(g)] = 1,$$

$$\begin{aligned}
q_{15,2} &= -x_6\{p_1x_3 + p_2x_3x_5 - p_3[x_2 - (1-x_3)x_4]\},\\
M^2_{15,2} &= \frac{x_6}{x_1(1-x_1)}\{m_t^2 - \hat{t}x_1x_3[(1-x_1)x_2 + x_1(1-x_3)x_4] - \hat{u}x_1x_3x_5[(1-x_1)x_2 + x_1(1-x_3)x_4] -\\
&\quad - sx_1x_3x_5(1-x_1x_3) - m_{H_1}^2[(1-x_1)x_2 + x_1(1-x_3)x_4][1-(1-x_1)x_2 - x_1(1-x_3)x_4]\}.
\end{aligned} \tag{3.20}$$

$$\begin{aligned}
\tilde{\Delta}_{15} =& \frac{x_6}{x_1(1-x_1)}\Big\{1 + \rho_s x_1x_3x_5(1 - x_1x_3 - (1-x_1)x_3x_6) -\\
&- x_1x_3\hat{\rho}_t[(1-x_1)x_2(1-x_6) + (1-x_3)x_4(x_1 + (1-x_1)x_6)] -\\
&- x_1x_3x_5\hat{\rho}_u[(1-x_1)x_2(1-x_6) + (1-x_3)x_4(x_1 + (1-x_1)x_6)] -\\
&- \rho_1\{x_2(1-x_2) - x_1(1-2x_2)[x_2 - (1-x_3)x_5] - x_1[x_1 + (1-x_1)x_6][x_2 - (1-x_3)x_5]^2\}\Big\},\\
&\tilde{\Delta}_{15} = \frac{x_6}{x_1(1-x_1)}\Delta_{15}.
\end{aligned}$$

Finally, after the integration over the loop momentum k_2, the integral $I_{j,15}$ gets the following form:

$$\begin{aligned}
I_{j,15} &= \sum_{\alpha,\beta=0}^{3}(-1)^{(7-\alpha-\beta)}\frac{\Gamma(7-\alpha-\beta-d)\Gamma(\alpha+\frac{d}{2})\Gamma(\beta+\frac{d}{2})}{\Gamma(\frac{d}{2})\Gamma(\frac{d}{2})}\times\\
&\qquad\times\int_0^1 d\mathbf{x}_6\frac{[x_1(1-x_1)]^{1-\beta-\frac{d}{2}}\det[J(g_{15})]B^{(\alpha,\beta)}_{j,15}(\mathbf{x})}{x_6^{2-\beta-\frac{d}{2}}\Delta_{15}^{7-\alpha-\beta-d}}\\
&= \sum_{\alpha,\beta=0}^{3}(-1)^{(7-\alpha-\beta)}\frac{\Gamma(3-\alpha-\beta+2\epsilon)\Gamma(\alpha+\frac{d}{2})\Gamma(\beta+\frac{d}{2})}{\Gamma(\frac{d}{2})\Gamma(\frac{d}{2})}\times\\
&\qquad\times\int_0^1 d\mathbf{x}_6\frac{x_3(1-x_3)x_6^{\beta-\epsilon}B^{(\alpha,\beta)}_{j,15}(\mathbf{x})}{x_1^{\beta-2-\epsilon}(1-x_1)^{\beta-\epsilon}\Delta_{15}^{3-\alpha-\beta+2\epsilon}}.
\end{aligned} \tag{3.21}$$

The Δ_{15} is always positive for $\mathbf{x} \in [0,1]^6 \wedge \rho_i < 4$, hence below the top-mass threshold the tadpole-like mass term is well-defined. Moreover, no divergences can arise from the numerator.

There is still the possibility that $I_{j,15}$ developes a singular behaviour on the boundaries of the integration region. Such terms are the source of the ultraviolet divergences. Since the aim is to arrive at an expression which can be integrated numerically, a particular treatment is needed to single them out.

3.1.3 Extracting the singularities

The singularities of the form factor under consideration comes from an interplay between the integration over the Feynman parameters and the β-rank integrals. The highest possible rank for $I_{j,15}$ is 6, from which follows the constraint $\alpha + \beta \leq 3$.

Divergences arising from the integral comes from the following terms:

$$I_{j,15}|_{\text{div}} \subset \int_0^1 dx_1\frac{B^{(\alpha,\beta)}_{j,15}(x_1)}{x_1^{\beta-2-\epsilon}(1-x_1)^{\beta-\epsilon}} \quad \text{for some } \beta. \tag{3.22}$$

The numerator $B^{(\alpha,\beta)}_{j,15}(x_1)$ has a polynomial dependence on x_1 that may influence the divergency, so it must be taken into account. Hence, $I_{j,15}$ diverges in $x_1 = 0$ for $\beta = 3$ and in $x_1 = 1$ for $\beta \geq 1$.

An additional constraint on diverging β-rank tensors can be set by taking into account the numerator. Purely k_2 tensor integrals have at most $\beta \leq 1$: higher β-rank tensor integrals comes from the shift of the first loop momenta $k_1 \to k_1 - q_{15,1}$. Each shift introduces a $(1-x_1)$ on the numerator,

which cancels against the denominator $(1-x_1)^{\beta-\epsilon}$. This fact implies that the divergences have the following form:

$$I_{j,15}|_{\rm div} \subset \left\{ \int_0^1 dx_1 \frac{f(x_1)}{x_1^{1-\epsilon}}, \int_0^1 dx_1 \frac{f(x_1)}{(1-x_1)^{1-\epsilon}} \right\}. \tag{3.23}$$

and it also ensures that there can not be simultaneous divergences in both the integration boundaries.

The idea for extracting the singular behaviour of the integrals is the so-called *end-point subtraction*: manipulating the numerator, it can be arranged such that it converges faster than the denominator on the boundaries. The strategy is to add a clever zero on the numerator:

$$\begin{aligned} \int_0^1 dx_1 \frac{f(x_1)}{x_1^{1-\epsilon}} &= \int_0^1 dx_1 \frac{f(0)}{x_1^{1-\epsilon}} + \int_0^1 dx_1 \frac{f(x_1)-f(0)}{x_1^{1-\epsilon}} \\ &= \frac{f(0)}{\epsilon} + \int_0^1 dx_1 \frac{f(x_1)-f(0)}{x_1^{1-\epsilon}} \\ \int_0^1 dx_1 \frac{f(x_1)}{(1-x_1)^{1-\epsilon}} &= \frac{f(1)}{\epsilon} + \int_0^1 dx_1 \frac{f(x_1)-f(1)}{x_1^{1-\epsilon}} \end{aligned} \tag{3.24}$$

The converge is facilitated by noticing that $f(x_1)-f(0)$ is the Taylor series of $f(x_1)$ starting from the second term, proportional to x_1.

An additional source of ultraviolet singularities comes from the Gamma function which multiplies Eq. (3.21) when $\alpha+\beta=3$:

$$\Gamma(2\epsilon) = \frac{1}{2}\frac{\Gamma(1+2\epsilon)}{\epsilon}, \tag{3.25}$$

This is a completely independent behaviour, which can happen simultaneously to the poles coming from the integrals ${}_{j,15}|_{\rm div}$. Therefore, $I_{j,15}$ developes second order poles in ϵ, that have to be renormalized. For later purposes, notice that

$$\Gamma(1+2\epsilon) = \frac{\Gamma(1+\epsilon)\Gamma(1-\epsilon)}{\Gamma(1+2\epsilon)} + O(\epsilon^2). \tag{3.26}$$

Once that every ultraviolet divergency has been singled out, the form factor $I_{j,15}$ can be ϵ-expanded and its coefficient will be suitable for a numerical integration.

For kinematic region above the top-mass production threshold ($\rho_i > 4$), threshold singularities enter into the game. These kind of divergences can be avoided by introducing an imaginary mass regulator to the top-mass, which acts as a parameter for the analytical continuation of the form factor:

$$m_t^2 \to m_t^2(1-i\epsilon_t). \tag{3.27}$$

For small values of ϵ_t, the dependence of form factor from ϵ_t is completely negligible, and it ensures the finiteness of its real (and imaginary) part. But, as we can expect, the numerical stability gets lower when ϵ_t decreases. To avoid integrations with high statistic, integration by parts represents a useful tool to decrease the power of the denominator, at the price of increasing the number of integrands. A single integral with $\alpha=\beta=0$ occuring in the form factor can be written as:

$$I_{j,15}^{(n)} = -2\int_0^1 d\mathbf{x}_6 \frac{x_1^2 x_3(1-x_3) B_{j,15}^{(0,0),(n)}(\mathbf{x})}{\Delta_{15}^3}. \tag{3.28}$$

Focusing on a single parameter, Δ_{15} has at most a quadratic dependence on a Feynman parameter, and a linear dependence on x_5 and x_6. Integration by parts on such parameter yields:

$$I_{j,15}^{(n)} \propto \int_0^1 dx_5 \frac{f(x_5)}{(ax_5+b)^3} = \frac{f(0)}{2ab^2} - \frac{f(1)}{2a(a+b)^2} + \frac{1}{2a}\int_0^1 dx_5 \frac{f'(x_5)}{(ax_5+b)^2}. \tag{3.29}$$

Therefore, when a term of a form factor is linear dependent on a Feynman parameters, it is convenient to apply integration by parts such that the power of the denominator decreases. The numerical stability will be significantly increased.

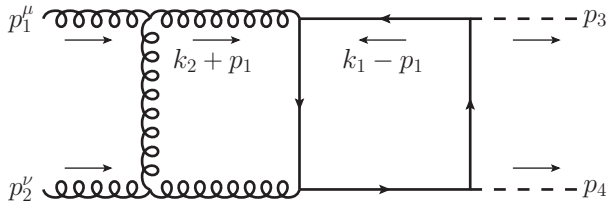

Figure 3.2: *External momenta convention for Box 45.*

3.1.4 Infrared divergences

Infrared divergences come from a particular set of diagrams, belonging to topology 6. They are characterized by the rescattering of a virtual gluon emitted and reabsorbed by the initial state gluons (Fig. 3.2). The explicit expression for the j-th form factor is

$$\begin{aligned}\widetilde{\mathcal{A}}_{j,45} &= -\left(-\frac{3}{2}\delta^{ab}\right)(i)^4(-i)^3\left(-i\frac{m_t}{v}\right)^2 Y_1 Y_2 I_{j,45} \\ &= -i\frac{3}{2}\frac{m_t^2}{v^2}\delta^{ab} Y_1 Y_2 I_{j,45},\end{aligned}$$

$$\begin{aligned}I_{j,45} = P_j^{\mu\nu}\int_{k_1,k_2} &\frac{\lambda_3^{\mu\rho\eta}(p_1,-k_2-p_1,k_2)\lambda_3^{\nu\eta\sigma}(p_2,-k_2,k_2-p_2)}{k_2^2(k_2+p_1)^2(k_2-p_2)^2}\times \\ &\times \mathrm{Tr}\left[\gamma_\rho\Delta_t(k_1-p_1)\Delta_t(k_1-p_1+p_3)\Delta_t(k_1+p_2)\gamma_\sigma\Delta_t(k_1+k_2)\right],\end{aligned} \tag{3.30}$$

$$\lambda_3^{\mu_1\mu_2\mu_3}(p_1,p_2,p_3) = g^{\mu_1\mu_2}(p_1-p_2)^{\mu_3} + g^{\mu_2\mu_3}(p_2-p_3)^{\mu_1} + g^{\mu_1\mu_3}(p_3-p_1)^{\mu_2}$$

Expanding the form factor, it assume the usual structure of a Feynman integral:

$$I_{j,45} = \int_{k_1,k_2}\frac{N_{j,45}(k_1,k_2)}{D_1D_2D_3D_4D_5D_6D_7} \tag{3.31}$$

where

$$\begin{aligned}D_1 &= (k_1-p_1)^2 - m_t^2, & D_5 &= k_2^2, \\ D_2 &= (k_1-p_2)^2 - m_t^2, & D_6 &= (k_2+p_1)^2, \\ D_3 &= (k_1-p_1+p_3)^2 - m_t^2, & D_7 &= (k_2-p_2)^2. \\ D_4 &= (k_1+k_2)^2 - m_t^2,\end{aligned} \tag{3.32}$$

Here, we summarize the quantities coming from the Feynman parametrization:

First integration

$$g_{45,1}:\mathcal{C}\to[0,1]^3,\quad g_{45,1}(\mathbf{x}) = \begin{pmatrix}(1-x_1)\\ x_1(1-x_2)\\ x_1x_2x_3\end{pmatrix},\quad \det[J(g_{45,1})] = x_1^2x_2,$$

$$\begin{aligned}q_{45,1} &= (1-x_1)k_2 - x_1x_2p_1 + x_1(1-x_2)p_2 + x_1x_2x_3p_3, \\ M_{45,1}^2 &= m_t^2 - (1-x_1)k_2^2 - x_1x_2x_3t,\end{aligned} \tag{3.33}$$

$$\begin{aligned}q_{45,1}^2 + M_{45,1}^2 = m_t^2 - x_1(1-x_1)k_2^2 - 2x_1(1-x_1)k_2\cdot\{x_2p_1 - (1-x_2)p_2 - x_2x_3p_3\} - sx_1^2x_2(1-x_2) - \\ - \hat{t}x_1x_2x_3(1-x_1x_2) - \hat{u}x_1^2x_2x_3(1-x_2) - m_{H_1}^2x_1x_2x_3(1-x_1x_2x_3) \\ q_{45,1}^2 + M_{45,1}^2 = -x_1(1-x_1),\end{aligned}$$

hence

$$I_{j,45} = \sum_{\alpha=0}^{3}(-1)^{\frac{d}{2}}\frac{\Gamma(4-\alpha-\frac{d}{2})\Gamma(\alpha+\frac{d}{2})}{\Gamma(\frac{d}{2})}\int_0^1 d\mathbf{x}_3\frac{\det[J(g_{45,1})]}{[x_1(1-x_1)]^{4-\alpha-\frac{d}{2}}}\int_{k_2}\frac{\widetilde{B}_{j,45}^{(\alpha)}(k_2)}{D_5D_8^{4-\alpha-\frac{d}{2}}D_6D_7}. \tag{3.34}$$

Second integration

$$g_{45,2}:\mathcal{C}\to[0,1]^3,\quad g_{45,1}(\mathbf{x})=\begin{pmatrix}x_4x_5\\1-x_5\\(1-x_4)x_5x_6\end{pmatrix},\quad \det[J(g_{45,2})]=(1-x_4)x_5^2,$$

$$\begin{aligned}q_{45,2}&=(1-x_5+x_2x_4x_5)p_1-[x_4x_5(1-x_2)+(1-x_4)x_5x_6]p_2+x_2x_3x_4x_5p_3,\\M^2_{45,2}&=\frac{x_4x_5m_t^2}{x_1(1-x_1)}-s\frac{x_1x_2x_4x_5(1-x_2)}{(1-x_1)}-\hat{t}\frac{x_2x_3x_4x_5(1-x_1x_2)}{(1-x_1)}-\\&\quad-\hat{u}\frac{x_1x_2x_3x_4x_5(1-x_2)}{(1-x_1)}-m^2_{H_1}\frac{x_2x_3x_4x_5(1-x_1x_2x_3)}{(1-x_1)},\end{aligned}$$

$$\begin{aligned}\tilde{\Delta}_{45}=\frac{x_5}{x_1(1-x_1)}\Big\{&x_4-x_1\left[x_1x_2x_4(1-x_2)+(1-x_1)(1-x_5+x_2x_4x_5)\{x_6(1-x_4)+x_4(1-x_2)\}\right]\rho_s-\\&-x_1x_2x_3x_4\left[1-x_1x_2-(1-x_1)(1-x_5+x_2x_4x_5)\right]\hat{\rho}_t-\\&-x_1x_2x_3x_4\left[x_1(1-x_2)+(1-x_1)x_5\{(1-x_4)x_6+x_4(1-x_2)\}\right]\hat{\rho}_u\\&-x_1x_2x_3x_4[1-x_1x_2x_3-(1-x_1)x_2x_3x_4x_5]\rho_1\Big\},\\\tilde{\Delta}_{45}&=\frac{x_5}{x_1(1-x_1)}\Delta_{45},\end{aligned}\tag{3.35}$$

hence

$$\begin{aligned}I_{j,45}=&\sum_{\alpha,\beta=0}^{2}(-1)^{7-\alpha-\beta}\frac{\Gamma(3-\alpha-\beta+2\epsilon)\Gamma(\alpha+\frac{d}{2})\Gamma(\beta+\frac{d}{2})}{\Gamma(\frac{d}{2})\Gamma(\frac{d}{2})}\times\\&\times\int_0^1 d\mathbf{x}_6\left[x_1^{3-\beta+\epsilon}(1-x_1)^{1-\beta+\epsilon}x_2(1-x_4)x_4^{1-\alpha+\epsilon}x_5^{\beta-\epsilon}\right]\frac{B^{(\alpha,\beta)}_{j,45}(\mathbf{x})}{\Delta_{45}^{3-\alpha-\beta+2\epsilon}}.\end{aligned}\tag{3.36}$$

Even if it can develope UV divergences, their treatment is completely analogous to how it has been presented before. Hence, in order to focus on the analysis of the IR divergences, we set $\alpha=0$, $\beta=0$ and factorize the x_4 from $B^{(0,0)}_{j,45}(\mathbf{x})$:

$$I_{j,45}\propto\int_0^1 dx_4\frac{(1-x_4)x_4^{1+\eta+\epsilon}B^{(0,0)}_{j,45}(\hat{\mathbf{x}}_4,x_4)}{(ax_4^2+bx_4+c)^{3+2\epsilon}}.\tag{3.37}$$

where the new index η has been introduce to take into account the x_4 factors coming from the numerator. Moreover, the quadratic dependence on x_4 has been made explicit. Its roots for $c\neq0$ fall outside the integration domain, so we focus on the case where $x_4=0$ and $c=0$. At last, $\hat{\mathbf{x}}_4$ is the set of Feynman parameters with x_4 excluded.

The quadratic formula can be rewritten as

$$\begin{aligned}\Delta_{45}&=ax_4^2+bx_4+c=c(1+r_-x_4)(1+r_+x_4)\\r_\pm&=\frac{b}{2c}\left[1\pm\sqrt{1-\frac{4ac}{b^2}}\right],\end{aligned}\tag{3.38}$$

In the limit of $c\to0$:

$$\begin{aligned}r_+(c)\sim_0\frac{b}{c}\left(1+\frac{ac}{b^2}\right)\sim_0\frac{b}{c}\quad&\Longrightarrow\quad\lim_{c\to0}r_+=\infty,\\r_-(c)\sim_0\frac{b}{c}\left(\frac{ac}{b^2}\right)\sim_0\frac{a}{b}\quad&\Longrightarrow\quad\lim_{c\to0}r_-=\frac{a}{b}.\end{aligned}\tag{3.39}$$

The behaviour of Δ_{45} in the limit of $x_4,c\to0$ is exactly what we can expect from the heavy-top limit of this amplitude. The reason behind this lies in the *universality of the infrared singular structure*. From the form factor in the heavy-top limit, it is known that only the coefficient b and c gives contributions

to the IR structure. Therefore, subtracting the limit we have found for Δ_{45} is equivalent to subtract the heavy-top limit form factor from it.

The explicit subtraction yields:

$$\begin{aligned} I_{j,45} \propto \int_0^1 dx_4\ (1-x_4) x_4^{1+\eta+\epsilon} \left[\frac{B_{j,45}^{(0,0)}(\hat{\mathbf{x}}_4, x_4)}{(a x_4^2 + b x_4 + c)^{3+2\epsilon}} - \frac{B_{j,45}^{(0,0)}(\hat{\mathbf{x}}_4, 0)}{\left[c(1+\frac{b}{c}x_4)\right]^{3+2\epsilon}} \right] + \\ + \frac{B_{j,45}^{(0,0)}(\hat{\mathbf{x}}_4, 0)}{c^{3+2\epsilon}} \int_0^1 dx_4\ x_4^{1+\eta+\epsilon}(1-x_4) \left(1+\frac{b}{c}x_4\right)^{-3-2\epsilon}. \end{aligned} \tag{3.40}$$

The latter integral can be integrated analytically, involving the integral reporesentation of the hypergeometric function

$${}_2F_1(a,b;c;z) = \frac{\Gamma(c)}{\Gamma(b)\Gamma(c-b)} \int_0^1 dt\ t^{b-1}(1-t)^{c-b-1}(1-zt)^{-a}. \tag{3.41}$$

Therefore:

$$\int_0^1 dx_4\ x_4^{1+\eta+\epsilon}(1-x_4)\left(1+\frac{b}{c}x_4\right)^{-3-2\epsilon} = \frac{\Gamma(2+\eta+\epsilon)}{\Gamma(3+\eta+\epsilon)} {}_2F_1\left(3+2\epsilon, 2+\eta+\epsilon; 3+\eta+\epsilon; -\frac{b}{c}\right). \tag{3.42}$$

By using the properties of the hypergeometric function, the divergence can be factorized from ${}_2F_1$:

$$\begin{aligned} {}_2F_1(a,b;c;z) &= \frac{\Gamma(c)\Gamma(b-a)}{\Gamma(b)\Gamma(c-a)}(-z)^{-a}\,{}_2F_1\left(a, 1-c+a; 1-b+a; z^{-1}\right) \\ &= \frac{\Gamma(c)\Gamma(a-b)}{\Gamma(a)\Gamma(c-b)}(-z)^{-b}\,{}_2F_1\left(b, 1-c+b; 1-a+b; z^{-1}\right) \\ &\Downarrow \\ \frac{\Gamma(2+\eta+\epsilon)}{\Gamma(3+\eta+\epsilon)} {}_2F_1\left(3+2\epsilon, 2+\eta+\epsilon; 3+\eta+\epsilon; -\frac{b}{c}\right) &= \\ &= \frac{\Gamma(-1+\eta-\epsilon)}{\Gamma(\eta-\epsilon)}\left(\frac{c}{b}\right)^{3+2\epsilon} {}_2F_1\left(3+2\epsilon, 1-\eta+\epsilon; 2-\eta+\epsilon; -\frac{c}{b}\right) \\ &\quad + \frac{\Gamma(2+\eta+\epsilon)\Gamma(1-\eta+\epsilon)}{\Gamma(3+2\epsilon)}\left(\frac{c}{b}\right)^{2+\eta+\epsilon} {}_2F_1\left(2+\eta+\epsilon, 0; \eta-\epsilon; -\frac{c}{b}\right) \\ &= \frac{\Gamma(\eta-1-\epsilon)}{\Gamma(\eta-\epsilon)}\left(\frac{c}{b}\right)^{3+2\epsilon} {}_2F_1\left(3+2\epsilon, 1-\eta+\epsilon; 2-\eta+\epsilon; -\frac{c}{b}\right) \\ &\quad + \frac{\Gamma(2+\eta+\epsilon)\Gamma(1-\eta+\epsilon)}{\Gamma(3+2\epsilon)}\left(\frac{c}{b}\right)^{2+\eta+\epsilon} \end{aligned} \tag{3.43}$$

where ${}_2F_1(a,0;c;z) = 1$. Now, the expression is suitable for an analysis of the pole structure. Plugging Eq. (3.43) in Eq. (3.40):

$$\begin{aligned} I_{j,45}|_{\text{poles}} \propto B_{j,45}^{(0,0)}(\hat{\mathbf{x}}_4, 0) \Bigg\{ \frac{\Gamma(\eta-1-\epsilon)}{\Gamma(\eta-\epsilon)} \frac{{}_2F_1\left(3+2\epsilon, 1-\eta+\epsilon; 2-\eta+\epsilon; -\frac{c}{b}\right)}{b^{3+2\epsilon}} + \\ + \frac{\Gamma(2+\eta+\epsilon)\Gamma(1-\eta+\epsilon)}{\Gamma(3+2\epsilon)}\left(\frac{1}{b^{2+\eta+\epsilon}c^{1-\eta+\epsilon}}\right)\Bigg\}. \end{aligned} \tag{3.44}$$

Since the hypergeometric functions in Eq. (3.44) are regular for every η, the singular behaviour of the form factor shows up for $\eta = 0$ and $\eta = 1$. The latter case is a pole generated by a gamma function, for which no subtraction is needed. The $\eta = 0$ divergence lies into the term $c^{-1-\epsilon}$, for which the end point subtraction is needed. For this, we need the explicit expression of c, which is

$$c = -\rho_s x_1(1-x_1)(1-x_5)x_6. \tag{3.45}$$

The divergent part of $\alpha = \beta = 0$ added of the form factor $I_{j,45}$ is:

$$I_{j,45}|_{\text{poles}} \subset (-1)^{-\epsilon}\Gamma(2+\epsilon)\Gamma(1+\epsilon) \int_0^1 d\hat{\mathbf{x}}_4 \left(\frac{x_1^2 x_2 x_5^{-\epsilon}\rho_s^{-1-\epsilon}}{(1-x_5)^{1+\epsilon}x_6^{1+\epsilon}}\right) \frac{B_{j,45}^{(0,0)}(\hat{\mathbf{x}}_4, 0)}{b^{2+\epsilon}}, \tag{3.46}$$

which developes poles for $x_5 = 1$ and $x_6 = 0$. Since these two divergent behaviours can happen simultaneosly, a proper subtraction term is needed:

$$\int_0^1 dx_5 dx_6 \frac{f(x_5,x_6)}{(1-x_5)^{1+\epsilon}x_6^{1+\epsilon}} = \int_0^1 dx_5 dx_6 \frac{f(x_5,x_6)-f(1,x_6)-f(x_5,0)+f(1,0)}{(1-x_5)^{1+\epsilon}x_6^{1+\epsilon}} + \frac{f(1,0)}{\epsilon^2} - \\ - \frac{1}{\epsilon}\left[\int_0^1 dx_6 \frac{f(1,x_6)-f(1,0)}{x_6^{1+\epsilon}} + \int_0^1 dx_5 \frac{f(x_5,0)-f(1,0)}{(1-x_5)^{1+\epsilon}}\right]. \tag{3.47}$$

Therefore, Box 45 can have ϵ^{-2} and ϵ^{-1} poles. It can be shown that an additional pole can arise from the remaining dependence from x_1, x_2 or x_3, but it is properly canceled after summing all the diagrams belonging to topology 6.

Finally, after having end point-subtracted all the divergences arising from the loop integrals, the finite part is numerically integrable and, with the help of the integration by parts technique, the integration results are stable.

3.2 Renormalisation

The NLO form factor have a divergent behaviour for the physical limit $\epsilon \to 0$. From the previous section we know that both ultraviolet and infrared divergence appear in the amplitude, leading to a definite pole structure that we have singled out explicitely.

Infrared divergences cancels against the real corrections. Ultraviolet divergences have to be renormalized by chosing a renormalisation scale and scheme and adding the proper counterterms. Different choices of renormalisation will not affect the physically relevant quantities if we were able to perform the calculation at every order of the perturbative expansion. Since we truncate the series at the NLO, we end up with a renormalisation-dependent result. The variation of the renormalisation scales and schemes are useful to estimate the theoretical uncertainties arising from the truncation of the perturbative series expansion.

Every parameter involved in this calculation have a running with respect of the energy of the process. These quantities are the strong coupling constant $\alpha_s = \alpha_s(\mu_R)$ and the top-quark mass $m_t = m_t(\mu_R)$.

In the whole calculation, we have consider these parameters as bare quantities ($\alpha_{s,0}$ and $m_{t,0}$), which lead to the usual divergent behaviour of higher order contributions. An UV finite result can be achieved by considering the renormalized quantities:

$$\begin{aligned} m_{t,0} &= m_t + \delta m_t + O(\delta m_t^2) \\ \alpha_{s,0} &= \alpha_s + \delta\alpha_s + O(\delta\alpha_s^2). \end{aligned} \tag{3.48}$$

The counterterms δm_t and $\delta\alpha_s$ have scheme and scale dependence, but all schemes are employed in such a way that the UV poles at NLO are canceled against them. Different schemes will only lead to different finite parts.

We start by considering the *on-shell (OS) renormalisation scheme* for δm_t: the quark propagator can be writteng as

$$iG_{2,0}(\not{p}) = \frac{i}{\not{p} - m_{t,0} + \Sigma_2(\not{p})} = iZ_2 G_{2,R}(\not{p}). \tag{3.49}$$

The term $\Sigma_2(\not{p})$ contains all the one-loop contributions to the quark propagator. We also have explicitely shown the relation between the bare and renormalized propagator.

Expanding the renormalisation constant up to the first order:

$$\begin{aligned} iG_{2,R}(\not{p}) &= \frac{i}{\not{p} - m_{t,0} + \Sigma_2(\not{p}) + \delta_2\not{p} - \delta_2 m_{t,0}} \\ &= \frac{i}{\not{p} - m_t - \delta m_t m_t + \Sigma_2(\not{p}) + \delta_2\not{p} - \delta_2 m_t} \\ &= \frac{i}{\not{p} - m_t + \Sigma_R(\not{p})}. \end{aligned} \tag{3.50}$$

The on-shell condition for the top mass is translated into the two following conditions:

$$\Sigma_R(m_t) = 0, \qquad \frac{d}{d\not{p}}\Sigma_R(\not{p})\bigg|_{\not{p}=m_t} = 0 \tag{3.51}$$

which fix the conditions on δm_t and δ_2. Since we are only interested in the mass counterterm, its explicit expression in the OS scheme is

$$\frac{\delta m_t}{m_t} = \frac{\alpha_s}{(4\pi)}\Gamma(1+\epsilon)\left(\frac{4\pi\mu^2}{m_t^2}\right)^{\epsilon}\left(\frac{1}{\epsilon}+\frac{4}{3}\right). \tag{3.52}$$

The OS scheme counterterm has a finite part. Later on, the $\overline{\text{MS}}$ counterterm will be considered, therefore its expression is

$$\frac{\delta\overline{m}_t}{\overline{m}_t(\mu_t)} = \frac{\alpha_s}{(4\pi)}\Gamma(1+\epsilon)\left(\frac{4\pi\mu^2}{\mu_t^2}\right)^{\epsilon}\frac{1}{\epsilon}. \tag{3.53}$$

For the α_s counterterms we will use the $\overline{\text{MS}}$ scheme. It is designed to cancel only the poles, without generating a finite part. The expression for the 5 flavour massless QCD is:

$$\frac{\delta\alpha_s}{\alpha_s} = \frac{\alpha_s}{(4\pi)}\left(\frac{4\pi\mu^2}{\mu_R^2}\right)^{\epsilon}\Gamma(1+\epsilon)\left[-\frac{11C_A-2(N_f)}{3\epsilon}\right]. \tag{3.54}$$

Since we have to add the divergences due to the top-quark involved in the calculation, the $\overline{\text{MS}}$ scheme is modified by adding the missing pole:

$$\frac{\delta\alpha_s}{\alpha_s} = \frac{\alpha_s}{(4\pi)}\left(\frac{4\pi\mu^2}{\mu_R^2}\right)^{\epsilon}\Gamma(1+\epsilon)\left[-\frac{11C_A-2(N_f+1)}{3\epsilon}\right]. \tag{3.55}$$

However, the $\overline{\text{MS}}$ scheme is mass-independent scheme. The remaining top-mass dependent terms depends on μ_R logarithmly, like $\log\frac{m_t^2}{\mu_R^2}$. This might break the perturbative expansion, since these logarithm can be arbitrarily high. The way to avoid such logarithms is *to decouple the top-quark mass from the running of* α_s. This procedure leads to the following counterterm:

$$\frac{\delta\alpha_s}{\alpha_s} = \frac{\alpha_s}{(4\pi)}\left(\frac{4\pi\mu^2}{\mu_R^2}\right)^{\epsilon}\Gamma(1+\epsilon)\left[-\left(\frac{11C_A-2(N_f+1)}{3}\right)\frac{1}{\epsilon}+\frac{2}{3}\log\left(\frac{\mu_R^2}{m_t^2}\right)\right]. \tag{3.56}$$

where the finite term milds the logarithmic behaviour introduced by the $\overline{\text{MS}}$ scheme.

Since we have considered the input parameters of the calculation to be "bare", we have to express the form factors in terms of the running variables:

$$\begin{aligned}
F_j(\alpha_{s,0}, m_{t,0}) &\simeq F_j^{(0)}(\alpha_s+\delta\alpha_s, m_t-\delta m_t) + F_j^{(1)}(\alpha_s, m_t) \\
&= F_j^{(0)}(\alpha_s, m_t) + \delta\alpha_s\frac{\partial F_j^{(0)}}{\partial\alpha_s}(\alpha_s, m_t) - \delta m_t\frac{\partial F_j^{(0)}}{\partial m_t}(\alpha_s, m_t) + F_j^{(1)}(\alpha_s, m_t) \\
&= F_j^{(0)}(\alpha_s, m_t) + \frac{\delta\alpha_s}{\alpha_s}F_j^{(0)}(\alpha_s, m_t) - 2\frac{\delta m_t}{m_t}m_t^2\frac{\partial F_j^{(0)}}{\partial m_t^2}(\alpha_s, m_t) + F_j^{(1)}(\alpha_s, m_t) \\
&= F_j^{(0)}(\alpha_s, m_t) + F_j^{(CT,1)}(\alpha_s, m_t) + F_j^{(1)}(\alpha_s, m_t) \\
&= F_j^{(0)}(\alpha_s, m_t) + \overline{F}_j^{(1)}(\alpha_s, m_t)
\end{aligned} \tag{3.57}$$

where the linearity of $F_j^{(0)}(\alpha_s)$ with respect to α_s has been exploited. The terms proportional to $\delta\alpha_s$ and δm_t contribute to the NLO form factors, and they correspond exactly to the UV counterterms that cancel the UV divergences of the NLO form factor shown in the previous section.

The $\delta\alpha_s$ counterterm has been prepared to cancel the divergences that appear as external vacuum polarization diagrams. This contribution can be found by considering the vacuum polarization diagram (Appendix G) in the on-shell limit. It gives the following contribution

$$\Pi_{m_t}(0)F_j^{(0)}(\alpha_s) = -\frac{\alpha_s}{(4\pi)}\left(\frac{4\pi\mu^2}{m_t^2}\right)^{\epsilon}\Gamma(1+\epsilon)\frac{2}{3}\frac{1}{\epsilon}F_j, \tag{3.58}$$

and calling $\delta_{\alpha_s} = \Pi_{m_t}(0) + \frac{\delta\alpha_s}{\alpha_s}$, the complete counterterm for α_s is

$$\begin{aligned}\delta_{\alpha_s} F_j^{(0)}(\alpha_s, m_t) &= -\frac{\alpha_s}{(4\pi)} \left(\frac{4\pi\mu^2}{\mu_R^2}\right)^{\epsilon} \Gamma(1+\epsilon) \left(\frac{11C_A - 2N_f}{3}\right) \frac{1}{\epsilon} F_j^{(0)}(\alpha_s, m_t) \\ &\Downarrow \\ \delta_{\alpha_s} F_j^{(0)}(\alpha_s, m_t) &= \frac{i\alpha_s^2}{(4\pi)^2} \frac{m_t^2}{v^2} \left(\frac{4\pi\mu^2}{m_t^2}\right)^{2\epsilon} \Gamma^2(1+\epsilon) \left(\frac{11C_A - 2N_f}{3}\right) \left[\frac{1}{\epsilon} - \log\left(\frac{\mu_R^2}{m_t^2}\right)\right] \mathcal{A}_j.\end{aligned} \tag{3.59}$$

Moving the discussion on the top-mass counterterm, we set

$$\delta_{m_t} F_j^{(0)}(\alpha_s, m_t) = -2\frac{\delta m_t}{m_t} m_t^2 \frac{\partial F_j^{(0)}}{\partial m_t^2}(\alpha_s, m_t). \tag{3.60}$$

Therefore:

$$\delta_{m_t} F_j^{(0)}(\alpha_s, m_t) = 2\frac{i\alpha_s^2}{(4\pi)^2} \frac{m_t^2}{v^2} Y_1 Y_2 \Gamma^2(1+\epsilon) \left(\frac{4\pi\mu^2}{m_t^2}\right)^{2\epsilon} \left(\frac{1}{\epsilon} + \frac{4}{3}\right) \left[(1-\epsilon)\mathcal{A}_j + \frac{\partial \mathcal{A}_j}{\partial m_t^2}\right], \tag{3.61}$$

and

$$F_j^{(CT,1)}(\alpha_s, m_t) = \delta_{\alpha_s} F_j^{(0)}(\alpha_s, m_t) + \delta_{m_t} F_j^{(0)}(\alpha_s, m_t). \tag{3.62}$$

Notice that the form factor of the $\overline{\text{MS}}$ counterterm is the same, but without the factor 4/3 coming from the OS part.

Since we know the heavy-top limit behaviour of the form factors at NLO, we can exploit the universality of the infrared structure to build a term containing the infrared singularities. The NLO form factor in the heavy-top limit can be written as,

$$F_{\text{HTL},j}^{(1)}(\alpha_s) = \frac{\alpha_s}{(4\pi)} \frac{\Gamma(1-\epsilon)}{\Gamma(1-2\epsilon)} \left(\frac{4\pi\mu^2}{-\hat{s}}\right)^{\epsilon} \left[\frac{6}{\epsilon^2} + \frac{11C_A - 2N_f}{3\epsilon} \left(\frac{\mu^2}{-\hat{s}}\right)^{-\epsilon} - 11 + \pi^2\right] F_j^{(0)}(\alpha_s), \tag{3.63}$$

and summing it with the α_s counterterm, we get

$$\begin{aligned}\delta_{\text{IR}} F_j(\alpha_s, m_t) = -\frac{i\alpha_s^2}{(4\pi)^2} \frac{m_t^2}{v^2} Y_1 Y_2 \frac{\Gamma(1-\epsilon)\Gamma(1+\epsilon)}{\Gamma(1-2\epsilon)} \left(\frac{4\pi\mu^2}{-\hat{s}}\right)^{2\epsilon} \times \\ \times \left[\frac{12}{\epsilon^2} - \frac{6}{\epsilon}\log\left(\frac{-\hat{s}}{m_t^2}\right) + 3\log^2\left(\frac{-\hat{s}}{m_t^2}\right) - 22 + 2\pi^2\right] \mathcal{A}_j^{(0)},\end{aligned} \tag{3.64}$$

where we used the following replacement:

$$\Gamma^2(1+\epsilon) \to \frac{\Gamma(1-\epsilon)\Gamma(1+\epsilon)}{\Gamma(1-2\epsilon)}. \tag{3.65}$$

This term encodes the infrared behaviour that is common both for the HTL form factor and the full m_t dependent one.

This last term, once added to the virtual form factor $F_j^{(1)}$, will lead to a finite result which can be integrated without having any numerical issue, like instability or diverging behaviour.

3.3 Virtual cross-section

The form factors of the partonic process $gg \to H_1 H_2$ at NLO QCD get contributions from the box diagrams, one-particle-reducible diagrams and triangle diagrams. Each diagram has been processed by the calculation strategy presented in the previous section, and the form factors $F_j^{(1)}$ are found by summing the whole set of diagrams.

The UV finite virtual contributions to the cross section $\overline{F}_j^{(1)}$ is still IR divergent. However, the IR divergent part of the form factor with the full m_t dependence is the same as the HTL one. This fact implies the following:

$$\frac{\overline{F}_j^{(1)}}{F_j^{(0)}} - \frac{\overline{F}_{\text{HTL},j}^{(1)}}{F_{\text{HTL},j}^{(0)}} \sim O(\epsilon^0), \tag{3.66}$$

which means that they have the same IR pole structure. Hence, we define

$$R_j^{(1)} = \frac{\overline{F}_j^{(1)}}{F_j^{(0)}} - \frac{\overline{F}_{\mathrm{HTL},j}^{(1)}}{F_{\mathrm{HTL},j}^{(0)}} \propto \frac{\overline{\mathcal{A}}_j^{(1)}}{\mathcal{A}_j^{(0)}} - \frac{\overline{\mathcal{A}}_{\mathrm{HTL},j}^{(1)}}{\mathcal{A}_{\mathrm{HTL},j}^{(0)}}, \tag{3.67}$$

such that the virtual cross section split into a finite part $d\hat{\sigma}_{\mathrm{virt}}^{\mathrm{fin}}$ and divergent one $d\hat{\sigma}_{\mathrm{HTL}}$:

$$\hat{\sigma}_{\mathrm{virt}} = \hat{\sigma}_{\mathrm{virt}}^{\mathrm{fin}} + \hat{\sigma}_{\mathrm{HTL}}. \tag{3.68}$$

Therefore, the virtual cross section is:

$$\begin{aligned}
\hat{\sigma}_{\mathrm{virt}} &= C_{\mathrm{sym}} C_{\mathrm{flux}} 2\mathrm{Re} \int d\mathrm{PS}_2 C_{\mathrm{av}} \left[\left(C_\Delta F_\Delta^{(0)} + F_1^{(0)} \right)^* \left(C_\Delta F_\Delta^{(1)} + F_1^{(1)} \right) + F_2^{*(0)} F_2^{(1)} \right], \\
\hat{\sigma}_{\mathrm{virt}}^{\mathrm{fin}} &= \frac{\alpha_s^3}{(4\pi)^3} \frac{G_F^2 m_t^4}{32\pi\hat{s}^2} \int_{t^-}^{t^+} dt \Bigg[\left| C_\Delta \mathcal{A}_\Delta^{(0)} \right|^2 R_\Delta^{(1)} + Y_1^2 Y_2^2 \left| \mathcal{A}_1^{(0)} \right|^2 R_1^{(1)} + Y_1^2 Y_2^2 \left| \mathcal{A}_2^{(0)} \right|^2 R_2^{(1)} \\
&\qquad + Y_1 Y_2 C_\Delta \mathcal{A}_\Delta^{*(0)} \mathcal{A}_1^{(0)} \left(R_\Delta^{(1)} + R_1^{(1)} \right) \Bigg], \\
\hat{\sigma}_{\mathrm{HTL}} &= \frac{\alpha_s^3}{(4\pi)^3} \frac{G_F^2 m_t^4}{32\pi\hat{s}^2} \int_{t^-}^{t^+} dt \Bigg[\left| C_\Delta \mathcal{A}_\Delta^{(0)} \right|^2 \frac{\overline{\mathcal{A}}_{\mathrm{HTL},\Delta}^{(1)}}{\mathcal{A}_{\mathrm{HTL},\Delta}^{(0)}} + Y_1^2 Y_2^2 \left| \mathcal{A}_1^{(0)} \right|^2 \frac{\overline{\mathcal{A}}_{\mathrm{HTL},1}^{(1)}}{\mathcal{A}_{\mathrm{HTL},1}^{(0)}} + Y_1^2 Y_2^2 \left| \mathcal{A}_2^{(0)} \right|^2 \frac{\overline{\mathcal{A}}_{\mathrm{HTL},2}^{(1)}}{\mathcal{A}_{\mathrm{HTL},2}^{(0)}} \\
&\qquad + Y_1 Y_2 C_\Delta \mathcal{A}_\Delta^{*(0)} \mathcal{A}_1^{(0)} \left(\frac{\overline{\mathcal{A}}_{\mathrm{HTL},\Delta}^{(1)}}{\mathcal{A}_{\mathrm{HTL},\Delta}^{(0)}} + \frac{\overline{\mathcal{A}}_{\mathrm{HTL},1}^{(1)}}{\mathcal{A}_{\mathrm{HTL},1}^{(0)}} \right) \Bigg].
\end{aligned} \tag{3.69}$$

It is useful to define also the ratio between the NLO and LO partonic cross section:

$$C_{\mathrm{mass}} = 2\mathrm{Re} \left[\frac{\hat{\sigma}_{\mathrm{virt}}^{\mathrm{fin}}}{\hat{\sigma}_{\mathrm{LO}}} \right], \tag{3.70}$$

such that the virtual contribution to the NLO cross section becomes:

$$\Delta\sigma_{\mathrm{virt}} = \frac{\alpha_s}{4\pi} \int_{\tau_0}^1 \frac{d\mathcal{L}_{gg}}{d\tau} \hat{\sigma}_{\mathrm{LO}}(\tau s) C_{\mathrm{mass}}. \tag{3.71}$$

Let us stress that $\hat{\sigma}_{\mathrm{HTL}}$ contains IR divergences, but they will cancel against the real corrections, once that the phase space integration is performed.

3.4 Real corrections

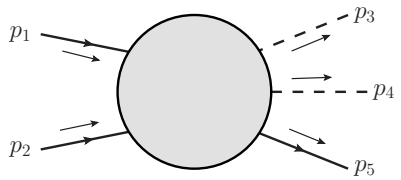

Figure 3.3: *Kinematics convention for the real amplitude*

The missing piece to complete the calculation is the real contribution cross section. They consist of one-loop diagrams with an additional emission of a massless parton in the final state. The integration over the sphase space will lead to IR divergences which will cancel against σ_{HTL} coming from the virtual correction.

There are three channels for the real corrections: $q\bar{q} \to H_1 H_2 g$, $qg \to H_1 H_2 q$ and $gg \to H_1 H_2 g$. The number of diagrams amounts to 43, up to fermion-loop flow. For the first two channel, only triangle and box integrals are needed. For the last channel, there are pentagon integrals involved.

Finding the Lorentz projector is not an easy task: for the $gg \to H_1 H_2 g$ there are 14 form factors, and building 14 orthogonal tensors and projector can introduce overcomplexity into this calculation. The approach exploited is to immediately square the total amplitude, without performing any projection onto their tensor structure.

Let us introduce the actual calculation by considering the following kinematics (Figure 3.3):

$$\begin{gathered} s = 2p_1 \cdot p_2, \qquad t = -2p_1 \cdot p_5, \qquad u = -2p_2 \cdot p_5 \\ s + t + u = (p_3 + p_4)^2 = Q^2 \end{gathered} \tag{3.72}$$

3.4.1 Heavy top limit

To illustrate how the procedure has been done, let us focus on the $q\bar{q} \to H_1 H_2 g$ process in the heavy-top limit. This process can be build from the effective verteces we have calculated in the Chapter 2.

The triangle contributions are:

$$\begin{aligned} \mathcal{M}_\Delta = \bar{v}(p_2)\gamma^\sigma u(p_1)\epsilon^*_\mu(p_5)(-ig_s)\frac{ig_{\sigma\rho}}{(p_1+p_2)^2}\sum_j Y_j \frac{i}{(p_1+p_2-p_5)^2 - m^2_{H_j}}\left(-i3\frac{\lambda_{j12}}{v}\right)\times \\ \times\left[\frac{i\alpha_s}{3\pi v}\delta^{ab}\left(\frac{4\pi\mu^2}{m_t^2}\right)^\epsilon \Gamma(1+\epsilon)[p_5\cdot(p_1+p_2)g^{\mu\rho} - p_5^\rho(p_1+p_2)^\mu]\right] \end{aligned} \tag{3.73}$$

$$= \bar{v}(p_2)\gamma_\rho u(p_1)\epsilon^*_\mu(p_5)\frac{i\alpha_s g_s}{3\pi v^2}\delta^{ab}\sum_j \frac{3Y_j\lambda_{j12}}{Q^2 - m^2_{H_j}}\left(\frac{4\pi\mu^2}{m_t^2}\right)^\epsilon \Gamma(1+\epsilon)\left[\frac{1}{2}\frac{(t+u)}{s}g^{\mu\rho} + \frac{p_5^\rho(p_1+p_2)^\mu}{s}\right],$$

and the box one is

$$\begin{aligned} \mathcal{M}_\Box = \bar{v}(p_2)\gamma^\sigma u(p_1)\epsilon^*_\mu(p_5)(-ig_s)\frac{ig_{\sigma\rho}}{(p_1+p_2)^2}\times \\ \times\left[-i\frac{\alpha_s}{3\pi v^2}Y_1Y_2\delta^{ab}\left(\frac{4\pi\mu^2}{m_t^2}\right)^\epsilon \Gamma(1+\epsilon)[p_5\cdot(p_1+p_2)g^{\mu\rho} - p_5^\rho(p_1+p_2)^\mu]\right] \\ = -\bar{v}(p_2)\gamma_\rho u(p_1)\epsilon^*_\mu(p_5)\frac{i\alpha_s g_s}{3\pi v^2}\delta^{ab}\left(\frac{4\pi\mu^2}{m_t^2}\right)^\epsilon \Gamma(1+\epsilon)\left[\frac{1}{2}\frac{(t+u)}{s}g^{\mu\rho} + \frac{p_5^\rho(p_1+p_2)^\mu}{s}\right]. \end{aligned} \tag{3.74}$$

Already with this contribution we can find a feature that happens to all the channels: there is a common factor related with the couplings that can be factorized. Let us define

$$\sqrt{\kappa} = \sum_j \left(\frac{3Y_j\lambda_{j12}}{Q^2 - m^2_{H_j}}\right) - Y_1Y_2. \tag{3.75}$$

Summing these contributions we arrive at the following amplitude:

$$\mathcal{M}_{q\bar{q}} = \bar{v}(p_2)\gamma_\rho u(p_1)\epsilon^*_\mu(p_5)\sqrt{\kappa}\frac{i\alpha_s g_s}{3\pi v^2}\delta^{ab}\left(\frac{4\pi\mu^2}{m_t^2}\right)^\epsilon \Gamma(1+\epsilon)\left[\frac{1}{2}\frac{(t+u)}{s}g^{\mu\rho} + \frac{p_5^\rho(p_1+p_2)^\mu}{s}\right], \tag{3.76}$$

Let us evaluate the square amplitude explicitely. Since the polarization sum gives a factor[2] $\epsilon_\mu(p_5)\epsilon_\nu(p_5) \to -g_{\mu\nu}$, and the spin sum gives us

$$\sum_{\text{spins}} \bar{u}(p_1)\gamma_\sigma v(p_2)\bar{v}(p_2)\gamma_\rho u(p_1) = \text{Tr}\left[\not{p}_2\gamma_\rho\not{p}_1\gamma_\sigma\right] \tag{3.77}$$

the square of the tensor structure yields:

$$\begin{aligned} -\text{Tr}\left[\not{p}_2\gamma_\rho\not{p}_1\gamma_\sigma\right]\left[\frac{1}{2}\frac{(t+u)}{s}g^{\mu\rho} + \frac{p_5^\rho(p_1+p_2)^\mu}{s}\right]\left[\frac{1}{2}\frac{(t+u)}{s}g_\mu{}^\sigma + \frac{p_5^\sigma(p_1+p_2)_\mu}{s}\right] = \\ -\left[\frac{1}{4}\frac{(t+u)^2}{s^2}\text{Tr}\left[\not{p}_2\gamma^\sigma\not{p}_1\gamma_\sigma\right] + \text{Tr}\left[\not{p}_2\not{p}_5\not{p}_1\not{p}_5\right]\right] = \frac{(d-2)}{2}\frac{(t+u)^2}{s} - 2tu = \\ = \frac{t^2+u^2}{s} - \epsilon\frac{(t+u)^2}{s}. \end{aligned} \tag{3.78}$$

[2]Since there is only one external on-shell gluon, the Ward identities grant that we can neglect the "axial gauge" added.

Therefore, the averaged square amplitude is

$$\sum_{\text{pol,spin}} \overline{\left|\mathcal{M}_{q\bar{q}}^{\text{HTL}}\right|}^2 = \kappa \frac{8\alpha_s^3 G_F^2}{81\pi} \left(\frac{4\pi\mu^2}{m_t^2}\right)^{2\epsilon} \Gamma^2(1+\epsilon) \left[\frac{t^2+u^2}{s} - \epsilon\frac{(t+u)^2}{s}\right], \tag{3.79}$$

For completeness, the HTL square amplitude for the other channels is

$$\begin{aligned}
\sum_{\text{pol,spin}} \overline{\left|\mathcal{M}_{qg}^{\text{HTL}}\right|}^2 &= \kappa \frac{\alpha_s^3 G_F^2}{27\pi} \left(\frac{4\pi\mu^2}{m_t^2}\right)^{2\epsilon} \frac{\Gamma^2(1+\epsilon)}{(1-\epsilon)} \left[\frac{s^2+u^2}{-t} + \epsilon\frac{(s+u)^2}{t}\right], \\
\sum_{\text{pol,spin}} \overline{\left|\mathcal{M}_{gg}^{\text{HTL}}\right|}^2 &= \kappa \frac{\alpha_s^3 G_F^2}{12\pi} \left(\frac{4\pi\mu^2}{m_t^2}\right)^{2\epsilon} \frac{\Gamma^2(1+\epsilon)}{(1-\epsilon)^2} \left[(1-\epsilon)\frac{s^4+t^4+u^4+Q^8}{stu} - 4\epsilon Q^2\right].
\end{aligned} \tag{3.80}$$

A little sidenote on the gluon-gluon channel. The sum over the polarization must be done on the *physical* polarization states: the QED Ward identities does not hold anymore for QCD contribution with triple gluon interaction. Therefore, the sum have to be restricted on the physical polarization, meaning

$$\sum_{\text{pol}} \epsilon_\mu^*(p_1)\epsilon_\mu(p_1) = -g^{\mu\nu} + \frac{p_1^\mu p_r^\nu + p_1^\nu p_r^\mu}{p_1 \cdot p_r} \tag{3.81}$$

where p_r is an auxiliary momentum such that $p_1 \cdot p_r \neq 0$. If one would like to not introduce these additional tensors, the external ghost contributions have to be considered. The square amplitude of these contribution will cancel the unphysical degrees of freedom contributions from the gluon-gluon amplitude. We have chosen to sum over the physical polarization, and to introduce the additional tensor. Further details for the polarization sum are presented in Appendix C.

3.4.2 Full m_t dependence

The full top-mass dependence contribution requires the evaluation of one-loop Feynman integrals. Since the Feynman integrals appearing into the real correction are at most of rank-5, we have applyed the Passarino-Veltmann reduction to the amplitude and, in a second step, we have prepared the square amplitude to be integrated over the phase space.

We chose to not reduce the tensor integrals down to scalar ones. This strategy is aimed at obtaining manageable expressions and localize the possible numerical instabilities due to small Gram determinants. Such instabilities are more severe in the gluon-gluon channel because of the presence of the pentagon integrals involving many Gram determinants. We have prefered to decompose the integrals in the internal momenta basis (see Chapter 2) in order to keep the length of the expressions under control. The coefficients of the Lorentz tensors are Feynman integrals of rank up to 4, and they depend only on the scale parameters, i.e. the kinematic invariants and the masses. We will not present the calculation in details, since it has been completely automatized, and the procedure we exploited is in the end completely analogous to the LO amplitude one. We present the strategy with the $q\bar{q}$ channel as an example:

$$\mathcal{M}_{q\bar{q},j} = \frac{ig_s^3}{(4\pi)^2} \frac{m_t^2}{v^2} \delta^{ab} \left(\frac{4\pi\mu^2}{m_t^2}\right)^{\epsilon} \Gamma(1+\epsilon) \bar{v}(p_2)\gamma_\nu u(p_1)\epsilon_\mu^*(p_5) K_j \mathcal{A}_j^{\mu\nu}, \tag{3.82}$$

where K_j encodes the normalization, remaining factors and the dependence on λ_{j12}, Y_1 and $\mathcal{A}_j^{\mu\nu}$ is the j-th Feynman integral. Taking as an example the gauge-invariant triangle subprocesses, the internal momenta basis for $\mathcal{A}_j^{\mu\nu}$ reads

$$\begin{aligned}
\mathcal{A}_j^{\mu\nu} &= \sum_{ik} C_{00i} g^{(\mu\nu} q_i^{\rho)} q_{k,\rho} + \sum_{iklm} q_i^\mu q_k^\nu (q_l \cdot q_m) C_{ikl} \\
&+ C_{00} g^{\mu\nu} + \sum_{ik} q_i^\mu q_k^\nu C_{ik} + \sum_{ik} q_i^\mu q_k^\nu C_i \\
&+ g^{\mu\nu} \sum_i B_{00}^{(i)} + \sum_{ik} q_i^\mu q_k^\nu B_{ij} + g^{\mu\nu} A_{00},
\end{aligned} \tag{3.83}$$

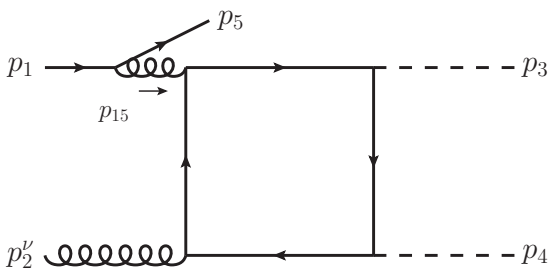

Figure 3.4: *Infrared divergent diagram belonging to the qg channel.*

where q_j are linear combinations of the external momenta. More details on the structure of the coefficients of Eq. (3.83) can be found in Appendix D.

In the actual calculation, this expression drastically simplifies with massless particles, Ward identities, same propagator mass in the loops, and in general with low number of scales. The coefficient of the tensors are known using standard recursion relations. Once that the projection of the amplitude on the internal momenta basis has been applied, we take the modulus square of the result and the spin, polarization and color average. This constitute the building block for the real cross section.

The generation of the amplitude and the PV reduction has been performed within `Mathematica`. We have used the libraries `FeynArts` [146] and `FeynCalc` [147] to perform the algebra and the square amplitude function, that later on has been exported in `Fortran` subroutines. The evaluation of the tensor integrals has been left to the package `LoopTools` [146], which has a `Mathematica` interface that has been extremely useful for internal crosschecks.

3.5 Real cross section

The square amplitude is now ready to be integrated over the 3-particle phase space. As for the virtual correction, we split the real corrections in a finite term and a IR divergent part:

$$\frac{|\mathcal{M}_{ij}|^2}{|\mathcal{M}_{\rm LO}|^2} - \frac{|\mathcal{M}_{ij}^{\rm HTL}|^2}{|\mathcal{M}_{\rm LO}^{\rm HTL}|^2} = (\text{IR finite}). \tag{3.84}$$

which expresses the fact that the ratio between the matrix elements and the Born term of the square amplitude and its heavy top-quark limit have the same IR structure.

Defining the IR safe quantity

$$R^{(r)} = \frac{|\mathcal{M}_{ij}|^2}{|\mathcal{M}_{\rm LO}|^2} - \frac{|\mathcal{M}_{ij}^{\rm HTL}|^2}{|\mathcal{M}_{\rm LO}^{\rm HTL}|^2}, \tag{3.85}$$

it is possible to express the cross section as the sum of IR divergent and IR safe terms. Therefore, the partonic real cross section $\hat{\sigma}_{ij}(\hat{s})$:

$$\begin{aligned}\hat{\sigma}_{ij}(\hat{s}) &= \int d\text{PS}_3 \left[|\mathcal{M}_{\rm LO}|^2 R^{(r)} + |\mathcal{M}_{\rm LO}|^2 \frac{|\mathcal{M}_{ij}^{\rm HTL}|^2}{|\mathcal{M}_{\rm LO}^{\rm HTL}|^2} \right] \\ &= \int d\text{PS}_3 \left[|\mathcal{M}_{\rm LO}|^2 R^{(r)} \right] + \hat{\sigma}_{ij}^{\rm HTL}\end{aligned} \tag{3.86}$$

The $\hat{\sigma}_{ij}^{\rm HTL}$ will cancel against the $\hat{\sigma}_{\rm HTL}$ coming from the calculation of the virtual cross section.

It is necessary a clarification on the meaning of the ratio $R^{(r)}$. Since the two processes do not share the same number of external legs (and so the kinematic invariants), the 3-particle phase space have to be projected over the 2-particle one. The IR behaviour comes from the soft and collinear limit related to the emission of the additional parton since each parton is massless. From this simple argument follows that the pentagon topologies can not generate IR divergences: the massive loop prevents both limits to happen.

Therefore, we can give an explicit example by looking at the diagram in Figure 3.4. The structure of this diagram shows an explicit factorization into a quark-flow and a LO box diagram with an off-shell gluon. The LO box represents the $2 \to 2$ subprocess onto which the 3-particle phase space needs to be projected. The factorization reads

$$\mathcal{M}_{qg} \supset \frac{f^{\mu}(p_1; p_5)}{p_{15}^2} \mathcal{M}_{\mathrm{LO}}^{\mu\nu}(\tilde{p}_{15}, \tilde{p}_2; \tilde{p}_3, \tilde{p}_4), \tag{3.87}$$

where the tilded momenta have to be defined, according to the embedding we are aiming at. They will be linear combinations of the external on-shell momenta with the coefficients depending on the kinematics.

For the incoming particles, the transformed momenta are

$$\begin{aligned} \widetilde{p}_{15}^{\mu} &= \frac{p_1 \cdot p_2 - p_1 \cdot p_5 - p_2 \cdot p_5}{p_1 \cdot p_2}\, p_1^{\mu} = \frac{Q^2}{\hat{s}}\, p_1^{\mu}, \\ \widetilde{p}_2^{\nu} &= p_2^{\nu}, \end{aligned} \tag{3.88}$$

and the outgoing ones are

$$\begin{aligned} \widetilde{p}_{3,4}^{\mu} &= p_{3,4}^{\mu} - \frac{2p_{3,4} \cdot (K + \widetilde{K})}{(K + \widetilde{K})^2}(K + \widetilde{K})^{\mu} + \frac{2p_{3,4} \cdot K}{K^2}\widetilde{K}^{\mu}, \\ K^{\mu} &= p_1^{\mu} + p_2^{\mu} - p_5^{\mu}, \qquad \widetilde{K}^{\mu} = \widetilde{p}_1^{\mu} + \widetilde{p}_2^{\mu}. \end{aligned} \tag{3.89}$$

Further details on the factorization of the $2 \to 2$ phase space out of the $2 \to 3$ can be found in Ref. [51].

The phase space integral has been built such that the LO factor factorizes (Appendix C.2), and the integral over the 2-particle phase space factor can be performed, obtaining the following result

$$\begin{aligned} \hat{\sigma}_{ij}(\hat{s}) &= \int d\mathrm{PS}_3 \, \left[|\mathcal{M}_{\mathrm{LO}}|^2 R^{(r)} \right] + \hat{\sigma}_{ij}^{\mathrm{HTL}} \\ &= \frac{\alpha_s}{(4\pi)} \int_{\frac{\tau_0}{\tau}}^1 \frac{dz}{z} \hat{\sigma}_{\mathrm{LO}}(z\hat{s}) D_{ij}(z). \end{aligned} \tag{3.90}$$

The coefficients D_{ij} have the following structure:

$$\begin{aligned} D_{q\bar{q}}(z) &= d_{q\bar{q}}(z), \\ D_{qg}(z) &= d_{qg}(z) - \frac{z}{2\epsilon}\frac{\Gamma(1-\epsilon)}{\Gamma(1-2\epsilon)}\left(\frac{4\pi\mu_R^2}{\mu_F^2}\right)^{\epsilon} P_{qg}(z), \\ D_{gg}(z) &= d_{gg}(z) - \frac{z}{\epsilon}\frac{\Gamma(1-\epsilon)}{\Gamma(1-2\epsilon)}\left(\frac{4\pi\mu_R^2}{\mu_F^2}\right)^{\epsilon} P_{gg}(z) + 6[1 - z^4 + (1-z)^4]\left[\frac{\log(1-z)}{1-z}\right]_+. \end{aligned} \tag{3.91}$$

The coefficients $d_{ij}(z)$ contain the top-mass dependence of the partonic cross section, and they have an already-known heavy-top limit:

$$\begin{aligned} d_{q\bar{q}}(z) &\xrightarrow{m_t \to \infty} \frac{32}{27}(1-z)^3, \\ d_{qg}(z) &\xrightarrow{m_t \to \infty} \frac{2}{3}z^2 - (1-z)^2, \\ d_{gg}(z) &\xrightarrow{m_t \to \infty} -\frac{11}{2}(1-z). \end{aligned} \tag{3.92}$$

The functions $P_{ij}(z)$ are the Altarelli-Parisi splitting functions:

$$\begin{aligned} P_{qg} &= \frac{4}{3}\frac{1 + (1-z)^2}{z}, \\ P_{gg} &= 6\left\{\left[\frac{1}{1-z}\right]_+ + \frac{1}{z} - 2 + z(1-z)\right\} + \delta(1-z)\frac{33 - 2N_f}{6}, \end{aligned} \tag{3.93}$$

and

$$[f(z)]_+ = f(z) - \delta(1-z)\int_0^1 dz' f(z') \tag{3.94}$$

is the plus prescription.

Notice that there are still some residual collinear initial-state singularities located into the coefficient of the splitting function. These divergences can be absorbed into a redefinition of the *bare* NLO gluon densities located into the gluon luminosity.

We would need a term that cancels against the initial-state singularities acting as:

$$\hat{\sigma}_{R,ij}(\mu_F) = \hat{\sigma}_{ij} - \frac{\alpha_s}{(4\pi)}\int dz \left[-\frac{1}{2\epsilon}\frac{\Gamma(1-\epsilon)}{\Gamma(1-2\epsilon)}\left(\frac{4\pi\mu_R^2}{\mu_F^2}\right)^{\epsilon} P_{ij}(z) + K_{ij,\mathrm{FS}}(z)\right]\hat{\sigma}_{\mathrm{LO}}(z\hat{s}), \tag{3.95}$$

where $K_{ij,\mathrm{FS}}(z)$ is an arbitrary function of z. It is possible to show that such term arises from the renormalisation of the partonic distribution functions. Recalling that

$$\sigma_{ij} = \int_0^1 dx_1 dx_2 \; f_{g,0}(x_1) f_{g,0}(x_2)\hat{\sigma}_{ij}(x_1 x_2 s), \tag{3.96}$$

the bare gluon densities can be renormalized in the following way

$$\begin{aligned} f_{g,0}(x) = f_g(x,\mu_F) &+ \frac{\alpha_s}{(4\pi)}\left[-\frac{1}{2\epsilon}\frac{\Gamma(1-\epsilon)}{\Gamma(1-2\epsilon)}\left(\frac{4\pi\mu_R^2}{\mu_F^2}\right)^{\epsilon} P_{gg} + K_{gg,\mathrm{FS}}\right]\otimes f_g(x,\mu_F) \\ &+ \frac{\alpha_s}{(4\pi)}\left[-\frac{1}{2\epsilon}\frac{\Gamma(1-\epsilon)}{\Gamma(1-2\epsilon)}\left(\frac{4\pi\mu_R^2}{\mu_F^2}\right)^{\epsilon} P_{gq} + K_{gq,\mathrm{FS}}\right]\otimes f_q(x,\mu_F), \end{aligned} \tag{3.97}$$

where

$$f\otimes g(x,\mu_F) = \int_x^1 \frac{dz}{z} f(z,\mu_F) g\left(\frac{x}{z},\mu_F\right). \tag{3.98}$$

The functions $K_{ij,\mathrm{FS}}(z)$, as for the UV renormalisation, are completely arbitrary. They can be fixed by chosing a renormalisation scheme. The simplest choice will be the $\overline{\mathrm{MS}}$ scheme, which sets these functions to zero everywhere: $K_{ij,\mathrm{FS}} = 0$. Therefore:

$$f_{g,0}(x) = f_g(x,\mu_F) + \frac{\alpha_s}{(4\pi)}\frac{1}{2\epsilon}\frac{\Gamma(1-\epsilon)}{\Gamma(1-2\epsilon)}\left(\frac{4\pi\mu_R^2}{\mu_F^2}\right)^{\epsilon}\left[P_{gg}\otimes f_g(x,\mu_F) + P_{gq}\otimes f_q(x,\mu_F)\right] \tag{3.99}$$

Finally, the finite parts of the real contribution to the cross sections are

$$\begin{aligned} \Delta\sigma_{gg} &= \frac{\alpha_s}{(4\pi)}\int_{\tau_0}^1 d\tau \sum_q \frac{d\mathcal{L}_{gg}}{d\tau}\int_{\frac{\tau_0}{\tau}}^1 \frac{dz}{z}\hat{\sigma}_{\mathrm{LO}}(z\tau s) C_{q\bar{q}}(z), \\ \Delta\sigma_{gq} &= \frac{\alpha_s}{(4\pi)}\int_{\tau_0}^1 d\tau \sum_{q,\bar{q}} \frac{d\mathcal{L}_{gg}}{d\tau}\int_{\frac{\tau_0}{\tau}}^1 \frac{dz}{z}\hat{\sigma}_{\mathrm{LO}}(z\tau s) C_{gq}(z), \\ \Delta\sigma_{gg} &= \frac{\alpha_s}{(4\pi)}\int_{\tau_0}^1 d\tau \frac{d\mathcal{L}_{gg}}{d\tau}\int_{\frac{\tau_0}{\tau}}^1 \frac{dz}{z}\hat{\sigma}_{\mathrm{LO}}(z\tau s) C_{gg}(z), \end{aligned} \tag{3.100}$$

where

$$\begin{aligned} C_{q\bar{q}}(z) &= d_{q\bar{q}}(z), \\ C_{gq}(z) &= d_{gq}(z) - \frac{z}{2}P_{gq}(z)\log\left(\frac{\mu_F^2}{\tau s(1-z)^2}\right), \\ C_{gg}(z) &= d_{gg}(z) - zP_{gg}(z)\log\left(\frac{\mu_F^2}{\tau s}\right) + 6[1+z^4+(1-z)^4]\left[\frac{\log(1-z)}{1-z}\right]_+. \end{aligned} \tag{3.101}$$

Chapter 4

Numerical integration

In this Chapter, the technicalities related to the numerical integration of the quantities found in Chapter 3 are presented. The main ingredients are: the Vegas algorithm [148] for Monte Carlo integrations and the Richardson extrapolation [149]. The Vegas algorithm is an adaptive method to drastically decrease the numerical error on the integration, keeping the statistic under control, based on the importance sampling. For each form factor, a relative statistical error of 10^{-5} has been required.

The Richardson extrapolation is a method to obtain the value of a function in a specific point by a proper linear combination of its values on a set of points. It will be used for extract the differential cross section for the narrow width top quark, also known as the "limit" $\epsilon_t \to 0$ (defined in the previous Chapter). In this context, it can be seen as the analytical continuation of the differential distribution in $\epsilon_t = 0$. The convergence of the Richardson extrapolation will be discussed in details, and some explicit example will be presented.

The Richardson extrapolation, together with the trapezoidal rule, will be also exploit in the integration of the differential distribution in order to obtain the total NLO cross section.

4.1 Integrating the Box form factors

The procedure described in Section (3.1) provides form factors depending on the Feynman parameters, the Higgs-pair invariant mass $\hat{s}$ and the transferred momentum square $\hat{t}$, the top-quark mass m_t and the two Higgs masses m_{H_1} and m_{H_2}. The threshold singularities corresponding to the production of two on-shell top quarks have been regularized by introducing the regulator ϵ_t.

In the context of this work, the virtual differential cross section is the sum of the interferences of the the LO and NLO form factors:

$$\tau \frac{d\sigma}{ds}(\tau s) = \hat{\sigma}^{\text{fin}}_{\text{virt}}(\hat{s}) = \hat{\sigma}_{\Delta\Delta} + \hat{\sigma}_{1\Delta} + \sum_k^{\text{diags}} \hat{\sigma}^{(k)}_{\Delta 1} + \sum_k^{\text{diags}} \hat{\sigma}^{(k)}_{11} + \sum_k^{\text{diags}} \hat{\sigma}^{(k)}_{22}, \tag{4.1}$$

where $\hat{\sigma}^{(k)}_{ij}$ is partial partonic cross sections constituted by the interference of the (total) LO form factor i with the NLO form factor j belonging to the diagram k. Each term has the following structure

$$\hat{\sigma}^{(k)}_{ij}(\hat{s}, \epsilon_t) = \int_{\hat{t}^-}^{\hat{t}^+} d\hat{t} \int_0^1 d\mathbf{x}\; I^{(k)}_{ij}(\hat{t}, \mathbf{x}), \tag{4.2}$$

where $\mathbf{x}$ are the Feynman parameters and $t^\pm$ is defined in Appendix C. Each integral depends on at most 6 parameters.

The integration over $\mathbf{x}$ and $\hat{t}$ leads to logarithmic divergences which only cancel in the total sum; this will lead to strong numerical instabilities. It is possible to mild the behaviour of the integral on

the boundaries. Notice first that

$$\begin{gathered}\frac{d\hat{t}}{\hat{s}p_T^2} = \frac{d\hat{t}}{(\hat{t}^+ - \hat{t}^-)}\left[\frac{1}{(\hat{t}-\hat{t}^-)} + \frac{1}{(\hat{u}-\hat{t}^-)}\right] \\ \Downarrow \\ \int_{\hat{t}^-}^{\hat{t}^+} d\hat{t} I_{ij}^{(k)}(\hat{t},\mathbf{x}) = \hat{s}p_T^2 \int_{\hat{t}^-}^{\hat{t}^+} \frac{d\hat{t}}{(\hat{t}-\hat{t}^-)} \frac{I_{ij}^{(k)}(\hat{t},\mathbf{x}) + I_{ij}^{(k)}(\hat{u},\mathbf{x})}{(\hat{t}^+ - \hat{t}^-)},\end{gathered} \tag{4.3}$$

where we exploited the relation between the kinematic variables $\hat{s}+\hat{t}+\hat{u} = m_{H_1}^2 + m_{H_2}^2$ (see Appendix F). To avoid numerical instabilities, the following change of variable will smooth the convergence of the integral:

$$y = \log \frac{\hat{t}-\hat{t}^-}{m_t^2}, \qquad dy = \frac{d\hat{t}}{\hat{t}-\hat{t}^-} \tag{4.4}$$

and the integral becomes

$$\int_{\hat{t}^-}^{\hat{t}^+} d\hat{t}\ I_{ij}^{(k)}(\hat{t},\mathbf{x}) = \hat{s}p_T^2 \int_{y^-}^{y^+} \frac{dy}{(\hat{t}^+ - \hat{t}^-)} \left[I_{ij}^{(k)}(\hat{t}(y),\mathbf{x}) + I_{ij}^{(k)}(\hat{u}(y),\mathbf{x})\right]. \tag{4.5}$$

We have to regulate the behaviour of the boundaries since applying the change of variables of Eq. (4.4), the lower boundary becomes $y^- = -\infty$. Introducing a technical cut-off regulator $\bar{\epsilon}$ it reads

$$\hat{t}^- \to \hat{t}^- + (\hat{t}^+ - \hat{t}^-)\bar{\epsilon}, \quad \hat{t}^+ \to \hat{t}^+ - (\hat{t}^+ - \hat{t}^-)\bar{\epsilon}. \tag{4.6}$$

After the change of variable $\hat{t} = \hat{t}(y)$, the integration boundaries become

$$y^- = \log \frac{(\hat{t}^+ - \hat{t}^-)\bar{\epsilon}}{m_t^2}, \qquad y^+ = \log \frac{(\hat{t}^+ - \hat{t}^-)(1-\bar{\epsilon})}{m_t^2}. \tag{4.7}$$

A last change of variable will turn the integration domain into the unit segment:

$$y = y^- + (y^+ - y^-)x_7, \qquad dy = \log \frac{1-\bar{\epsilon}}{\bar{\epsilon}} \tag{4.8}$$

so that it can be treated like an additional Feynman parameter. The integral become:

$$\hat{\sigma}_{ij}^{(k)}(\hat{s},\epsilon_t) = sp_T^2 \left(\log \frac{1-\bar{\epsilon}}{\bar{\epsilon}}\right) \int_0^1 d\mathbf{x} dx_7 \ \left[I_{ij}^{(k)}(\hat{t}(x_7),\mathbf{x}) + I_{ij}^{(k)}(\hat{u}(x_7),\mathbf{x})\right], \tag{4.9}$$

A regulator can be introduced for each Feynman parameter, in the same manner as depicted in Eq. (4.6), and by introducing a cut-off regulator $\bar{\epsilon_i}$ for each parameter x_i, the convergence is even better. This brings the contribution to the total cross section to become

$$\begin{gathered}x_i \to \bar{\epsilon_i} + (1-2\bar{\epsilon_i})x_i, \qquad dx_i \to (1-2\bar{\epsilon_i})x_i \\ \Downarrow \\ \hat{\sigma}_{ij}^{(k)}(\hat{s},\epsilon_t) = sp_T^2 \left(\log \frac{1-\bar{\epsilon}}{\bar{\epsilon}}\right) \prod_i^6 (1-2\epsilon_i) \int_0^1 d\mathbf{x} dx_7 \ \left[I_{ij}^{(k)}(\hat{t}(x_7),\mathbf{x}) + I_{ij}^{(k)}(\hat{u}(x_7),\mathbf{x})\right].\end{gathered} \tag{4.10}$$

The numerical integration of each $\hat{\sigma}_{ij}^{(k)}(\hat{s})$ has been performed using a Monte Carlo integration method based on the VEGAS algorithm: it reduces the integration error through the *importance sampling*, aimed at optimizing the sampling in the integration region that contributes the most to the integral. Consider a function $f(x)$ that has to be integrate between 0 and 1. The numerical integration can be written as

$$\int_0^1 f(x)dx \approx \frac{1}{N}\sum_n^N f(x_n) = \mathrm{E}(f), \tag{4.11}$$

where x_n comes from an uniform distribution. If x_n comes from a distribution $g(x)$ instead, it is possible to show that

$$\int_0^1 f(x)dx \approx \frac{1}{N}\sum_n^N \frac{f(x_n)}{g(x_n)} = \mathrm{E}_g\left(f\right), \qquad \mathrm{Var}_g(f) = \mathrm{E}\left(\frac{f^2}{g^2}\right) - \mathrm{E}^2\left(\frac{f}{g}\right), \tag{4.12}$$

where g must respect the following requirement

$$\mathrm{E}\left(f\right) = \mathrm{E}_g\left(f\right). \tag{4.13}$$

It is easy to show that:

$$g(x) = \frac{|f(x)|}{\int_0^1 f(x)dx} \implies \mathrm{Var}_g(f) = 0. \tag{4.14}$$

Since it is not possible to choose this distribution at numerical level, it will provide a simple way to reduce drastically the error by concentrating the distribution around the bulk of $f(x)$. Therefore, preliminar integration of $f(x)$ with uniform distribution will provide an estimation of the distribution $g(x)$ that will be used to integrate $f(x)$ with an incresed precision. The process can be iterated as far as the aimed precision has not been reach.

The VEGAS algorithm has been implemented into the `Fortran` code XVEGAS, and it has been run into the computer cluster, which granted us access to 4000 CPUs for a maximum runtime of individual jobs of 96 hours.

The energy bins chosen for the integration runs from $270 - 2500$ GeV, with a scan of 25 GeV around the theshold region ($\hat{s} = 245$ GeV for $m_t = 172.5$ GeV in the OS scheme), 50 in the region $500 - 1500$ GeV and two additional bins in the tails at 2000 GeV and 2500 GeV. For all integrations, the Feynman parameters regulator have been fixed to $\bar{\epsilon} = \bar{\epsilon}_i = 10^{-8}$. The top-mass regulator have been set to the values $\epsilon_t = 0.1 \cdot 2^k$ with $k = \{1, \cdots, 8\}$, with two additional values ($k = -1, -2$) for the bins around the threshold. The reason for this will be clear later.

For each integral, a number of 10 preliminar sampling with lower statistics have been generated, and this leads to an optimization of the integration method. The number of sampling points has been adapted for each form factor to reach the ideal statistical error $\delta\sigma_{ij}^{(k)} \sim 10^{-5}$. Due to limitations related with the hugeness of the calculation, we choose to split the integration on multiple random number seeds, and combining the result afterwards by combining the single estimates for each seed. For the majority of the form factors, for the regulators set to $\epsilon_t > 0.4$ and $\bar{\epsilon} = \bar{\epsilon}_i = 10^{-8}$, two runs with number of sampling points $N \sim 10^8$ can be combined to obtain the aimed precision. The lower is ϵ_t and the higher is the partonic $\hat{s}$, the lower is the convergence of the integration and the numerical stability: for $\epsilon_t = 0.1$ and $\hat{s} > 1000$ GeV and for the whole tail the differential cross section distribution, 50 runs were needed to achieve $\delta\sigma_{ij}^{(k)} \sim 10^{-5}$ for topologies 1, 2, 3 and 4 and up to 1000 for topologies 5 and 6 (diagrams depicted in Appendix H).

All the runs have been performed a total of 4 times: one with the top-mass in the OS scheme, fixing its value to 172.5 GeV; the other 3 times considering the top-mass in the $\overline{\mathrm{MS}}$ scheme. For this last run, we performed the calculation with $\overline{m}_t(\overline{m}_t) = 163.015161017019$ GeV, $\overline{m}_t(\hat{s})$ and $\overline{m}_t(\hat{s}/4)$. Since these last three runs have a role into the estimation of the uncertainties related with the top mass scheme, a simplified energy scan have been chosen, keeping the same energy range but, with half the number of bins.

As it is clear from this picture, the integration of the virtual form factors represented the bottleneck of this calculation, with a total running time of around 9 months in more than 2000 CPUs.

4.2 Richardson Extrapolation

The imaginary part ϵ_t introduced to the top mass as $m_t^2 \to m_t^2(1 - i\epsilon_t)$ plays the role of the finite width of the top quark. In accordance with the literature, we consider the top quark in the narrow width approximation, which induces us to take the limit $\epsilon_t \to 0$. Since we build a numerical setup, the "limit" is not a viable option, and the numerical integration for $\epsilon_t < 10^{-2}$ becomes highly unstable.

The way to take this "limit" into our numerical framework lies in the *Richardson extrapolation method*. Consider a function $f(h)$ depending *polynomially*[1] on h. We are interested in its value for $h = 0$ knowing it for $h = h_0$ and $h = 2h_0$. Expanding f around $h = 0$:

$$\begin{cases} f(h_0) = f(0) + h_0 f'(0) + O(h_0^2) \\ f(2h_0) = f(0) + 2h_0 f'(0) + O(h_0^2) \end{cases} . \tag{4.15}$$

Combining the two expressions:

$$\begin{gathered} f(0) = 2f(h_0) - f(2h_0) + O(h_0^2) \\ \Downarrow \\ \mathrm{RiEx}_{2,h_0}[f(0)] = 2f(h_0) - f(2h_0) \end{gathered} \tag{4.16}$$

where we have introduced the $\mathrm{RiEx}_{n,h_0}[f(0)]$ to be the Richardson extrapolation of $f(0)$ with n nodes and pivot node h_0. One more example with three node yields

$$\begin{gathered} f(0) = \frac{1}{3}[8f(h_0) - 6f(2h_0) + f(4h_0)] + O(h_0^3) \\ \Downarrow \\ \mathrm{RiEx}_{3,h_0}[f(0)] = \frac{1}{3}[8f(h_0) - 6f(2h_0) + f(4h_0)] \end{gathered} \tag{4.17}$$

The key feature of the Richardson extrapolation is that the error is inversely proportional to the number of nodes. Beyond a certain number of nodes, the extrapolation reaches a plateau where the approximation can not be improved further.

Coming back to the virtual differential cross section $\hat{\sigma}^{\mathrm{fin}}_{\mathrm{virt}}(\hat{s})$, the role of the variable h is played by the top-mass regulator ϵ_t. The pivot value for ϵ_t has been set to different values depending on the energy region: for $\sqrt{\hat{s}}$ between 300 GeV and 350 GeV, we set $\epsilon_t = 0.025$; for $\sqrt{\hat{s}}$ between 375 GeV and 475 GeV, we set $\epsilon_t = 0.05$; for all the other energies $\epsilon_t = 0.1$. The reason for chosing different pivot with respect to the energy region will be clear later.

For each of the energy bins, a 9-nodes Richardson extrapolation for each form factor contribution $\hat{\sigma}^{(k)}_{ij}(\hat{s}, \epsilon_t)$ has been performed:

$$\mathrm{RiEx}_{9,2^m\cdot 0.025}[\hat{\sigma}^{(k)}_{ij}(\hat{s}, 0)] = \sum_{n=m}^{m+8} c_n \hat{\sigma}^{(k)}_{ij}(\hat{s}, 2^n \cdot 0.025), \qquad m = \{0, 1, 2\}. \tag{4.18}$$

Since the plateau region is reached already for 4 of 5 nodes for almost all form factors, increasing the number of the nodes may lead to an underestimation of the error, which decreases with the number of nodes. In order to obtain a conservative extrapolation, the error associated to each extrapolation has been chosen to be the difference of the extrapolations with 4 and 5 nodes. To conclude, the Richardson extrapolation leads to the following narrow width approximation of the differential cross section

$$\hat{\sigma}^{(k)}_{ij}(\hat{s}, 0) = \mathrm{RiEx}_{9,2^m\cdot 0.025}[\hat{\sigma}^{(k)}_{ij}(\hat{s}, 0)] \pm 2^{\Theta(m)} \left| \mathrm{RiEx}_{5,2^m\cdot 0.025}[\hat{\sigma}^{(k)}_{ij}(\hat{s}, 0)] - \mathrm{RiEx}_{4,2^m\cdot 0.025}[\hat{\sigma}^{(k)}_{ij}(\hat{s}, 0)] \right|, \tag{4.19}$$

where a factor 2 is added in order to obtain a conservative estimate of the error around the $t\bar{t}$-production threshold. The Richardson extrapolation error will be summed quadratically with the statistical error coming from the Monte Carlo integration. These errors represent the complete statistical uncertainties introduced by the numerical setup at the differential cross section level. An additional Richardson extrapolation will be applied to obtain the integrated total cross section.

4.2.1 Convergence of the Richardson extrapolation: two examples

An analysis of the Richardson extrapolation for specific cases will clarify its convergence behaviour. The notion of convergence will be identified with considering the following sequence and convergence

[1] The polynomial requirement is demanded for having a good convergence of the method.

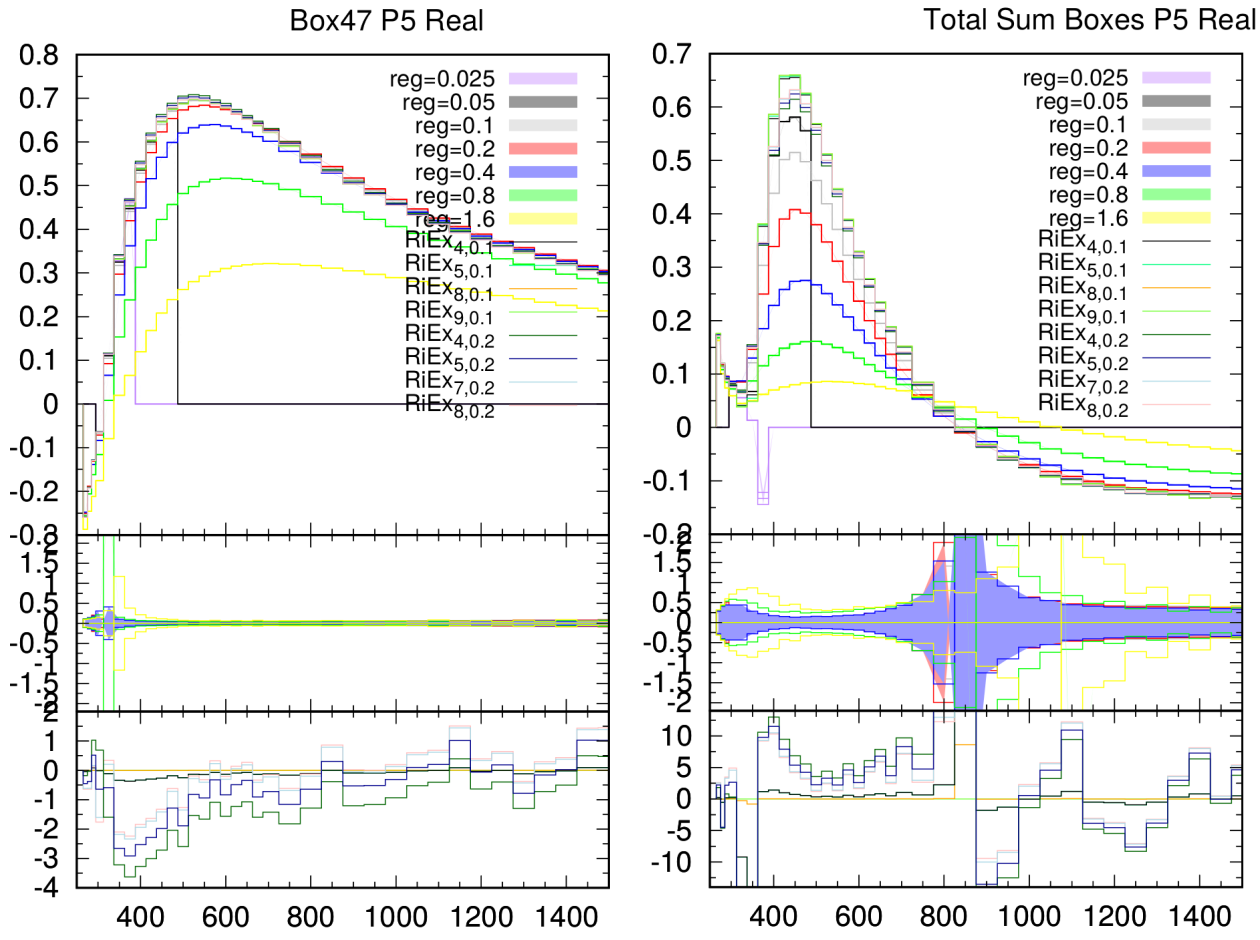

Figure 4.1: *Richardson extrapolation of the narrow width m_t of the NLO 2HDM H_1H_2 production differential cross section of the Box 47 (left panel) and the total contribution of the boxes (right). P5 is the contribution $\hat{\sigma}^{(j)}_{\Delta 1} + \hat{\sigma}^{(j)}_{11} + \hat{\sigma}^{(j)}_{22}$.* Upper panels*: Richardson extrapolation of the narrow width approximation of $RiEx_{n,h_0}[\hat{\sigma}^{(47)}_{ij}(\hat{s},0)]$ for different pivot and number of nodes;* middle panels*: relative error for each bin;* lower panels*: deviation between $RiEx_{9,0.1}[\hat{\sigma}^{(47)}_{ij}(\hat{s},0)]$ and all the other extrapolations.*

ratio:

$$(\mathrm{RiEx}_{n,h_0})_{n\leq 9}, \qquad \delta_n = \frac{|\mathrm{RiEx}_{n,h_0} - \mathrm{RiEx}_{n-1,h_0}|}{\mathrm{RiEx}_{n-1,h_0}}. \tag{4.20}$$

The sequence will be consider "quickly" convergent if $\delta_n \lesssim 1\%$ for $n > 5$ and $\delta_n \lesssim 0.1\%$ for $n > 8$: in other words, if the estimated error is below the percent level and the plateau of the extrapolation is reached starting from the 7-nodes[2].

It can be shown that an 8-nodes Richardson extrapolation with pivot value $\epsilon_t = 0.2$ does not satisfy the criteria expressed in Eq. (4.20) for many box diagrams and energy bins, i.e. its convergence is not sufficiently good. This fact brought us to consider the 9-nodes one with pivot $\epsilon_t = 0.1$. The $\mathrm{RiEx}_{8,0.2}$ is anyhow useful for two reasons: at first instance, its computational requirements are small compared to the $\mathrm{RiEx}_{9,0.1}$, of about one order of magnitude less in runtime; in addition, $\mathrm{RiEx}_{8,0.2}$ can be used as a test of compatibility with $\mathrm{RiEx}_{9,0.1}$ since the 8-nodes Richardson extrapolation is affected by a larger statistical error, and the central value of the 9-nodes one will likely falls within its error band.

The box 47 (Appendix H) is an infrared divergent diagram that have been massively run such that the statistical error is negligible for this purpose (around the per-mille level). The convergence of the Richardson extrapolation for the complete contribution of this box to the differential cross section can be better understood in Figure 4.1. The upper panel shows the differential distributions with

[2]These criteria are mostly empiric.

different widths and the Richardson extrapolations of the narrow width approximation with different nodes; in particular, it shows how good the convergence of the extrapolations becomes once more nodes are considered. In the lower panel it is shown the convergence of the extrapolations around $\mathrm{RiEx}_{9,0.1}[\hat{\sigma}_{ij}^{(47)}(\hat{s},0)]$, which has been taken as central value.

In more details, the behaviour of the Richardson extrapolation can be better understood by looking at the single curves. The yellow curve represents the partonic cross section evaluated with regulator $\epsilon_t = 1.6$, the green represents the one with regulator $\epsilon_t = 0.8$, the blue represents the one with regulator $\epsilon_t = 0.4$. It is visible how the differents partonic cross sections tends to approach a "limit" distribution, until the red curve starts to be undistiguishable from the upper curves. The latter ones are the partonic cross section with regulator $\epsilon_t = 0.1$ and various Richardson extrapolations with different nodes and pivot. The Richardson extrapolation that takes into account all the curves we have described here is the $\mathrm{RiEx}_{5,0.1}$ (light green curve in the left plot in Figure 4.1). In this case, the difference between the Richardson extrapolation and the pivot value $\epsilon_t = 0.1$ (grey curve) is about the per-cent level, and its robustness has been checked by varying the pivot and the number of nodes. The lower panel in the left plot shows that, setting $\mathrm{RiEx}_{9,0.1}$ as expectation value, a 4-nodes extrapolation already introduces deviations of around the per-mille level, and an 8-nodes Richardson extrapolated falls within the statistical error of the estimated value (including its Richardson extrapolation error), and it is completely undistiguishable from $\mathrm{RiEx}_{9,0.1}$. For the majority of the bins, the $\mathrm{RiEx}_{9,0.1}$ has a sufficient fast convergence such that it can be considered the most robust estimate of the differential cross section.

The right plot in Figure 4.1 shows a case where the pivot $\epsilon_t = 0.1$ may be not enough for a reliable extrapolation. The differential distributions for different regulators do not show a manifest convergent behaviour on the $\mathrm{RiEx}_{9,0.1}$, since its deviation from the pivot value $\epsilon_t = 0.1$ (grey curve of the right plot) in the threshold region is more than 25% in the peak. In addition, $\mathrm{RiEx}_{8,0.2}$ and $\mathrm{RiEx}_{9,0.1}$ are not compatible within a standard deviation, a hint that pivots closer to $\epsilon_t = 0$ have to be taken into account. Therefore, to test the reliability of the Richardson extrapolation, additional regulators have been introduced: $\epsilon_t = 0.05$ and $\epsilon_t = 0.025$. Adding these new regulator is very expensive from the computational point of view since Monte Carlo integrations with many sample points have to be considered[3]. However, the $\epsilon = 0.1$ curve still offers a reliabile Richardson extrapolation for $\sqrt{\hat{s}} > 500$ GeV and $\sqrt{\hat{s}} < 300$ GeV. The black curve, namely the distribution with $\epsilon_t = 0.05$ (right plot of Figure 4.1) adds a 10% to the grey curve in the peak region, which attests the beginning of a convergence to some curve. There can be shown that $\mathrm{RiEx}_{9,0.05}$ and $\mathrm{RiEx}_{9,0.025}$ reach their plateau value and the deviation between them is lower than their respective errors. Therefore, the $\mathrm{RiEx}_{9,0.025}$ has been chosen to be the expectation value for the bins $\sqrt{\hat{s}} = \{300, 325, 350\}$ GeV, $\mathrm{RiEx}_{9,0.05}$ the one for $\sqrt{\hat{s}} = \{375, \cdots, 475\}$ GeV, $\mathrm{RiEx}_{9,0.1}$ for all the other bins.

4.3 Total Cross Section

The total cross section is found by integrating the differential distribution built with the partonic cross section $\hat{\sigma}_{ij}^{(k)}(\hat{s},0)$. The numerical framework that has been setup in the previous section is suitable for the trapezoidal rule:

$$\begin{aligned}\sigma_{\mathrm{NLO}} = \int_{\hat{s}_-}^{\hat{s}_+} \frac{d\sigma_{\mathrm{NLO}}}{d\hat{s}}(\hat{s})d\hat{s} &= \frac{\delta\hat{s}}{2}\left[\frac{d\sigma_{\mathrm{NLO}}}{d\hat{s}}(\hat{s}_-) + 2\sum_{j=1}^{n-1}\frac{d\sigma_{\mathrm{NLO}}}{d\hat{s}}(\hat{s}_- + j\delta\hat{s}) + \frac{d\sigma_{\mathrm{NLO}}}{d\hat{s}}(\hat{s}_+)\right] + O(\delta\hat{s}^2) \\ &= \sigma_{\mathrm{NLO}}(\delta\hat{s}) + O(\delta\hat{s}^2),\end{aligned} \tag{4.21}$$

where $\delta\hat{s}$ is the step size of the energy bins. The trapezoidal rule introduces a dependence on $\delta\hat{s}$, and an error proportional to $\delta\hat{s}^2$. The analytical integration, in the spirit of the Riemann integral, is the limit when the small steps $\delta\hat{s}$ goes to 0 and the number of steps goes to infinity. Since the two quantities are related, the limit $\delta\hat{s} \to 0$ is sufficient to describe the continuos limit.

[3]For our setup, the number of sampling points were the same. Instead, it has been exploited the multi-seeds structure of the codes. For problematic boxes, around a thousand seeds have been combined.

We can assume a polynomial dependence on $\delta\hat{s}$, such that the limit $\delta\hat{s} \to 0$ can be extrapolate by the Richardson extrapolation:

$$\sigma_{\mathrm{NLO}} = \mathrm{RiEx}_{n,\delta\hat{s}}[\sigma_{\mathrm{NLO}}(0)] + O(\delta\hat{s}^{2n+2}), \tag{4.22}$$

Different pivot value have been selected depending on the region. Empirical argument have shown that for the threshold region, namely for 300 GeV $< \sqrt{\hat{s}} <$ 700 GeV, a 25 GeV energy scan must be consider in order to achieve a Richardson extrapolation which converges sufficiently quick; for the remaining energy bins, a 50 GeV scan has been chosen. This energy scan grants a Richardson extrapolation of the NLO total cross section with an error below the per-mille level. The remaining region 260 GeV $< \sqrt{\hat{s}} <$ 300 GeV can be integrated by using the Boole's rule with 5-points, achieving an error comparable with the other method.

Chapter 5

Results and Discussion

The method presented in the previous Chapters have been applied and studied extensively in Refs. [54, 55] for the SM case, where $m_{H_1} = m_{H_2} = 125.09$ GeV and $Y_1 = Y_2 = 1$. The 2HDM neutral scalar Higgs-pair production will be treated in a future work. However, the arguments presented in this Chapter can be generalized to the analysis of the 2HDM case.

In this last Chapter, the major outcomes of the works discussed in this thesis are presented. The PDFs considered in the calculation are the `PDF4LHC` and `MMHT2014` sets [150, 151]. The NLO differential cross section in the HTL [32] will be compared with the full-m_t dependent one, and cross-checked with the first calculation [139, 152]. The mass effects become sizeable for increasing values of the Higgs-pair invariant mass.

Three main topics will be discussed in details: the size of the uncertainties due to the top-mass renormalisation scale and scheme, the proper top-mass renormalisation scale choice for the main Higgs-pair invariant mass regions and how to combine the top-mass uncertainties with the state-of-the-art calculation [153].

5.1 SM Differential and Total cross section

The addition of the virtual and real contributions constitute the differential cross section which reads

$$\hat{s}\frac{d\Delta\sigma_{\rm NLO}}{d\hat{s}} = \frac{\alpha_s(\mu_R)}{4\pi}\left[\frac{d\mathcal{L}_{gg}}{d\tau}\hat{\sigma}_{\rm LO}C_{\rm mass}(\hat{s})\bigg|_{\tau=\frac{\hat{s}}{s}} + \int\frac{dz}{z^2}\,\frac{d\mathcal{L}_{ij}}{d\tau}\hat{\sigma}_{\rm LO}C_{ij}(\hat{s},z)\bigg|_{\tau=\frac{\hat{s}}{zs}}\right]. \tag{5.1}$$

For the SM calculation, we have set $m_{H_1} = m_{H_2} = m_H = 125.09$ GeV and $m_t = 172.5$ GeV.

As discussed in the previous Chapter, we provided the result for Higgs-pair invariant mass from 250 GeV to 1500 GeV with steps of 5 GeV for 250-300 GeV, of 25 GeV from 300 GeV to 700 GeV, and 50 GeV for the rest. To have control on the tail of the distribution, additional bins at 2000 GeV and 2500 GeV have been included. The Richardson extrapolation has been performed with 9 nodes with pivot node $\epsilon_t = 0.025$ from 300 GeV to 375 GeV, since the presence of the OS top-mass threshold had bad impact on the stability of the integration, making the convergence slow. For higher energies, we choose the pivot at $\epsilon_t = 0.05$ up to 475 GeV and pivot $\epsilon_t = 0.1$ up to 1500 GeV with 9 nodes. The multiseeds approach has been extremely useful to obtain the total statistical and Richardson extrapolation error at per-mille level.

The NLO partonic cross section has been implemented into the program `Hpair` [32], already used to derive the NLO HTL cross section. The `PDF4LHC` and `MMHT2014` PDFs are used to obtain the numerical results [150, 151]. The distributions we provide are built for centre-of-mass energy of $\sqrt{s}$ =14, 27, 100 TeV. The renormalisation and factorization scheme have been set to $\mu_R = \mu_F = \frac{\hat{s}}{2}$. We presente the comparison between the NLO distribution of the full top-mass dependence against the LO and HTL calculations which has been studied in previous works [32].

In Figure 5.1 the differential distribution of the invariant mass of the Higgs-pair system is shown. The finite top-mass effects introduced by the virtual contributions (the green line) have a huge impact on the differential distributions, leading to a -20% deviation with respect to the HTL starting from

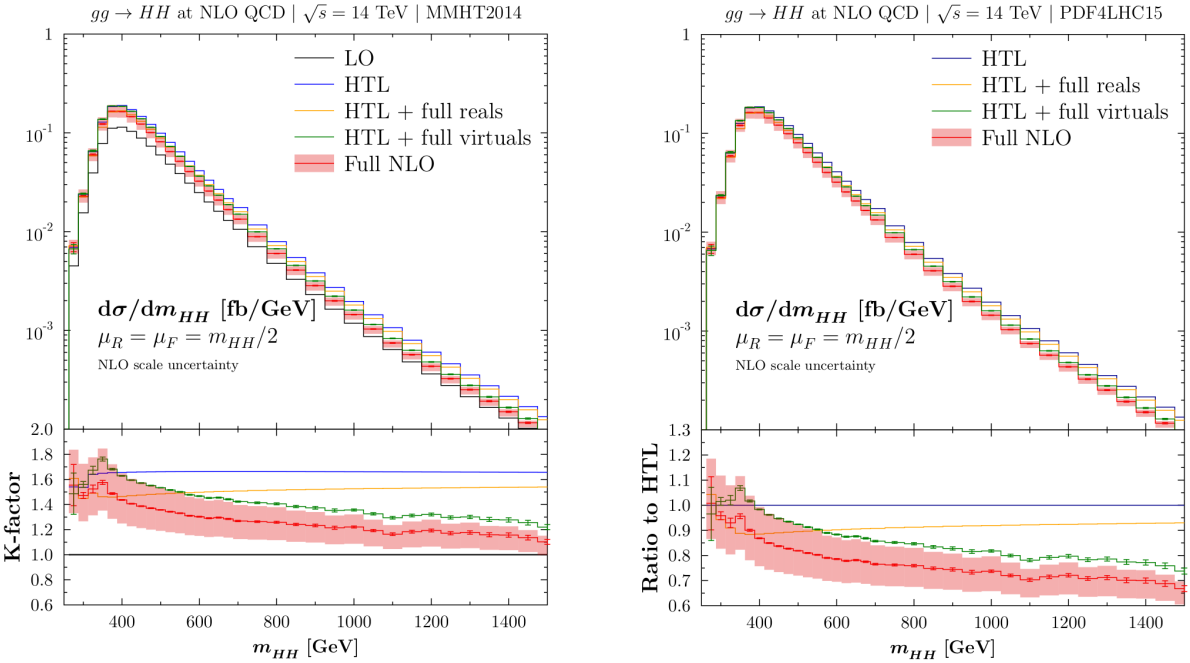

Figure 5.1: *Differential cross section distribution for the NLO SM Higgs-pair production at* 14 TeV. *Left panels: result with* `MMHT2014` *and bin-by-bin K-factor; right panel: result with* `PDF4LHC` *PDF and bin-by-bin ratio to the HTL. Black line: LO calculation; blue line: NLO HTL calculation; yellow line: NLO HTL + reals with full* m_t *dependence; NLO HTL + virtuals with full* m_t *dependence; red line: full NLO calculation, with renormalisation and factorization uncertainties included as red band. Here* $m_{HH} = \sqrt{\hat{s}}$ *is the Higgs-pair invariant mass.*

$\sqrt{\hat{s}} = 1000$ GeV. This deviation becomes even larger at centre-of-mass energies of $\sqrt{s} = 100$ TeV, with a decreasing of -40% when the real correction are taken into accoung (red line). This behaviour does not show up to Higgs-pair invariant mass around the threshold region, since this is the region of validity of the HTL approximation. The red band represents the scale and scheme uncertainties, estimated as an envelope of the differential distributions evaluated at $\mu_R = \mu_F = \hat{s}$ and $\mu_R = \mu_F = \frac{\hat{s}}{4}$. They amount to around 15% from the central value at low Higgs-pair invariant mass, and decrease to around 10% in the tails. It can be shown that the bulk of the mass effect to the NLO K-factor is carried by the continuum diagrams (the ones not containing that do not contain the triple Higgs interaction), that can be used to describe this process within a deviation of at most 5%.

$\sqrt{s}$ (TeV)	σ_{NLO} (fb)
13	$27.73^{+13.8\%}_{-12.8\%}$
14	$32.81^{+13.5\%}_{-12.5\%}$
27	$127.0^{+11.7\%}_{-10.7\%}$
100	$1140^{+10.7\%}_{-10.0\%}$

$\sqrt{s}$ (TeV)	σ_{HTL} (fb)
13	$32.51^{+18\%}_{-15\%}$
14	$38.65^{+18\%}_{-15\%}$
27	$156.2^{+17\%}_{-13\%}$
100	$1521^{+16\%}_{-13\%}$

Table 5.1: *Total cross section for SM Higgs-pair production. On the left, the full top-mass dependence, on the right the HTL calculation. The numbers in the brackets are the numerical errors.*

The total cross section has been calculated by means of a numerical integration. The Richardson extrapolation of the trapezoidal method offered a reliable numerical integration: as already mentioned in Chapter 4, the numerical integral of the differential distribution can be treated as a function of the bin size, and its value at vanishing bin size can be extrapolated with the Richardson extrapolation. This strategy has been adopted for $\sqrt{\hat{s}} > 300$ GeV. For lower value the Boole's rule with five nodes

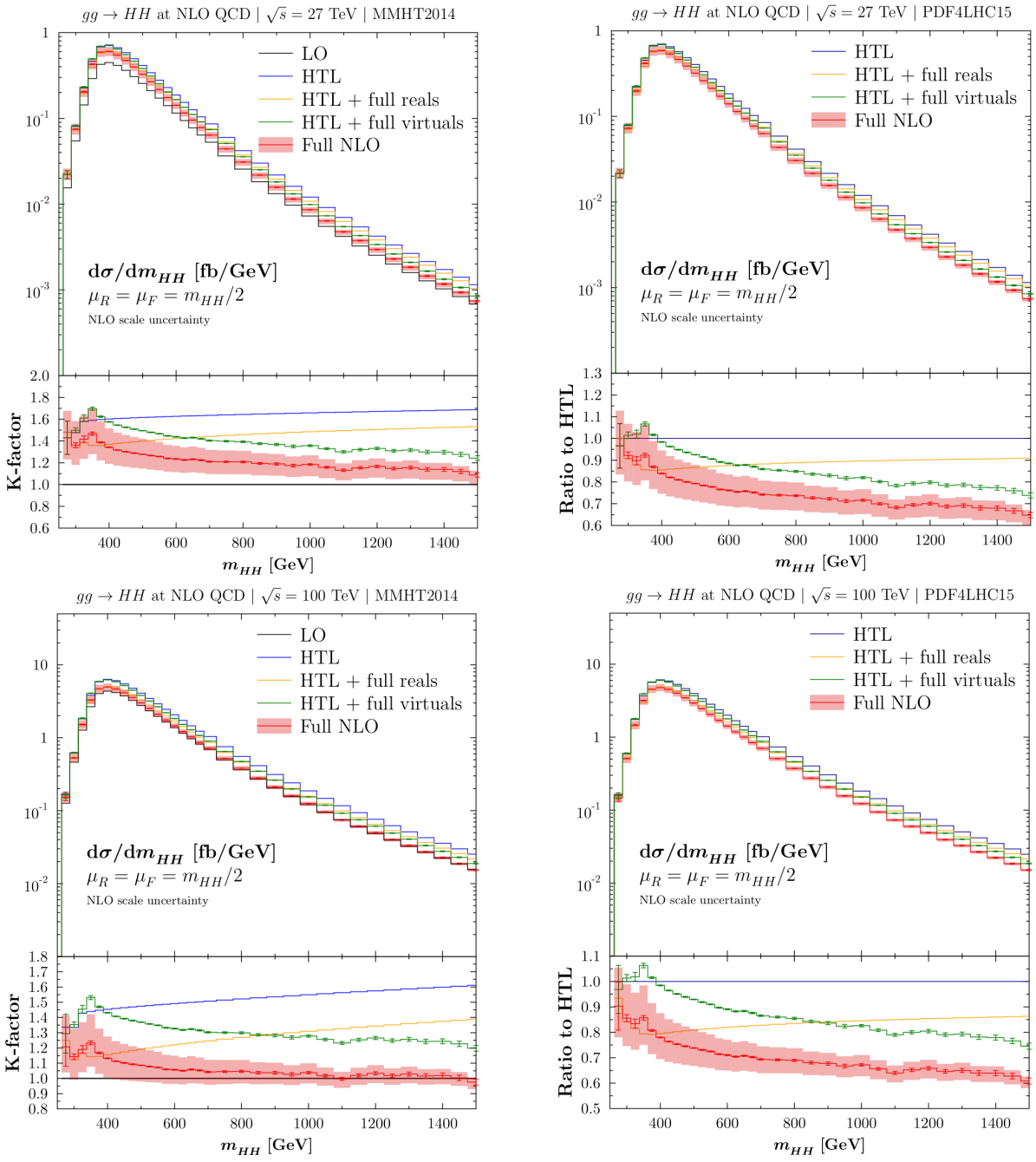

Figure 5.2: *Same description of Figure 5.1, with* $\sqrt{s} = 27$ TeV *and* $\sqrt{s} = 100$ TeV

.

has been considered.

The procedures yield the total cross section depicted in Table 5.1, together with renormalisation and factorization scale uncertainties. As we can infer from the comparison between the left and right tables, the top-mass effects have decreased the total cross section with respect to the NLO HTL approximation [54] of around 15%; the inclusion of the mass effect have reduced the scale uncertainties too. These cross sections show complete agreement with the literature [139].

5.1.1 Dependence on the trilinear Higgs coupling

The NLO total cross section of the Higgs-boson pair production is the key to access the trilinear Higgs coupling λ_{3H}. We recall [23] that the total cross section have an inverse proportionality relation with

the trilinear Higgs coupling close to the SM value

$$\frac{\Delta\sigma}{\sigma} \sim -\frac{\Delta\lambda_{3\mathrm{H}}}{\lambda_{\mathrm{SM}}}. \tag{5.2}$$

Therefore, the sensitivity of the Higgs-pair production total cross section can be probed by varying the trilinear Higgs coupling. The study of these variations can be also interpreted as due to BSM effects to the trilinear Higgs coupling. They can be treated systematically by considering the SM Lagrangian with dimension-6 operators in the scalar sector only [154]. A more general approach including all dimension-6 operators has been studied up to the NNLO HTL [128, 155, 156].

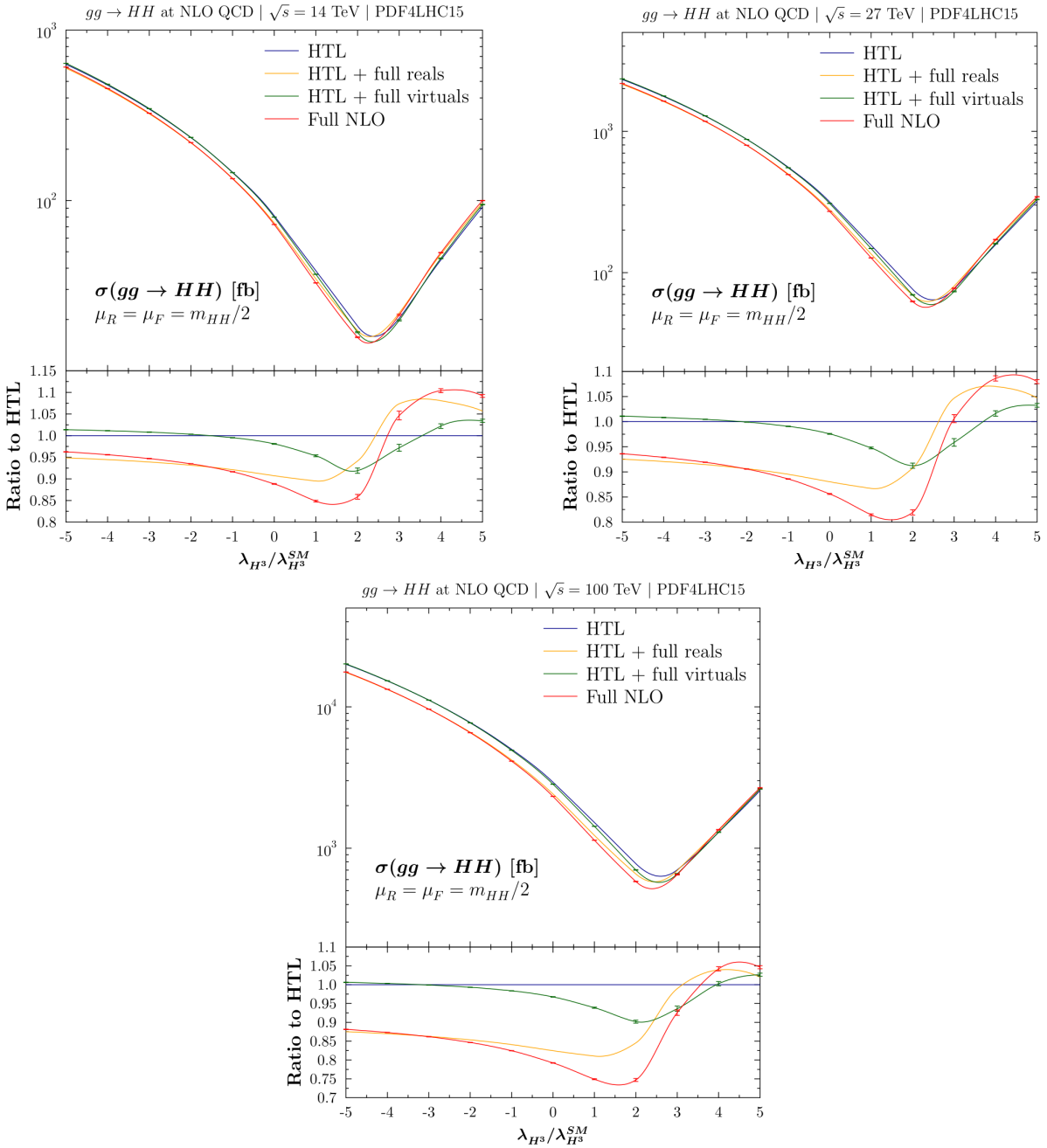

Figure 5.3: *Total Higgs-pair production as function of the trilinear Higgs coupling in units of SM coupling. The centre-of-mass energy is fixed to* $\sqrt{s} = 14$ TeV *(left),* $\sqrt{s} = 27$ TeV *(right) and* $\sqrt{s} = 100$ TeV *(down). The* `PDF4LHC15` *PDFs have been used and the renormalisation scale is fixed to* $\sqrt{\hat{s}}/2$*. The error bars are statistical uncertainties combined with the Richardson extrapolation error.*

We have studied the behaviour of the NLO total cross section of the Higgs-pair production process

with respect to λ_{3H} in units of SM coupling λ_{SM}. It can be expressed as follows

$$\sigma_{NLO} = \sigma_1 + \sigma_2 \frac{\lambda_{3H}}{\lambda_{SM}} + \sigma_3 \left(\frac{\lambda_{3H}}{\lambda_{SM}}\right)^2 \tag{5.3}$$

In Figure 5.3, the dependence of the integrated Higgs-pair production cross section with respect to the Higgs self-coupling is presented. The parabolic behaviour of the curves in the upper panels is distorted by the logarithmic scale of the y-axis. The minimum of the full NLO total cross section is shifted from 2.4 to 2.3 SM units w.r.t. the HTL calculation [23, 32, 157]. The NLO mass effects amount to 10-15% with respect to the HTL. The sign of the correction changes in correspondence to the passage from constructive to destructive interference between the box and triangle diagrams in the form factor $F_1^{(i)}$. The meaning of constructive and destructive interference for $F_1^{(i)}$ is manifest in the HTL [115, 116, 158], and it can be seen in Eq. (3.79) and (3.80).

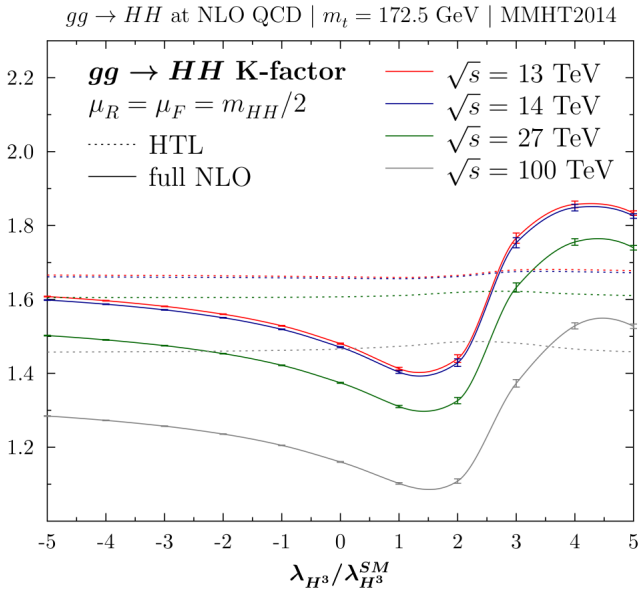

Figure 5.4: *K-factors comparison between different full NLO cross sections and HTL one as function of the trilinear Higgs coupling in SM units. The error bars are statistical uncertainties.*

The Figure 5.4 gathers all the NLO K-factors for different collider energies. The dotted lines correspond to the HTL K-factors, the solid ones to the full top-mass dependence NLO K-factors. The top-mass effects increase with the collider energy in the constructive interference region ($\lambda_{3H} < 0$), ranging from 10% to 15%. As it is clear from the behaviour of the solid curves, the top-mass effects introduce a strong dependence on the trilinear Higgs coupling, including a change of slope for $\lambda_{3H} > 1$, where the interference between box and triangles becomes destructive. At last, using Eq. (5.3), the expressions for the curves represented in Figure 5.3 are

$$\begin{aligned}
\sigma_{NLO}|_{14TeV} &= \left(72.27(7) - 50.70(6)\frac{\lambda_{3H}}{\lambda_{SM}} + 11.23(9)\left(\frac{\lambda_{3H}}{\lambda_{SM}}\right)^2\right) \text{fb}, \\
\sigma_{NLO}|_{27TeV} &= \left(270.9(3) - 183.1(2)\frac{\lambda_{3H}}{\lambda_{SM}} + 39.5(4)\left(\frac{\lambda_{3H}}{\lambda_{SM}}\right)^2\right) \text{fb}, \\
\sigma_{NLO}|_{100TeV} &= \left(2323(2) - 1496(2)\frac{\lambda_{3H}}{\lambda_{SM}} + 313(3)\left(\frac{\lambda_{3H}}{\lambda_{SM}}\right)^2\right) \text{fb},
\end{aligned} \tag{5.4}$$

where the `PDF4LHC` PDFs have been used and the central scales $\mu_R = \mu_F = \sqrt{\hat{s}}/2$ have been chosen.

5.2 Top-mass uncertainties

A consequence of the truncation of the perturbative QCD series is the introduction of theoretical uncertainties due to the choice of the renormalisation scheme and scale. The uncertainties due to the renormalisation μ_R and factorization μ_F scales have already been taken into account in previous studies [53, 139] and they have been represented in the previous Section in Figure 5.1 and Figure 5.2 as a red band around the central value (red curve). The top-quark mass is a renormalisation scheme and scale dependent variable as well. Different choices of the renormalisation scheme and scale will lead to different runnings of the top mass, and introduce an additional source of theoretical uncertainties. Such uncertainties and the ones coming from the renormalisation of the strong coupling have to be combined.

In single-Higgs production, the finite top-mass effects were negligible due to the small Higgs mass. This is also the reason why the HTL approximation works very well for that process. Since it has been shown that the finite top-mass effects on the Higgs-pair production are sizeble, a dedicated study of the uncertainties due to the choice of different mass renormalisation scheme and scales have been performed.

We have evaluated the top-mass uncertainties by evaluating the whole differential cross section by chosing four different top-mass scenarios: $m_t = 172.5$ GeV in the on-shell renormalisation scheme and $\overline{m}_t(\overline{m}_t) = 163.01516101$ GeV, $\overline{m}(\hat{s})$ and $\overline{m}(\hat{s}/4)$ in the $\overline{\text{MS}}$ renormalisation scheme[1]. The running of the $\overline{\text{MS}}$ top mass has been considered at N^{3}LL:

$$\begin{aligned} \overline{m}_t(\mu_t) &= \overline{m}_t(m_t)\frac{c(\alpha_s(\mu_t)/\pi)}{c(\alpha_s(m_t)/\pi)}, \\ c(x) &= \left(\frac{7}{2}\right)^{\frac{4}{7}}[1 + 1.398x + 1.793x^2 - 0.6834x^3], \end{aligned} \tag{5.5}$$

and $\overline{m}_t(m_t)$ has been calculated using the relation between the top pole mass and $\overline{\text{MS}}$ top mass at N^{3}LO [159–163]. The integration of the partonic cross section has been repeated for every mass configuration taking into account the running of Eq. (5.5) with the same setup used for the OS scheme calculation shown in the previous section. Since the role of these runs is to estimate the top-mass uncertainties, a rougher energy scan has been chosen: 25 GeV scan between $\sqrt{\hat{s}} = 300$ GeV and $\sqrt{\hat{s}} = 400$ GeV and 100 GeV for $\sqrt{\hat{s}} > 400$ GeV.

Figure 5.5 shows the distributions obtained for the four top-mass scheme chosen. For $\sqrt{\hat{s}} > 400$ GeV the maximum value for each bin is the OS scheme and the minimum is the distribution for $\overline{m}_t(\hat{s})$.

Chosing the OS scheme as central value, we estimated the mass uncertainties by taking the envelope of the different mass distributions bin-by-bin. This procedure make the top-mass uncertainties to be strongly asymmetric at the differential cross section level (Table 5.2): for $\sqrt{\hat{s}} > 400$ GeV the upper uncertainty vanishes, since the OS distribution provides the maximum for each bin. As it is clear from the Table 5.2, the mass uncertainties are very large: going from LO to NLO, they decrease of about a factor two, being of order 30% at 600 GeV. This same behaviour have been seen for off-shell single-Higgs production, where the top-mass effects are noticeable.

5.2.1 Preferred scale choice

An appropriate choice of the top-mass renormalisation scheme is mandatory to avoid that large logarithms involving the Higgs-pair invariant mass $\sqrt{\hat{s}}$ do not spoil the convergence of the QCD perturbative expansion.

In Figure 5.6 the differential distributions for different choice of top-mass scale and scheme are presented, and important information can be infered from them. The OS scheme and the $\overline{\text{MS}}$ scheme with $\overline{m}_t(\overline{m}_t)$ in the ratio with the NLO HTL are shown respectively in red and blue. These ratios are decreasing with respect of the Higgs-pair invariant mass. The $\overline{\text{MS}}$ scheme with $\overline{m}_t(\hat{s})$ and $\overline{m}_t(\hat{s}/4)$,

[1]Note that since different top-quark masses has to be used, this study can only be performed nowadays woth the method presented in this thesis.

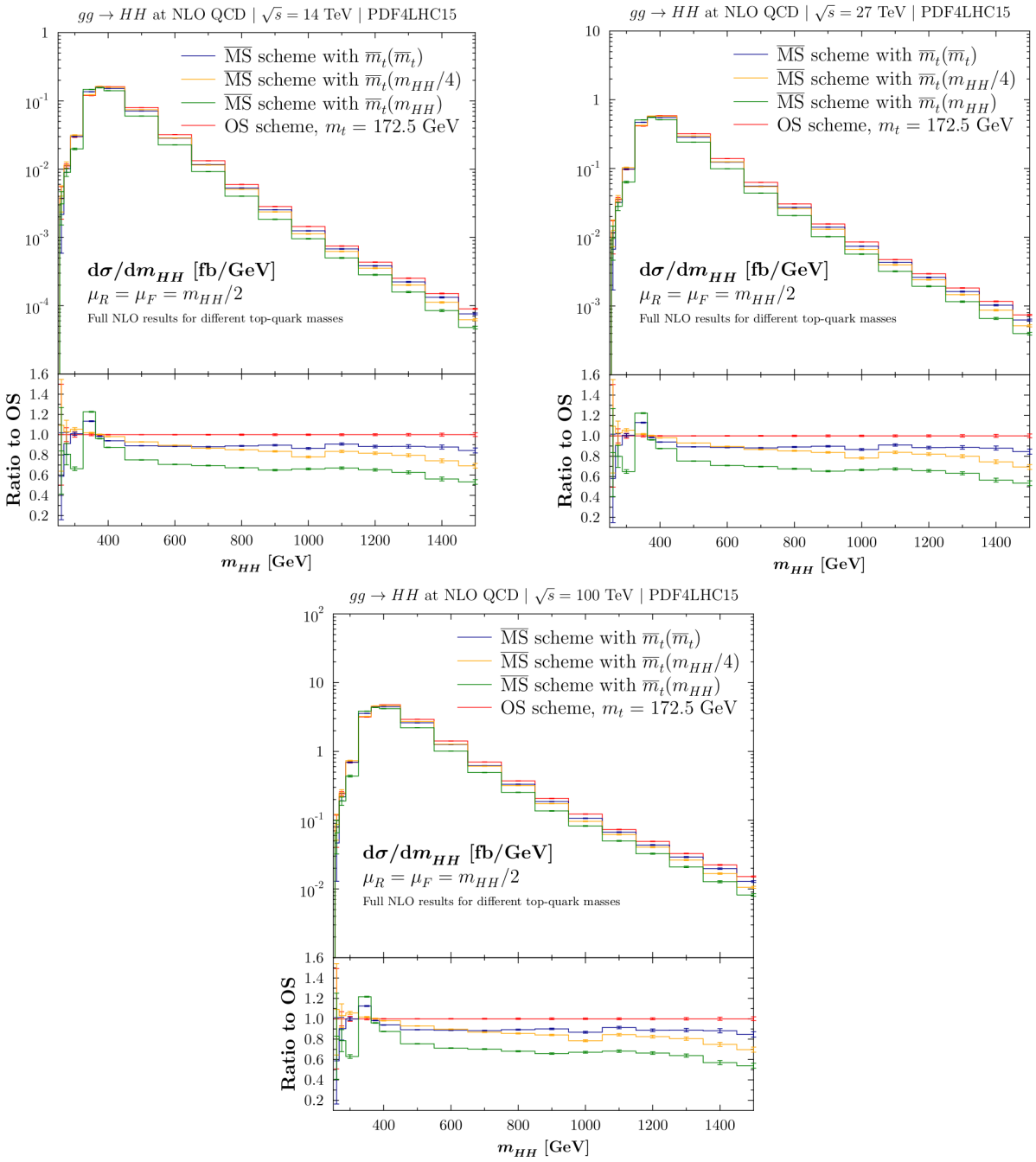

Figure 5.5: *Differential cross section of NLO SM Higgs-pair production for different values of the top mass at $\sqrt{s} = 14$ TeV, $\sqrt{s} = 27$ TeV and $\sqrt{s} = 100$ TeV. The PDF4LHC15 PDFs have been used.*

respectively in green and blue, are rather constants for Higgs-pair invariant mass $\sqrt{\hat{s}} > 500$ GeV. This behaviour of the ratios reflect two distinct effect of the scale choice:

1. *decreasing top-mass effect* for the choice of fixes value of the mass renormalisation scale;
2. *constant top-mass effects* for dynamical scale choice.

These trends can be clearly understand from the theory, by looking at the low and high energy limits of the process. For energies below the double Higgs production threshold, the HTL is a good approximation of the process. We notice that the HTL can be described by the SM effective field theory where the top mass has been integrated out [32, 35, 164, 165], which manifests an effective vertex between gluons and Higgs boson:

$$\mathcal{L}_{\text{eff}} = \frac{\alpha_s}{12\pi} \text{Tr}\left[G^{\mu\nu} G_{\mu\nu}\right] \left(\frac{C_1}{v} H - \frac{C_2}{2v^2} H^2\right). \tag{5.6}$$

$\sqrt{\hat{s}}$ (GeV)	$\frac{d\sigma_{\text{LO}}}{d\sqrt{\hat{s}}}$ (fb/GeV)	$\frac{d\sigma_{\text{NLO}}}{d\sqrt{\hat{s}}}$ (fb/GeV)
300	$0.01656^{+62\%}_{-2.4\%}$	$0.02978(7)^{+6\%}_{-34\%}$
400	$0.09391^{+0\%}_{-20\%}$	$0.1609(4)^{+0\%}_{-13\%}$
600	$0.02132^{+0\%}_{-48\%}$	$0.03204(9)^{+0\%}_{-30\%}$
1200	$0.0003223^{+0\%}_{-56\%}$	$0.000435(4)^{+0\%}_{-35\%}$

$\sqrt{s}$ (TeV)	σ_{NLO} (fb)
13	$27.73^{+4\%}_{-18\%}$
14	$32.81^{+4\%}_{-18\%}$
27	$127.0^{+4\%}_{-18\%}$
100	$1140^{+3\%}_{-18\%}$

$$\Downarrow$$

$$\sigma_{\text{NLO}} = 32.81(7)^{+4\%}_{-18\%}\text{fb}$$

Table 5.2: *Left table: Differential cross section values for $\sqrt{s} = 14$ TeV at LO and NLO. The NLO corrections make the mass uncertainties decrease by a factor 2. The total cross section is shown below. Right table: total cross section including top mass scheme and scale uncertainties for $\sqrt{s} = 13, 24, 27, 100$ TeV.*

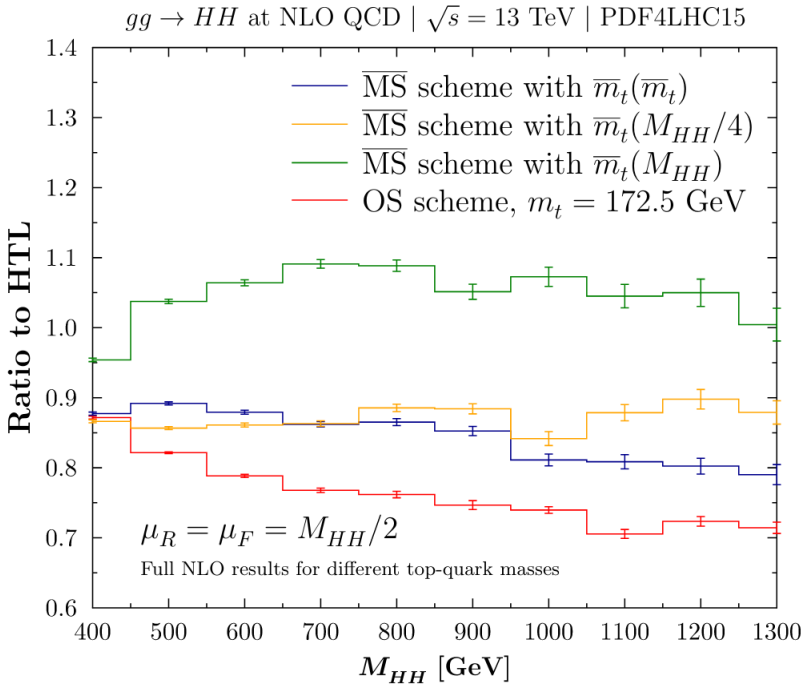

Figure 5.6: *Ratio of the NLO differential cross section with the HTL NLO one for the mass schemes considered for $\sqrt{s} = 13\,TeV$.*

The Wilson coefficients C_i of the HTL Lagrangian, independents from the scattering process, are determined by the matching to the SM Lagrangian. These coefficients at NLO are

$$C_1 = 1 + \frac{11}{4}\left(\frac{\alpha_s}{\pi}\right) + \left\{\frac{2777}{288} + \frac{19}{16}\log\left(\frac{\mu_R^2}{m_t^2}\right) + N_f\left[\frac{1}{2}\log\left(\frac{\mu_R^2}{m_t^2},\right) - \frac{67}{96}\right]\right\}\left(\frac{\alpha_s}{\pi}\right)^2 + O(\alpha_s^3),$$
$$C_2 = C_1 + \left(\frac{35}{24} + \frac{2}{3}N_f\right)\left(\frac{\alpha_s}{\pi}\right)^2 + O(\alpha_s^3). \tag{5.7}$$

Therefore, the natural choice of the matching scale is the top pole mass $\mu_R = m_t$. This fact shows why at low Higgs-pair invariant mass the OS scheme offers a good scale choice.

The large $\sqrt{\hat{s}}$ behaviour can be understood by considering the analytical high energy expansion of the Higgs-pair production form factors [45, 46]. First of all, the triangle contributions are strongly suppressed, because of the off-shell Higgs propagator, so the dominant contribution comes from the

virtual corrections. The analytical expressions of the form factors in terms of the top pole mass are

$$F_i^{(1)} \sim \frac{\alpha_s}{\pi}\left\{2F_i^{(0)}\log\left(\frac{m_t^2}{\hat{s}}\right)+\frac{m_t^2}{\hat{s}}G_i(\hat{s},\hat{t})\right\}, \tag{5.8}$$

where G_i are complicated functions of the partonic kinematic invariants. Notice that the dependence of $F_i^{(1)}$ on the top mass is completely isolated. However, the logarithm involving the top mass introduce large contribution proportional to the LO. A different behaviour shows up when the form factors are expanded in term of the $\overline{\text{MS}}$ mass:

$$F_i^{(1)} \sim \frac{\alpha_s}{\pi}\left\{2F_i^{(0)}\left[\log\left(\frac{\mu_t^2}{\hat{s}}\right)+\frac{4}{3}\right]+\frac{\overline{m}_t^2(\mu_t)}{\hat{s}}G_i(\hat{s},\hat{t})\right\}. \tag{5.9}$$

Setting $\mu_t = \kappa\hat{s}$ the logarithm is under control and behaves good at high $\sqrt{\hat{s}}$. This provides the explanation of why a dynamical scale choice of the $\overline{\text{MS}}$ mass renormalisation scale provides a good scale choice for the high energy regime. Notice that Figure 5.6 shows in particular that a proper choice of the mass renormalisation scale makes the NLO finite top-mass effects to be independent on the Higgs-pair invariant mass, and their size assest to around 10-15% for $\mu_t = \sqrt{\hat{s}}/4$.

5.2.2 Combining the uncertainties

Collecting all the results we have found in our analysis, the uncertainties on the NLO SM total cross section are summarized in Table 5.3. It shows NLO cross sections at different centre-of-mass energies with theoretical uncertainties. The left table displays the uncertainties related to the renormalisation and factorization scale choice; the central one shows the uncertainties related to the top-mass renormalisation scale and scheme choice; the right table shows the combination of the two uncertainties. Since both sources of uncertainties have been estimated from the envelope, their interplay is an envelope too, leading to the linear sum of the uncertainties. Additional corrections to the Higgs-pair

$\sqrt{s}$ (TeV)	σ_{NLO} (fb)
13	$27.73^{+13.8\%}_{-12.8\%}$
14	$32.81^{+13.5\%}_{-12.5\%}$
27	$127.0^{+11.7\%}_{-10.7\%}$
100	$1140^{+10.7\%}_{-10.0\%}$
Ren.+fac. uncertainties	

$\oplus$

$\sqrt{s}$ (TeV)	σ_{NLO} (fb)
13	$27.73^{+4\%}_{-18\%}$
14	$32.81^{+4\%}_{-18\%}$
27	$127.0^{+4\%}_{-18\%}$
100	$1140^{+3\%}_{-18\%}$
top-mass uncertainties	

$=$

$\sqrt{s}$ (TeV)	σ_{NLO} (fb)
13	$27.73^{+17.8\%}_{-30.8\%}$
14	$32.81^{+17.5\%}_{-30.5\%}$
27	$127.0^{+15.7\%}_{-28.7\%}$
100	$1140^{+13.7\%}_{-28.0\%}$
Combined uncertainties	

Table 5.3: *Left table: NLO SM total cross sections with renormalisation and factorization scheme uncertainties. Central table: NLO SM total cross section with top-mass uncertainties. Right table: NLO SM total cross section with combined uncertainties.*

production have been studied. The recommended prediction is the NNLO QCD corrections in the full-theory approximation (FTapprox), i.e. LO and NLO with full top-mass dependence, HTL virtual and real-virtual contributions and full top-mass dependence for the double real contributions [29, 153]. This calculation estimates a renormalisation and factorization scale uncertainties up to 5%.

To analyze how to combine these uncertainties with the state-of-the-art calculation, a comment of the structure of the n-th order of the total cross section is useful:

$$d\sigma_n = d\sigma_{n-1}\left(K_{\text{SV}}^{(n)} + K_{\text{rem}}^{(n)}\right), \tag{5.10}$$

where $K_{\text{SV}}^{(n)}$ is the soft+virtual contribution in the HTL (independent on the top mass) and $K_{\text{rem}}^{(n)}$ is the top mass contribution to the differential cross section in the ratio with the previous perturbative order [39, 55].

$\sqrt{s}$ (TeV)	$\sigma_{\text{NNLO}}^{\text{FTapprox}}$ (fb)
13	$31.05^{+2.2\%}_{-5.0\%}$
14	$36.69^{+2.1\%}_{-4.9\%}$
27	$139.9^{+1.3\%}_{-3.9\%}$
100	$1224^{+0.9\%}_{-3.2\%}$

Ren.+fac. uncertainties

$\oplus$

$\sqrt{s}$ (TeV)	σ_{NLO} (fb)
13	$27.73^{+4\%}_{-18\%}$
14	$32.81^{+4\%}_{-18\%}$
27	$127.0^{+4\%}_{-18\%}$
100	$1140^{+3\%}_{-18\%}$

top-mass uncertainties

$=$

$\sqrt{s}$ (TeV)	$\sigma_{\text{NNLO}}^{\text{FTapprox}}$ (fb)
13	$31.05^{+6\%}_{-23\%}$
14	$36.69^{+6\%}_{-23\%}$
27	$139.9^{+5\%}_{-22\%}$
100	$1224^{+4\%}_{-21\%}$

Combined uncertainties

Table 5.4: *Left table: Recommended NNLO FTapprox SM total cross sections with renormalisation and factorization scheme uncertainties. Central table: NLO SM total cross section with top-mass uncertainties. Right table: NNLO FTapprox SM total cross section with combined uncertainties.*

Both the soft+virtual and remainder terms are multiplied for the same factor and $K_{\text{SV}}^{(n)}$ is dominant. The $K_{\text{rem}}^{(n)}$ provides a correction of 10-15% of the $K_{\text{SV}}^{(n)}$ contribution. The latter term occurs both in the HTL approximation and the FTapprox, which is why these approximations are reliable. These statements have been tested at NLO and NNLO [153]. The explicit form of the NLO differential cross section shown in Eq. (3.69) and (3.100) are provided such that the factorization of Eqs. (5.10) is explicit. Since the SV part of the NNLO differential cross section, which is known in literature, scales with the full NLO contribution, and the top-mass uncertainties are independent on the renormalisation and factorization scale choice, we are legitimate to consider the combined uncertainties to be the *envelope* of the two *relative*, leading to a linear sum of the uncertainties. Therefore, the NNLO QCD total cross section for Higgs-pair production are recommended to be considered affected by the theoretical uncertainties in Table 5.4.

Chapter 6

Conclusions

In this thesis, a framework for the NLO QCD Higgs-pair production via gluon fusion cross section with full top-mass dependence has been described. It is suitable for BSM extensions of the scalar sector, such as the 2HDM. In particular, in Chapter 1 it has been explained how the different final states can be implemented into the calculation and how to deal with the dimensional regularisation in the presence of pseudoscalar and charged Higgs bosons.

The building block of the NLO contributions are the amplitudes built with up to four-points two-loops Feynman diagrams with five mass scales and five-points one-loop ones. The first are the virtual contributions, the latter are the real ones. Since there is no systematic strategy for two-loop diagrams, a specific calculation method for such amplitude is presented. No reduction methods have been performed during the calculation. For each of the 47 box diagrams belonging to the virtual amplitude, the projection into their form factors has been performed, and a topology-wise Feynman parametrization has been chosen, allowing the isolation of UV and IR divergences by means of the end-point subtraction. Particular care has been dedicated to the end-point subtraction of the divergences coming from the diagrams belonging to the topology 6: the universality of the IR divergences have been exploited to build a subtraction term from the heavy-top limit of the form factors. The addition of the renormalisation counterterms to the virtual amplitude yields UV finite quantities. The $\overline{\text{MS}}$ scheme with five active flavours and the on-shell top quark decoupled from the running has been used to renormalize the strong coupling. Finally, after the UV renormalisation and the end-point subtraction of the IR divergences, the box form factors are ready to be integrated over the Feynman parameters and the two-particles phase space. The one-particle reducible diagrams have been obtained by combining two Higgs decay into on-shell and off-shell gluon LO amplitudes, employed as effective verteces. At last, the NLO triangle contributions have been built from the single-Higgs production form factors.

The numerical setup have involved the *Vegas* algorithm for Monte Carlo integration [148], implemented into a *Fortran* code built with a multi-seed approach. Numerical instabilities arise for energies laying above the diagram thresholds, which can be $t\bar{t}$ or gg production thresholds. A small imaginary parameter ϵ_t introduced as top-quark mass finite width increases the stability of the Monte Carlo, and it can be used for an analytical continuation of the cross section to extract the narrow top-quark width. Moreover, integration by parts have been performed to decrease the power of the denominators, and the numerical stability has been improved further. The narrow width top quark has been extracted from combining linearly evaluations of the differential cross section for different ϵ_t regulator values. This is the core of the Richardson extrapolation method, whose extrapolation error is inversly proportional to the number of nodes. Nine nodes for each energy bins have been combined to obtain the final differential distribution for each interference terms, leading to a complete virtual differential cross section contributions.

The real corrections have been obtained through standard algorithms, involving the decomposition of the real amplitude into the Passarino-Veltman tensor basis, and by taking its analytical square average. Every analytical step has been implemented into a *Mathematica* code that provide the square amplitude of every real correction channel. The IR divergences have been subtracted by the same term used for subtracting the virtual IR singularities. The integration over the three-particle

phase space has led to the real differential cross section.

The SM case has been studied in detail. The finite top-mass effects to the NLO total cross section introduce a 15% correction to the NLO HTL calculation. More noticeable effects can be seen at the level of the differential distribution, where the finite top mass introduces a deviation in its tail down to -40%. The results for the central values at different centre-of-mass energies are in complete agreement with the literature, as well as the reduction of the renormalisation and factorization scale uncertainties. The total cross section as function of the trilinear Higgs coupling shows significant deviation from the HTL due to top-mass effects, leading to a noticeable shift of its minimum.

The framework built for this calculation allows the choice of different top-mass renormalisation scheme and scales, suitable for the first estimation the uncertainties they introduce. The $\overline{\text{MS}}$ top mass to different scale choice has underlined the importance of these uncertainties, that amounts to 15% at the total cross section level and down to -35% at the differential cross section level. The behaviour of the differential cross section at different renormalisation scales has been discussed, and it has been shown how a dynamical renormalisation scale is the most natural choice for large Higgs-pair invariant mass. The quasi-independence of the top-mass uncertainties from the renormalisation and factorization scheme lead to a linear addition of the uncertainties since they have been defined as envelopes of multiple distributions. The combination of the NLO top-mass uncertainties and the NNLO renormalisation and factorization uncertainties have been discussed, and from a factorization of the cross section argument, the most conservative treatment of the uncertainties has been identified as their linear sum.

The framework described in this thesis has already been applied successfully to the 2HDM; some results regarding the neutral scalar Higgs-pair production has been shown in Chapter 5. Further future application will involve final states containing pseudoscalars and charged scalars. Moreover, the dependence on the β angle of the Yukawa couplings in the 2HDM may lead to non-negligible contributions from bottom quark loops, for which additional treatments on the form factors are needed to increase the numerical stability, like bottom-quark mass expansions and integration by parts.

Appendix A

HTL gluon-Higgs effective vertex

The low-energy Higgs effective Lagrangian contains the effective gluon-Higgs interaction verteces. Such interactions can be obtained from the SM Lagrangian by taking the heavy-top limit of the QCD induced Higgs production via gluon fusion. This amplitude has been calculated in Chapter 2 in the case where an incoming gluon is off-shell. Starting from that expression, the analytical limit can be calculated.

For both the HTL limit and the on-shell limit, the parameters λ and τ behave in the same way:

$$\lambda, \tau \xrightarrow[m_t^2 \to \infty]{p_2^2 \to 0} \infty, \tag{A.1}$$

therefore the functions $f(\lambda)$ and $g(\lambda)$ have the same behaviour in both limits. The functions $f(\lambda)$ and $g(\lambda)$ are defined as follows:

$$\begin{gathered} f(\lambda) = -\frac{1}{4}\log^2\left(-\frac{\alpha_+}{\alpha_-}\right), \qquad g(\lambda) = \frac{\sqrt{1-\lambda}}{2}\log\left(-\frac{\alpha_+}{\alpha_-}\right), \\ \alpha_\pm = 1 \pm \sqrt{1-\lambda}, \end{gathered} \tag{A.2}$$

The limit of $\alpha_\pm$ for $\lambda \to \infty$ is

$$\alpha_\pm \sim_{\lambda\to\infty} 1 \pm i\sqrt{\lambda}\left(1 - \frac{1}{2\lambda}\right) = 1 \mp \frac{i}{2\sqrt{\lambda}} \pm i\sqrt{\lambda}, \tag{A.3}$$

and the inverse of α_- has the following behaviour:

$$\begin{aligned} \frac{1}{\alpha_-} \sim_{\lambda\to\infty} \frac{1}{1 + \frac{i}{2\sqrt{\lambda}} - i\sqrt{\lambda}} &= \frac{i}{\sqrt{\lambda}}\frac{1}{1 + \frac{i}{\sqrt{\lambda}} - \frac{1}{2\lambda}} \sim_{\lambda\to\infty} \frac{i}{\sqrt{\lambda}}\left(1 - \frac{i}{\sqrt{\lambda}} - \frac{1}{2\lambda}\right) \\ &= \frac{i}{\sqrt{\lambda}} + \frac{1}{\lambda} - \frac{i}{2\lambda\sqrt{\lambda}}. \end{aligned} \tag{A.4}$$

Hence

$$\begin{aligned} -\frac{\alpha_+}{\alpha_-} &= -\left(1 - \frac{i}{2\sqrt{\lambda}} + i\sqrt{\lambda}\right)\left(\frac{i}{\sqrt{\lambda}} + \frac{1}{\lambda} - \frac{i}{2\lambda\sqrt{\lambda}}\right) \\ &= 1 - \frac{2i}{\sqrt{\lambda}} - \frac{2}{\lambda} + \frac{i}{\lambda\sqrt{\lambda}}, \end{aligned} \tag{A.5}$$

and from

$$\begin{aligned} \log(1 + ax + bx^2 + cx^3) &\sim_{x\to 0} (ax + bx^2 + cx^3) - \frac{1}{2}(ax + bx^2)^2 + \frac{1}{3}(ax)^3 \\ &\sim ax + \left(b - \frac{1}{2}a^2\right)x^2 + \left(c - ab + \frac{1}{3}a^3\right)x^3, \end{aligned} \tag{A.6}$$

the logarithm occuring into the definitions of $f(\lambda)$ and $g(\lambda)$ is

$$\begin{aligned}\log\left[-\frac{\alpha_+}{\alpha_-}\right] &\sim_{\lambda\to\infty} \log\left[1-2i\frac{1}{\sqrt{\lambda}}-2\left(\frac{1}{\sqrt{\lambda}}\right)^2+i\left(\frac{1}{\sqrt{\lambda}}\right)^3\right]\\ &\sim_{\lambda\to\infty} -\frac{2i}{\sqrt{\lambda}}+(-2+2)\left(\frac{1}{\sqrt{\lambda}}\right)^2+\left(i-4i+\frac{8}{3}i\right)\left(\frac{1}{\sqrt{\lambda}}\right)^3\\ &\sim_{\lambda\to\infty} -i\left(2\frac{1}{\sqrt{\lambda}}+\frac{1}{3}\frac{1}{\lambda\sqrt{\lambda}}\right).\end{aligned} \tag{A.7}$$

Therefore, $f(\lambda)$ in the limit $\lambda\to\infty$ has the following series expansion:

$$\begin{aligned}f(\lambda)=-\frac{1}{4}\log^2\left[-\frac{\alpha_+}{\alpha_-}\right] &= \left(\frac{1}{\sqrt{\lambda}}+\frac{1}{6}\frac{1}{\lambda\sqrt{\lambda}}\right)^2+O\left(\frac{1}{\lambda^3}\right)\\ &= \frac{1}{\lambda}+\frac{1}{3\lambda^2}+O\left(\frac{1}{\lambda^3}\right)\end{aligned} \tag{A.8}$$

Going further with the expansion, the third expansion term is

$$f(\lambda)=\frac{1}{\lambda}+\frac{1}{3\lambda^2}+\frac{8}{45\lambda^3}+O\left(\frac{1}{\lambda^4}\right) \tag{A.9}$$

Moving the discussion to the function $g(\lambda)$:

$$\begin{aligned}g(\lambda)=\frac{\sqrt{1-\lambda}}{2}\log\left(-\frac{\alpha_+}{\alpha_-}\right) &= \sqrt{1-\frac{1}{\lambda}}\left(1+\frac{1}{6\lambda}\right)+O\left(\frac{1}{\lambda^2}\right)\\ &= \left(1-\frac{1}{2\lambda}\right)\left(1+\frac{1}{6\lambda}\right)+O\left(\frac{1}{\lambda^3}\right)\\ &= 1-\frac{1}{3\lambda}+O\left(\frac{1}{\lambda^2}\right)\end{aligned} \tag{A.10}$$

and, adding an additional order to $g(\lambda)$:

$$g(\lambda)\sim_{\lambda\to\infty} 1-\frac{1}{3\lambda}-\frac{2}{15\lambda^2} \tag{A.11}$$

A.1 ggH_j effective vertex

From the result of Chapter 2, the gluon-Higgs effective vertex is the on-shell and heavy-top limit of the $gg\to H_j$ amplitude:

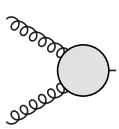

$$= \lim_{\tau,\lambda\to\infty}\mathcal{M}_\Delta^{\mu\nu,ab}=i\left(\frac{\alpha_s}{\pi v}\right)\delta^{ab}\left(\frac{4\pi\mu^2}{m_t^2}\right)^\epsilon\Gamma(1+\epsilon)\left[(p\cdot q)g^{\mu\nu}-q^\mu p^\nu\right]\lim_{\tau,\lambda\to\infty}\mathcal{I}(\tau,\lambda), \tag{A.12}$$

where

$$\mathcal{I}(\tau,\lambda)=\frac{\tau\lambda}{2(\tau-\lambda)}+\frac{\tau^2\lambda}{(\tau-\lambda)^2}\left[g(\tau)-g(\lambda)\right]+\frac{\tau^2\lambda^2}{2(\tau-\lambda)^2}[f(\tau)-f(\lambda)]+\frac{\tau\lambda}{2(\tau-\lambda)}[f(\tau)-f(\lambda)]. \tag{A.13}$$

The on-shell limit $\lambda \to \infty$ yields:

$$\begin{aligned}
\frac{\tau\lambda}{2(\tau-\lambda)} &\sim -\frac{\tau}{2} - \frac{\tau^2}{2\lambda} \\
\frac{\tau^2\lambda}{(\tau-\lambda)^2}\left[g(\tau)-g(\lambda)\right] &\sim -\frac{\tau^2}{\lambda} + \frac{\tau^2}{\lambda} g(\tau) \\
\frac{\tau^2\lambda^2}{2(\tau-\lambda)^2}[f(\tau)-f(\lambda)] &\sim \frac{\tau^2}{2} f(\tau) + \frac{\tau^2}{\lambda}\frac{(2\tau f(\tau)-1)}{2} \\
\frac{\tau\lambda}{2(\tau-\lambda)}[f(\tau)-f(\lambda)] &\sim -\frac{\tau}{2} f(\tau) - \frac{\tau}{\lambda}\frac{(\tau f(\tau)-1)}{2} \\
&\Downarrow \\
\mathcal{I}(\tau,\infty) = \lim_{\lambda\to\infty} \mathcal{I}(\tau,\lambda) &= -\frac{\tau}{2}\left[1-\tau f(\tau)+f(\tau)\right],
\end{aligned} \tag{A.14}$$

and the HTL:

$$\begin{aligned}
\mathcal{I}(\tau,\infty) &\sim -\frac{\tau}{2}\left[-\frac{1}{3\tau}+\frac{1}{\tau}\right] \\
&\Downarrow \\
\lim_{\lambda,\tau\to\infty} \mathcal{I}(\tau,\lambda) &= -\frac{1}{3}.
\end{aligned} \tag{A.15}$$

Therefore, the gluon-Higgs effective vertex is

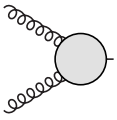

$$= -i\left(\frac{\alpha_s}{3\pi v}\right)\delta^{ab}\left(\frac{4\pi\mu^2}{m_t^2}\right)^{\epsilon}\Gamma(1+\epsilon)\left[(p\cdot q)g^{\mu\nu}-q^\mu p^\nu\right]. \tag{A.16}$$

Notice that the two limits do commute.

Appendix B

General tensors for the $gg \to H_1 H_2$ process

The amplitude of $gg \to H_1 H_2$ is a rank-2 tensor depending on the external momenta p_1, p_2, p_3:

$$\mathcal{M}^{\mu\nu} = a_{00} g^{\mu\nu} + \sum_{i,j=1}^{3} a_{ij} p_i^\mu p_j^\nu \tag{B.1}$$

where a_{00} and a_{ij} are the coefficients of the tensor basis, which will depend on the process. First of all, the incoming gluons are physical, i.e. transverse with respect to their momentum:

$$p_i^\sigma \epsilon_\sigma(p_i) = 0. \tag{B.2}$$

Consider the gluon with momentum p_1 contracted with the first index μ, and the gluon with momentum p_2 contracted with the second index μ of $\mathcal{M}^{\mu\nu}$. With this consideration, since $p_1^\mu \epsilon_\mu(p_1) = p_2^\nu \epsilon_\nu(p_2) = 0$, the general tensor $\mathcal{M}^{\mu\nu}$ reads:

$$\mathcal{M}^{\mu\nu} = a_{00} g^{\mu\nu} + a_{21} p_2^\mu p_1^\nu + a_{31} p_3^\mu p_1^\nu + a_{23} p_2^\mu p_3^\nu + a_{33} p_3^\mu p_3^\nu \tag{B.3}$$

If one performs the calculation in the axial gauge, in general there will be complicated tensor structures for propagators and polarization sum. However, it allow to use the QED-like Ward identities for on-shell gluons:

$$p_{1\mu} \mathcal{M}^{\mu\nu} = 0, \qquad p_{2\nu} \mathcal{M}^{\mu\nu} = 0. \tag{B.4}$$

The Ward identities provide the following conditions

$$\begin{cases} p_{1\mu} p_{1\nu} T^{\mu\nu} = 0 \\ p_{1\mu} p_{2\nu} T^{\mu\nu} = 0 \\ p_{2\mu} p_{2\nu} T^{\mu\nu} = 0 \end{cases},$$

$$\begin{cases} a_{23}(p_1 \cdot p_2) + a_{33}(p_1 \cdot p_3) = 0 \\ a_{00}(p_1 \cdot p_2) + a_{21}(p_1 \cdot p_2)^2 + a_{31}(p_1 \cdot p_3)(p_1 \cdot p_2) + a_{23}(p_1 \cdot p_2)(p_2 \cdot p_3) + a_{33}(p_1 \cdot p_3)(p_2 \cdot p_3) = 0 \\ a_{31}(p_1 \cdot p_2) + a_{33}(p_2 \cdot p_3) = 0 \end{cases}. \tag{B.5}$$

The first and the last equation give

$$a_{23} = -\frac{(p_1 \cdot p_3)}{(p_1 \cdot p_2)} a_{33}, \qquad a_{31} = -\frac{(p_2 \cdot p_3)}{(p_1 \cdot p_2)} a_{33}, \tag{B.6}$$

and replacing these results in the second equation it follows that

$$a_{00} = \frac{a_{33}(p_1 \cdot p_3)(p_2 \cdot p_3) - a_{21}(p_1 \cdot p_2)^2}{(p_1 \cdot p_2)}. \tag{B.7}$$

The amplitude becomes

$$\begin{aligned} T^{\mu\nu} &= a_{12}\left[-(p_1\cdot p_2)g^{\mu\nu}+p_2^\mu p_1^\nu\right] \\ &\quad + a_{33}\left(\frac{(p_1\cdot p_3)(p_2\cdot p_3)}{(p_1\cdot p_2)}g^{\mu\nu}-\frac{(p_2\cdot p_3)}{(p_1\cdot p_2)}p_1^\mu p_3^\nu-\frac{(p_1\cdot p_3)}{(p_1\cdot p_2)}p_2^\mu p_3^\nu+p_3^\mu p_3^\nu\right), \end{aligned} \tag{B.8}$$

and factoring out the terms proportioanl to $g^{\mu\nu}$, the tensor reads:

$$\begin{aligned} a_{12}\to -\frac{a_{21}}{(p_1\cdot p_2)}, \qquad a_{33}\to \frac{(p_1\cdot p_2)}{(p_1\cdot p_3)(p_2\cdot p_3)}a_{33} \\ \mathcal{M}^{\mu\nu} = a_{12}\left(g^{\mu\nu}-\frac{p_2^\mu p_1^\nu}{(p_1\cdot p_2)}\right)+a_{33}\left(g^{\mu\nu}-\frac{(p_2\cdot p_3)p_1^\mu p_3^\nu+(p_1\cdot p_3)p_2^\mu p_3^\nu-(p_1\cdot p_2)p_3^\mu p_3^\nu}{(p_1\cdot p_3)(p_2\cdot p_3)}\right) \\ = a_{12}\widetilde{T}_1^{\mu\nu}+a_{33}\widetilde{T}_2^{\mu\nu} \end{aligned} \tag{B.9}$$

The tensors $\widetilde{T}_1^{\mu\nu}$ and $\widetilde{T}_2^{\mu\nu}$ are not orthogonal in four dimensions. Using $\widetilde{T}_1^{\mu\nu}$ as reference, the Gram-Schmidt orthogonalization yields:

$$\begin{aligned} T_1^{\mu\nu} &= \widetilde{T}_1^{\mu\nu} \\ T_2^{\mu\nu} &= \widetilde{T}_2^{\mu\nu}-\frac{(\widetilde{T}_2^{\mu\nu}T_{1\mu\nu})}{(T_1^{\mu\nu}T_{1\mu\nu})}T_{1\mu\nu} \end{aligned} \tag{B.10}$$

that can be enforced by the shift

$$a_{12} = F_1-\frac{(\widetilde{T}_2^{\mu\nu}T_{1\mu\nu})}{(T_1^{\mu\nu}T_{1\mu\nu})} = F_1-\frac{1}{2}\frac{(p_1\cdot p_2)p_3^2}{(p_1\cdot p_3)(p_2\cdot p_3)}. \tag{B.11}$$

Therefore, the amplitude is

$$\begin{aligned} \mathcal{M}^{\mu\nu} = F_1T_1^{\mu\nu}+a_{33}\Bigg(&\frac{2(p_1\cdot p_3)(p_2\cdot p_3)-(p_1\cdot p_2)p_3^2}{2(p_1\cdot p_3)(p_2\cdot p_3)}g^{\mu\nu} \\ &+\frac{p_3^2p_2^\mu p_1^\nu-2(p_2\cdot p_3)p_1^\mu p_3^\nu-2(p_1\cdot p_3)p_2^\mu p_3^\nu+2(p_1\cdot p_2)p_3^\mu p_3^\nu}{2(p_1\cdot p_3)(p_2\cdot p_3)}\Bigg) \end{aligned} \tag{B.12}$$

and defining the transverse momentum by

$$p_T^2 = \frac{2(p_1\cdot p_3)(p_2\cdot p_3)}{(p_1\cdot p_2)}-p_3^2, \tag{B.13}$$

it becomes

$$\begin{aligned} a_{33} &= \frac{2(p_1\cdot p_3)(p_2\cdot p_3)}{(p_1\cdot p_2)p_T^2}F_2 \\ \mathcal{M}^{\mu\nu} &= F_1T_1^{\mu\nu}+F_2\left(g^{\mu\nu}+\frac{p_3^2p_2^\mu p_1^\nu-2(p_2\cdot p_3)p_1^\mu p_3^\nu-2(p_1\cdot p_3)p_2^\mu p_3^\nu+2(p_1\cdot p_2)p_3^\mu p_3^\nu}{(p_1\cdot p_2)p_T^2}\right) \\ &= F_1T_1^{\mu\nu}+F_2T_2^{\mu\nu} \end{aligned} \tag{B.14}$$

and

$$\begin{aligned} T_1^{\mu\nu} &= g^{\mu\nu}-\frac{p_2^\mu p_1^\nu}{(p_1\cdot p_2)}, \\ T_2^{\mu\nu} &= g^{\mu\nu}+\frac{p_3^2p_2^\mu p_1^\nu-2(p_2\cdot p_3)p_1^\mu p_3^\nu-2(p_1\cdot p_3)p_2^\mu p_3^\nu+2(p_1\cdot p_2)p_3^\mu p_3^\nu}{(p_1\cdot p_2)p_T^2}. \end{aligned} \tag{B.15}$$

It is easy to show that in d dimensions, the tensor basis satisfies $T_1^{\mu\nu}T_{1\mu\nu} = T_2^{\mu\nu}T_{2\mu\nu} = d-2$ and $T_1^{\mu\nu}T_{2\mu\nu} = d-4$. The projectors onto $T_1^{\mu\nu}$ and $T_2^{\mu\nu}$ can be defined by using the following relations:

$$P_i^{\mu\nu}T_{j\mu\nu} = \delta_{ij}, \qquad P_i^{\mu\nu} = a_{i1}T_{1\mu\nu}+a_{i2}T_{2\mu\nu}, \tag{B.16}$$

and the solution of this system yields

$$P_1^{\mu\nu} = \frac{(d-2)T_1^{\mu\nu} + (d-4)T_2^{\mu\nu}}{4(d-3)}, \qquad P_2^{\mu\nu} = \frac{(d-4)T_1^{\mu\nu} + (d-2)T_2^{\mu\nu}}{4(d-3)}. \tag{B.17}$$

The projection of the amplitude onto the tensor basis $T_{1,2\mu\nu}$ is done by contracting $\mathcal{M}^{\mu\nu}$ with the projectors of Eq. (B.17); they give the form factors F_1 and F_2 which depend only on the kinematic variables and the space-time dimension d.

Appendix C

Phase space integral

The total cross section for a $2 \to n$ scattering process is the integral over the phase space of its square amplitude. The number of dimension of the phase space depends on the number of particle involved in the process, and increases fastly with n. In this Appendix the phase space elements for the $2 \to 2$ and $2 \to 3$ particles will be presented. In particular, the treatment of the $2 \to 3$ phase space involves a factorization, of crucial importance to define the infrared subtraction terms needed for isolating the soft and collinear divergences.

C.1 $2 \to 2$ process

C.1.1 Kinematics

Consider the process

$$g(p_1) + g(p_2) \to H_1(p_3) + H_2(p_4). \tag{C.1}$$

The definitions of the four-momenta (omitting the transpose notation) are: $p_1 = (E_1, E_1\hat{a})$, $p_2 = (E_2, E_2\hat{b})$ for the gluons and $p_3 = (\omega_3, \bar{p}_3 = |\bar{p}_3|\hat{c})$ and $p_4 = (\omega_4, \bar{p}_4 = |\bar{p}_4|\hat{d})$ for the two Higgs bosons, where we defined $\hat{a}, \hat{b}, \hat{c}, \hat{d}$ to be unitary length vectors. In the center-of-mass frame, we have

$$\begin{aligned} & p_1 + p_2 = p_3 + p_4 = (\sqrt{\hat{s}}, \bar{0}) \\ \implies & \begin{cases} (E_1 + E_2, E_1\hat{a} + E_2\hat{b}) = (\sqrt{\hat{s}}, \bar{0}) \\ (\omega_1 + \omega_2, |\bar{p}_3|\hat{c} + |\bar{p}_4|\hat{d}) = (\sqrt{\hat{s}}, \bar{0}) \end{cases} . \end{aligned} \tag{C.2}$$

From the tri-momenta components, we obtain:

$$\begin{aligned} E_1\hat{a} = -E_2\hat{b} &\implies E_1 = E_2 \quad \wedge \quad \hat{a} = -\hat{b} \\ |\bar{p}_3|\hat{c} = -|\bar{p}_4|\hat{d} &\implies |\bar{p}_3| = |\bar{p}_4| \quad \wedge \quad \hat{c} = -\hat{d}, \end{aligned} \tag{C.3}$$

and from the conservation of the energy:

$$E_1 + E_2 = 2E_1 = \sqrt{\hat{s}} \implies E_1 = \frac{\sqrt{\hat{s}}}{2}. \tag{C.4}$$

Therefore, incoming and outgoing particles lie on two different straight lines respectively. We chose the reference frame such that the incoming particles lie on the $\hat{z}$ axis, and the outgoing ones lie on a straight line generated by the unit vector $\hat{v}$. Moreover, by momentum conservation, we set $|\bar{p}_3| = |\bar{p}_4| = p_{\text{cm}}$. The kinematic of the process becomes

$$\begin{aligned} p_1 = \frac{\sqrt{\hat{s}}}{2}(1, \hat{z}), \qquad & p_2 = \frac{\sqrt{\hat{s}}}{2}(1, -\hat{z}) \\ p_3 = (\omega_3, p_{\text{cm}}\hat{v}), \qquad & p_4 = (\omega_4, -p_{\text{cm}}\hat{v}) \\ \omega_3 + \omega_4 = \sqrt{\hat{s}}. & \end{aligned} \tag{C.5}$$

The on-shell conditions state that $\omega_i^2 = p_{\rm cm}^2 + m_{H_i}^2$, so that

$$\begin{gathered} \omega_3^2 - m_{H_1}^2 = \omega_4^2 - m_{H_2}^2 \\ \omega_3^2 - m_{H_1}^2 = (\sqrt{\hat{s}} - \omega_3)^2 - m_{H_2}^2, \qquad (\sqrt{\hat{s}} - \omega_2)^2 - m_{H_1}^2 = \omega_4^2 - m_{H_2}^2 \\ \omega_3 = \frac{\hat{s} + m_{H_1}^2 - m_{H_2}^2}{2\sqrt{\hat{s}}}, \qquad \omega_4 = \frac{\hat{s} - m_{H_1}^2 + m_{H_2}^2}{2\sqrt{\hat{s}}}, \end{gathered} \tag{C.6}$$

and defining $\Delta = \frac{m_{H_2}^2 - m_{H_1}^2}{\hat{s}}$, we get

$$\begin{gathered} \Delta = \frac{m_{H_2}^2 - m_{H_1}^2}{\hat{s}} \\ \Downarrow \\ \omega_3 = \frac{\sqrt{\hat{s}}}{2}(1 - \Delta), \qquad \omega_4 = \frac{\sqrt{\hat{s}}}{2}(1 + \Delta). \end{gathered} \tag{C.7}$$

The Higgs bosons momentum $p_{\rm cm}$ in the CM frame is

$$\begin{aligned} p_{\rm cm}^2 &= \frac{\hat{s}}{4}(1 - \Delta)^2 - m_{H_1}^2 \\ &= \frac{\hat{s}}{4}\left(1 + \Delta^2 - 2\left(\Delta + \frac{2m_{H_1}^2}{\hat{s}}\right)\right) \\ &= \frac{\hat{s}}{4}\left(1 + \Delta^2 - 2\Sigma\right) \\ \implies p_{\rm cm} &= \frac{\sqrt{\hat{s}}}{2}\sqrt{1 + \Delta^2 - 2\Sigma} = \frac{\sqrt{\hat{s}}}{2}\beta, \end{aligned} \tag{C.8}$$

where we defined

$$\Sigma = \frac{m_{H_1}^2 + m_{H_2}^2}{\hat{s}}. \tag{C.9}$$

With these constraints, the transferred momentum square $\hat{t}$ is

$$\begin{aligned} \hat{t} = (p_3 - p_1)^2 &= -2(p_1 \cdot p_3) + p_3^2 \\ &= m_{H_1}^2 + p_{\rm cm}\sqrt{\hat{s}}(\hat{z} \cdot \hat{v}) - \sqrt{\hat{s}}\omega_1 \\ &= m_{H_1}^2 + \frac{\hat{s}}{2}\beta\cos\theta - \frac{s}{2}(1 - \Delta) \\ &= m_{H_1}^2 - \frac{\hat{s}}{2}(1 - \Delta - \beta\cos\theta) \\ &= -\frac{\hat{s}}{2}(1 - \Sigma - \beta\cos\theta). \end{aligned} \tag{C.10}$$

Using momentum conservation, the missing kinematic variable is $\hat{u}$, which is

$$\hat{u} = -\frac{\hat{s}}{2}(1 - \Sigma + \beta\cos\theta). \tag{C.11}$$

The independent variables are $\hat{s}$ and $\hat{t}$. Since the total cross section at fixed $\hat{s}$ is of interest, the phase space element will be integrated over $\hat{t}$.

C.1.2 d-dimensional Phase space integrals

The $a + b \to 1 + \cdots + n$ differential cross section is

$$d\sigma \propto (\mu^2)^{\frac{4-d}{2}} \int \frac{d^{d-1}\mathbf{p}_1}{(2\pi)^{d-1}} \cdots \frac{d^{d-1}\mathbf{p}_n}{(2\pi)^{d-1}} \frac{1}{(2\omega_1)} \cdots \frac{1}{(2\omega_n)} (2\pi)^d \delta^d(P - p_1 - \cdots - p_n) \overline{|\mathcal{M}|^2}, \tag{C.12}$$

where the integration is performed over the d.o.f. for which the amplitude does not depend on and $\hat{t}$, $\overline{|\mathcal{M}|^2}$ is the square amplitude averaged over the polarizations and $P = p_a + p_b$ is the total incoming momentum. Hence, we can define

$$dR_n = (\mu^2)^{\frac{4-d}{2}} \int \frac{d^{d-1}\mathbf{p}_1}{(2\pi)^{d-1}} \cdots \frac{d^{d-1}\mathbf{p}_n}{(2\pi)^{d-1}} \frac{1}{(2\omega_1)} \cdots \frac{1}{(2\omega_n)} (2\pi)^d \delta^d(P - p_1 - \cdots - p_n). \tag{C.13}$$

We are interested in dR_2 i.e. the phase space element of the $2 \to 2$ scattering process:

$$dR_2 = (\mu^2)^{\frac{4-d}{2}} \int \frac{d^{d-1}\mathbf{p}_3}{(2\pi)^{d-1}} \frac{d^{d-1}\mathbf{p}_4}{(2\pi)^{d-1}} \frac{1}{(2\omega_3)} \frac{1}{(2\omega_4)} (2\pi)^d \delta^d(P - p_3 - p_4), \tag{C.14}$$

where $P = p_1 + p_2 = (\sqrt{\hat{s}}, \bar{0}_{d-1})$ and p_3, p_4 are the two Higgs bosons momenta. Using the identity

$$\int \frac{d^{d-1}\mathbf{p}_4}{(2\pi)^{d-1}} \frac{1}{2\omega_4} = \int \frac{d^d p_4}{(2\pi)^{d-1}} \delta(p_4^2 - m_{H_2}^2) \Theta(\omega_4), \tag{C.15}$$

we obtain

$$\begin{aligned} dR_2 &= (\mu^2)^{\frac{4-d}{2}} \int \frac{d^{d-1}\mathbf{p}_3}{(2\pi)^{d-1}} \frac{d^d p_4}{(2\pi)^{d-1}} \frac{1}{2\omega_3} \delta(p_4^2 - m_{H_2}^2) \Theta(\omega_4) (2\pi)^d \delta^d(P - p_3 - p_4) \\ &= \frac{(\mu^2)^{\frac{4-d}{2}}}{(2\pi)^{d-2}} \int \frac{d^{d-1}\mathbf{p}_3}{2\omega_3} \delta((P - p_3)^2 - m_{H_2}^2) \Theta(\sqrt{\hat{s}} - \omega_3). \end{aligned} \tag{C.16}$$

The delta function can be transformed as follows

$$\begin{aligned} (P - p_3)^2 - m_{H_2}^2 &= s - 2\sqrt{\hat{s}}\omega_3 + m_{H_1}^2 - m_{H_2}^2, \\ \delta\left((P - p_3)^2 - m_{H_2}^2\right) &= \frac{1}{2\sqrt{\hat{s}}} \delta\left(\omega_3 - \frac{\sqrt{\hat{s}}}{2}(1 - \Delta)\right). \end{aligned} \tag{C.17}$$

The integration of the momenta in d-dimensional spherical coordinates reads

$$d^{d-1}\mathbf{p}_3 = p_{\rm cm}^{d-2} dp_{\rm cm} d\Omega = p_{\rm cm}^{d-3} \omega_3 d\omega_3 d\Omega_{d-2}, \tag{C.18}$$

the integral reads as

$$\begin{aligned} dR_2 &= \frac{(\mu^2)^{\frac{4-d}{2}}}{4(2\pi)^{d-2}} \int \frac{d\omega_3 d\Omega_{d-2}}{\sqrt{\hat{s}}} p_{\rm cm}^{d-3} \delta\left(\omega_3 - \frac{\sqrt{\hat{s}}}{2}(1 - \Delta)\right) \Theta(\sqrt{\hat{s}} - \omega_3) \\ &= (\mu^2)^{\frac{4-d}{2}} \frac{p_{\rm cm}^{d-3}}{4(2\pi)^{d-2}\sqrt{\hat{s}}} \int d\Omega_{d-2} \Theta\left(\frac{\sqrt{\hat{s}}}{2}(1 + \Delta)\right) \\ &= (\mu^2)^{\frac{4-d}{2}} \frac{\hat{s}^{\frac{d-4}{2}} \beta^{d-3}}{2^{2d-3}\pi^{d-2}} \int d\Omega_{d-2}. \end{aligned} \tag{C.19}$$

The condition on the Heaviside function is always satisfied ($\Delta > 0$).

The $(d-2)$-dimensional sphere can be integrated over $(d-3)$ angles since does not have any role in the scattering, and can be integrated out directly. The integration yields:

$$\begin{aligned} \int d\Omega_{d-2} &= d\theta \sin^{d-3}\theta \left[\int_0^\pi d\phi_2 \sin^{d-4}\phi_2\right] \cdots \left[\int_0^\pi d\phi_{d-3} \sin\phi_{d-3}\right] \left[\int_0^{2\pi} d\phi_{d-2}\right] \\ &= d\theta \sin^{d-3}\theta \int d\Omega_{d-3}, \end{aligned} \tag{C.20}$$

The angle element $d\theta$ has been factorized since the integrand will depend explicitely on it.

Using the following identity

$$\int_0^{\frac{\pi}{2}} d\phi_j \sin^n\phi_j \cos^m\phi_j = \frac{1}{2} \frac{\Gamma(\frac{1}{2}(n+1))\Gamma(\frac{1}{2}(m+1))}{\Gamma(\frac{1}{2}(n+m)+1)}, \tag{C.21}$$

for $m = 0$, the volume element becomes

$$\begin{aligned}\int d\Omega_{d-2} &= \left[\frac{\Gamma(\frac{d-3}{2})\Gamma(\frac{1}{2})}{\Gamma(\frac{d-2}{2})}\right]\left[\frac{\Gamma(\frac{d-4}{2})\Gamma(\frac{1}{2})}{\Gamma(\frac{d-3}{2})}\right]\cdots\left[\frac{\Gamma(1)\Gamma(\frac{1}{2})}{\Gamma(\frac{3}{2})}\right]\left[\int_0^{2\pi} d\phi_{d-2}\right]\sin^{d-3}\theta d\theta \\ &= \left[\frac{\Gamma^{d-4}(\frac{1}{2})}{\Gamma(\frac{d-2}{2})}\right]\left[\int_0^{2\pi} d\phi_{d-2}\right]\sin^{d-3}\theta d\theta,\end{aligned} \tag{C.22}$$

which contains a remarkable value of the Gamma function, such as

$$\Gamma\left(\frac{1}{2}\right) = \pi^{\frac{1}{2}}. \tag{C.23}$$

Therefore, we get

$$\int d\Omega_{d-2} = \frac{2\pi^{1-\epsilon}}{\Gamma(1-\epsilon)}\sin^{d-3}\theta d\theta, \tag{C.24}$$

where we have integrated over the ϕ_{d-2} angle since the scattering occur on the $\widehat{xz}$ plane. We will see that we are not legitimate to integrate away this variable for the calculation of dR_3 since the $2 \to 3$ scattering does not happen on a single plane. An important result of this integration states that:

$$d\Omega_{n-1} = \frac{2\pi^{\frac{n}{2}}}{\Gamma\left(\frac{n}{2}\right)} = \frac{2\pi^{\frac{n-1}{2}}}{\Gamma\left(\frac{n-1}{2}\right)}\sin^{n-2}\theta d\theta \tag{C.25}$$

We can first present the result of the integration over the whole phase space:

$$\begin{aligned}\int dR_2 &= \left(\frac{\mu^2}{\hat{s}}\right)^{\epsilon}\frac{\beta^{1-2\epsilon}}{4^{2-2\epsilon}\pi^{1-\epsilon}}\frac{1}{\Gamma(1-\epsilon)}\int\sin^{d-3}\theta d\theta \\ &= \left(\frac{\mu^2}{\hat{s}}\right)^{\epsilon}\frac{\beta^{1-2\epsilon}}{4^{2-2\epsilon}\pi^{1-\epsilon}}\frac{1}{\Gamma(1-\epsilon)}\left[\frac{\Gamma(1-\epsilon)\Gamma(\frac{1}{2})}{\Gamma(\frac{1}{2}+1-\epsilon)}\right].\end{aligned} \tag{C.26}$$

A useful identity involving the Gamma function is:

$$\Gamma(2n) = \frac{4^n}{\sqrt{4\pi}}\Gamma(n)\Gamma\left(\frac{1}{2}+n\right), \tag{C.27}$$

which brings the phase space integral to the following form

$$\int dR_2 = \left(\frac{4\pi\mu^2}{\hat{s}}\right)^{\epsilon}\frac{\beta^{1-2\epsilon}}{8\pi}\frac{\Gamma(1-\epsilon)}{\Gamma(2-2\epsilon)}. \tag{C.28}$$

If we keep the dependence on the θ angle, the expression is more involved

$$dR_2 = \left(\frac{4\pi\mu^2}{\hat{s}}\right)^{\epsilon}\frac{\beta^{1-2\epsilon}}{16\pi}\frac{1}{\Gamma(1-\epsilon)}\left(\frac{1-\cos^2\theta}{4}\right)^{-\epsilon}d\cos\theta, \tag{C.29}$$

but the factor involving the cosine square can be simplified by using the explicit expression of $\cos\theta$ in Eq. (C.10) and the relations contained into Appendix F:

$$\begin{aligned}\frac{1-\cos^2\theta}{4} = -\frac{1}{\beta^2}\left[\frac{\left(\hat{t}-m_{H_1}^2\right)\left(\hat{t}-m_{H_2}^2\right)+\hat{s}\hat{t}}{\hat{s}^2}\right] &= \frac{1}{\beta^2}\frac{p_T^2}{\hat{s}} \\ \Downarrow \\ dR_2 = \left(\frac{4\pi\mu^2}{p_T^2}\right)^{\epsilon}\frac{\beta}{16\pi}\frac{1}{\Gamma(1-\epsilon)}&d\cos\theta.\end{aligned} \tag{C.30}$$

The integral over the θ angle is related to the trasferred momentum square $\hat{t}$:

$$\hat{t} = -\frac{\hat{s}}{2}(1-\Sigma-\beta\cos\theta) \implies d\hat{t} = \frac{\hat{s}\beta}{2}d\cos\theta, \tag{C.31}$$

hence we get the following final expression:

$$dR_2 = \left(\frac{4\pi\mu^2}{p_T^2}\right)^{\epsilon} \frac{1}{\Gamma(1-\epsilon)} \frac{d\hat{t}}{8\pi\hat{s}}. \tag{C.32}$$

where p_T^2 depends on $\hat{t}$. For the LO and the NLO virtual corrections, the dR_2 can be expanded around $\epsilon \to 0$:

$$dR_2|_{\epsilon=0} = \frac{d\hat{t}}{8\pi\hat{s}}. \tag{C.33}$$

C.1.3 Differential partonic cross section: setup

The differential cross section for the partonic scattering under investigation is

$$d\hat{\sigma} = C_{\text{flux}} C_{\text{sym}} \int d\text{PS}_2 \overline{|\mathcal{M}_{\text{LO}}|^2} \tag{C.34}$$

where C_{flux} is the flux factor and C_{sym} is the symmetry factor. The flux coefficient C_{flux} for the QCD Higgs-pair production via gluon fusion process is

$$C_{\text{flux}} = \frac{1}{4\sqrt{(p_1 \cdot p_2)^2 - p_1^2 p_2^2}} = \frac{1}{4|p_1 \cdot p_2|} = \frac{1}{2\hat{s}} \tag{C.35}$$

hence the differential cross section becomes

$$\begin{aligned} d\hat{\sigma} &= C_{\text{sym}} \frac{dR_2}{2s} \overline{|\mathcal{M}|^2} \\ &= C_{\text{sym}} \frac{d\hat{t}}{16\pi\hat{s}^2} \overline{|\mathcal{M}|^2}. \end{aligned} \tag{C.36}$$

We now extract the factor coming from the averaged square amplitude: each gluon in the initial state can have 2 polarizations and $(N_c^2 - 1)$ colors. Therefore

$$\begin{aligned} d\hat{\sigma} &= \frac{d\hat{t}}{16\pi\hat{s}^2} \frac{1}{4} \frac{C_{\text{sym}}}{(N^2-1)^2} \sum_{a,b} \sum_{h_1,h_2} |\mathcal{M}|^2 \\ &= \frac{d\hat{t}}{16\pi\hat{s}^2} \frac{1}{4} \frac{C_{\text{sym}}}{64} \sum_{a,b} \sum_{h_1,h_2} |\mathcal{M}|^2, \end{aligned} \tag{C.37}$$

where C_{sym} is the factor which takes into account the permutation of the external legs. We can permute the initial state gluon but not the Higgs in the final state. Moreover, the final state Higgs bosons are different: no identical final state factor is needed. This implies $C_{\text{sym}} = 2$ and

$$\begin{aligned} d\hat{\sigma} &= \frac{d\hat{t}}{16\pi\hat{s}^2} \frac{1}{4} \frac{2}{64} \sum_{a,b} \sum_{h_1,h_2} |\mathcal{M}|^2 \\ &= \frac{d\hat{t}}{16\pi\hat{s}^2} \frac{1}{128} \sum_{a,b} \sum_{h_1,h_2} |\mathcal{M}|^2. \end{aligned} \tag{C.38}$$

C.1.4 Polarization sum

Assuming that a gluon is moving along the $\hat{z}$ axis with momentum $p_1^\mu = \omega_1(1, \hat{z})$, its two polarization physical polarization vectors can be written as[1]

$$\epsilon_\mu^+(p_1) = \frac{1}{\sqrt{2}}(0, 1, i, 0), \qquad \epsilon_\mu^-(p_1) = \frac{1}{\sqrt{2}}(0, 1, -i, 0). \tag{C.39}$$

[1]The Lorentz gauge is implicitely assumed.

These polarization vector satisfy the following relations:

$$p_1^\mu \epsilon_\mu^\pm(p_1) = 0, \qquad \epsilon_\mu^{h_1}(p_1)\epsilon^{*h_2\mu}(p_1) = -\delta^{h_1 h_2}. \tag{C.40}$$

The basis can be completed by adding the longitudinal polarization and an additional light-like polarization vector:

$$\epsilon_L^\mu(p_1) = \frac{1}{\sqrt{2}}(1,\hat{z}) = \frac{p_1^\mu}{\sqrt{2}\omega_1}, \qquad \tilde{\epsilon}_L^\mu(q) = \frac{1}{\sqrt{2}}(1,-\hat{z}) = \frac{q^\mu}{\sqrt{2}\omega_q}, \qquad q^\mu = \omega_q(1,-\hat{z}), \tag{C.41}$$

where q^μ is a *reference momentum*, whose 3-momentum is anti-parallel to the gluon 3-momentum. The completeness relation of this basis reads

$$-\epsilon_\mu^+(p_1)\epsilon_\nu^{*+}(p_1) - \epsilon_\mu^-(p_1)\epsilon_\nu^{*-}(p_1) + \epsilon_{L\mu}(p_1)\tilde{\epsilon}_{L\nu}^*(q) + \tilde{\epsilon}_{L\mu}(q)\epsilon_{L\nu}^*(p_1) = g_{\mu\nu}, \tag{C.42}$$

and using the explicit expressions for the longitudinal four-vectors, the polarization sum takes the following form:

$$\sum_{h=\pm} \epsilon_\mu^h(p_1)\epsilon_\nu^{*h}(p_1) = -g_{\mu\nu} + \frac{p_{1\mu}q_\nu + q_\mu p_{1\nu}}{p_1\cdot q} = -g_{\mu\nu} + \frac{p_{1\{\mu}q_{\nu\}}}{p_1\cdot q}, \tag{C.43}$$

where the $\{\cdots\}$ is the symmetrization of the tensor with respect to the index they wrap.

For QCD processes, if one wants to perform the QED-like polarization sum, namely

$$\sum_{h=\pm} \epsilon_\mu^h(p_1)\epsilon_\nu^{*h}(p_1) = -g_{\mu\nu} \tag{C.44}$$

the ghost contributions are needed, otherwise the general polarization sum of Eq. (C.43) is mandatory in order to avoid not sum over the unphysical degrees of freedom. To make clear this point, the amplitude of the process under consideration can be written as

$$\mathcal{M} = \epsilon_\mu(p_1)\epsilon_\nu(p_2)\mathcal{M}^{\mu\nu}. \tag{C.45}$$

The sum of over the physical polarization yields:

$$\begin{aligned}
\sum_{h_1,h_2=\pm} |\mathcal{M}|^2 &= \sum_{h_1,h_2=\pm} \epsilon_\mu^{h_1}(p_1)\epsilon_\rho^{*h_1}(p_1)\epsilon_\nu^{h_2}(p_2)\epsilon_\sigma^{*h_2}(p_2)\mathcal{M}^{\mu\nu}\mathcal{M}^{\rho\sigma}, \\
\sum_{h_1,h_2=\pm} |\mathcal{M}|^2 &= \sum_{h_1=\pm} \epsilon_\mu^{h_1}(p_1)\epsilon_\rho^{*h_1}(p_1)\left[-g_{\nu\sigma} + \frac{p_{2\{\nu}q'_{\sigma\}}}{p_2\cdot q'}\right]\mathcal{M}^{\mu\nu}\mathcal{M}^{*\rho\sigma} \\
&= \left[-\sum_{h_1=\pm} \epsilon_\mu^{h_1}(p_1)\epsilon_\rho^{*h_1}(p_1)g_{\nu\sigma} + \sum_{h_1=\pm} \epsilon_\mu^{h_1}(p_1)\epsilon_\rho^{*h_1}(p_1)\frac{p_{2\{\nu}q'_{\sigma\}}}{p_2\cdot q'}\right]\mathcal{M}^{\mu\nu}\mathcal{M}^{*\rho\sigma},
\end{aligned} \tag{C.46}$$

The polarization sum depicted into Eq. (C.46) is rather complex, but it can be simplified. It can be shown that,

$$p_{1\mu}\epsilon_\nu^h(p_2)\mathcal{M}^{\mu\nu} \propto p_2^\nu \epsilon_\nu^h(p_2), \tag{C.47}$$

which implies that, for longitudinal polarization:

$$p_{1\mu}\epsilon_{L\nu}(p_2)\mathcal{M}^{\mu\nu} \propto p_2^\nu \epsilon_{L\nu}(p_2) = 0, \qquad p_2^2 = 0, \tag{C.48}$$

therefore

$$p_{1\mu}p_{2\nu}\mathcal{M}^{\mu\nu} = 0. \tag{C.49}$$

In particular, it means that $p_{2\mu}\epsilon_\nu^h(p_2)\mathcal{M}^{\mu\nu} = 0$ if $\epsilon_\nu^h(p_2)p_2^\nu = 0$ for $h = \pm$ (meaning that such gluon is transverse).

Therefore, the second term in the parenthesis of Eq. (C.46) vanishes because of Eq. (C.47) for physical gluons:

$$\begin{aligned}\sum_{h_1,h_2=\pm}|\mathcal{M}|^2 &= \left[-\sum_{h_1=\pm}\epsilon_\mu^{h_1}(p_1)\epsilon_\rho^{*h_1}(p_1)g_{\nu\sigma}\right]\mathcal{M}^{*\rho\sigma}\mathcal{M}^{\mu\nu}\\ &= \left[g_{\mu\rho}g_{\nu\sigma}-g_{\nu\sigma}\frac{p_{1\{\mu}q_{\rho\}}}{p_1\cdot q}\right]\mathcal{M}^{*\rho\sigma}\mathcal{M}^{\mu\nu}\\ &= \left[g_{\mu\rho}g_{\nu\sigma}+\left(\sum_{h_2=\pm}\epsilon_\nu^{h_2}(p_2)\epsilon_\sigma^{*h_2}(p_2)\right)\frac{p_{1\{\mu}q_{\rho\}}}{p_1\cdot q}-\frac{p_{1\{\mu}q_{\rho\}}}{p_1\cdot q}\frac{p_{2\{\nu}q'_{\sigma\}}}{p_2\cdot q'}\right]\mathcal{M}^{*\rho\sigma}\mathcal{M}^{\mu\nu}\\ &= \left[g_{\mu\rho}g_{\nu\sigma}-\frac{p_{1\{\mu}q_{\rho\}}}{p_1\cdot q}\frac{p_{2\{\nu}q'_{\sigma\}}}{p_2\cdot q'}\right]\mathcal{M}^{*\rho\sigma}\mathcal{M}^{\mu\nu},\end{aligned} \tag{C.50}$$

where again the transversality of $\epsilon^\nu(p_2)$ has been exploited. Finally, expanding the symmetrical combination into the parenthesis, the square amplitude reads:

$$\sum_{h_1,h_2=\pm}|\mathcal{M}|^2=\left[g_{\mu\rho}g_{\nu\sigma}-\frac{p_{1\rho}q_\mu p_{2\nu}q'_\sigma+p_{1\mu}q_\rho p_{2\sigma}q'_\nu}{(p_1\cdot q)(p_2\cdot q')}\right]\mathcal{M}^{*\rho\sigma}\mathcal{M}^{\mu\nu}. \tag{C.51}$$

A convenient choice of the reference momenta will introduce a further simplification: setting $q=p_2$ and $q'=p_1$, Eq. (C.46) becomes

$$\sum_{h_1,h_2=\pm}|\mathcal{M}|^2=\left[g_{\mu\rho}g_{\nu\sigma}-\frac{p_{2\mu}p_{2\nu}p_{1\rho}p_{1\sigma}+p_{1\mu}p_{1\nu}p_{2\rho}p_{2\sigma}}{(p_1\cdot p_2)^2}\right]\mathcal{M}^{*\rho\sigma}\mathcal{M}^{\mu\nu}. \tag{C.52}$$

In general, the second term of Eq. (C.52) yields non-vanishing contribution of the polarization sum. However, in Appendix B the axial gauge has been used to extract the form factors; the expression of the amputated amplitude is

$$\mathcal{M}^{\mu\nu}=\delta_{ab}\left(F_1T_1^{\mu\nu}+F_2T_2^{\mu\nu}\right). \tag{C.53}$$

It is possible to show that

$$p_{1\mu}p_{1\nu}T_j^{\mu\nu}=p_{2\mu}p_{2\nu}T_j^{\mu\nu}=0, \tag{C.54}$$

as expected from the tensors written in the axial gauge. Therefore, the second term of Eq. (C.52) will always lead to vanishing contribution, and therefore it can be neglected:

$$\sum_{h_1,h_2=\pm}|\mathcal{M}|^2=g_{\mu\rho}g_{\nu\sigma}\mathcal{M}^{*\rho\sigma}\mathcal{M}^{\mu\nu}. \tag{C.55}$$

It is important to underline that Eq. (C.55) is a direct consequence of considering the polarization vectors in the axial gauge for the $2\to2$ process. For the $2\to3$ process no axial gauge form factors will be provided, and the general polarization sum of Eq. (C.43) have to be used.

C.1.5 Differential partonic cross section: Virtual corrections

At LO, the square amplitude (in $d=4$) is

$$\begin{aligned}|\mathcal{M}_{\rm LO}|^2 &= g_{\mu\rho}g_{\nu\sigma}\mathcal{M}_{\rm LO}^{*\rho\sigma}\mathcal{M}_{\rm LO}^{\mu\nu}\\ &= \delta_{ab}\delta_{ba}\left[F_1^{(0)}T_1^{\mu\nu}+F_2^{(0)}T_2^{\mu\nu}\right]^*\left[F_1^{(0)}T_{1\mu\nu}+F_2^{(0)}T_{2\mu\nu}\right]\\ &= 2\delta_{ab}\delta_{ba}\left(|F_1^{(0)}|^2+|F_2^{(0)}|^2\right).\end{aligned} \tag{C.56}$$

Putting all the ingredients together, the LO partonic cross sections reads

$$\begin{aligned} d\hat{\sigma}_{\rm LO} &= \frac{d\hat{t}}{16\pi s^2}\frac{1}{128}\sum_{a,b}\sum_{h_1,h_2}|\mathcal{M}_{\rm LO}|^2 \\ &= \frac{d\hat{t}}{16\pi \hat{s}^2}\frac{1}{64}\left(\sum_{a,b}\delta_{ab}\delta_{ba}\right)\left(|F_1^{(0)}|^2+|F_2^{(0)}|^2\right) \\ &= \frac{d\hat{t}}{16\pi \hat{s}^2}\frac{{\rm Tr}\left[\delta_{N_c^2-1}\right]}{64}\left(\left|F_1^{(0)}\right|^2+|F_2^{(0)}|^2\right) \\ &= \frac{d\hat{t}}{128\pi \hat{s}^2}\left(|F_1^{(0)}|^2+|F_2^{(0)}|^2\right), \end{aligned} \tag{C.57}$$

where $N_c = 3$.

At NLO, the intereference between the one-loop and two-loop virtual amplitude have to be considered:

$$\begin{aligned} \sum_{h_1,h_2=\pm} 2{\rm Re}\mathcal{M}^*_{\rm LO}\mathcal{M}_{\rm NLO} &= 2g_{\mu\rho}g_{\nu\sigma}{\rm Re}\mathcal{M}^{\mu\nu}_{\rm LO}\mathcal{M}^{*\rho\sigma}_{\rm NLO} \\ &= 2\delta_{ab}\delta_{ba}{\rm Re}\left[F_1^{(0)}T_1^{\mu\nu}+F_2^{(0)}T_2^{\mu\nu}\right]^*\left[F_1^{(1)}T_{1\mu\nu}+F_2^{(1)}T_{2\mu\nu}\right] \\ &= 4\delta_{ab}\delta_{ba}{\rm Re}\left(F_1^{*(0)}F_1^{(1)}+F_2^{*(0)}F_2^{(1)}\right) \end{aligned} \tag{C.58}$$

which leads to

$$d\Delta\hat{\sigma}_{\rm NLO} = \frac{d\hat{t}}{64\pi\hat{s}^2}{\rm Re}\left(F_1^{*(0)}F_1^{(1)}+F_2^{*(0)}F_2^{(1)}\right). \tag{C.59}$$

C.2 $2 \to 3$ process

The 5-points kinematic is more involved than the 4-point one. Consider the $2 \to 3$ process

$$g(p_1)+g(p_2) \to H_1(p_3)+H_1(p_4)+g(p_5), \tag{C.60}$$

where additional outgoing particle with four-momentum

$$p_5 = (E_5, \bar{p}_5), \tag{C.61}$$

is considered. After applying the conservation of the four-momentum, the kinematic of the process can be written as

$$\begin{gathered} p_1+p_2 = p_3+p_4+p_5 \\ \Downarrow \\ \begin{cases} (E_1+E_2, E_1\hat{a}+E_2\hat{b}) = (\sqrt{\hat{s}},\bar{0}) \\ (E_3+E_4+E_5, E_3\hat{c}+E_4\hat{d}+E_5\hat{e}) = (\sqrt{\hat{s}},\bar{0}) \end{cases} \\ \Downarrow \\ E_1\hat{a}+E_2\hat{b}=0 \implies E_1\hat{a} = -E_2\hat{b} \implies E_1 = E_2 = \frac{\sqrt{\hat{s}}}{2}, \\ E_3+E_4+E_5 = \sqrt{\hat{s}} \implies x_3+x_4+x_5 = 2, \qquad E_i = x_i\frac{\sqrt{\hat{s}}}{2}, \end{gathered} \tag{C.62}$$

where x_i is the fraction of center-of-mass energy $\hat{s}$. The momentum p_3 is parametrized such that it lies on $\hat{z}$ axis. Before explaining the details of the phase space, we introduce the relevant kinematic variables

$$2p_1\cdot p_2 = \hat{s}, \qquad -2p_1\cdot p_5 = \hat{t}, \qquad -2p_2\cdot p_5 = \hat{u}, \qquad (p_3+p_4)^2 = \hat{s}+\hat{t}+\hat{u} = Q^2. \tag{C.63}$$

The incoming particles four momenta can be parametrize as follows

$$p_1 = \frac{\sqrt{\hat{s}}}{2}(1, \cos\theta_{15}, 0, \sin\theta_{15}), \qquad p_2 = \frac{\sqrt{\hat{s}}}{2}(1, -\cos\theta_{15}, 0, -\sin\theta_{15}), \tag{C.64}$$

where the scattering occur int the $\hat{xz}$ plane and the radiating parton p_5 lays on the $\hat{z}$ axis; θ_{15} is the angle between p_1 and p_5 on the $\hat{xz}$ plane:

$$p_5 = \frac{\sqrt{\hat{s}}}{2}x_5(1, 0, 0, 1). \tag{C.65}$$

At last, we define the angle θ_{35} and φ_{35} to be the projected angles that in spherical coordinates parametrize the direction of p_3; due to momentum conservation, these directions are sufficient to parametrize the scattering. Note that the same setup can be applied by choosing any of the outgoing momentum, and we can define the angles θ_{ij} and φ_{ij} for every couple of momenta.

Therefore, the kinematic of the process is:

$$\begin{gathered}
p_3 = \frac{\sqrt{\hat{s}}}{2}x_3(1, \beta_3\cos\varphi_{35}\sin\theta_{35}, \beta_3\sin\varphi_{35}\sin\theta_{35}, \beta_3\cos\theta_{35}), \\
p_4 = \frac{\sqrt{\hat{s}}}{2}(x_4, -x_3\beta_3\cos\varphi_{35}\sin\theta_{35}, -x_3\beta_3\sin\varphi_{35}\sin\theta_{35}, -x_5 - x_3\beta_3\cos\theta_{35}), \\
\mu_i = \frac{m_i}{\sqrt{\hat{s}}}, \\
\beta_i = \sqrt{1 - 4\frac{\mu_i^2}{x_i^2}}, \qquad \cos\theta_{ij} = \frac{2}{x_i x_j \beta_i \beta_j}\left(1 - x_i - x_j + \frac{x_i x_j}{2} + \mu_i + \mu_j - \mu_k\right).
\end{gathered} \tag{C.66}$$

These definitions set boundaries on the parameters we have chosen. The particles production thresholds state that $(p_i + p_j) \geq (m_i + m_j)^2$. For x_5, we have

$$\begin{gathered}
\begin{cases} p_5^0 \geq 0 \\ (p_3 + p_4)^2 = (p_1 + p_2 - p_5)^2 \geq (m_{H_1} + m_{H_2})^2 \end{cases} \\
\Downarrow \\
0 \leq x_5 \leq 1 - (\mu_{H_1} + \mu_{H_2})^2.
\end{gathered} \tag{C.67}$$

The constraint on x_3 comes from the image of $\cos\theta_{35}$, meaning that it can be read from

$$\begin{gathered}
-1 \leq \cos\theta_{35} \leq 1 \implies \cos^2\theta_{35} \leq 1 \\
\Downarrow \\
x_3^2(1 - x_5) - x_3(2 - x_5)(1 - x_5 - \Delta) + (1 - x_5 - \Delta)^2 + \mu_{H_1}^2 x_5^2 \leq 0,
\end{gathered} \tag{C.68}$$

and solving for x_3, we obtain the following condition:

$$\begin{gathered}
x_3^- \leq x_3 \leq x_3^+ \\
x_3^\pm = \frac{(2 - x_5)(1 - x_5 - \Delta) \pm x_5(1 - x_5)\beta_{x_5}}{2(1 - x_5)} \\
\beta_{x_5} = \sqrt{\left[1 - \frac{(\mu_{H_2} + \mu_{H_1})^2}{(1 - x_5)}\right]\left[1 - \frac{(\mu_{H_2} - \mu_{H_1})^2}{(1 - x_5)}\right]}.
\end{gathered} \tag{C.69}$$

C.2.1 d-dimensional Phase space integrals

Recalling the definition presented in Eq. (C.1.2), the phase space element dR_3 is

$$dR_3 = (\mu^2)^{\frac{4-d}{2}} \int \frac{d^{d-1}\mathbf{p}_3}{(2\pi)^{d-1}} \frac{d^{d-1}\mathbf{p}_4}{(2\pi)^{d-1}} \frac{d^{d-1}\mathbf{p}_5}{(2\pi)^{d-1}} \frac{1}{(2\omega_3)} \frac{1}{(2\omega_4)} \frac{1}{(2\omega_5)} (2\pi)^d \delta^d(P - p_3 - p_4 - p_5), \tag{C.70}$$

where $P = p_1 + p_2 = (\sqrt{s}, \bar{0}_{d-1})$ and p_3, p_4, p_5 are the two Higgs bosons momenta and the additional parton. Similarly to the steps described for the 2-particle phase space, the integraation over p_4 yields

$$\begin{aligned} dR_3 &= \frac{(\mu^2)^{4-d}}{(2\pi)^{2d-3}} \int \frac{d^{d-1}\mathbf{p}_3}{(2\omega_3)} \frac{d^{d-1}\mathbf{p}_5}{(2\omega_5)} d^d p_4 \delta(p_4^2 - m_{H_2}^2)\Theta(p_4^0)\delta^d(P - p_3 - p_4 - p_5) \\ &= \frac{(\mu^2)^{4-d}}{4(2\pi)^{2d-3}} \int \frac{d^{d-1}\mathbf{p}_3}{\omega_3} \frac{d^{d-1}\mathbf{p}_5}{\omega_5} \delta((P - p_3 - p_5)^2 - m_{H_2}^2). \end{aligned} \tag{C.71}$$

The argument of the Dirac delta is

$$\begin{aligned} (P - p_3 - p_5)^2 - m_{H_2}^2 &= \hat{s} - \hat{s}(x_3 + x_5) + \frac{\hat{s}}{2} x_3 x_5 (1 - \beta_3 \cos\theta_{35}) + m_{H_1}^2 - m_{H_2}^2 \\ &= \hat{s}\left[1 - x_3 - x_5 + \frac{x_3 x_5}{2}(1 - \beta_3 \cos\theta_{35}) - \Delta\right], \end{aligned} \tag{C.72}$$

and we define the angle for which this expression vanished as

$$\cos\theta_{35}^0 = \frac{2}{\beta_3 x_3 x_5}\left[1 - \Delta - x_3 - x_5 + \frac{1}{2} x_3 x_5\right]. \tag{C.73}$$

Moreover, the integration measurements in spherical coordinates becomes

$$d^{d-1}\mathbf{p}_3 = \frac{\hat{s}^{\frac{d-2}{2}}(x_3\beta_3)^{d-3}}{2^{d-2}} \omega_3 dx_3 d\Omega_{d-2}^{(3)}, \tag{C.74}$$

hence

$$dR_3 = \frac{(\mu^2)^{4-d}\hat{s}^{d-2}}{4(2\pi)^{2d-3}4^{d-2}} \int dx_3 dx_5 d\Omega_{d-2}^{(3)} d\Omega_{d-2}^{(5)} (\beta_3 x_3 x_5)^{d-3} \frac{2}{s\beta_3 x_3 x_5} \delta(\cos\theta_{35} - \cos\theta_{35}^0). \tag{C.75}$$

The angle elements are:

$$\begin{aligned} d\Omega_{d-2}^{(3)} &= \int \sin^{d-3}\theta_{35} \sin^{d-4}\phi_2 \cdots \sin\phi_{d-3} d\theta_{35} d\phi_2 \cdots d\phi_{d-2} \\ &= \left[\int \sin^{d-4}\phi_2 \cdots \sin\phi_{d-3} d\phi_2 \cdots d\phi_{d-2}\right] (1 - \cos^2\theta_{35})^{\frac{d-4}{2}} d\cos\theta_{35} \\ &= \Omega_{d-3}(1 - \cos^2\theta_{35})^{\frac{d-4}{2}} d\cos\theta_{35}, \end{aligned} \tag{C.76}$$

$$d\Omega_{d-2}^{(5)} = \Omega_{d-4}(1 - \cos^2\theta_{15})^{\frac{d-4}{2}} \sin^{d-4}\varphi_{35}\ d\cos\theta_{15} d\varphi_{35}.$$

The integral over the solid angle yields:

$$\Omega_n = \frac{2\pi^{\frac{n+1}{2}}}{\Gamma(\frac{n+1}{2})}, \tag{C.77}$$

therefore

$$\begin{aligned} dR_3 &= \frac{(\mu^2)^{4-d}\hat{s}^{d-3}}{(2\pi)^{2d-3}4^{d-2}} \frac{2\pi^{\frac{d-2}{2}}\pi^{\frac{d-3}{2}}}{\Gamma(\frac{d-2}{2})\Gamma(\frac{d-3}{2})} \times \\ &\quad \times dx_3 dx_5 d\cos\theta_{15} d\varphi_{35} (1 - \cos^2\theta_{35}^0)^{\frac{d-4}{2}} (1 - \cos^2\theta_{15})^{\frac{d-4}{2}} \sin^{d-4}\varphi_{35}\ (\beta_3 x_3 x_5)^{d-4} \\ &= \frac{\hat{s}}{(4\pi)^4} \frac{4^{2\epsilon}\pi^{\frac{1}{2}}}{\Gamma(1-\epsilon)\Gamma\left(\frac{1}{2} - \epsilon\right)} \left(\frac{4\pi\mu^2}{\hat{s}}\right)^{2\epsilon} \times \\ &\quad \times dx_3 dx_5 d\cos\theta_{15} d\varphi_{35} (1 - \cos^2\theta_{35}^0)^{-\epsilon} (1 - \cos^2\theta_{15})^{-\epsilon} \sin^{-2\epsilon}\varphi_{35}\ (\beta_3 x_3 x_5)^{-2\epsilon}. \end{aligned} \tag{C.78}$$

At last, using the following identity:

$$\Gamma\left(\frac{1}{2} - n\right) = 4^n \sqrt{\pi} \frac{\Gamma(1-2n)}{\Gamma(1-n)}, \tag{C.79}$$

the phase-space integral becomes

$$dR_3 = \frac{\hat{s}}{(4\pi)^4}\left(\frac{4\pi\mu^2}{\hat{s}x_3x_5}\right)^{2\epsilon}\left(\beta_3^2\frac{1-\cos^2\theta_{35}^0}{4}\right)^{-\epsilon}\frac{(1-\cos^2\theta_{15})^{-\epsilon}\sin^{-2\epsilon}\varphi_{35}}{\Gamma(1-2\epsilon)}dx_3dx_5d\cos\theta_{15}d\varphi_{35}. \tag{C.80}$$

The dR_3 can be manipulae such that a R_2 factors, and the integration boundaries of the fraction of the momenta x_3 and x_5 are set from 0 to 1. Notice that

$$\begin{aligned}\frac{1-\cos\theta_{35}^0}{2} &= \frac{1}{2\beta_3}\left[\beta_3 - 1 + 2\frac{(1-x_4)+\Delta}{x_3x_5}\right],\\ \frac{1+\cos\theta_{35}^0}{2} &= \frac{1}{2\beta_3}\left[\beta_3 - 1 + 2\frac{(1-x_3)(1-x_5)-\Delta}{x_3x_5}\right],\\ x_3^2x_5^2\beta_3^2\frac{1-\cos^2\theta_{35}^0}{4} &= (1-x_4)(1-x_3)(1-x_5) - \mu_{H_1}^2x_5^2 + \Delta[2(1-x_3-x_5)+x_3x_5-\Delta].\end{aligned} \tag{C.81}$$

Defining the variable z to be the fraction of the invariant Higgs-pair mass Q^2 with respect to $\sqrt{\hat{s}}$

$$z = \frac{Q^2}{\hat{s}} = \frac{(p_3+p_4)^2}{\hat{s}} = 1 - x_5 \implies x_5 = 1-z, \qquad dx_5 = -dz, \tag{C.82}$$

the Eq. (C.81) simplifies:

$$x_3^2x_5^2\beta_3^2\frac{1-\cos^2\theta_{35}^0}{4} = (x_3-z)(1-x_3)z - \mu_{H_1}^2(1-z)^2 + \Delta[2(z-x_3)+x_3(1-z)-\Delta]. \tag{C.83}$$

Defining $x_3 = 1-y$, the expression reads

$$x_3^2x_5^2\beta_3^2\frac{1-\cos^2\theta_{35}^0}{4} = (1-y-z)yz - \mu_{H_1}^2(1-z)^2 + \Delta[-2(1-y-z)+(1-y)(1-z)-\Delta]. \tag{C.84}$$

Finally, letting $y = (1-z)x$, Eq. (C.81) reads

$$\begin{aligned}x_3^2x_5^2\beta_3^2\frac{1-\cos^2\theta_{35}^0}{4} &= (1-z)^2z(1-x)x - \mu_{H_1}^2(1-z)^2 - (1-z)\Delta[1-(1+z)x] - \Delta^2,\\ &= z(1-z)^2\left[(1-x)x - \frac{\mu_{H_1}^2}{z} - \frac{\Delta[1-(1+z)x]}{z(1-z)} - \frac{\Delta^2}{z(1-z)^2}\right]\end{aligned} \tag{C.85}$$

These change of variables lead to the following integration measure:

$$\begin{aligned}\int_0^{1-(\mu_{H_1}+\mu_{H_2})^2}dx_5\int_{x_3^-}^{x_3^+}dx_3 &= \int_{(\mu_{H_1}+\mu_{H_2})^2}^1 dz\int_{x_-}^{x_+}dx(1-z),\\ x^\pm = \frac{1}{2}\left(1+\frac{\Delta(1+z)}{z(1-z)}\pm\beta_z\right), \qquad \beta_z &= \sqrt{\left[1-\frac{(\mu_{H_2}+\mu_{H_1})^2}{z}\right]\left[1-\frac{(\mu_{H_2}-\mu_{H_1})^2}{z}\right]}.\end{aligned} \tag{C.86}$$

Notice that the parameter β_z strongly resemble the β defined in the context of the $2\to2$ scattering: recalling the definition of Σ and Δ, a simple manipulation of its expression yields

$$\beta_z = \sqrt{1-\frac{2\Sigma}{z}+\frac{\Delta^2}{z^2}}, \tag{C.87}$$

that shows an explicit dependence on the fraction of total energy of the Higgs-pair invariant mass.

Important quantities are related with a combination of the boundaries of $x_\pm$:

$$x_+ - x_- = \beta_z, \qquad x_+x_- = \frac{\mu_{H_1}^2}{z} + \frac{\Delta}{(1-z)z} + \frac{\Delta^2}{(1-z)^2z}, \tag{C.88}$$

that can be plugged into Eq. (C.85) to obtain a very compact form.

Introducing a variable r such that it runs through the limit of integration of x, the term involving the $\cos^2\theta_{35}^0$ becomes:

$$\begin{aligned} x &= x_- + (x_+ - x_-)r, \\ x_3^2 x_5^2 \beta_3^2 \frac{1-\cos^2\theta_{35}^0}{4} &= -(1-z)^2 z(x-x_-)(x-x_+) \\ &= (1-z)^2 z(x_+-x_-)^2 r(1-r) \\ &= (1-z)^2 z\beta_z^2 r(1-r). \end{aligned} \tag{C.89}$$

The 3-particle phase space element therefore becomes:

$$dR_3 = \frac{\hat{s}\beta_z^{1-2\epsilon}}{(4\pi)^4}\left(\frac{4\pi\mu^2}{\hat{s}}\right)^{2\epsilon}\left[r^{-\epsilon}(1-r)^{-\epsilon}\sin^{-2\epsilon}\varphi_{35} dr d\varphi_{35}\right]\frac{z^{-\epsilon}(1-z)^{1-2\epsilon}(1-\cos^2\theta_{15})^{-\epsilon}}{\Gamma(1-2\epsilon)} dz d\cos\theta_{15}. \tag{C.90}$$

The term into the parenthesis can be integrated

$$\begin{aligned} \int_0^\pi \sin^{-2\epsilon}\varphi_{35} d\varphi_{35} &= 4^\epsilon \pi \frac{\Gamma(1-2\epsilon)}{\Gamma^2(1-\epsilon)}, \\ \int_0^1 r^{-\epsilon}(1-r)^{-\epsilon} dr &= \frac{\Gamma^2(1-\epsilon)}{\Gamma(2-2\epsilon)}, \end{aligned} \tag{C.91}$$

therefore

$$\begin{aligned} dR_3 &= 4^\epsilon \pi \frac{\hat{s}\beta_z^{1-2\epsilon}}{(4\pi)^4}\left(\frac{4\pi\mu^2}{\hat{s}}\right)^{2\epsilon}\frac{z^{-\epsilon}(1-z)^{1-2\epsilon}(1-\cos^2\theta_{15})^{-\epsilon}}{\Gamma(2-2\epsilon)} dz d\cos\theta_{15} \\ &= \left[\frac{\beta_z^{1-2\epsilon}}{8\pi}\left(\frac{4\pi\mu^2}{\hat{s}z}\right)^\epsilon \frac{\Gamma(1-\epsilon)}{\Gamma(2-2\epsilon)}\right]\left(\frac{4\pi\mu^2}{\hat{s}z}\right)^\epsilon \frac{\hat{s}z}{32\pi^2}\frac{z^{-1+\epsilon}(1-z)^{1-2\epsilon}}{\Gamma(1-\epsilon)}\left(\frac{1-\cos^2\theta_{15}}{4}\right)^{-\epsilon} dz d\cos\theta_{15}. \end{aligned} \tag{C.92}$$

The variable z can be expressed again in terms of the invariant Higgs-pair momentum Q^2 as follows

$$\begin{aligned} dR_3 &= \left[\frac{\beta_z^{1-2\epsilon}}{8\pi}\left(\frac{4\pi\mu^2}{Q^2}\right)^\epsilon \frac{\Gamma(1-\epsilon)}{\Gamma(2-2\epsilon)}\right]\frac{Q^2}{32\pi^2}\left(\frac{4\pi\mu^2}{Q^2}\right)^\epsilon \frac{z^{-1+\epsilon}(1-z)^{1-2\epsilon}}{\Gamma(1-\epsilon)}\left(\frac{1-\cos^2\theta_{15}}{4}\right)^{-\epsilon} dz d\cos\theta_{15} \\ &= R_2 \frac{Q^2}{32\pi^2}\left(\frac{4\pi\mu^2}{Q^2}\right)^\epsilon \frac{z^{-1+\epsilon}(1-z)^{1-2\epsilon}}{\Gamma(1-\epsilon)}\left(\frac{1-\cos^2\theta_{15}}{4}\right)^{-\epsilon} dz d\cos\theta_{15} \end{aligned} \tag{C.93}$$

We remark that β_z is essentially the same β defined for the 2-particle phase space since it has been factorized from the 3-particle one and it contains informations only on the $2 \to 2$ subprocess. This factorization is crucial for a coherent definition of the infrared subtraction terms expressed in Chapter 3.

C.2.2 Differential cross section: real corrections

As for the virtual corrections, the real contributions have the following differential partonic cross section:

$$\begin{aligned} d\Delta\hat{\sigma}_{ij} &= \frac{dR_3}{2\hat{s}}\overline{|\mathcal{M}_{ij}|^2} \\ &= R_2 \frac{dz d\cos\theta_{15}}{64\pi^2}\left(\frac{4\pi\mu^2}{Q^2}\right)^\epsilon \frac{z^\epsilon(1-z)^{1-2\epsilon}}{\Gamma(1-\epsilon)}\left(\frac{1-\cos^2\theta_{15}}{4}\right)^{-\epsilon}\overline{|\mathcal{M}_{ij}|^2} \\ &= R_2 \frac{dz d\cos\theta_{15}}{64\pi^2}\left(\frac{4\pi\mu^2}{Q^2}\right)^\epsilon \frac{z^\epsilon(1-z)^{1-2\epsilon}}{\Gamma(1-\epsilon)}\left(\frac{1-\cos^2\theta_{15}}{4}\right)^{-\epsilon} C_{\rm col}^{ij} C_{\rm pol}^{ij} C_{\rm spin}^{ij} \sum_{\rm ext.} |\mathcal{M}_{ij}|^2. \end{aligned} \tag{C.94}$$

Each channel contributing to the real correction have different color, polarization and spin average. Here the definition of the quantities occuring in Eq. (C.94) are presented.

$q\bar{q} \to H_1 H_2 g$

$$C_{\rm pol}^{q\bar{q}} = 1, \qquad C_{\rm spin}^{q\bar{q}} = \frac{1}{4}, \qquad C_{\rm col}^{q\bar{q}} = \frac{1}{9},$$

$$\begin{aligned}
\sum_{\rm ext.} |\mathcal{M}_{q\bar{q}}|^2 &= \sum_{\rm spin}\sum_{\rm pol}\sum_{\rm col} T^a_{ij}T^a_{ji}\bar{v}(p_2)\gamma_\mu u(p_1)\bar{u}(p_1)\gamma_\rho v(p_2)\epsilon^{*h}_\sigma(p_5)\epsilon^h_\nu(p_5)\mathcal{M}^{*\rho\sigma}_{q\bar{q}}\mathcal{M}^{\mu\nu}_{q\bar{q}} \\
&= \left(\sum_{\rm spin}\bar{v}(p_2)\gamma_\mu u(p_1)\bar{u}(p_1)\gamma_\rho v(p_2)\right)\left(\sum_h \epsilon^{*h}_\sigma(p_5)\epsilon^h_\nu(p_5)\right)\left(\sum_{i,j,a} T^a_{ij}T^a_{ji}\right)\mathcal{M}^{*\rho\sigma}_{q\bar{q}}\mathcal{M}^{\mu\nu}_{q\bar{q}} \\
&= {\rm Tr}\left[\not{p}_1\gamma_\rho\not{p}_2\gamma_\mu\right](-g_{\sigma\nu})\,{\rm Tr}\left[\delta_{N_c^2-1}\right]\mathcal{M}^{*\rho\sigma}_{q\bar{q}}\mathcal{M}^{\mu\nu}_{q\bar{q}} \\
&= -32\left[p_{1\rho}p_{2\mu} - (p_1\cdot p_2)g_{\rho\mu} + p_{2\rho}p_{1\mu}\right]g_{\sigma\nu}\mathcal{M}^{*\rho\sigma}_{q\bar{q}}\mathcal{M}^{\mu\nu}_{q\bar{q}}.
\end{aligned} \tag{C.95}$$

$qg \to H_1 H_2 q$

$$C_{\rm pol}^{qg} = \frac{1}{2}, \qquad C_{\rm spin}^{qg} = \frac{1}{2}, \qquad C_{\rm col}^{qg} = \frac{1}{24},$$

$$\begin{aligned}
\sum_{\rm ext.} |\mathcal{M}_{qg}|^2 &= \sum_{\rm spin}\sum_{\rm pol}\sum_{\rm col} T^a_{ij}T^a_{ji}\bar{u}(p_5)\gamma_\mu u(p_1)\bar{u}(p_1)\gamma_\rho u(p_5)\epsilon^h_\sigma(p_2)\epsilon^{*h}_\nu(p_2)\mathcal{M}^{*\rho\sigma}_{qg}\mathcal{M}^{\mu\nu}_{qg} \\
&= \left(\sum_{\rm spin}\bar{u}(p_5)\gamma_\mu u(p_1)\bar{u}(p_1)\gamma_\rho u(p_5)\right)\left(\sum_h \epsilon^{*h}_\sigma(p_2)\epsilon^h_\nu(p_2)\right)\left(\sum_{i,j,a} T^a_{ij}T^a_{ji}\right)\mathcal{M}^{*\rho\sigma}_{qg}\mathcal{M}^{\mu\nu}_{qg} \\
&= {\rm Tr}\left[\not{p}_1\gamma_\rho\not{p}_5\gamma_\mu\right](-g_{\sigma\nu})\,{\rm Tr}\left[\delta_{N_c^2-1}\right]\mathcal{M}^{*\rho\sigma}_{qg}\mathcal{M}^{\mu\nu}_{qg} \\
&= -32\left[p_{1\rho}p_{5\mu} - (p_1\cdot p_5)g_{\rho\mu} + p_{5\rho}p_{1\mu}\right]g_{\sigma\nu}\mathcal{M}^{*\rho\sigma}_{qg}\mathcal{M}^{\mu\nu}_{qg}.
\end{aligned} \tag{C.96}$$

$gg \to H_1 H_2 g$

$$C_{\rm pol}^{gg} = \frac{1}{4}, \qquad C_{\rm spin}^{gg} = 1, \qquad C_{\rm col}^{gg} = \frac{1}{64},$$

$$\begin{aligned}
\sum_{\rm ext.} |\mathcal{M}_{gg}|^2 &= \sum_{\rm pol}\sum_{\rm col} f^{abc}f^{abc}\epsilon^{*h_1}_\rho(p_1)\epsilon^{h_1}_\mu(p_1)\epsilon^{*h_2}_\sigma(p_2)\epsilon^{h_2}_\nu(p_2)\epsilon^{h_5}_\beta(p_5)\epsilon^{*h_5}_\alpha(p_5)\mathcal{M}^{*\rho\sigma\beta}_{gg}\mathcal{M}^{\mu\nu\alpha}_{gg} \\
&= \left(\sum_{h_1}\epsilon^{*h_1}_\rho(p_1)\epsilon^{h_1}_\mu(p_1)\right)\left(\sum_{h_2}\epsilon^{*h_2}_\sigma(p_2)\epsilon^{h_2}_\nu(p_2)\right)\left(\sum_{h_5}\epsilon^{h_5}_\beta(p_5)\epsilon^{*h_5}_\alpha(p_5)\right)\left(\sum_{a,b,c} f^{abc}f^{abc}\right)\mathcal{M}^{*\rho\sigma\beta}_{gg}\mathcal{M}^{\mu\nu\alpha}_{gg}, \\
&= -N_c(N_c^2-1)\left[g_{\mu\rho}g_{\nu\sigma}g_{\alpha\beta} + A_{\mu\rho,\nu\sigma,\alpha\beta}\right]\mathcal{M}^{*\rho\sigma\beta}_{gg}\mathcal{M}^{\mu\nu\alpha}_{gg} \\
&= -24\left[g_{\mu\rho}g_{\nu\sigma}g_{\alpha\beta} + A_{\mu\rho,\nu\sigma,\alpha\beta}\right]\mathcal{M}^{*\rho\sigma\beta}_{gg}\mathcal{M}^{\mu\nu\alpha}_{gg}
\end{aligned}$$

$$A_{\mu\rho,\nu\sigma,\alpha\beta} = \left(-g_{\mu\rho} + \frac{p_{1\{\mu}q_{1\rho\}}}{p_1\cdot q_1}\right)\left(-g_{\nu\sigma} + \frac{p_{2\{\nu}q_{2\sigma\}}}{p_2\cdot q_2}\right)\left(-g_{\alpha\beta} + \frac{p_{5\{\alpha}q_{5\beta\}}}{p_5\cdot q_5}\right) - g_{\mu\rho}g_{\nu\sigma}g_{\alpha\beta}. \tag{C.97}$$

The amplitude contributing to the $q\bar{q}$ and qg channels can be built from the LO diagrams by putting an incoming gluon off-shell and attaching a fermion line to it (Appendix H). This fact allows to factor out from the amplitudes the quantities that have to be added. Moreover, the presence of a single on-shell gluon in the final state allows to use the QED-like Ward identities, and the axial term of the polarization can be dropped.

The gg channel is a bit different, since it contains pentagon diagrams. They cannot be constructed by the LO diagrams. The contributions do not even represent a gauge-invariant subset of the amplitude. In addition, if one does not want to consider the ghost contributions, the polarization sum have to be performed over the physical polarization states since in the usual Lorentz gauge no Ward identity ensures the cancellation of the unphysical ones. In Eq. (C.97), the tensor A would vanish in QED ones contracted with the full amplitude because of the on-shell Ward identities; in QCD this argument is not anymore valid, and in general it will give a non-zero contribution.

Appendix D

Passarino-Veltmann reduction

The Feynman integrals contributing at each order of a perturbative QFT expansion does not form an independent set: it can be shown [144] that every one-loop tensor integral can be expressed as a linear combination of scalar integrals. Such integrals, which are independent, are called *master integrals*. The decomposition of a tensor integral in terms of its master integrals is called *reduction*. Several algorithms allow the reduction to master integrals, both at integra*l* and integra*nd* level. In this Appendix the Passarino-Veltmann reduction algorithm is presented with explicit examples.

Consider the following set of denominators:

$$\begin{gathered} D_0 = k^2 - m_t^2, \qquad D_1 = (k-p_1)^2 - m_t^2, \qquad D_2 = (k+p_2)^2 - m_t^2, \\ p_1^2 = 0, \qquad p_2^2 \neq 0, \qquad (p_1+p_2)^2 = m_{H_j}^2, \\ D_{H_j} = (k+p_1+p_2)^2 - m_t^2, \end{gathered} \tag{D.1}$$

and the general scalar integrals:

$$A_0(m_0^2) = \int_k \frac{1}{[k^2 - m_0^2]}, \tag{D.2}$$

$$B_0(q^2; m_0^2, m_1^2) = \int_k \frac{1}{[k^2 - m_0^2][(k+q)^2 - m_1^2]}, \tag{D.3}$$

$$C_0(q_1^2, q_2^2, (q_2-q_1)^2; m_0^2, m_1^2, m_2^2) = \int_k \frac{1}{[k^2 - m_0^2][(k+q_1)^2 - m_1^2][(k+q_2)^2 - m_2^2]}. \tag{D.4}$$

When all denominators have the same mass, instead of writing the full list, a redefinition of the argument will be performed such that $\{m_t^2, \ldots, m_t^2\} = \overline{m}_t^2$. The integrals built with D_i, $i = \{0,1,2\}$ defined before are:

$$\begin{gathered} B_0(p_2^2; \overline{m}_t^2) = \int_k \frac{1}{D_0 D_2}, \qquad B_0(0; \overline{m}_t^2) = \int_k \frac{1}{D_0 D_1}, \\ C_0(0, p_2^2, m_{H_j}^2; \overline{m}_t^2) = \int_k \frac{1}{D_0 D_1 D_2}. \end{gathered} \tag{D.5}$$

and through a shift $k \to k + p_1$, an additional integral can be defined

$$\int_k \frac{1}{D_1 D_2} = \int_k \frac{1}{D_0 D_{H_j}} = B_0(m_{H_j}^2; \overline{m}_t^2). \tag{D.6}$$

In the following section, the reduction of the 2-points and 3-points integrals is presented

D.1 Reduction to scalar integrals

D.1.1 2-point tensor integrals

We firstly have to express the scalar products containing at least one loop momenta in terms of denominators, so that

$$k^2 = D_0 + m_t^2, \qquad k \cdot p_1 = -\frac{1}{2}\left(D_1 - D_0\right), \qquad k \cdot p_2 = \frac{1}{2}\left(D_2 - D_0 - p_2^2\right). \tag{D.7}$$

The strategy will be the same for each tensor integral:

- defining the tensor structure of the tensor integral;
- contracting both the tensor integral and the tensor structure for its tensor basis;
- inverting the system to find the tensor coefficients.

Coefficient B_i

The simplest example is the rank-1 $B_0(p_2^2, \overline{m}_t^2)$ integral. It can be written in terms of its tensor structure:

$$\int_k \frac{k^\mu}{D_0 D_2} = B_1 p_2^\mu, \tag{D.8}$$

where B_1 is a coefficient depending on the kinematic invariants and masses. Contracting both side of Eq. (D.8) with p_2^μ, the equation reads

$$\begin{aligned} B_1 p_2^2 &= \int_k \frac{k \cdot p_2}{D_0 D_2} \\ &= \frac{1}{2}\left(\int_k \frac{1}{D_0} - \int_k \frac{1}{D_2} - p_2^2 \int_k \frac{1}{D_0 D_2}\right) \\ &= -\frac{1}{2} B_0(p_2^2, \overline{m}_t^2) p_2^2, \end{aligned} \tag{D.9}$$

where we have used the identities of Eq. (D.7) and the identity

$$\int_k \frac{1}{D_0} = \int_k \frac{1}{D_2}, \tag{D.10}$$

follows from the shift $k \to k - p_2$. Inverting Eq. (D.9), the rank-1 $B_0(p_2^2, \overline{m}_t^2)$ is given by

$$\int_k \frac{k^\mu}{D_0 D_2} = -\frac{1}{2} B_0(p_2^2, \overline{m}_t^2) p_2^\mu. \tag{D.11}$$

Coefficient B_{ij}

Similarly, the rank-2 $B_0(p_2^2, \overline{m}_t^2)$ has the following tensor structure

$$\int_k \frac{k^\mu k^\nu}{D_0 D_2} = B_{00} g^{\mu\nu} + B_{11} p_2^\mu p_2^\nu. \tag{D.12}$$

Contracting both sides with its tensor basis, a system involving the coefficients B_{00} and B_{11} is defined:

$$\begin{pmatrix} 1 & m_t^2 \\ \frac{1}{2}p_2^2 & \frac{1}{4}(p_2^2)^2 \end{pmatrix} \begin{pmatrix} A_0(m_t^2) \\ B_0(p_2^2, \overline{m}_t^2) \end{pmatrix} = \begin{pmatrix} d & p_2^2 \\ p_2^2 & (p_2^2)^2 \end{pmatrix} \begin{pmatrix} B_{00} \\ B_{11} \end{pmatrix}, \tag{D.13}$$

which has as solution

$$\begin{aligned} \begin{pmatrix} B_{00} \\ B_{11} \end{pmatrix} &= \frac{1}{(d-1)(p_2^2)^2} \begin{pmatrix} (p_2^2)^2 & -p_2^2 \\ -p_2^2 & d \end{pmatrix} \begin{pmatrix} 1 & m_t^2 \\ \frac{1}{2}p_2^2 & \frac{1}{4}(p_2^2)^2 \end{pmatrix} \begin{pmatrix} A_0(m_t^2) \\ B_0(p_2^2, \overline{m}_t^2) \end{pmatrix} \\ &= \frac{1}{(d-1)(p_2^2)^2} \frac{1}{4} \begin{pmatrix} 2(p_2^2)^2 A_0(m_t^2) + (p_2^2)^2(4m_t^2 - p_2^2) B_0(p_2^2; \overline{m}_t^2) \\ 2p_2^2(d-2) A_0(m_t^2) - p_2^2(4m_t^2 - d p_2^2) B_0(p_2^2; \overline{m}_t^2) \end{pmatrix}, \end{aligned} \tag{D.14}$$

and

$$\begin{aligned} \int_k \frac{k^\mu k^\nu}{D_0 D_2} = &\left[\frac{2(p_2^2)^2 A_0(m_t^2) + (p_2^2)^2(4m_t^2 - p_2^2) B_0(p_2^2; \overline{m}_t^2)}{4(d-1)(p_2^2)^2}\right] g^{\mu\nu} \\ &+ \left[\frac{2p_2^2(d-2) A_0(m_t^2) - p_2^2(4m_t^2 - d p_2^2) B_0(p_2^2; \overline{m}_t^2)}{4(d-1)(p_2^2)^2}\right] p_2^\mu p_2^\nu. \end{aligned} \tag{D.15}$$

D.2 3-points tensor integrals

Coefficient C_i

The rank-1 C_0 is

$$\int_k \frac{k^\mu}{D_0 D_1 D_2} = C_1 p_1^\mu + C_2 p_2^\mu. \tag{D.16}$$

where the tensor integral has already been set. Contracting both sides of Eq. (D.16) for the tensor basis, the system for evaluating the coefficients A_1 and A_2 can be written as

$$\mathbf{I} = \int_k \frac{1}{D_0 D_1 D_2} \begin{pmatrix} k\cdot p_1 \\ k\cdot p_2 \end{pmatrix} = \begin{pmatrix} 0 & p_1\cdot p_2 \\ p_1\cdot p_2 & p_2^2 \end{pmatrix} \begin{pmatrix} A_1 \\ A_2 \end{pmatrix} = \mathbb{G}\mathbf{C}, \tag{D.17}$$

where $\mathbb{G}$ is the Gram matrix. Its determinant is

$$G = -(p_1\cdot p_2)^2, \tag{D.18}$$

and its inverse is

$$\mathbb{G}^{-1} = \frac{1}{G}\begin{pmatrix} p_2^2 & -p_1\cdot p_2 \\ -p_1\cdot p_2 & 0 \end{pmatrix}. \tag{D.19}$$

The left-hand side written in terms of scalar integrals is

$$\mathbf{I} = \frac{1}{2}\begin{pmatrix} B_0(q_2^2;\overline{m}_t^2) - B_0(m_{H_j}^2;\overline{m}_t^2) \\ B_0(0;\overline{m}_t^2) - B_0(m_{H_j}^2;\overline{m}_t^2) - p_2^2 C_0(0,p_2^2,m_{H_j}^2;\overline{m}^2) \end{pmatrix}. \tag{D.20}$$

Finally, inverting the Gram matrix, the coefficients of the tensor expansion are given by

$$\begin{aligned} C_1 =& \frac{1}{2G}\left[p_2^2(p_1\cdot p_2)C_0(0,p_2^2,m_{H_j}^2;\overline{m}_t^2) + ((p_1\cdot p_2) - p_2^2)B_0(m_{H_j}^2;\overline{m}_t^2)\right. \\ &\left. + q_2^2 B_0(q_2^2;\overline{m}_t^2) - (p_1\cdot p_2)B_0(0;\overline{m}_t^2)\right], \\ C_2 =& \frac{(p_1\cdot p_2)}{2G}\left[B_0(m_{H_j}^2;\overline{m}_t^2) - B_0(q_2^2;\overline{m}_t^2)\right], \end{aligned} \tag{D.21}$$

and the rank-1 integral becomes

$$\begin{aligned} \int_k \frac{k^\mu}{D_0 D_1 D_2} =& \frac{1}{2G}\left[p_2^2(p_1\cdot p_2)C_0(0,p_2^2,m_{H_j}^2;\overline{m}_t^2) + ((p_1\cdot p_2) - p_2^2)B_0(m_{H_j}^2;\overline{m}_t^2)\right. \\ &\left. + q_2^2 B_0(q_2^2;\overline{m}_t^2) - (p_1\cdot p_2)B_0(0;\overline{m}_t^2)\right] p_1^\mu \\ &+ \frac{(p_1\cdot p_2)}{2G}\left[B_0(m_{H_j}^2;\overline{m}_t^2) - B_0(q_2^2;\overline{m}_t^2)\right] p_2^\mu. \end{aligned} \tag{D.22}$$

Coefficient C_{ij}

Similarly, the rank-2 integral can be decomposed as

$$\int_k \frac{k^\mu k^\nu}{D_0 D_1 D_2} = C_{00} g^{\mu\nu} + \sum_{i=1}^{2} C_{ij} p_i^\mu p_j^\nu, \tag{D.23}$$

where we already expressed it as a general tensor depending on p_1 and p_2.

Contracting the r.h.s. with respectively $g^{\mu\nu}$, $p_1^\mu p_1^\nu$, $p_1^\mu p_2^\nu$, $p_2^\mu p_1^\nu$ and $p_2^\mu p_2^\nu$ we can generate a system:

$$\mathbb{M}\mathbf{A} = \begin{pmatrix} d & 0 & (p_1\cdot p_2) & (p_1\cdot p_2) & p_2^2 \\ 0 & 0 & 0 & 0 & (p_1\cdot p_2)^2 \\ (p_1\cdot p_2) & 0 & 0 & (p_1\cdot p_2)^2 & (p_1\cdot p_2)p_2^2 \\ (p_1\cdot p_2) & 0 & (p_1\cdot p_2)^2 & 0 & (p_1\cdot p_2)p_2^2 \\ p_2^2 & (p_1\cdot p_2) & (p_1\cdot p_2)p_2^2 & (p_1\cdot p_2)p_2^2 & (p_2^2)^2 \end{pmatrix} \begin{pmatrix} C_{00} \\ C_{11} \\ C_{12} \\ C_{21} \\ C_{22} \end{pmatrix}. \tag{D.24}$$

The contraction of the l.h.s. is:

$$\mathbf{I} = \begin{pmatrix} B_0(m_{H_j}^2;\overline{m}_t^2) + m_t^2 C_0(0,p_2^2,m_{H_j}^2;\overline{m}_t^2) \\ \frac{1}{4}B_0(p_2^2;\overline{m}_t^2)(p_1\cdot p_2) - \frac{1}{4}B_0(m_{H_j}^2;\overline{m}_t^2)(p_1\cdot p_2) \\ \frac{1}{4}B_0(p_2^2;\overline{m}_t^2)p_2^2 - \frac{1}{4}B_0(m_{H_j}^2;\overline{m}_t^2)(p_2^2 - p_1\cdot p_2) \\ \frac{1}{4}B_0(p_2^2;\overline{m}_t^2)p_2^2 - \frac{1}{4}B_0(m_{H_j}^2;\overline{m}_t^2)(p_2^2 - p_1\cdot p_2) \\ \frac{1}{4}B_0(0;\overline{m}_t^2)(p_1\cdot p_2 - p_2^2) + \frac{1}{4}B_0(m_{H_j}^2;\overline{m}_t^2)(2p_2^2 - p_1\cdot p_2) + \frac{1}{4}(p_2^2)^2 C_0(0,p_2^2,m_{H_j}^2;\overline{m}_t^2) \end{pmatrix}. \tag{D.25}$$

The determinant of the matrix $\mathbb{M}$ can be written in terms of the Gram determinant:

$$\det\mathbb{M} = (d-2)[(p_1\cdot p_2)^2]^4 = (d-2)G^4. \tag{D.26}$$

Finally, inverting $\mathbb{M}$, we can get the expression of the coefficients $\mathbf{A}$ with $\mathbf{A} = \mathbb{M}^{-1}\mathbb{P}$. Due to gauge invariance, we are only interested in A_{00} and A_{21}, whose values are

$$\begin{aligned} C_{00} &= -\frac{(p_1\cdot p_2)(p_2^2 + 2(p_1\cdot p_2))B_0(m_{H_j}^2;\overline{m}_t^2) - (p_1\cdot p_2)p_2^2 B_0(p_2^2;\overline{m}_t^2) + 4m_t^2(p_1\cdot p_2)^2 C_0(0,p_2^2,m_{H_j}^2;\overline{m}_t^2)}{4(d-2)G}, \\ C_{21} &= -\frac{(p_1\cdot p_2)((d-4)(p_1\cdot p_2) - p_2^2)B_0(m_{H_j}^2;\overline{m}_t^2) + (p_1\cdot p_2)p_2^2 B_0(p_2^2;\overline{m}_t^2) - 4m_t^2(p_1\cdot p_2)^2 C_0(0,p_2^2,m_{H_j}^2;\overline{m}_t^2)}{4(d-2)G}. \end{aligned} \tag{D.27}$$

The procedure explained in this Appendix is the core of the Passarino-Veltmann reduction, which can be extended to boxes D_0 and pentagons E_0. The complexity of the tensor coefficients rapidly increases with the number of external legs and tensor-rank. The Gram determinants G strongly depend on the kinematics, and they introduce strong numerical instabilities when the phase space integral is performed: high-rank integrals increase its power of G in the denominator, and regions where G becomes small can lead to strong cancellation and loss of numerical precision.

D.3 Recurrence relations

An alternative to the reduction down to scalar integrals is represented by the recurrence relations. Once that the scalar integrals are defined, a rank-r integral can be expressed in terms of a tensor basis, where its coefficients depend on the rank-$(r-1)$ ones. This means that the coefficients of such tensors are can be obtained by iteration starting from the scalar integrals. In general, every rank contributes with one power of inverse Gram determinant, which lead to the potential numerical problems expressed in the previous Section.

B_{ij} coefficients

Consider the tensor structure of the rank-2 2-point integrals

$$\int_k \frac{k^\mu k^\nu}{D_0 D_2} = B_{00} g^{\mu\nu} + B_{11} p_2^\mu p_2^\nu. \tag{D.28}$$

In complete analogy of what has been done in the previous section, contracting both sides for the momentum p^μ and the metric tensor $g^{\mu\nu}$, two equations can be obtained

$$\begin{aligned} g_{\mu\nu}\int_k \frac{k^\mu k^\nu}{D_0 D_2} &= B_{00} d + B_{11} p_2^2, \\ p_2^\nu \int_k \frac{k^\mu k^\nu}{D_0 D_2} &= B_{00} p_2^\mu + B_{11} p_2^2 p_2^\mu. \end{aligned} \tag{D.29}$$

Using the relations of Eq. (D.7), and expressing the rank-1 integrals with their tensor structure, the l.h.s. becomes

$$\begin{aligned} g_{\mu\nu}\int_k \frac{k^\mu k^\nu}{D_0 D_2} &= A_0(m_t^2) + m_t^2 B_0(p_2^2;\overline{m}_t^2), \\ p_2^\nu \int_k \frac{k^\mu k^\nu}{D_0 D_2} &= \frac{p_2^\mu}{2}\int_k \frac{1}{D_0} - \frac{p_2^2}{2}\int_k \frac{k^\mu}{D_0 D_2} \\ &= \frac{1}{2}A_0(m_t^2)p_2^\mu - \frac{p_2^2}{2}B_1 p_2^\mu. \end{aligned} \tag{D.30}$$

Therefore, the system of equations can be solved for the coefficients B_{ij}

$$\begin{pmatrix} B_{00} \\ B_{11} \end{pmatrix} = \frac{1}{2(d-1)p_2^2} \begin{pmatrix} 2p_2^2 & -p_2^2 \\ -2 & d \end{pmatrix} \begin{pmatrix} A_0(m_t^2) + m_t^2 B_0(p_2^2; \overline{m}_t^2) \\ A_0(m_t^2) - p_2^2 B_1 \end{pmatrix}, \tag{D.31}$$

and using the fact that $G = p_2^2$, the coefficients B_{ij} are given by

$$\begin{aligned} B_{00} &= \frac{1}{2(d-1)} \left[A_0(m_t^2) + 2m_t^2 B_0(p_2^2; \overline{m}_t^2) + p_2^2 B_1(p_2^2; \overline{m}_t^2) \right], \\ B_{11} &= \frac{1}{2(d-1)G} \left[(d-2) A_0(m_t^2) - 2m_t^2 B_0(p_2^2; \overline{m}_t^2) - d p_2^2 B_1(p_2^2; \overline{m}_t^2) \right]. \end{aligned} \tag{D.32}$$

Therefore, the coefficients B_{00} and B_{11} of the rank-2 2-points integrals depend explicitely on B_1, namely the coefficient of the rank-1 2-points tensor integral, which in turn is related to the scalar integral B_0 through the Eq. (D.9).

C_{ij} coefficients

The rank-2 3-points integrals have the following tensor structure:

$$\int_k \frac{k^\mu k^\nu}{D_0 D_1 D_2} = C_{00} g^{\mu\nu} + \sum_{i=1}^{2} C_{ij} p_i^\mu p_j^\nu, \tag{D.33}$$

Contracting both sides for the external momenta, a system of four equations can be built:

$$\begin{aligned} p_1^\nu \int_k \frac{k^\mu k^\nu}{D_0 D_1 D_2} &= +\frac{1}{2} \left[B_1(m_{H_j}^2; \overline{m}_t^2) + B_0(m_{H_j}^2; \overline{m}_t^2) \right] p_1^\mu \\ &\quad + \frac{1}{2} \left[B_1(m_{H_j}^2; \overline{m}_t^2) - B_1(p_2; \overline{m}_t^2) \right] p_2^\mu \\ &= [C_{00} + C_{12}(p_1 \cdot p_2)] p_1^\mu + C_{22} p_2^\mu, \\ p_2^\nu \int_k \frac{k^\mu k^\nu}{D_0 D_1 D_2} &= \frac{1}{2} \left[B_1(p_2^2; \overline{m}_t^2) - B_1(m_{H_j}^2; \overline{m}_t^2) - B_0(m_{H_j}^2; \overline{m}_t^2) - p_2^2 C_1 \right] p_1^\mu \\ &\quad + \frac{1}{2} \left[B_1(m_{H_j}^2; \overline{m}_t^2) + p_2^2 C_2 \right] p_2^\mu \\ &= [C_{11}(p_1 \cdot p_2) + C_{12} p_2^2] p_1^\mu + [C_{00} + C_{21}(p_1 \cdot p_2) + C_{22} p_2^2] p_2^\mu, \end{aligned} \tag{D.34}$$

which lead to the following system and its solution

$$\begin{pmatrix} B_1(m_{H_j}^2; \overline{m}_t^2) + B_0(m_{H_j}^2; \overline{m}_t^2) - 2C_{00} \\ B_1(p_2^2; \overline{m}_t^2) - B_1(m_{H_j}^2; \overline{m}_t^2) - B_0(m_{H_j}^2; \overline{m}_t^2) - p_2^2 C_1 \\ B_1(m_{H_j}^2; \overline{m}_t^2) - B_1(p_2^2; \overline{m}_t^2) \\ B_1(m_{H_j}^2; \overline{m}_t^2) + p_2^2 C_2 - 2C_{00} \end{pmatrix} = 2 \begin{pmatrix} 0 & (p_1 \cdot p_2) & 0 & 0 \\ (p_1 \cdot p_2) & p_2^2 & 0 & 0 \\ 0 & 0 & 0 & (p_1 \cdot p_2) \\ 0 & 0 & (p_1 \cdot p_2) & p_2^2 \end{pmatrix} \begin{pmatrix} C_{11} \\ C_{21} \\ C_{12} \\ C_{22} \end{pmatrix}$$

$$\Downarrow$$

$$\begin{pmatrix} C_{11} \\ C_{21} \\ C_{12} \\ C_{22} \end{pmatrix} = \frac{1}{2G} \begin{pmatrix} p_2^2 & -(p_1 \cdot p_2) & 0 & 0 \\ -(p_1 \cdot p_2) & 0 & 0 & 0 \\ 0 & 0 & p_2^2 & -(p_1 \cdot p_2) \\ 0 & 0 & -(p_1 \cdot p_2) & 0 \end{pmatrix} \begin{pmatrix} B_1(m_{H_j}^2; \overline{m}_t^2) + B_0(m_{H_j}^2; \overline{m}_t^2) - 2C_{00} \\ B_1(p_2^2; \overline{m}_t^2) - B_1(m_{H_j}^2; \overline{m}_t^2) - B_0(m_{H_j}^2; \overline{m}_t^2) - p_2^2 C_1 \\ B_1(m_{H_j}^2; \overline{m}_t^2) - B_1(p_2^2; \overline{m}_t^2) \\ B_1(m_{H_j}^2; \overline{m}_t^2) + p_2^2 C_2 - 2C_{00} \end{pmatrix}$$

$$\Downarrow$$

$$\begin{aligned} C_{11} &= \frac{(p_2^2 + p_1 \cdot p_2) B_1(m_{H_j}^2; \overline{m}_t^2) + (p_2^2 + p_1 \cdot p_2) B_0(m_{H_j}^2; \overline{m}_t^2) - 2p_2^2 C_{00} - (p_1 \cdot p_2) B_1(p_2^2; \overline{m}_t^2) + p_2^2 (p_1 \cdot p_2) C_1}{2G}, \\ C_{12} &= \frac{(p_2^2 - p_1 \cdot p_2) B_1(m_{H_j}^2; \overline{m}_t^2) - p_2^2 B_1(p_2^2; \overline{m}_t^2) - (p_1 \cdot p_2) p_2^2 C_2 + (p_1 \cdot p_2) 2C_{00}}{2G}, \\ C_{21} &= \frac{B_1(p_2^2; \overline{m}_t^2) - B_1(m_{H_j}^2; \overline{m}_t^2) - B_0(m_{H_j}^2; \overline{m}_t^2) - p_2^2 C_1}{2}, \\ C_{22} &= \frac{B_1(m_{H_j}^2; \overline{m}_t^2) + p_2^2 C_2 - 2C_{00}}{2} \end{aligned} \tag{D.35}$$

where we defined the Gram determinant $G = -(p_1 \cdot p_2)^2$. The remaining C_{00} coefficient can be found by contracting the Eq. (D.33) for the metric tensor $g^{\mu\nu}$ and using the results found in Eq. (D.35).

As for the previous example, the C_{ij} tensor coefficients are related to the C_i and B_i ones, which in turn are related to the C_0 and B_0 scalar integrals. The generalization of this procedure for the rank-r n-points tensor integrals is straightforward: 1. find the Lorentz basis on which the rank-r tensor integral can be projected; 2. define the equality between the tensor integral and its decomposition of such tensor basis; 3. contract both side of the equation found in 2. for every external momenta; 4. express the rank-$(r-1)$ in terms of its tensor structure; 5. solve the system for the coefficient of the rank-r tensor structure. It can be shown that it is possible to build a master equation which holds for any rank-r n-points tensor integral and relates its tensor coefficients to the rank-$(r-1)$ n-points (or lower) ones (See e.g. Ref. [166, 167]).

Appendix E

Evaluating the basis of one-loop integrals

One-loop amplitudes can be written as a combination of scalar integrals: the minimal requirement for the evaluation of such amplitude is to know how to calculate the integral basis. There exist many methods [168–173] for expressing one-loop scalar integrals into a series expansion in ϵ. In this Appendix the calculation of the simpler scalar integral will be presented by using the standard technique involving Feynman parametrization and the tadpole integral.

The tadpole integral is defined by:

$$A_0(m_t^2) = \int_k \frac{1}{k^2 - m_t^2}. \tag{E.1}$$

The integral over the loop momentum is

$$\int_k \frac{(k^2)^\alpha}{[k^2 - q^2 - M^2]^n} = (-1)^{(n-\alpha)} \frac{\Gamma(n - \alpha - \frac{d}{2})\Gamma(\alpha + \frac{d}{2})}{\Gamma(n)\Gamma(\frac{d}{2})} \frac{1}{[q^2 + M^2]^{n-\alpha-\frac{d}{2}}}, \tag{E.2}$$

and it can be applied directly on Eq. (E.1). It reads

$$\begin{aligned} A_0(m_t^2) &= -\frac{\Gamma(1 - \frac{d}{2})}{\Gamma(1)} \frac{1}{(m_t^2)^{1-\frac{d}{2}}} \\ &= -m_t^2 \frac{\Gamma(1+\epsilon)}{\epsilon(\epsilon - 1)} (m_t^2)^{-\epsilon} \\ &= m_t^2 (m_t^2)^{-\epsilon} \Gamma(1+\epsilon) \left(\frac{1}{\epsilon} + 1\right) + O(\epsilon). \end{aligned} \tag{E.3}$$

For more complex integrand, the Feynman parametrization allows the integrand to take the tadpole-like form. However, additional integrations over the Feynman parameters have to be performed, making the calculation of one-loop scalar integrals highly non-trivial. In the following Section, the 2-points and 3-points scalar integrals will be calculated up to the order $O(1)$.

E.1 2-points scalar integrals

$B_0(q^2, \overline{m}_t^2)$

The integral $B_0(q^2, \overline{m}_t^2)$ is

$$B_0(q^2, \overline{m}_t^2) = \int_k \frac{1}{[k^2 - m_t^2][(k+q)^2 - m_t^2]}. \tag{E.4}$$

Writing $B_0(q^2, \overline{m}_t^2)$ in terms of Feynman parameters, it reads:

$$B_0(q^2, \overline{m}_t^2) = \frac{\Gamma(2)}{\Gamma(1)\Gamma(1)} \int_k \int_0^1 dx_1 dx_2 \frac{\delta(1 - x_1 - x_2)}{[(k^2 - m_t^2)x_1 + ((k+q)^2 - m_t^2)x_2]^2}, \tag{E.5}$$

Rearranging the terms in the denominator and integrate over x_1 it becomes

$$\begin{aligned} B_0(q^2, \overline{m}_t^2) &= \int_k \int_0^1 dx_2 \frac{1}{[k^2 + (2k \cdot q + q^2)x_2 - m_t^2]^2} \\ &= \int_k \int_0^1 dx_2 \frac{1}{[k^2 + q^2 x_2(1 - x_2) - m_t^2]^2}, \end{aligned} \tag{E.6}$$

where the shift $k \to k - qx_1$ has been applied. Using Eq. (E.2) the integral becomes

$$B_0(q^2, \overline{m}_t^2) = \frac{\Gamma(2 - \frac{d}{2})}{\Gamma(2)} \int_0^1 \frac{dx_2}{[m_t^2 - q^2 x_2(1 - x_2)]^{2 - \frac{d}{2}}}, \tag{E.7}$$

and by setting $d = 4 - 2\epsilon$ and renaming $x_2 = x$ it reads

$$\begin{aligned} B_0(q^2, \overline{m}_t^2) &= \Gamma(\epsilon) \int_0^1 \frac{dx}{[m_t^2 - q^2 x_2(1 - x)]^\epsilon} \\ &= (m_t^2)^{-\epsilon} \frac{\Gamma(1 + \epsilon)}{\epsilon} \int_0^1 \frac{dx}{\left[1 - \frac{q^2}{m_t^2} x(1 - x)\right]^\epsilon}. \end{aligned} \tag{E.8}$$

Expanding the last expression up to the finite order and defining $\frac{q^2}{m_t^2} = \rho$, $B_0(q^2, \overline{m}_t^2)$ reads

$$B_0(q^2, \overline{m}_t^2) = \Gamma(1 + \epsilon)(m_t^2)^{-\epsilon} \left[\frac{1}{\epsilon} - \int_0^1 dx \log\left[1 - \rho x(1 - x)\right]\right]. \tag{E.9}$$

The integral in the parenthesis can be evaluated analytically:

$$\begin{gathered} \tau = \frac{4}{\rho}, \qquad g(\tau) = \frac{\sqrt{1 - \tau}}{2} \log\left(-\frac{1 + \sqrt{1 - \tau}}{1 - \sqrt{1 - \tau}}\right), \\ \Downarrow \\ \int_0^1 dx \log\left[1 - \rho x(1 - x)\right] = 2[g(\tau) - 1], \end{gathered} \tag{E.10}$$

Therefore, the analytical expansion of the 2-point scalar integral is

$$B_0(q^2, \overline{m}_t^2) = \Gamma(1 + \epsilon)(m_t^2)^{-\epsilon} \left[\frac{1}{\epsilon} + 2 - 2g(\tau)\right]. \tag{E.11}$$

An important limit of this integral is obtained for $q^2 \to 0$:

$$B_0(0, \overline{m}_t^2) = (m_t^2)^{-\epsilon} \frac{\Gamma(1 + \epsilon)}{\epsilon}. \tag{E.12}$$

The derivative of $B_0(p^2; \overline{m}_t)$ is given by:

$$\frac{d}{dq^2} B_0(q^2, \overline{m}_t^2) = -\Gamma(1 + \epsilon)(m_t^2)^{-\epsilon} 2g'(\tau(q^2)), \tag{E.13}$$

$$g'(\tau(q^2)) = \frac{\tau^2}{8m_t^2} \left(\frac{g(\tau)}{1 - \tau} + \frac{1}{\tau}\right), \tag{E.14}$$

and the on-shell limit of the derivative of $B_0(q^2, \overline{m}_t^2)$ is

$$\frac{d}{dq^2} B_0(0, \overline{m}_t^2) \sim \Gamma(1 + \epsilon)(m_t^2)^{-\epsilon} \frac{1}{6m_t^2}. \tag{E.15}$$

$B_0(p^2;\overline{0})$

A particular case arises when we set the internal masses to zero, i.e. $m_t^2 \to 0$.

$$\begin{aligned} B_0(q^2,\overline{0}) &= \frac{\Gamma(2-\frac{d}{2})}{\Gamma(2)}\int_0^1 dx \frac{1}{[-q^2x(1-x)]^{2-\frac{d}{2}}} \\ &= (-q^2)^{\frac{d}{2}-2}\Gamma\left(2-\frac{d}{2}\right)\int_0^1 dx x^{\frac{d}{2}-2}(1-x)^{\frac{d}{2}-2}, \end{aligned} \tag{E.16}$$

the last term can be written in terms of Gamma functions:

$$\int_0^1 t^{x-1}(1-t)^{y-1}dt = \frac{\Gamma(x)\Gamma(y)}{\Gamma(x+y)}. \tag{E.17}$$

Hence

$$\begin{aligned} B_0(q^2,\overline{m_t^2}) &= (-q^2)^{\frac{d}{2}-2}\Gamma\left(2-\frac{d}{2}\right)\frac{\Gamma(\frac{d}{2}-1)\Gamma(\frac{d}{2}-1)}{\Gamma(d-2)} \\ &= (-q^2)^{-\epsilon}\Gamma\left(\epsilon\right)\frac{\Gamma(1-\epsilon)\Gamma(1-\epsilon)}{\Gamma(2(1-\epsilon))}. \end{aligned} \tag{E.18}$$

$B_0(p^2;m_t,0)$

Consider the integral

$$B_0(p^2;m_t^2,0) = \int_k \frac{1}{[k^2-m_t^2](k+p)^2}. \tag{E.19}$$

Using the same steps did for the equal mass case, the 2-point integral reads

$$\begin{aligned} B_0(p^2;m_t^2,0) &= \int_k\int_0^1 \frac{dx}{[k^2+2k\cdot px+p^2x-m_t^2(1-x)]^2} \\ &= \int_k\int_0^1 \frac{dx}{[k^2+p^2x(1-x)-m_t^2(1-x)]^2} \\ &= \frac{\Gamma(2-\frac{d}{2})}{\Gamma(2)}\int_0^1 \frac{dx}{[m_t^2(1-x)-p^2x(1-x)]^{2-\frac{d}{2}}} \\ &= (m_t^2)^{\frac{d}{2}-2}\Gamma\left(2-\frac{d}{2}\right)\int_0^1 (1-x)^{\frac{d}{2}-2}\left(1-\frac{p^2}{m_t^2}x\right)^{\frac{d}{2}-2}dx \\ &= (m_t^2)^{\frac{d}{2}-2}\Gamma\left(2-\frac{d}{2}\right)\int_0^1 (1-x)^{\frac{d}{2}-2}\left(1-\rho x\right)^{\frac{d}{2}-2}dx. \end{aligned} \tag{E.20}$$

The Hypergeometric function is defined as

$$B(b,c-b)_2F_1(a,b;c;z) = \int_0^1 x^{b-1}(1-x)^{c-b-1}(1-zx)^{-a}dx, \tag{E.21}$$

where

$$B(x,y) = \frac{\Gamma(x+y)}{\Gamma(x)\Gamma(y)}. \tag{E.22}$$

With these definition, the Eq. (E.20) reads

$$\begin{aligned} B_0(p^2;m_t^2,0) &= (m_t^2)^{\frac{d}{2}-2}\Gamma\left(2-\frac{d}{2}\right)\int_0^1 (1-x)^{\frac{d}{2}-1-1}\left(1-\rho x\right)^{-(2-\frac{d}{2})}dx \\ &= (m_t^2)^{\frac{d}{2}-2}\Gamma\left(2-\frac{d}{2}\right)B\left(1,\frac{d}{2}-1\right){}_2F_1\left(2-\frac{d}{2},1;\frac{d}{2};\rho\right) \\ &= (m_t^2)^{\frac{d}{2}-2}\Gamma\left(2-\frac{d}{2}\right)\left(\frac{d}{2}-1\right){}_2F_1\left(2-\frac{d}{2},1;\frac{d}{2};\rho\right) \\ &= (m_t^2)^{-\epsilon}\Gamma(\epsilon)(1-\epsilon){}_2F_1\left(\epsilon,1;2-\epsilon;\rho\right). \end{aligned} \tag{E.23}$$

Hypergeometric functions can be expanded as follows

$$\begin{aligned} {}_2F_1\left(a,b;c;z\right) &= \sum_{n=0}^{\infty} \frac{(a)_n (b)_n}{(c)_n} \frac{z^n}{n!} \\ &= {}_2F_1\left(b,a;c;z\right), \end{aligned} \tag{E.24}$$

$$(x)_n = \begin{cases} 1 & n = 0 \\ x(x+1)\cdots(x+n-1) & n > 0 \end{cases} = \frac{\Gamma(x+n)}{\Gamma(x)},$$

hence, they can be written as

$$\begin{aligned} {}_2F_1\left(1,\epsilon;2-\epsilon;\frac{p^2}{m_t^2}\right) &= \sum_{n=0}^{\infty} \frac{(a)_n (b)_n}{(c)_n} \frac{\rho^n}{n!} \\ &= \sum_{n=0}^{\infty} \frac{(1)_n (\epsilon)_n}{(2-\epsilon)_n} \frac{\rho^n}{n!} \\ &= \frac{\Gamma(2-\epsilon)}{\Gamma(1)\Gamma(\epsilon)} \sum_{n=0}^{\infty} \frac{\Gamma(1+n)\Gamma(\epsilon+n)}{\Gamma(2-\epsilon+n)} \frac{\rho^n}{\Gamma(1+n)} \\ &= \frac{\Gamma(2-\epsilon)}{\Gamma(\epsilon)} \sum_{n=0}^{\infty} \frac{\Gamma(\epsilon+n)}{\Gamma(2-\epsilon+n)} \rho^n \\ &= \frac{\Gamma(2-\epsilon)}{\Gamma(\epsilon)} \left[\frac{\Gamma(\epsilon)}{\Gamma(2-\epsilon)} + \frac{\Gamma(1+\epsilon)}{\Gamma(3-\epsilon)}\rho + \frac{\Gamma(2+\epsilon)}{\Gamma(4-\epsilon)}\rho^2 + \cdots \right] \\ &= 1 + \frac{\Gamma(2-\epsilon)}{\Gamma(\epsilon)} \frac{\Gamma(1+\epsilon)}{\Gamma(3-\epsilon)}\rho + \frac{\Gamma(2-\epsilon)}{\Gamma(\epsilon)} \frac{\Gamma(2+\epsilon)}{\Gamma(4-\epsilon)}\rho^2 + \cdots \\ &= 1 + \frac{\epsilon}{(2-\epsilon)}\rho + \frac{\epsilon(1+\epsilon)}{(2-\epsilon)(3-\epsilon)}\rho^2 + \cdots . \end{aligned} \tag{E.25}$$

Looking closely at the definition of ${}_2F_1$, the m-th term is

$$\frac{\epsilon(\epsilon+1)(\epsilon+2)\cdots(\epsilon+n-1)}{(2-\epsilon)(3-\epsilon)\cdots(2-\epsilon+n-1)} = \frac{\epsilon((n-1)! + O(\epsilon))}{(n+1)! + O(\epsilon)}. \tag{E.26}$$

Thanks to this expression, and using the derivative of a rational function, the m-th term becomes

$$\begin{aligned} \frac{d}{d\epsilon}\frac{f(\epsilon)}{g(\epsilon)} &= \frac{f'(\epsilon)g(\epsilon) - f(\epsilon)g'(\epsilon)}{g^2(\epsilon)} \\ \implies \frac{[(n-1)! + O(\epsilon)][(n+1)! + O(\epsilon)] - O(\epsilon)}{[(n+1)! + O(\epsilon)]^2} &= \frac{(n-1)!}{(n+1)!} + O(\epsilon). \end{aligned} \tag{E.27}$$

Thus, the expansion around $\epsilon = 0$ yields

$$\begin{aligned} {}_2F_1\left(1,\epsilon;2-\epsilon;\frac{p^2}{m_t^2}\right) &= {}_2F_1\left(1,0;2;\rho\right) + \epsilon \frac{d}{d\epsilon} {}_2F_1\left(1,\epsilon;2-\epsilon;\rho\right)\Big|_{\epsilon=0} + O(\epsilon^2) \\ &= 1 + \epsilon\left[\frac{\rho}{2} + \frac{\rho^2}{6} + \cdots\right] + O(\epsilon^2) \\ &= 1 + \epsilon \sum_{n=1}^{\infty} \frac{(n-1)!}{(n+1)!}\rho^n + O(\epsilon^2) \\ &= 1 + \epsilon\rho \sum_{n=0}^{\infty} \frac{n!}{(n+2)!}\rho^n + O(\epsilon^2) \\ &= 1 + \epsilon\rho \sum_{n=0}^{\infty} \frac{\Gamma(1+n)\Gamma(1+n)}{\Gamma(3+n)} \frac{\rho^n}{n!} + O(\epsilon^2) \\ &= 1 + \epsilon\rho \frac{\Gamma(1)\Gamma(1)}{\Gamma(3)} {}_2F_1\left(1,1;3;\rho\right) + O(\epsilon^2) \\ &= 1 + \epsilon\frac{\rho}{2} {}_2F_1\left(1,1;3;\rho\right) + O(\epsilon^2). \end{aligned} \tag{E.28}$$

The hypergeometric function in the last identity is

$$\begin{aligned} F_1\left(1,1;3;\rho\right) &= 2\int_0^1 dx \frac{(1-x)}{(1-\rho x)} \\ &= \frac{2}{\rho}\left[\frac{(1-\rho)}{\rho}\int_0^1 \frac{(-\rho)dt}{(1-\rho t)} + 1\right] \\ &= \frac{2}{\rho}\left[\frac{(1-\rho)}{\rho}\log(1-\rho) + 1\right]. \end{aligned} \tag{E.29}$$

Hence

$${}_2F_1\left(1,\epsilon;2-\epsilon;\frac{p^2}{m_t^2}\right) = 1+\epsilon\left[\frac{(1-\rho)}{\rho}\log(1-\rho)+1\right]+O(\epsilon^2), \tag{E.30}$$

and finally, the $B_0(p^2;m_t^2,0)$ around $\epsilon=0$ is

$$\begin{aligned} B_0(p^2;m_t^2,0) &= (m_t^2)^{-\epsilon}\Gamma(1+\epsilon)\left(\frac{1}{\epsilon}-1\right){}_2F_1\left(\epsilon,1;2-\epsilon;\rho\right) \\ &= (m_t^2)^{-\epsilon}\Gamma(1+\epsilon)\left[\frac{1}{\epsilon}+\frac{(1-\rho)}{\rho}\log(1-\rho)\right]+O(\epsilon). \end{aligned} \tag{E.31}$$

E.2 3-points scalar integrals

$C_0(0,p_2^2,m_{H_j}^2;\overline{m}_t^2)$

Consider the integral

$$\begin{aligned} C_0(0,p_2^2,m_{H_j}^2;\overline{m}_t^2) &= \int_k \frac{1}{[k^2-m_t^2][(k-p_1)^2-m_t^2][(k+p_2)^2-m_t^2]}, \\ p_1^2 &= 0, \qquad p_2^2 = m_{H_j}^2. \end{aligned} \tag{E.32}$$

Doing the same steps done for the 2-points integrals, $C_0(0,p_2^2,m_{H_j}^2;\overline{m}_t^2)$ reads

$$\begin{aligned} C_0(0,p_2^2,m_{H_j}^2;\overline{m}_t^2) &= \frac{\Gamma(3)}{\Gamma(1)\Gamma(1)\Gamma(1)}\int_k\int_0^1 \frac{dx_1dx_2dx_3\delta(1-x_1-x_2-x_3)}{[(k^2-m_t^2)x_3+((k-p_1)^2-m_t^2)x_1+((k+p_2)^2-m_t^2)x_2]^3} \\ &= 2\int_0^1 dx_2\int_0^{1-x_2} dx_1\int_k \frac{1}{[k^2-2k\cdot(p_1x_1-p_2x_2)+p_2^2x_2-m_t^2]^3} \\ &= 2\int_0^1 dx_2\int_0^{1-x_2} dx_1\int_k \frac{1}{[k^2+2(p_1\cdot p_2)x_1x_2+p_2^2x_2(1-x_2)-m_t^2]^3}. \end{aligned} \tag{E.33}$$

Shifting the Feynman parameters as $x_1 \to x_1(1-x_2)$ and $x_2 \to x_2$, and rewriting $(p_1\cdot p_2) = (p_1+p_2)^2 - p_2^2 = m_{H_j}^2 - p_2^2$, C_0 reads

$$\begin{aligned} C_0(0,p_2^2,m_{H_j}^2;\overline{m}_t^2) &= 2\int_0^1 dx_1dx_2\int_k \frac{1-x_2}{[k^2+2(p_1\cdot p_2)x_1x_2(1-x_2)+p_2^2x_2(1-x_2)-m_t^2]^3} \\ &= 2\int_0^1 dx_1dx_2\int_k \frac{1-x_2}{[k^2+m_{H_j}^2x_1x_2(1-x_2)-p_2^2x_1x_2(1-x_2)+p_2^2x_2(1-x_2)-m_t^2]^3}. \end{aligned} \tag{E.34}$$

After integrating the expression in the loop momenta, and expressing it in terms of ϵ, C_0 becomes:

$$C_0(0,p_2^2,m_{H_j}^2;\overline{m}_t^2) = -\Gamma(1+\epsilon)\int_0^1 \frac{(1-x_2)dx_1dx_2}{[m_t^2-p_2^2x_2(1-x_2)+(m_{H_j}^2-p_2^2)x_2(1-x_2)x_1]^{1+\epsilon}}. \tag{E.35}$$

This expression is already finite, so one can immediately set $\epsilon=0$ at integrand level. Furthermore, defining $\rho_H = m_{H_j}^2/m_t^2$ and $\rho_2 = p_2^2/m_t^2$

$$C_0(0,p_2^2,m_{H_j}^2;\overline{m}_t^2) = -\frac{\Gamma(1+\epsilon)}{m_t^2}(m_t^2)^{-\epsilon}\int_0^1 \frac{(1-x_2)dx_1dx_2}{[1-\rho_2x_2(1-x_2)+(\rho_H-\rho_2)x_2(1-x_2)x_1]}. \tag{E.36}$$

Integrating over x_1 this expression:

$$\begin{aligned}
&\int_0^1 \frac{(1-x_2)dx_1dx_2}{[1-\rho_2 x_2(1-x_2)+(\rho_H-\rho_2)x_2(1-x_2)x_1]} = \\
&= \frac{1}{(\rho_H-\rho_2)}\int_0^1 \frac{dx_2}{x_2}\int_0^1 dx_1 \frac{(\rho_H-\rho_2)x_2(1-x_2)dx_1}{[1-\rho_2 x_2(1-x_2)+(\rho_H-\rho_2)x_2(1-x_2)x_1]} = \\
&= \frac{1}{(\rho_H-\rho_2)}\int_0^1 \frac{dx_2}{x_2}\log\left[1-\rho_2 x_2(1-x_2)+(\rho_H-\rho_2)x_2(1-x_2)x_1\right]\Big|_{x_1=0}^{x_1=1} \\
&= \frac{1}{(\rho_H-\rho_2)}\left[\int_0^1 \frac{dx}{x}\log\left[1-\rho_H x(1-x)\right]-\int_0^1 \frac{dx}{x}\log\left[1-\rho_2 x(1-x)\right]\right].
\end{aligned} \tag{E.37}$$

Lastly, defining

$$\begin{aligned}
\tau = \frac{4}{\rho_H}, \quad \lambda = \frac{4}{\rho_2}, \quad f(\tau) = -\frac{1}{4}\log^2\left[-\frac{1+\sqrt{1-\tau}}{1-\sqrt{1-\tau}}\right], \\
\int_0^1 \frac{dx}{x}\log\left[1-\rho_2 x(1-x)\right] = -2f(\lambda), \\
\int_0^1 \frac{dx}{x}\log\left[1-\rho_H x(1-x)\right] = -2f(\tau),
\end{aligned} \tag{E.38}$$

the integral can be performed analytically

$$\int_0^1 \frac{(1-x_2)dx_1dx_2}{[1-\rho_2 x_2(1-x_2)-(\rho_H-\rho_2)x_2(1-x_2)x_1]} = -\frac{2}{(\rho_H-\rho_2)}[f(\tau)-f(\lambda)]. \tag{E.39}$$

and, expressing ρ_2 and ρ_H respectively in terms of λ and τ:

$$\int_0^1 \frac{(1-x_2)dx_1dx_2}{[1-\rho_2 x_2(1-x_2)-(\rho_H-\rho_2)x_2(1-x_2)x_1]} = -\frac{1}{2}\frac{\tau\lambda}{\tau-\lambda}[f(\tau)-f(\lambda)]. \tag{E.40}$$

Finally, $C_0(0,p_2^2,m_{H_j}^2;\overline{m}_t^2)$ takes the following analytical expression

$$C_0(0,p_2^2,m_{H_j}^2;\overline{m}_t^2) = \frac{\Gamma(1+\epsilon)}{m_t^2}(m_t^2)^{-\epsilon}\left[\frac{\tau\lambda}{2}\frac{f(\tau)-f(\lambda)}{\tau-\lambda}\right]. \tag{E.41}$$

The one-loop integrals evaluated in this Appendix have direct application both at LO and at NLO, where they are involved in the real corrections. 4-points and 5-points integrals are much more complex, and when it is needed, a numerical approach would be more convenient.

E.2.1 Scaleless scalar integrals

Within the dimensional regularisation, the scaleless Feynman integrals vanish [174]. Consider the integral

$$J_\alpha = \int_k (k^2)^\alpha, \qquad [J_\alpha] = [M]^{d-2\alpha}. \tag{E.42}$$

A first naive argument for it to vanish is the dimensionality. The integral J_α does not contain any physical scale apart from the loop momentum k; the loop momentum is integrated out, so that its dimensionality have to by absorbed by some other dimensionful quantity. Since such scale is absent, it must vanish: $J_\alpha = 0,\ \forall\alpha$.

Another argument is related with a constructive definition of the Feynman integrals as a function of the dimension $d \in \mathbb{C}$ and its analytical continuation. Consider the integral

$$\int_k \frac{(k^2)^\alpha}{(k^2-m^2)} + \frac{J_\alpha}{m^2} = \int_k \frac{(k^2)^{\alpha+1}}{(k^2-m^2)m^2}. \tag{E.43}$$

The left and the right-hand side are exact identities. The analytical evaluation of the integrals appearing in Eq. (E.43) is

$$\begin{aligned}\int_k \frac{(k^2)^\alpha}{(k^2-m^2)} &= (-1)^{1-\alpha}\frac{\Gamma(\alpha+\frac{d}{2})\Gamma(1-\alpha-\frac{d}{2})}{\Gamma(1)\Gamma(\frac{d}{2})}(m^2)^{\frac{1}{2}-1-\alpha}\\ \frac{1}{m^2}\int_k \frac{(k^2)^{\alpha+1}}{(k^2-m^2)} &= (-1)^{-\alpha}\frac{\Gamma(1+\alpha+\frac{d}{2})\Gamma(-\alpha-\frac{d}{2})}{\Gamma(1)\Gamma(\frac{d}{2})}(m^2)^{\frac{1}{2}-1-\alpha}\\ &= (-1)^{1-\alpha}\frac{\Gamma(\alpha+\frac{d}{2})\Gamma(1-\alpha-\frac{d}{2})}{\Gamma(1)\Gamma(\frac{d}{2})}(m^2)^{\frac{1}{2}-1-\alpha}.\end{aligned} \tag{E.44}$$

The two integrals have the same analytical expression: this fact brings Eq. (E.43) to state that

$$\int_k \frac{(k^2)^\alpha}{(k^2-m^2)} + \frac{J_\alpha}{m^2} = \int_k \frac{(k^2)^\alpha}{(k^2-m^2)} \implies J_\alpha = 0. \tag{E.45}$$

Rigorously, this result is true for $-2(\alpha+1) < d \leq -2\alpha$. The extension for every $d \in \mathbb{C}$ can be done by means of the analytical continuation. More details on the constructive approach to the $d-$dimensional integrations can be found in Ref. [174]. A direct consequence of Eq. (E.45) is that the general one-loop massless tadpoles vanish

$$A_0(0) = \int_k \frac{1}{k^2} = J_{-1} = 0. \tag{E.46}$$

In dimensional regularisation, the scaleless integrals vanish because of Eq. (E.45) and (E.46). The n-points scaleless one-loop integrals is:

$$\begin{aligned} I_1^n\left(\overline{0};\overline{0}\right) &= \int_k \frac{1}{D_0\cdots D_n},\\ D_i = (k+q_i)^2, \quad q_0 = 0, &\qquad (q_i\cdot q_j) = 0 \ \ \forall\ i,j \in \{1,\ldots,n\}.\end{aligned} \tag{E.47}$$

The Feynman parameterisation of $I_1^n\left(\overline{0};\overline{0}\right)$ yields

$$\begin{aligned} I_1^n\left(\overline{0};\overline{0}\right) &= \int_k\int_0^1 \frac{\delta(1-x_0-\cdots-x_n)}{(x_0D_0+\cdots+D_nx_n)^{n+1}}dx_0\cdots dx_n\\ &= \int_k\int_0^1 dx_1\int_0^{1-x_1} dx_2\cdots\int_0^{1-x_1-\cdots-x_n} dx_n\frac{dx_1\cdots dx_n}{[k^2+2k\cdot Q]^{n+1}}\\ &= \int_k\int_0^1 dx_1\cdots dx_n\frac{(1-x_1)^{n-1}(1-x_2)^{n-2}\cdots(1-x_{n-1})}{[k^2+2k\cdot Q]^{n+1}},\end{aligned} \tag{E.48}$$

such that $Q = \sum_{i=1}^n p_ix_i$ and $Q^2 = 0$. Completing the square in the denominator and shifting $k \to k-Q$, the integration over the Feynman parameters yields:

$$\begin{aligned} I_1^n\left(\overline{0};\overline{0}\right) &= \int_k\int_0^1 dx_1\cdots dx_n\frac{(1-x_1)^{n-1}(1-x_2)^{n-2}\cdots(1-x_{n-1})}{[(k+Q)^2]^{n+1}}\\ &= \int_k\int_0^1 dx_1\cdots dx_n\frac{x_1^{n-1}x_2^{n-2}\cdots x_{n-1}}{(k^2)^{n+1}}\\ &= \frac{1}{n!}\int_k\frac{1}{(k^2)^{n+1}} = \frac{J_{-n-1}}{n!}.\end{aligned} \tag{E.49}$$

This fact shows that each scaleless n-points one-loop scalar integrals can be related to a generic massless tadpole integral with the denominator equal to the number of external legs. The Eq. (E.49) can be generalized by taking into account denominators with positive indices[1]. This generalization implies only the change $n \to \sum_{i=1}^n a_i$ where a_i is the (positive) power of the denominator D_i.

[1]For negative indices one can use integral or integrand reduction methods in order to obtain a combination of scalar integrals with positive powers of the denominators.

The vanishing of the scaleless one-loop integrals can be generalize at multi-loop level:

$$\begin{gathered} I_l^n\left(\overline{0};\overline{0}\right)=\int_{k_1\cdots k_l}\frac{1}{\prod_{i=1}^{l}\prod_{j=1}^{n_l}D_{ij}}, \\ D_{ij}=(k_i+q_{ij})^2, \quad q_{i0}=0, \qquad (q_{ij}\cdot q_{rs})=0, \\ \forall\ i,r\in\{1,\ldots,l\},\ j\in\{1,\ldots,n_i\}, j\in\{1,\ldots,n_i\}\ s\in\{1,\ldots,n_r\}. \end{gathered} \tag{E.50}$$

The Feynman parametrization yields

$$\begin{aligned} I_l^n\left(\overline{0};\overline{0}\right)&=\int_{k_1\cdots k_l}\int_0^1\frac{\delta(1-x_1-\cdots-x_n)}{(x_1D_{11}+\cdots+D_{lnl}x_n)^n}dx_1\cdots dx_n \\ &=\int_{k_1\cdots k_l}\int_0^1\frac{\delta(1-x_1-\cdots-x_n)}{(\mathbf{k}^T\cdot A\mathbf{k}+2\mathbf{q}^T\cdot\mathbf{k})^n}dx_1\cdots dx_n, \end{aligned} \tag{E.51}$$

where $n=\sum_{i,j}n_{ij}$, $\mathbf{k}^T=(k_1,\cdots,k_l)$ is the vector containing all the loop momenta k_i and $\mathbf{q}$ contains a combination of the internal momenta q with coefficients depending on the parameters x_i. The matrix A (symmetric) admits a decomposition $A=S^TS$ such that $S^T=S$. Hence,

$$I_l^n\left(\overline{0};\overline{0}\right)=\int_{k_1\cdots k_l}\int_0^1\frac{\delta(1-x_1-\cdots-x_n)}{[(S\mathbf{k})^T\cdot S\mathbf{k}+2\mathbf{q}^T\cdot\mathbf{k}]^n}dx_1\cdots dx_n. \tag{E.52}$$

Applying the rotation $k\to S^{-1}k$, the Jacobian is $d^dk_1\cdots d^dk_l\to\det(S^{-1})d^dk_1\cdots d^dk_l$,

$$\begin{aligned} I_l^n\left(\overline{0};\overline{0}\right)&=\int_{k_1\cdots k_l}\int_0^1\frac{1}{\det^l(S)}\frac{\delta(1-x_1-\cdots-x_n)}{[\mathbf{k}^2+2\mathbf{q}^T\cdot(S^{-1}\mathbf{k})]^n}dx_1\cdots dx_n \\ &=\int_{k_1\cdots k_l}\int_0^1\frac{1}{\det(S)}\frac{\delta(1-x_1-\cdots-x_n)}{[\mathbf{k}^2+2(S^{-1}\mathbf{q})^T\cdot\mathbf{k}]^n}dx_1\cdots dx_n, \end{aligned} \tag{E.53}$$

and the shift $k\to k-S^{-1}\mathbf{q}$

$$\begin{aligned} I_l^n\left(\overline{0};\overline{0}\right)&=\int_0^1\frac{\delta(1-x_1-\cdots-x_n)}{\det^l(S)}dx_1\cdots dx_n\int_{k_1\cdots k_l}\frac{1}{[\mathbf{k}^2]^n} \\ &=C\int_{k_1\cdots k_l}\frac{1}{[k_1^2+\cdots+k_l^2]^n}, \end{aligned} \tag{E.54}$$

where C is the factor containing the integral over the Feynman parameters. Notice that the loop integral has the following structure

$$I_l^n\left(\overline{0};\overline{0}\right)=\frac{C}{(i\pi^{\frac{d}{2}})^l}\int\frac{dk_{0,1}\cdots dk_{0,l}d^{d-1}\overline{k}_1\cdots d^{d-1}\overline{k}_l}{[(k_{0,1})^2+\cdots+(k_{0,l})^2-|\overline{k}_1|^2-\cdots-|\overline{k}_l|^2]^n}. \tag{E.55}$$

The time and space components can be grouped as follows:

$$\begin{aligned} dk_{0,1}\cdots dk_{0,l}&=d\Omega_{l-1}|K_0|^{l-1}d|K_0|=d^lK_0 \\ d^{d-1}\overline{k}_1\cdots d^{d-1}\overline{k}_l=d\overline{k}_{11}\cdots d\overline{k}_{1d-1}d\overline{k}_{21}\cdots d\overline{k}_{ld-1}&=d\Omega_{l(d-1)-1}|\mathbf{K}|^{l(d-1)-1}d|\mathbf{K}|=d^{l(d-1)}\mathbf{K}, \end{aligned} \tag{E.56}$$

therefore

$$I_l^n\left(\overline{0};\overline{0}\right)=\frac{C}{(i\pi^{\frac{d}{2}})^l}\int\frac{d^lK_0d^{l(d-1)}\mathbf{K}}{(K_0^2-|\mathbf{K}|^2)^n}=C\int_K\frac{d^{ld}K}{[K^2]^n}=CJ_{-n}. \tag{E.57}$$

The Eq. (E.57) hides a subtlety: its metric tensor is not anymore the standard Minkowsky metric with signature $(1,d-1)$, but $(l,d-l)$. However, this very same calculation could have been done in the Euclidean space by means of the Wick rotation, leading to a non-ambiguous definition of the scalar products. Moreover, it can be shown [174] that for dimensionally regularized integral the following relation holds:

$$\int d^{d_1}k_1\int d^{d_2}k_2f(k_1^2+k_2^2)=\int d^{d_1+d_2}Kf(K^2), \qquad K=(k_1,k_2), \tag{E.58}$$

from which Eq. (E.57) follows, after inverting the Wick rotation.

It is important to notice that there are scaleless integrals for which their vanishing value comes from a non-trivial interplay between UV and IR divergences. This fact can be shown explicitely from the massless bubble:

$$B_0(0;0,0) = \int_k \frac{1}{k^2(k+p)^2}, \qquad p^2 = 0. \tag{E.59}$$

The Feynman parametrization yields

$$B_0(0;0,0) = \int_0^1 \int_k \frac{dx}{[k^2+2x(k\cdot p)]^2} = \int_0^1 \int_k \frac{dx}{[k^2]^2} = \int_k \frac{1}{[k^2]^2} = J_{-2}. \tag{E.60}$$

Instead of directly setting it to zero, there can be shown the reason why it vanish by analytically integrating the loop momentum:

$$\begin{aligned} B_0(0;0,0) &= \frac{1}{i\pi^{\frac{d}{2}}} \int \frac{dk^0 d^{(d-1)}\overline{k}}{[(k^0)^2 - |\overline{k}|^2]^2} \\ &= -\frac{\pi^{1-\frac{d}{2}}}{2} \int \frac{d^{(d-1)}\overline{k}}{[\overline{k}^2]^{\frac{3}{2}}} \\ &= -\frac{\pi^{1-\frac{d}{2}}}{4} \int d\Omega_{d-2} \int_0^\infty \frac{d\overline{k}^2}{[\overline{k}^2]^{3-\frac{d}{2}}}. \end{aligned} \tag{E.61}$$

Renaming $\overline{k}^2 = y$, setting $d = 4-2\epsilon$ and integrating over the solid angle $d\Omega_{d-2}$:

$$B_0(0;0,0) = -4^{-\epsilon} \frac{\Gamma(1-\epsilon)}{\Gamma(2-2\epsilon)} \int_0^\infty \frac{dy}{y^{1+\epsilon}}. \tag{E.62}$$

There is no way to make the integral of Eq. (E.62) converge by acting on the ϵ parameter. However, an appropriate analytical continuation with respect of ϵ ensures its vanishing behaviour. It is possible to recover this behaviour by splitting the integration regions and imposing two different conditions on ϵ:

$$\int_0^\infty \frac{dy}{y^{1+\epsilon}} = \int_0^1 \frac{dy}{y^{1+\epsilon}} + \int_1^\infty \frac{dy}{y^{1+\epsilon}}. \tag{E.63}$$

The first term diverges if $\epsilon < 0$; the second one if $\epsilon > 0$. Imposing $\epsilon_{\text{IR}} = -\epsilon$ for the first term and $\epsilon_{\text{UV}} = \epsilon$ for the second, the integral is not divergent anymore:

$$\int_0^\infty \frac{dy}{y^{1+\epsilon}} = \frac{1}{\epsilon_{\text{IR}}} y^{\epsilon_{\text{IR}}}\Big|_0^1 + \frac{1}{\epsilon_{\text{UV}}} \frac{1}{y^{\epsilon_{\text{UV}}}}\Big|_1^\infty = \frac{1}{\epsilon_{\text{IR}}} - \frac{1}{\epsilon_{\text{UV}}}, \tag{E.64}$$

and

$$B_0(0;0,0) = 4^{-\epsilon} \frac{\Gamma(1-\epsilon)}{\Gamma(2-2\epsilon)} \left(\frac{1}{\epsilon_{\text{UV}}} - \frac{1}{\epsilon_{\text{IR}}} \right). \tag{E.65}$$

The vanishing behaviour of $B_0(0;0,0)$ lies in an exact cancellation between the UV and IR poles. The UV pole extracted in this way is the one that is cancel by $\overline{\text{MS}}$ counterterm for massless quarks self-energies.

Appendix F

Utilities

In this Appendix, some useful identities used for make the expressions compact are presented. In the first Section, identities involving the kinematical variables and the transverse momentum are presented. In the last Section, the transformations regarding the Feynman parameters are shown for the one-loop case.

F.1 Useful kinematical identities

In the context of this thesis, the transverse momentum p_T^2 has been defined as follows:

$$p_T^2 = \frac{(\hat{t} - m_{H_1}^2)(\hat{u} - m_{H_1}^2) - \hat{s} m_{H_1}^2}{\hat{s}}. \tag{F.1}$$

Momentum conservation relates the $\hat{s}$, $\hat{t}$ and $\hat{u}$, and p_T^2 can take different expressions, for examples:

$$\begin{aligned} \hat{s} p_T^2 &= (\hat{t} - m_{H_1}^2)(\hat{u} - m_{H_1}^2) - \hat{s} m_{H_1}^2 \\ &= -(\hat{t} - m_{H_1}^2)(\hat{t} - m_{H_2}^2) - \hat{s}\hat{t} \\ &= \hat{t}\hat{u} - m_{H_1}^2 m_{H_2}^2. \end{aligned} \tag{F.2}$$

Moreover, looking back to Appendix C, the $\hat{t}$ variable runs from t_- to t_+, defined as

$$\hat{t}_\pm = -\frac{\hat{s}}{2}(1 - \Sigma \mp \beta). \tag{F.3}$$

Combinations of $\hat{t}$ and $\hat{t}_\pm$ can be defined:

$$\begin{aligned} \hat{t}_+ \hat{t}_- &= m_{H_1}^2 m_{H_2}^2, \\ \hat{t}_+ - \hat{t}_- &= \hat{s}\beta, \\ \hat{t}_+ + \hat{t}_- &= -\hat{s}(1 - \Sigma), \\ \hat{t} - \hat{t}_+ &= -\frac{\hat{s}\beta}{2}(1 + \cos\theta) = -\frac{(\hat{t}_+ - \hat{t}_-)}{2}(1 + \cos\theta), \\ \hat{t} - \hat{t}_- &= \frac{\hat{s}\beta}{2}(1 - \cos\theta) = \frac{(\hat{t}_+ - \hat{t}_-)}{2}(1 - \cos\theta), \end{aligned} \tag{F.4}$$

so that

$$\begin{aligned} \hat{s} p_T^2 &= \hat{t}\hat{u} - m_{H_1}^2 m_{H_2}^2 \\ &= \frac{\hat{s}^2}{4}(1 - \Sigma - \beta\cos\theta)(1 - \Sigma + \beta\cos\theta) - \hat{t}_+\hat{t}_- \\ &= \frac{\hat{s}^2}{4}[(1 - \Sigma)^2 - \beta^2\cos^2\theta] - \hat{t}_+\hat{t}_- \\ &= \frac{1}{4}\left[(\hat{t}_+ + \hat{t}_-)^2 - (\hat{t}_+ - \hat{t}_-)^2\cos^2\theta\right] - \hat{t}_+\hat{t}_- \\ &= \frac{1}{4}(\hat{t}_+ - \hat{t}_-)^2(1 - \cos^2\theta) \\ &= -(\hat{t} - \hat{t}_+)(\hat{t} - \hat{t}_-). \end{aligned} \tag{F.5}$$

It is possible to define the $d\hat{t}$ element as follows

$$\frac{d\hat{t}}{\hat{s}p_T^2} = -\frac{d\hat{t}}{(\hat{t}-\hat{t}_-)(\hat{t}-\hat{t}_+)}. \tag{F.6}$$

The partial fractioning on the denominator yields

$$\frac{d\hat{t}}{\hat{s}p_T^2} = -\frac{d\hat{t}}{(\hat{t}_+-\hat{t}_-)}\left[\frac{1}{(\hat{t}-\hat{t}_+)} - \frac{1}{(\hat{t}-\hat{t}_-)}\right]. \tag{F.7}$$

It is easy to show that the identity

$$(\hat{t}-\hat{t}_+) = -(\hat{u}-\hat{t}_-), \tag{F.8}$$

therefore

$$\frac{d\hat{t}}{\hat{s}p_T^2} = \frac{d\hat{t}}{(\hat{t}_+-\hat{t}_-)}\left[\frac{1}{(\hat{t}-\hat{t}_-)} + \frac{1}{(\hat{u}-\hat{t}_-)}\right]. \tag{F.9}$$

The partonic cross section can be written as the integral of a function depending on the kinematic variables with respect to $\hat{t}$

$$\int_{\hat{t}_-}^{\hat{t}_+} \frac{d\hat{t}}{\hat{s}p_T^2} f(\hat{t},\hat{u}) = \int_{\hat{t}_-}^{\hat{t}_+} \frac{d\hat{t}}{(\hat{t}_+-\hat{t}_-)}\left[\frac{f(\hat{t},\hat{u})}{(\hat{t}-\hat{t}_-)} + \frac{f(\hat{t},\hat{u})}{(\hat{u}-\hat{t}_-)}\right]. \tag{F.10}$$

The second term can be written with the same denominator of the first one by noting that

$$\int_{\hat{t}_-}^{\hat{t}_+} d\hat{t}\frac{f(\hat{t},\hat{u})}{(\hat{u}-\hat{t}_-)} = \int_{\hat{t}_-}^{\hat{t}_+} d\hat{t}\frac{f(\hat{u},\hat{t})}{(\hat{t}-\hat{t}_-)}, \tag{F.11}$$

and therefore

$$\int_{\hat{t}_-}^{\hat{t}_+} \frac{d\hat{t}}{\hat{s}p_T^2} f(\hat{t},\hat{u}) = \int_{\hat{t}_-}^{\hat{t}_+} \frac{d\hat{t}}{(\hat{t}-\hat{t}_-)}\frac{f(\hat{t},\hat{u})+f(\hat{u},\hat{t})}{(\hat{t}_+-\hat{t}_-)}. \tag{F.12}$$

The integral of Eq. (F.12) shows manifestly the logarithmic instabilities that lie in the boundary of the integration region. In Chapter 4 these instabilites have been milded with a dedicated change of variables.

F.2 Feynman Parameters Tricks

The numerical integration of the Feynman integral requires a fixed boundaries, which for the Feynman parameters is an hypercube. In this Section the manipulations of the Feynman parameters which have been performed to obtain the convenient integration volume will be presented. The strategies presented in this Section have been employed for setting the integrands

F.2.1 Boundaries

Consider the integral measure occuring in a Feynman integral after its parameterization (for a 4-point integral):

$$\int_0^1 d\hat{x}_1 d\hat{x}_2 d\hat{x}_3 d\hat{x}_4 \delta\left(1-\sum_{i=1}^4 \hat{x}_i\right), \tag{F.13}$$

Extending a parameter domain to the real axis:

$$\int_{-\infty}^{\infty} d\hat{x}_1 d\hat{x}_2 d\hat{x}_3 d\hat{x}_4 \delta\left(1-\sum_{i=1}^4 \hat{x}_i\right)\prod_{i=1}^4 \theta(x_i)\theta(1-x_i). \tag{F.14}$$

Now the delta function can be legitimately integrated with respect to x_4

$$\int_{-\infty}^{\infty} d\hat{x}_1 d\hat{x}_2 d\hat{x}_3 \theta\left(\sum_{i=1}^3 \hat{x}_i\right)\theta\left(1-\sum_{i=1}^3 \hat{x}_i\right)\prod_{i=1}^3 \theta(\hat{x}_i)\theta(1-\hat{x}_i). \tag{F.15}$$

The first two Heaviside distributions yield the conditions

$$\theta(\hat{x}_1+\hat{x}_2+\hat{x}_3)\theta(1-\hat{x}_1-\hat{x}_2-\hat{x}_3)\geq 0 \iff -\hat{x}_1-\hat{x}_2\leq\hat{x}_3\leq 1-\hat{x}_1-\hat{x}_2. \tag{F.16}$$

Because of the $\theta(\hat{x}_3)\theta(1-\hat{x}_3)$ function, the lower limit for $\hat{x}_3$ has to be in between 0 and 1:

$$0\leq -\hat{x}_1-\hat{x}_2\leq 1 \iff \hat{x}_1=0\wedge\hat{x}_2=0. \tag{F.17}$$

Hence the lower limit for x_3 has to be 0.

Same argument holds for the upper limit for $\hat{x}_3$, except that now it does not get a single value, but a condition over $\hat{x}_2$:

$$0\leq 1-\hat{x}_1-\hat{x}_2\leq 1 \implies \hat{x}_2\geq -\hat{x}_1\wedge\hat{x}_2\leq 1-\hat{x}_1. \tag{F.18}$$

As for the first condition, for $\hat{x}_1>0$, the lower limit on $\hat{x}_2$ is zero.

Putting all the conditions together, the integration region is

$$\begin{aligned}&\theta\left(\sum_{i=1}^{3}\hat{x}_i\right)\theta\left(1-\sum_{i=1}^{3}\hat{x}_i\right)\prod_{i=1}^{3}\theta(\hat{x}_i)\theta(1-\hat{x}_i)\geq 0\\ \implies &0\leq\hat{x}_1\leq 1\wedge 0\leq\hat{x}_2\leq 1-\hat{x}_1\wedge 0\leq\hat{x}_3\leq 1-\hat{x}_1-\hat{x}_2,\end{aligned} \tag{F.19}$$

therefore,

$$\int_0^1 d\hat{x}_1 d\hat{x}_2 d\hat{x}_3 d\hat{x}_4\,\delta\left(1-\sum_{i=1}^{4}\hat{x}_i\right)=\int_0^1 d\hat{x}_1\int_0^{1-x_1}d\hat{x}_2\int_0^{1-x_1-x_2}d\hat{x}_3. \tag{F.20}$$

This argument can be extended for any number of Feynman parameters

$$\int_0^1 d^{n+1}\hat{x}\,\delta\left(1-\sum_{i=1}^{n+1}\hat{x}_i\right)=\int_0^1\cdots\int_0^{1-x_1-\cdots-x_n}d^n\hat{x},\quad d^n\hat{x}=\prod_{j=1}^{n}d\hat{x}_j. \tag{F.21}$$

Note that the order of the integrations it totally arbitrary:

$$\int_0^1 d\hat{x}_1 d\hat{x}_2 d\hat{x}_3\,\delta\left(1-\sum_{i=1}^{3}\hat{x}_i\right)=\int_0^1 d\hat{x}_1\int_0^{1-x_1}d\hat{x}_2=\int_0^1 d\hat{x}_2\int_0^{1-x_2}d\hat{x}_1. \tag{F.22}$$

This fact leads to the first trick: whenever a pattern that resambles the r.h.s. of Eq. (F.21) shows up, the integration order can be permuted in the most convenient one.

F.2.2 Transformations

To achieve the numerical integration, the variables have to be transformed such that the new integration volume is the n-dimensional unit cube $\mathcal{C}=[0,1]^n$. The easiest way is to use the following transformation

$$\begin{aligned}&\begin{cases}\hat{x}_i=\left[\prod_{j=1}^{i-1}(1-x_j)\right]x_i, & i>1\\ \hat{x}_i=x_i, & i=1\end{cases}\\ &d^n\hat{x}=\left(\prod_{i=1}^{n-1}(1-x_i)^{n-i}\right)d^n x,\end{aligned} \tag{F.23}$$

hence

$$\int_0^1 d^{n+1}\hat{x}\,\delta\left(1-\sum_{i=1}^{n+1}\hat{x}_i\right)=\int_0^1 d^n x\left(\prod_{i=1}^{n-1}(1-x_i)^{n-i}\right). \tag{F.24}$$

Focusing on the previous example, we can write:

$$\int_0^1 d\hat{x}_1 d\hat{x}_2 d\hat{x}_3 d\hat{x}_4\,\delta\left(1-\sum_{i=1}^{4}\hat{x}_i\right)=\int_0^1 dx_1 dx_2 dx_3(1-x_1)^2(1-x_2). \tag{F.25}$$

Note that the integration boundaries are invariant on the shift $x_i \to 1 - x_i$:

$$\int_0^1 dx f(x) = \int_0^1 dx f(1-x) \tag{F.26}$$

therefore sometimes can be convenient to shift our parameters

$$\begin{aligned}\int_0^1 d\hat{x}_1 d\hat{x}_2 d\hat{x}_3 d\hat{x}_4 \delta\left(1 - \sum_{i=1}^4 \hat{x}_i\right) &= \int_0^1 dx_1 dx_2 dx_3 (1-x_1)^2(1-x_2) \\ &= \int_0^1 dx_1 dx_2 dx_3 (x_1^2 x_2)\end{aligned} \tag{F.27}$$

The Eq. (F.23) offers a general change of variable for mapping the domain of the Feynman parameters in $[0,1]^n$. However, the complexity of the mapping increases with the number of Feynman parameters, and issues related with the endpoint subtraction can arise. At NLO, a dedicated change of variables have been chosen for treating the two-loop integrals for the virtual contributions, which has been presented in Chapter 3. Here below a sketch of the strategy employed in the construction of the change of variables at NLO is presented with LO examples.

Example 1

Let I be a one-loop 4-points integral. Using Feynman parametrization it reads

$$I = \int_0^1 d\hat{x}_2 \int_0^{1-\hat{x}_2} d\hat{x}_1 \int_0^{1-\hat{x}_1-\hat{x}_2} d\hat{x}_3 \frac{f(\hat{x}_1, \hat{x}_2, \hat{x}_3)}{[\hat{N}_1^2(\hat{x}_1, \hat{x}_2, \hat{x}_3)]^p},$$

$$\hat{N}_1^2(\hat{x}_1, \hat{x}_2, \hat{x}_3) = 1 - \hat{x}_2(1-\hat{x}_1-\hat{x}_2)\rho_s - \hat{x}_3(\hat{x}_1+\hat{x}_2)(\rho_t - \rho_{H_1}) - \hat{x}_2\hat{x}_3(\rho_u - \rho_{H_1}) - \hat{x}_3(1-\hat{x}_3)\rho_{H_1}. \tag{F.28}$$

Applying the first transformation $x_1 = 1 - \hat{x}_1 - \hat{x}_2$, the expression reads

$$I = \int_0^1 d\hat{x}_2 \int_0^{1-\hat{x}_2} dx_1 \int_0^{x_1} d\hat{x}_3 \frac{f(x_1, \hat{x}_2, \hat{x}_3)}{[\hat{N}_1^2(x_1, \hat{x}_2, \hat{x}_3)]^p} \tag{F.29}$$

$$\hat{N}_1^2(\hat{x}_1, \hat{x}_2, \hat{x}_3) = 1 - \hat{x}_2 x_1 \rho_s - \hat{x}_3(1-x_1)(\rho_t - \rho_{H_1}) - \hat{x}_2\hat{x}_3(\rho_u - \rho_{H_1}) - \hat{x}_3(1-\hat{x}_3)\rho_{H_1}$$

Switching the boundaries for $\hat{x}_2$ and x_1, I becomes

$$\int_0^1 d\hat{x}_2 \int_0^{1-\hat{x}_2} dx_1 \int_0^{x_1} d\hat{x}_3 \frac{f(x_1, \hat{x}_2, \hat{x}_3)}{[\hat{N}_1^2(x_1, \hat{x}_2, \hat{x}_3)]^p} = \int_0^1 dx_1 \int_0^{1-x_1} d\hat{x}_2 \int_0^{x_1} d\hat{x}_3 \frac{f(x_1, \hat{x}_2, \hat{x}_3)}{[\hat{N}_1^2(x_1, \hat{x}_2, \hat{x}_3)]^p}. \tag{F.30}$$

Finally, setting the boundaries from 0 to 1 through the trasformation $\hat{x}_2 = (1-x_1)x_2$ and $\hat{x}_3 = x_1 x_3$, the total transformation is

$$\begin{cases} \hat{x}_1 = (1-x_1)(1-x_2) \\ \hat{x}_2 = x_2(1-x_1) \\ \hat{x}_3 = x_1 x_3 \end{cases}. \tag{F.31}$$

Hence, the full integral reads

$$I = \int_0^1 dx_1 dx_2 dx_3 \frac{f(x_1, \hat{x}_2, \hat{x}_3)}{[\hat{N}_1^2(x_1, \hat{x}_2, \hat{x}_3)]^p} x_1(1-x_1). \tag{F.32}$$

Notive that the Jacobian depends on a single variable.

Example 2

The Feynman parameterisation brings the integral for $\mathcal{M}_2$ in the following form:

$$\begin{aligned} I &= \int_0^1 d\hat{x}_3 \int_0^{1-\hat{x}_3} d\hat{x}_2 \int_0^{1-\hat{x}_3-\hat{x}_2} d\hat{x}_1 \frac{f(\hat{x}_1,\hat{x}_2,\hat{x}_3)}{[\hat{N}_2^2(\hat{x}_1,\hat{x}_2,\hat{x}_3)]^p}, \\ \hat{N}_1^2(\hat{x}_1,\hat{x}_2,\hat{x}_3) &= 1-\hat{x}_3(1-\hat{x}_2-\hat{x}_3)\rho_{\hat{u}} - \hat{x}_3(1-\hat{x}_1-\hat{x}_2-\hat{x}_3)\rho_s + \\ &\quad -(\hat{x}_2+\hat{x}_3)(1-\hat{x}_1-\hat{x}_2-\hat{x}_3)\rho_{\hat{t}} - (\hat{x}_2+\hat{x}_3)(1-\hat{x}_1-\hat{x}_2-\hat{x}_3)\rho_{H_1}. \end{aligned} \tag{F.33}$$

The first replacement will be $\alpha = 1-\hat{x}_1-\hat{x}_2-\hat{x}_3 \implies \hat{x}_1 = 1-\alpha-\hat{x}_2-\hat{x}_3$. Therefore

$$I = \int_0^1 d\hat{x}_3 \int_0^{1-\hat{x}_3} d\hat{x}_2 \int_0^{1-\hat{x}_3-\hat{x}_2} d\alpha. \tag{F.34}$$

Exchanging the integration order and performing the change of variables $\beta = 1-\hat{x}_2-\hat{x}_3$, I becomes

$$\begin{aligned} \int_0^1 d\hat{x}_3 \int_0^{1-\hat{x}_3} d\hat{x}_2 \int_0^{1-\hat{x}_3-\hat{x}_2} d\alpha &= \int_0^1 d\alpha \int_0^{1-\alpha} d\hat{x}_3 \int_0^{1-\alpha-\hat{x}_3} d\hat{x}_2 \\ &= \int_0^1 d\alpha \int_0^{1-\alpha} d\hat{x}_3 \int_\alpha^{1-\hat{x}_3} d\beta. \end{aligned} \tag{F.35}$$

The domain for (α,β) is the upper triagle inscripted into the square $[0,1]^2$. Exchanging the integration variables, the boundaries can be mapped into the unit cube by means of the following identities

$$\begin{aligned} \int_0^1 d\alpha \int_0^{1-\alpha} d\hat{x}_3 \int_\alpha^{1-\hat{x}_3} d\beta &= \int_0^1 d\hat{x}_3 \int_0^{1-\hat{x}_3} d\alpha \int_\alpha^{1-\hat{x}_3} d\beta \\ &= \int_0^1 d\hat{x}_3 \int_0^{1-\hat{x}_3} d\beta \int_0^{\beta} d\alpha \\ &= \int_0^1 d\beta \int_0^{1-\beta} d\hat{x}_3 \int_0^{\beta} d\alpha \\ &= \int_{\mathcal{C}} d\overline{x} x_1(1-x_1). \end{aligned} \tag{F.36}$$

Collecting all the change of variables, the mapping reads

$$\begin{aligned} \hat{x}_1 = 1-\alpha-\hat{x}_2-\hat{x}_3 &\implies \hat{x}_1 = \beta-\alpha = x_1(1-x_2) \\ \hat{x}_2 = 1-\beta-\hat{x}_3 &\implies \hat{x}_2 = 1-\beta-(1-\beta)x_3 = (1-x_1)(1-x_3) \\ \hat{x}_3 = (1-\beta)x_3 &\implies \hat{x}_3 = (1-x_1)x_3. \end{aligned} \tag{F.37}$$

Appendix G

Running of α_s in QCD

In this Appendix, the evaluation of the counterterms for α_s in the $\overline{\text{MS}}$ scheme for the $N_f = 5$ active massless flavours with the top-quark mass decoupled from the running will be presented.

G.1 Gluon propagator

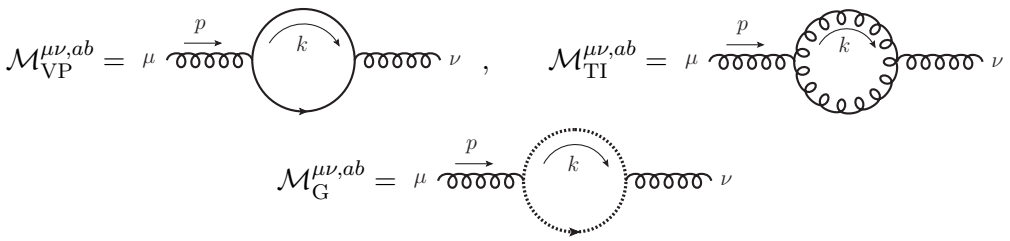

Figure G.1: Diagrams contributing to the gluon propagator.

The gluon propagator expressed into its form factor reads

$$i\delta^{ab}(p^2 g^{\mu\nu} - p^\mu p^\nu)\Pi_0(p^2) = \mathcal{M}^{\mu\nu,ab}_{\text{VP}} + \mathcal{M}^{\mu\nu,ab}_{\text{TI}} + \mathcal{M}^{\mu\nu,ab}_{\text{G}} \tag{G.1}$$

and the counterterm behave such that

$$\Pi_0(p^2) - \delta_3 = \text{finite}. \tag{G.2}$$

G.1.1 Massless flavours

$$\begin{aligned}
\mathcal{M}^{\mu\nu,ab}_{\text{VP}} &= -\frac{i}{(4\pi)^2}(4\pi\mu^2)^{2-\frac{d}{2}} \int_k (-ig_s\gamma^\mu T^a)\, \frac{i\not{k}}{k^2} \left(-ig_s\gamma^\nu T^b\right) \frac{i(\not{k}+\not{p})}{(k+p)^2} \\
&= -\frac{1}{2}\frac{ig_s^2}{(4\pi)^2}\delta^{ab}(4\pi\mu^2)^{2-\frac{d}{2}} \int_k \frac{\text{Tr}[\gamma^\mu \not{k}\gamma^\nu(\not{k}+\not{p})]}{k^2(k+p)^2} \\
&= -\frac{ig_s^2}{2(4\pi)^2}\delta^{ab}(4\pi\mu^2)^{2-\frac{d}{2}} 4 \left[2\int_k \frac{k^\mu k^\nu}{k^2(k+p)^2} + \int_k \frac{k^\mu p^\nu + p^\mu k^\nu}{k^2(k+p)^2} - g^{\mu\nu}\int_k \frac{(k^2 + k\cdot p)}{k^2(k+p)^2}\right] \\
&= -\frac{ig_s^2}{(4\pi)^2}\delta^{ab}\left[p^2 g^{\mu\nu} - p^\mu p^\nu\right]\left(\frac{4\pi\mu^2}{-p^2}\right)^\epsilon \Gamma(1+\epsilon)\frac{2}{3}\frac{1}{\epsilon}
\end{aligned} \tag{G.3}$$

Summing over the massless flavours, we obtain

$$\mathcal{M}^{\mu\nu,ab}_{\text{VP}} = -\frac{ig_s^2}{(4\pi)^2}\delta^{ab}\left[p^2 g^{\mu\nu} - p^\mu p^\nu\right]\left(\frac{4\pi\mu^2}{-p^2}\right)^\epsilon \Gamma(1+\epsilon)\frac{2N_f}{3}\frac{1}{\epsilon} + \text{finite}. \tag{G.4}$$

The triple gauge boson interaction diagram is given by

$$\begin{aligned}\mathcal{M}^{\mu\nu,ab}_{\rm TI} &= \frac{1}{2}\frac{i}{(4\pi)^2}(4\pi\mu^2)^{2-\frac{d}{2}}\int_k \left(-g_s f^{acd}[g^{\mu\alpha}(k+2p)^\beta + g^{\alpha\beta}(-2k-p)^\mu + g^{\beta\mu}(k-p)^\alpha]\right)\times \\ &\times\left(\frac{-ig_{\alpha\rho}\delta^{ce}}{k^2}\right)\left(-g_s f^{ebf}[g^{\rho\nu}(k+2p)^\sigma + g^{\nu\sigma}(k-p)^\rho + g^{\sigma\rho}(-2k-p)^\nu]\right)\left(\frac{-ig_{\sigma\beta}\delta^{df}}{(k+p)^2}\right) \\ &= \frac{1}{2}\frac{ig_s^2}{(4\pi)^2}f^{acd}f^{bcd}(4\pi\mu^2)^{2-\frac{d}{2}}\int_k \frac{\mathcal{N}^{\mu\nu}}{D_0 D_1},\end{aligned} \tag{G.5}$$

where

$$\begin{aligned}\mathcal{N}^{\mu\nu} &= [g^{\mu\rho}(k+2p)^\sigma + g^{\rho\sigma}(-2k-p)^\mu + g^{\sigma\mu}(k-p)^\rho][g^{\rho\nu}(k+2p)^\sigma + g^{\nu\sigma}(k-p)^\rho + g^{\sigma\rho}(-2k-p)^\nu] \\ &= 2(2d-3)k^\mu k^\nu + (2d-3)(k^\mu p^\nu + p^\mu k^\nu) + (d-6)p^\mu p^\nu + g^{\mu\nu}[2(k\cdot p) + 2k^2 + 5p^2]\end{aligned} \tag{G.6}$$

The PV reduction applied to the integral yields

$$\int_k \frac{\mathcal{N}^{\mu\nu}}{D_0 D_1} = \frac{[(6d-5)p^2 g^{\mu\nu} - (7d-6)p^\mu p^\nu]}{2(d-1)}B_0(p^2;\overline{0}), \tag{G.7}$$

so that

$$\mathcal{M}^{\mu\nu,ab}_{TI} = \frac{C_A}{2}\frac{ig_s^2}{(4\pi)^2}\delta^{ab}(4\pi\mu^2)^{2-\frac{d}{2}}\frac{[(6d-5)p^2 g^{\mu\nu} - (7d-6)p^\mu p^\nu]}{2(d-1)}B_0(p^2;\overline{0}), \tag{G.8}$$

which is not transverse.

The ghost contribution is needed to remove the contribution of the unphysical degrees of freedom:

$$\begin{aligned}\mathcal{M}^{\mu\nu,ab}_G &= -\frac{i}{(4\pi)^2}(4\pi\mu^2)^{2-\frac{d}{2}}\int_k (-g_s f^{cae}(k+p)^\mu)\left(\frac{i\delta^{cd}}{(k+p)^2}\right)(-g_s f^{fbd}k^\nu)\left(\frac{i\delta^{ef}}{k^2}\right) \\ &= -\frac{ig_s^2}{(4\pi)^2}f^{ace}f^{bce}(4\pi\mu^2)^{2-\frac{d}{2}}\left[\int_k \frac{k^\mu k^\nu}{k^2(k+p)^2} + p^\mu\int_k \frac{k^\nu}{k^2(k+p)^2}\right] \\ &= \frac{C_A}{2}\frac{ig_s^2}{(4\pi)^2}\delta^{ab}(4\pi\mu^2)^{2-\frac{d}{2}}\left[\frac{p^2 g^{\mu\nu} + (d-2)p^\mu p^\nu}{2(d-1)}\right]B_0(p^2;\overline{0})\end{aligned} \tag{G.9}$$

The sum of the ghost contribution and the non-abelian bubble contribution recovers the transversality of the propagator tensor:

$$\mathcal{M}^{\mu\nu,ab}_{TI} + \mathcal{M}^{\mu\nu,ab}_G = \frac{ig_s^2}{(4\pi)^2}\delta^{ab}\left(p^2 g^{\mu\nu} - p^\mu p^\nu\right)\left(\frac{4\pi\mu^2}{-p^2}\right)^\epsilon \Gamma(1+\epsilon)\frac{5C_A}{3}\frac{1}{\epsilon} + \text{finite}. \tag{G.10}$$

In massless QCD with N_f active flavours the divergent part is

$$\Pi_0^{\mu\nu} = \frac{g_s^2}{(4\pi)^2}\left(\frac{4\pi\mu^2}{-p^2}\right)^\epsilon \Gamma(1+\epsilon)\left(\frac{5C_A}{3} - \frac{2N_f}{3}\right)\frac{1}{\epsilon} + \text{finite}, \tag{G.11}$$

and the counterterm is

$$\delta_3' = \frac{g_s^2}{(4\pi)^2}\left(\frac{4\pi\mu^2}{\mu_R^2}\right)^\epsilon \Gamma(1+\epsilon)\left(\frac{5C_A}{3} - \frac{2N_f}{3}\right)\frac{1}{\epsilon}. \tag{G.12}$$

G.1.2 Top-mass contribution

$$\begin{aligned}\mathcal{M}^{\mu\nu,ab}_{\rm VP} &= -\frac{i}{(4\pi)^2}(4\pi\mu^2)^{2-\frac{d}{2}}\int_k (-ig_s\gamma^\mu T^a)\frac{i(\not{k}+m_t)}{[k^2-m_t^2]}\left(-ig_s\gamma^\nu T^b\right)\frac{i(\not{k}+\not{p}+m_t)}{[(k+p)^2-m_t^2]} \\ &= -\frac{ig_s^2}{(4\pi)^2}\mathrm{Tr}[T^a T^b](4\pi\mu^2)^{2-\frac{d}{2}}\int_k \frac{\mathrm{Tr}[\gamma^\mu(\not{k}+m_t)\gamma^\nu(\not{k}+\not{p}+m_t)]}{[k^2-m_t^2][(k+p)^2-m_t^2]} \\ &= -\frac{ig_s^2}{2(4\pi)^2}\delta^{ab}(4\pi\mu^2)^{2-\frac{d}{2}}\int_k \frac{\mathcal{N}^{\mu\nu}}{D_0 D_1}.\end{aligned} \tag{G.13}$$

Expanding the trace, we obtain

$$\begin{aligned}\mathcal{N}^{\mu\nu} &= \mathrm{Tr}[\gamma^\mu \not{k}\gamma^\nu(\not{k}+\not{p})] + m_t^2\mathrm{Tr}[\gamma^\mu\gamma^\nu] \\ &= 4[2k^\mu k^\nu + k^\mu p^\nu + p^\mu k^\nu - g^{\mu\nu}k\cdot(k+p) + m_t^2 g^{\mu\nu}],\end{aligned} \tag{G.14}$$

and the PV reduction of this amplitude (see Appendix D) yields

$$\begin{aligned}\mathcal{M}_{\mathrm{VP}}^{\mu\nu,ab} &= -\frac{2ig_s^2}{(4\pi)^2}\delta^{ab}(4\pi\mu^2)^{2-\frac{d}{2}}\left[2\int_k \frac{k^\mu k^\nu}{D_0 D_1} + \int_k \frac{k^\mu p^\nu + p^\mu k^\nu}{D_0 D_1} + g^{\mu\nu}\int_k \frac{m_t^2 - k\cdot(k+p)}{D_0 D_1}\right] \\ &= -\frac{ig_s^2}{(4\pi)^2}\delta^{ab}(4\pi\mu^2)^{2-\frac{d}{2}}\frac{[(d-2)p^2+4m_t^2]B_0(p^2;\overline{m}_t^2) - 2(d-2)A_0(m_t^2)}{(d-1)}\left(g^{\mu\nu} - \frac{p^\mu p^\nu}{p^2}\right) \\ &= -\frac{ig_s^2}{(4\pi)^2}\delta^{ab}(4\pi\mu^2)^{\epsilon}\left\{\frac{[2(1-\epsilon)p^2+4m_t^2]}{(3-2\epsilon)}B_0(p^2;\overline{m}_t^2) - \frac{4(1-\epsilon)}{(3-2\epsilon)}A_0(m_t^2)\right\}\left(g^{\mu\nu} - \frac{p^\mu p^\nu}{p^2}\right) \\ &= -\frac{ig_s^2}{(4\pi)^2}\delta^{ab}\left[p^2 g^{\mu\nu} - p^\mu p^\nu\right](4\pi\mu^2)^{\epsilon}\left(\frac{1}{3-2\epsilon}\right)\left\{\left[2(1-\epsilon) + \frac{4m_t^2}{p^2}\right]B_0(p^2;\overline{m}_t^2) - \frac{4(1-\epsilon)}{p^2}A_0(m_t^2)\right\}\end{aligned} \tag{G.15}$$

Therefore, the form factor $\Pi_t(p^2)$ of $\mathcal{M}_{\mathrm{VP}}^{\mu\nu,ab}$ with the top quark into the loop reads

$$\Pi_t(p^2) = -\frac{g_s^2}{(4\pi)^2}(4\pi\mu^2)^{\epsilon}\left(\frac{1}{3-2\epsilon}\right)\left\{\left[2(1-\epsilon) + \frac{4m_t^2}{p^2}\right]B_0(p^2;\overline{m}_t^2) - \frac{4(1-\epsilon)}{p^2}A_0(m_t^2)\right\}. \tag{G.16}$$

The on-shell limit of this form factor is useful to check the proper cancellation of the wave function corrections due to the top-quark contributions. Expanding Eq. (G.16) around $p^2 = 0$:

$$\begin{aligned}\Pi_t(p^2) &= -\frac{g_s^2}{(4\pi)^2}(4\pi\mu^2)^{\epsilon}\left(\frac{1}{3-2\epsilon}\right)\left\{\frac{1}{p^2}\left[4m_t^2 B_0(0;\overline{m}_t^2) - 4(1-\epsilon)A_0(m_t^2)\right]\right. \\ &\qquad \left. + \left[2(1-\epsilon)B_0(0;\overline{m}_t^2) + 4m_t^2\frac{d}{dp^2}B_0(0;\overline{m}_t^2)\right] + O(p^2)\right\} \\ &= -\frac{g_s^2}{(4\pi)^2}\left(\frac{4\pi\mu^2}{m_t^2}\right)^{\epsilon}\frac{\Gamma(1+\epsilon)}{3-2\epsilon}\left\{\frac{4m_t^2}{p^2}\epsilon + \left[\frac{2}{\epsilon} - \frac{4}{3}\right] + O(p^2)\right\},\end{aligned} \tag{G.17}$$

and around $\epsilon = 0$:

$$\Pi_t(p^2) = -\frac{g_s^2}{(4\pi)^2}\left(\frac{4\pi\mu^2}{m_t^2}\right)^{\epsilon}\Gamma(1+\epsilon)\frac{2}{3}\frac{1}{\epsilon} + O(p^2,\epsilon) \tag{G.18}$$

Here, the derivative of the bubble integral presented in Appendix E has been used. Therefore, the form factor for an on-shell gluon is

$$\Pi_t(0) = -\frac{g_s^2}{(4\pi)^2}\left(\frac{4\pi\mu^2}{m_t^2}\right)^{\epsilon}\Gamma(1+\epsilon)\frac{2}{3}\frac{1}{\epsilon}. \tag{G.19}$$

The on-shell limit presented in Eq. (G.19) takes part in the wave function correction of the NLO: their contribution, shown in Figure G.2, is the product of two form factors:

$$\Pi_t(0)F_j^{(0)} = -\frac{g_s^2}{(4\pi)^2}\left(\frac{4\pi\mu^2}{m_t^2}\right)^{\epsilon}\Gamma(1+\epsilon)\frac{2}{3}\frac{1}{\epsilon}F_j^{(0)}. \tag{G.20}$$

The vacuum polarization diagrams are the only ones that receive contribution depending on the top mass: this fact can be exploited to build a counterterm that makes the top quark decouple from the running of α_s. The decoupling can be enforced by the condition

$$\delta_3 - \delta_3' - \Pi_t(0) = \text{finite} \tag{G.21}$$

where δ_3 is the total vacuum polarization counterterm and δ_3' is the massless vacuum polarization counterterm. The explicit expression of δ_3 is

$$\delta_3 = \frac{g_s^2}{(4\pi)^2}\left(\frac{4\pi\mu^2}{\mu_R^2}\right)^{\epsilon}\Gamma(1+\epsilon)\left[\left(\frac{5C_A - 2(N_f+1)}{3}\right)\frac{1}{\epsilon} - \frac{2}{3}\log\left(\frac{\mu_R^2}{m_t^2}\right)\right]. \tag{G.22}$$

Later on, the decoupling of the top mass from the running of α_s will be shown explicitely.

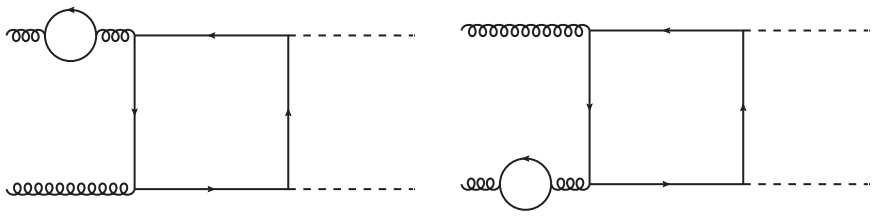

Figure G.2: Wave-function corrections due to top-quark loops.

G.2 Quark Self-energy

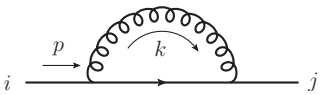

Figure G.3: Diagram contributing to the massless quark self-energy.

The self-energy diagram and its counterterm can be expressed as

$$\begin{aligned} -i\not{p}\delta^{ij}\Sigma(p^2) &= \mathcal{M}_0^{(f)}, \\ \Sigma(p^2) - \delta_2 &= \text{finite}. \end{aligned} \tag{G.23}$$

and the amplitude can be written as:

$$\begin{aligned} \mathcal{M}_0^{(f)} &= \frac{i}{(4\pi)^2}(4\pi\mu^2)^{2-\frac{d}{2}}\int_k(-ig_s\gamma^\mu T^a)\frac{i\not{k}}{k^2}(-ig_s\gamma^\nu T^b)\frac{-ig^{\mu\nu}\delta^{ab}}{(k-p)^2} \\ &= -\frac{ig_s^2}{(4\pi)^2}T^aT^a(4\pi\mu^2)^{2-\frac{d}{2}}\int_k\frac{\gamma^\mu\not{k}\gamma_\mu}{k^2(k-p)^2} \\ &= \frac{ig_s^2}{(4\pi)^2}C_F\delta^{ij}(4\pi\mu^2)^{2-\frac{d}{2}}\int_k\frac{(d-2)\not{k}}{k^2(k-p)^2} \\ &= \frac{ig_s^2}{(4\pi)^2}C_F\delta^{ij}(4\pi\mu^2)^{2-\frac{d}{2}}\frac{(d-2)}{2}\not{p}B_0(p^2,\overline{0}), \end{aligned} \tag{G.24}$$

where p^2 is the off-shellness of the quark propagator. The pole structure is:

$$\begin{aligned} \mathcal{M}_0^{(f)} &= \frac{ig_s^2}{(4\pi)^2}C_F\delta^{ij}\left(\frac{4\pi\mu^2}{-p^2}\right)^\epsilon\Gamma(1+\epsilon)\not{p}\frac{1}{\epsilon} + \text{finite} \\ \Sigma_0(p^2) &= -\frac{g_s^2}{(4\pi)^2}C_F\left(\frac{4\pi\mu^2}{-p^2}\right)^\epsilon\Gamma(1+\epsilon)\frac{1}{\epsilon} + \text{finite} \end{aligned} \tag{G.25}$$

and its counterter is

$$\delta_2 = -\frac{g_s^2}{(4\pi)^2}C_F\left(\frac{4\pi\mu^2}{\mu_R^2}\right)^\epsilon\Gamma(1+\epsilon)\frac{1}{\epsilon} \tag{G.26}$$

G.3 Verteces

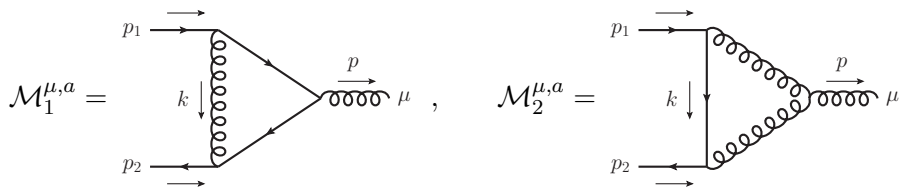

Figure G.4: Diagram contributing to the vertex corrections

Lastly, we need the vertex diagrams. This contribution has the following structure:

$$\begin{aligned} -ig_s T^a\gamma^\mu \Gamma_{\text{vert}}(p_1,p_2) &= \mathcal{M}_1^{\mu,a} + \mathcal{M}_2^{\mu,a} \\ \Gamma_{\text{vert}}(p_1,p_2) + \delta_1 &= \text{finite} \end{aligned} \tag{G.27}$$

The amplitude for $\mathcal{M}_1^{\mu,a}$ is

$$\begin{aligned} \mathcal{M}_1^{\mu,a} &= \frac{i}{(4\pi)^2}(4\pi\mu^2)^{2-\frac{d}{2}}\int_k (-ig_s\gamma^\sigma T^c)\frac{i(-\not{k}-\not{p}_2)}{(k+p_2)^2}(-ig_s\gamma^\mu T^a)\frac{i(-\not{k}+\not{p}_1)}{(k-p_1)^2}(-ig_s\gamma^\rho T^b)\frac{-ig^{\sigma\rho}\delta^{bc}}{k^2} \\ &= -\frac{ig_s^3}{(4\pi)^2}T^bT^aT^b(4\pi\mu^2)^{2-\frac{d}{2}}\int_k \frac{\gamma^\sigma(\not{k}+\not{p}_2)\gamma^\mu(\not{k}-\not{p}_1)\gamma_\sigma}{k^2(k-p_1)^2(k+p_2)^2} \end{aligned} \tag{G.28}$$

Since the scalar triangle C_0 is finite, we can already drop the terms which generates scalar triangles.

$$\mathcal{M}_1^{\mu,a} = -\frac{ig_s^3}{(4\pi)^2}T^bT^aT^b(4\pi\mu^2)^{2-\frac{d}{2}}\int_k \frac{\gamma^\sigma\not{k}\gamma^\mu\not{k}\gamma_\sigma - \gamma^\sigma\not{k}\gamma^\mu\not{p}_1\gamma_\sigma + \gamma^\sigma\not{p}_2\gamma^\mu\not{k}\gamma_\sigma}{k^2(k-p_1)^2(k+p_2)^2} + \text{finite} \tag{G.29}$$

Using the PV reduction, it is possible to show that the terms proportional to $\not{k}$ do not develope any pole. It relies on the pole structure of B_0, which is independent on the kinematics. Therefore, the rank-1 tensor integrals produce finite terms.

Neglecting rank-1 terms, the amplitude reads:

$$\begin{aligned} \mathcal{M}_1^{\mu,a} &= -\frac{ig_s^3}{(4\pi)^2}T^bT^aT^b(4\pi\mu^2)^{2-\frac{d}{2}}\int_k \frac{\gamma^\sigma\not{k}\gamma^\mu\not{k}\gamma_\sigma}{k^2(k-p_1)^2(k+p_2)^2} + \text{finite} \\ &= \frac{ig_s^3}{(4\pi)^2}T^bT^aT^b(4\pi\mu^2)^{2-\frac{d}{2}}\int_k \frac{(d-2)(2k^\mu\not{k}-k^2\gamma^\mu)}{k^2(k-p_1)^2(k+p_2)^2} + \text{finite} \end{aligned} \tag{G.30}$$

Applying the PV reduction on this last term, we obtain the following pole term:

$$\begin{aligned} \mathcal{M}_1^{\mu,a} &= -\frac{ig_s^3}{(4\pi)^2}T^bT^aT^b\left(\frac{4\pi\mu^2}{-p^2}\right)^\epsilon\Gamma(1+\epsilon)\frac{\gamma^\mu}{\epsilon} + \text{finite} \\ &= -\frac{ig_s^3}{(4\pi)^2}(C_F-\frac{1}{2}C_A)T^a\left(\frac{4\pi\mu^2}{-p^2}\right)^\epsilon\Gamma(1+\epsilon)\frac{\gamma^\mu}{\epsilon} + \text{finite} \end{aligned} \tag{G.31}$$

The second diagram can be written as

$$\begin{aligned} \mathcal{M}_2^{\mu,a} =& \frac{i}{(4\pi)^2}(4\pi\mu^2)^{2-\frac{d}{2}}\int_k (-ig_s\gamma^\beta T^c)\frac{i\not{k}}{k^2}(-ig_s\gamma^\alpha T^b)\frac{-ig^{\alpha\sigma}}{(k-p_1)^2}\frac{-ig^{\beta\rho}}{(k+p_2)^2})\times \\ & (-g_sf^{bac})[g^{\sigma\mu}(-k+2p_1+p_2)^\rho + g^{\mu\rho}(-k-p_1-2p_2)^\sigma + g^{\rho\sigma}(2k-p_1+p_2)^\mu] \\ =& \frac{g_s^3}{(4\pi)^2}f^{bac}T^cT^b(4\pi\mu^2)^\epsilon\int_k \frac{\gamma^\rho\not{k}\gamma^\sigma}{k^2(k-p_1)^2(k+p_2)^2}\times \\ & [g^{\sigma\mu}(-k+2p_1+p_2)^\rho + g^{\mu\rho}(-k-p_1-2p_2)^\sigma + g^{\rho\sigma}(2k-p_1+p_2)^\mu]. \end{aligned} \tag{G.32}$$

For reasons which are completely analogous to the previous diagram, terms which are proportional to rank-0 and rank-1 integrals will generate finite terms. Therefore:

$$\begin{aligned} \mathcal{M}_2^{\mu,a} =& \frac{g_s^3}{(4\pi)^2}f^{bac}T^cT^b(4\pi\mu^2)^\epsilon\int_k \frac{\gamma^\rho\not{k}\gamma^\sigma[2g^{\rho\sigma}k^\mu - g^{\sigma\mu}k^\rho - g^{\mu\rho}k^\sigma]}{k^2(k-p_1)^2(k+p_2)^2} + \text{finite} \\ =& \frac{g_s^3}{(4\pi)^2}f^{bac}T^cT^b(4\pi\mu^2)^\epsilon\int_k \frac{[2\gamma^\sigma\not{k}\gamma_\sigma k^\mu - \gamma^\mu\not{k}\not{k} - \not{k}\not{k}\gamma^\mu]}{k^2(k-p_1)^2(k+p_2)^2} + \text{finite} \\ =& \frac{g_s^3}{(4\pi)^2}f^{abc}T^cT^b(4\pi\mu^2)^\epsilon 2\int_k \frac{[(d-2)\not{k}k^\mu + k^2\gamma^\mu]}{k^2(k-p_1)^2(k+p_2)^2} + \text{finite}, \end{aligned} \tag{G.33}$$

and lastly, the PV reduction yields:

$$\mathcal{M}_2^{\mu,a} = -\frac{ig_s^3}{(4\pi)^2}\frac{3}{2}C_AT^a\left(\frac{4\pi\mu^2}{-p^2}\right)^\epsilon\Gamma(1+\epsilon)\frac{\gamma^\mu}{\epsilon} + \text{finite}, \tag{G.34}$$

which lead to the following total vertex contribution:

$$\Gamma_{\text{vert}}(p_1,p_2) = \frac{g_s^2}{(4\pi)^2}(C_F+C_A)\left(\frac{4\pi\mu^2}{-p^2}\right)^\epsilon\Gamma(1+\epsilon)\frac{1}{\epsilon}, \tag{G.35}$$

and to the following counterterm

$$\delta_1 = -\frac{g_s^2}{(4\pi)^2}(C_F + C_A)\left(\frac{4\pi\mu^2}{\mu_R^2}\right)^{\epsilon}\Gamma(1+\epsilon)\frac{1}{\epsilon}. \tag{G.36}$$

G.4 $\overline{\text{MS}}$ scheme for α_s with 5 massless flavour with the top quark decoupled

From the field and mass renormalisation of QCD Lagrangian we know how to renormalize the strong coupling constant

$$\alpha_{s,0} = \frac{Z_1^2}{Z_2^2 Z_3}\alpha_s \tag{G.37}$$

Expanding the latter with respect to the number of loops:

$$\begin{aligned}\alpha_{s,0} &= \alpha_s\left(1 + 2\delta_1 - 2\delta_2 - \delta_3\right) + O(\delta_i^2)\\ &= \alpha_s + \delta\alpha_s + O(\alpha_s^2).\end{aligned} \tag{G.38}$$

Therefore, the one-loop counterterm for the strong coupling reads:

$$\frac{\delta\alpha_s}{\alpha_s} = 2\delta_1 - 2\delta_2 - \delta_3 \tag{G.39}$$

which give the following explicit form:

$$\frac{\delta\alpha_s}{\alpha_s} = \frac{\alpha_s}{(4\pi)}\left(\frac{4\pi\mu^2}{\mu_R^2}\right)^{\epsilon}\Gamma(1+\epsilon)\left[-\frac{33 - 2(N_f+1)}{3\epsilon} + \frac{2}{3}\log\left(\frac{\mu_R^2}{m_t^2}\right)\right]. \tag{G.40}$$

It is possible to see explicitely the decoupling of the top mass from the running of α_s from the definition of the β-function [175–178]. Differentiating the Eq. (G.38) with respect to the renormalisation scale:

$$\mu_R^2\frac{d\alpha_{s,0}}{d\mu_R^2} = 0 = \mu_R^2\frac{d\alpha_s}{d\mu_R^2} + \mu_R^2\frac{d\delta\alpha_s}{d\mu_R^2} + O(\alpha_s^2) \tag{G.41}$$

since the bare coupling is independent on the renormalisation scale. The first term of the right hand side of Eq. (G.41) is by definition the one-loop beta function, the second term is its analytical expression, which gives:

$$\beta = \mu_R^2\frac{d\alpha_s}{d\mu_R^2}, \qquad \beta = \frac{\alpha_s}{(4\pi)}\left(\frac{4\pi\mu^2}{\mu_R^2}\right)^{\epsilon}\Gamma(1+\epsilon)\left(11 - \frac{2}{3}N_f\right). \tag{G.42}$$

The beta function is manifestly independent from the top mass, and it gets contributions only from the massless flavours.

Appendix H

Feynman Diagrams for $gg \to H_1 H_2$

Here the complete list of Feynman diagrams involved in the $gg \to H_1 H_2$ NLO cross section is presented.

H.1 Real corrections

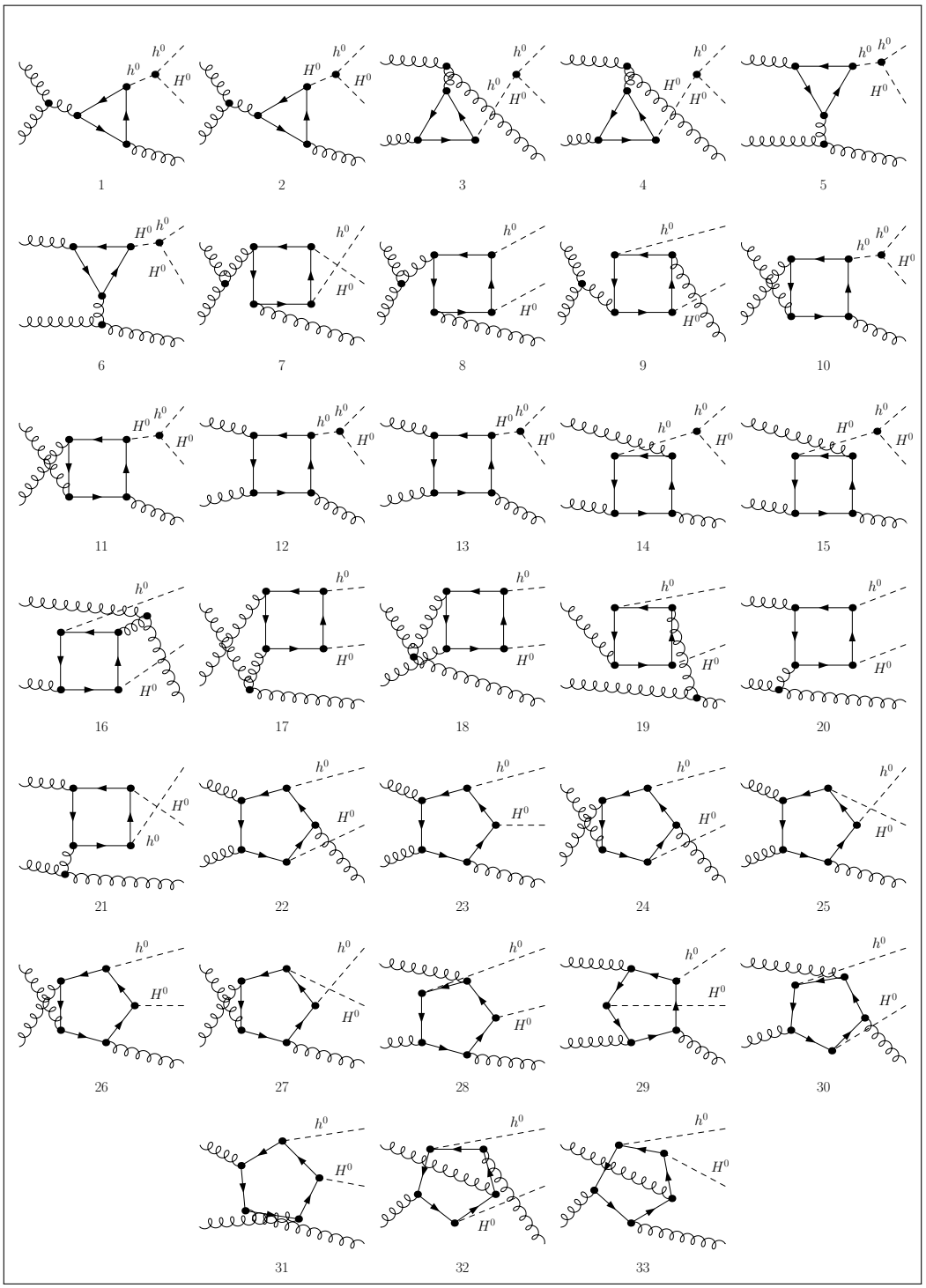

Figure H.1: Diagrams contributing to $\hat{\sigma}_{gg}$.

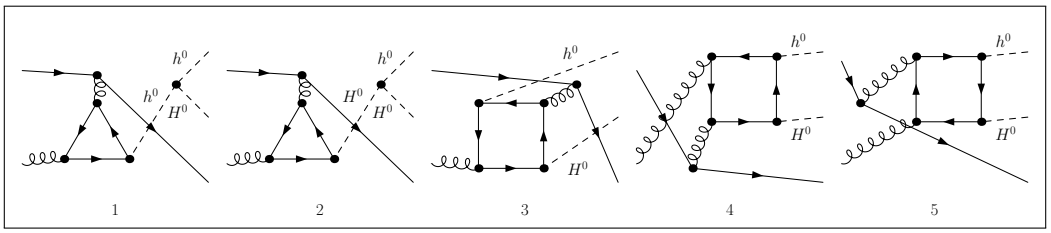

Figure H.2: Diagrams contributing to $\hat{\sigma}_{qg}$.

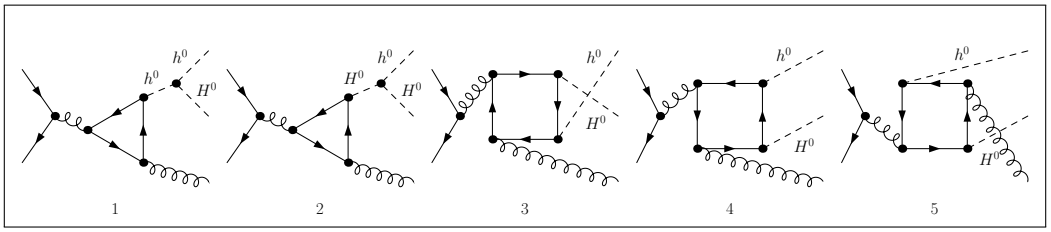

Figure H.3: Diagrams contributing to $\hat{\sigma}_{q\bar{q}}$.

H.2 Virtual contributions

H.2.1 Vertex contributions

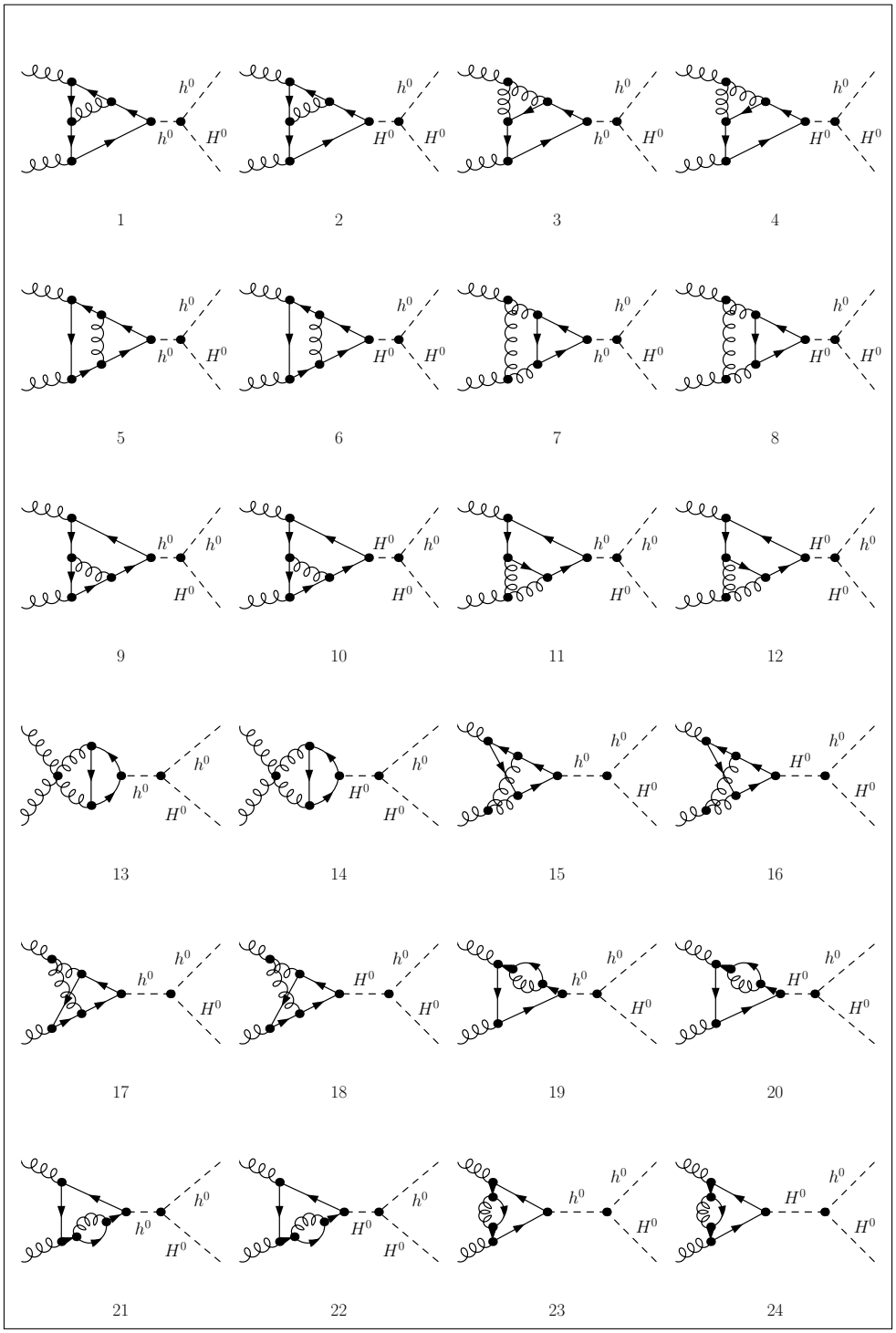

Figure H.4: Triangle contributions.

H.2.2 Box contributions

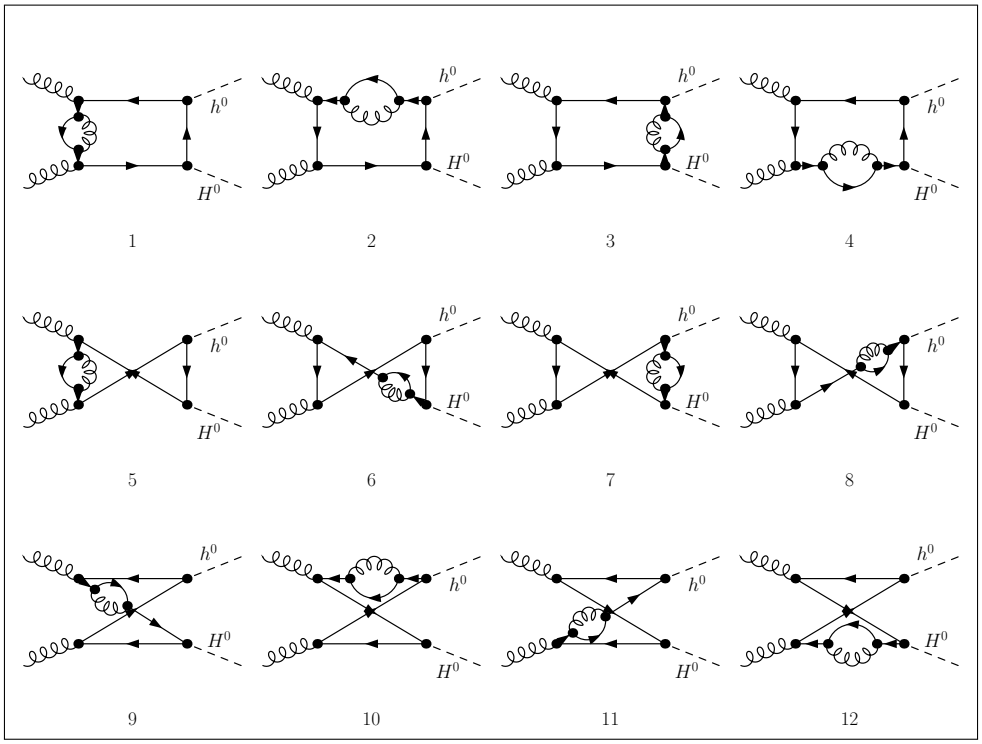

Figure H.5: Topology 1.

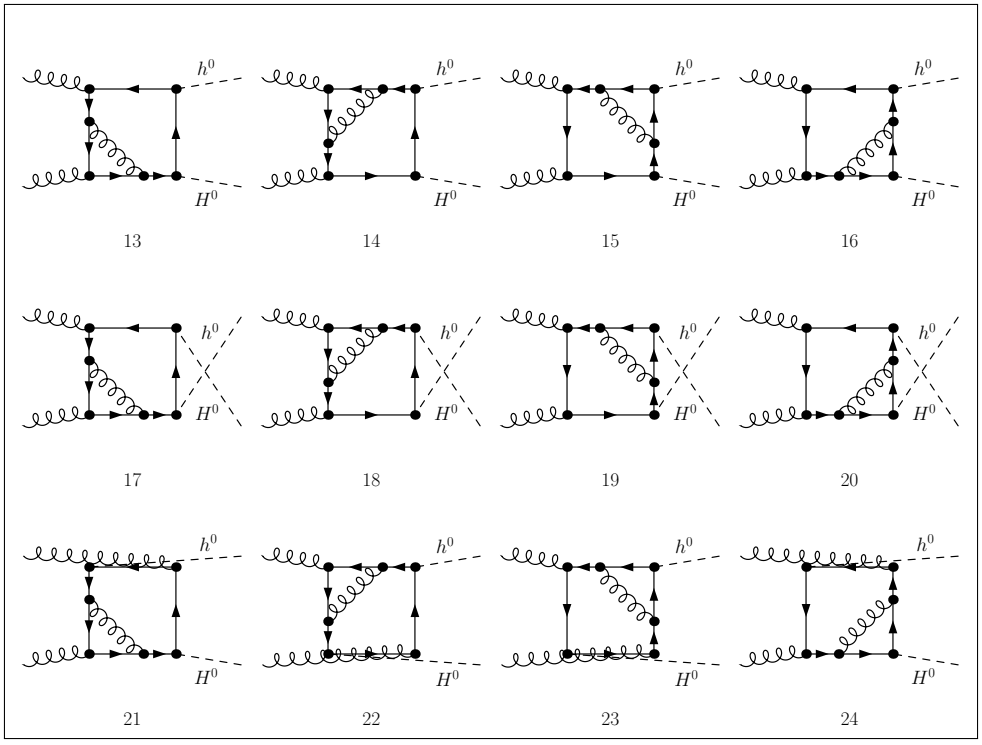

Figure H.6: Topology 2.

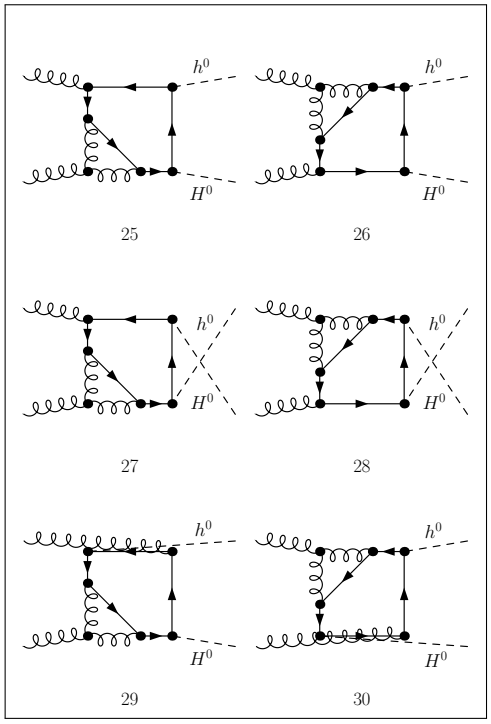

Figure H.7: Topology 3.

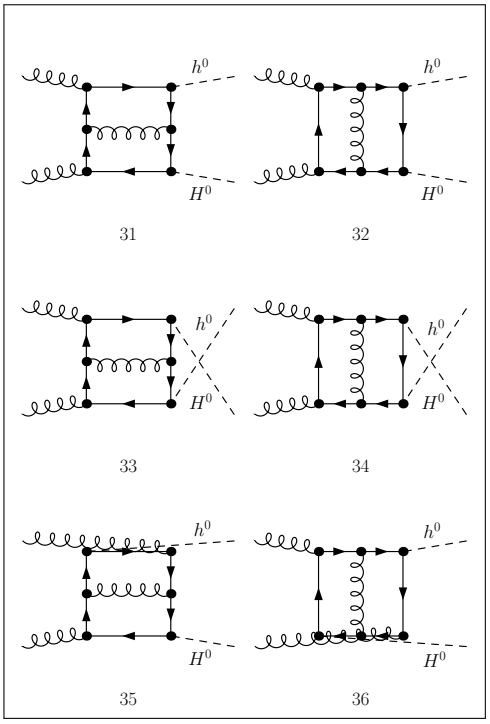

Figure H.8: Topology 4.

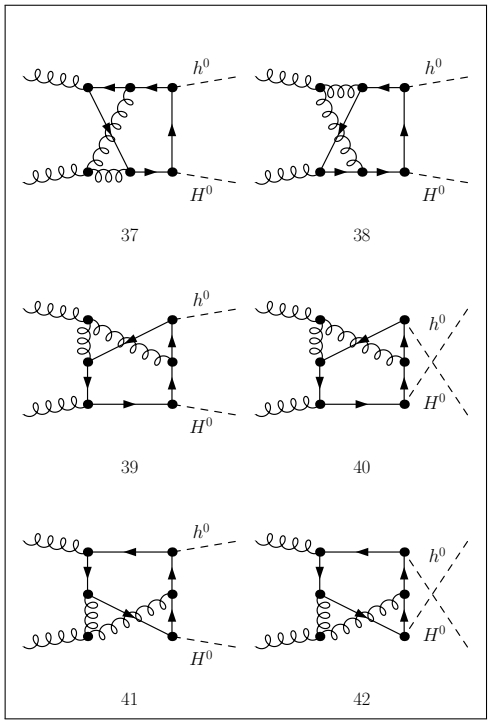

Figure H.9: Topology 5.

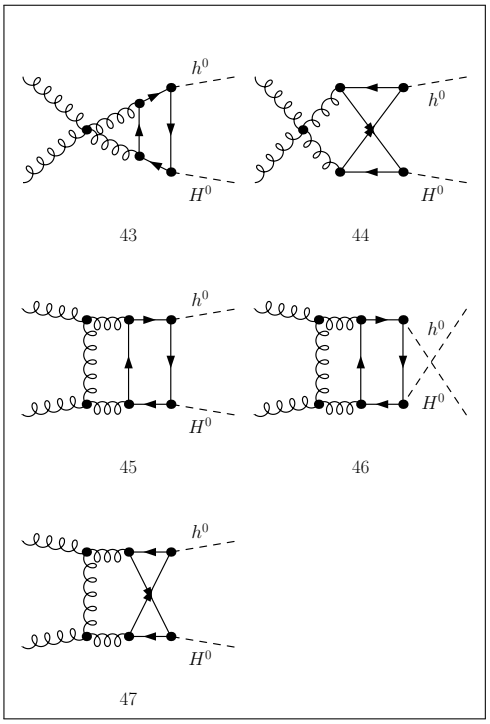

Figure H.10: Topology 6.

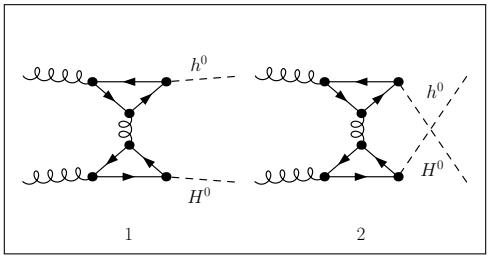

Figure H.11: One-particle reducible diagrams.

Appendix I

Feynman Rules

Here, the main Feynman rules coming from 2HDM and QCD relevant for this thesis are depicted.

I.1 2HDM scalar propagators and Yukawa couplings

Scalar propagators

$$\text{- - - - - - - - - } h \text{ - - - - - - - - -} = \frac{1}{q^2 - m_h^2}, \qquad h \in \{H_1, H_2, A, H^+, H^-\},$$

Yukawa couplings

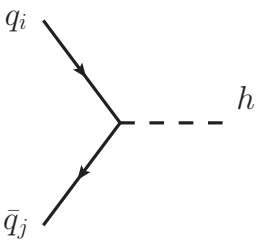

$h \in \{H_1, H_2, A, H^+, H^-\}$

$$\begin{aligned}
\bar{q}_i q_j H_1 &= -i\frac{m_q}{v}\delta_{ij} Y_1, \\
\bar{q}_i q_j H_2 &= -i\frac{m_q}{v}\delta_{ij} Y_2, \\
\bar{q}_i q_j A &= -\frac{m_q}{v}\gamma^5 \delta_{ij} Y_A, \\
\bar{u}_i d_j H^+ &= -\frac{i}{v} V_{ij} Y_+^{ij}, \\
\bar{d}_i u_j H^- &= -\frac{i}{v} V_{ij}^* Y_-^{ij}
\end{aligned}$$

		type I	type II	type X	type Y
Y_1	up quarks	$\frac{\cos\alpha}{\sin\beta}$	$\frac{\cos\alpha}{\sin\beta}$	$\frac{\cos\alpha}{\sin\beta}$	$\frac{\cos\alpha}{\sin\beta}$
	down quarks	$\frac{\cos\alpha}{\sin\beta}$	$-\frac{\sin\alpha}{\cos\beta}$	$\frac{\cos\alpha}{\sin\beta}$	$-\frac{\sin\alpha}{\cos\beta}$
Y_2	up quarks	$\frac{\sin\alpha}{\sin\beta}$	$\frac{\sin\alpha}{\sin\beta}$	$\frac{\sin\alpha}{\sin\beta}$	$\frac{\sin\alpha}{\sin\beta}$
	down quarks	$\frac{\sin\alpha}{\sin\beta}$	$\frac{\cos\alpha}{\cos\beta}$	$\frac{\sin\alpha}{\sin\beta}$	$\frac{\cos\alpha}{\cos\beta}$
Y_A	up quarks	$\cot\beta$	$\cot\beta$	$\cot\beta$	$\cot\beta$
	down quarks	$-\cot\beta$	$\tan\beta$	$-\cot\beta$	$\tan\beta$

	type I, type X	type II, type Y
Y_+^{ij}	$\sqrt{2}\left[m_{d_j}\cot\beta P_R - m_{u_i}\cot\beta P_L\right]$	$-\sqrt{2}\left[m_{d_j}\tan\beta P_R + m_{u_i} P_L \cot\beta\right]$
Y_-^{ij}	$\sqrt{2}\left[m_{d_i}\cot\beta P_L - m_{u_j}\cot\beta P_R\right]$	$-\sqrt{2}\left[m_{d_i}\tan\beta P_L + m_{u_j}\cot\beta P_R\right]$

I.2 2HDM trilinear Higgs couplings

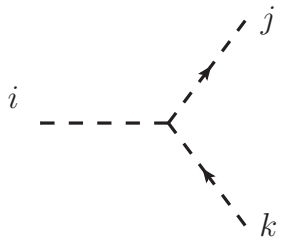

$$\lambda_{ijk} = -i3\frac{c_{ijk}}{v}$$

$i, j, k \in \{H_1, H_2, A, H^+, H^-\}$

$$c_{111} = \frac{m_{H_1}^2[2\cos(\alpha+\beta) + \sin 2\alpha \sin(\beta-\alpha)] - \lambda_5 v^2 \cos(\alpha+\beta)\cos^2(\beta-\alpha)}{\sin 2\beta},$$

$$c_{112} = \frac{\cos(\beta-\alpha)[2\sin 2\alpha(2m_{H_1}^2 + m_{H_2}^2) - \lambda_5 v^2(3\sin 2\alpha - \sin 2\beta)]}{6\sin 2\beta},$$

$$c_{122} = -\frac{\sin(\beta-\alpha)[2\sin 2\alpha(m_{H_1}^2 + 2m_{H_2}^2) - \lambda_5 v^2(3\sin 2\alpha + \sin 2\beta)]}{6\sin 2\beta},$$

$$c_{222} = -\frac{m_{H_2}^2[\cos(\beta-\alpha)\sin(2\alpha) - 2\sin(\alpha+\beta)] + \lambda_5 v^2 \sin(\alpha+\beta)\sin^2(\beta-\alpha)}{\sin 2\beta},$$

$$c_{1AA} = \sin(\beta-\alpha)(2m_A^2 - m_{H_1}^2) + \frac{\cos(\alpha+\beta)(2m_{H_1}^2 - \lambda_5 v^2)}{3\sin 2\beta},$$

$$c_{2AA} = \cos(\beta-\alpha)(2m_A^2 - m_{H_2}^2) + \frac{\sin(\alpha+\beta)(2m_{H_2}^2 - \lambda_5 v^2)}{3\sin 2\beta},$$

$$c_{1+-} = \sin(\beta-\alpha)(2m_+^2 - m_{H_1}^2) + \frac{\cos(\alpha+\beta)(2m_{H_1}^2 - \lambda_5 v^2)}{3\sin 2\beta},$$

$$c_{2+-} = \cos(\beta-\alpha)(2m_+^2 - m_{H_2}^2) + \frac{\sin(\alpha+\beta)(2m_{H_2}^2 - \lambda_5 v^2)}{3\sin 2\beta}.$$

I.3 SM QCD Feynman rules

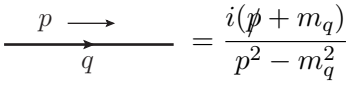

$$= \frac{i(\not{p} + m_q)}{p^2 - m_q^2}$$

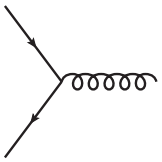

$$= -ig_s \gamma^\mu T^a$$

$$= \frac{-ig^{\mu\nu}\delta^{ab}}{p^2}$$

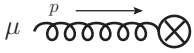

$$= \epsilon^\mu(p)$$

$$= 1$$

Bibliography

[1] Peter W. Higgs. Broken Symmetries and the Masses of Gauge Bosons. *Phys. Rev. Lett.*, 13:508–509, 1964.

[2] F. Englert and R. Brout. Broken Symmetry and the Mass of Gauge Vector Mesons. *Phys. Rev. Lett.*, 13:321–323, 1964.

[3] Peter W. Higgs. Spontaneous Symmetry Breakdown without Massless Bosons. *Phys. Rev.*, 145:1156–1163, 1966.

[4] G.S. Guralnik, C.R. Hagen, and T.W.B. Kibble. Global Conservation Laws and Massless Particles. *Phys. Rev. Lett.*, 13:585–587, 1964.

[5] G. Aad, T. Abajyan, B. Abbott, J. Abdallah, S. Abdel Khalek, A.A. Abdelalim, O. Abdinov, R. Aben, B. Abi, M. Abolins, and et al. Observation of a new particle in the search for the standard model higgs boson with the atlas detector at the lhc. *Physics Letters B*, 716(1):129, Sep 2012.

[6] S. Chatrchyan, V. Khachatryan, A.M. Sirunyan, A. Tumasyan, W. Adam, E. Aguilo, T. Bergauer, M. Dragicevic, J. Er, C. Fabjan, and et al. Observation of a new boson at a mass of 125 gev with the cms experiment at the lhc. *Physics Letters B*, 716(1):3061, Sep 2012.

[7] S. Chatrchyan, V. Khachatryan, A. M. Sirunyan, A. Tumasyan, W. Adam, E. Aguilo, T. Bergauer, M. Dragicevic, J. Er, C. Fabjan, and et al. Study of the mass and spin-parity of the higgs boson candidate via its decays tozboson pairs. *Physical Review Letters*, 110(8), Feb 2013.

[8] G. Aad, T. Abajyan, B. Abbott, J. Abdallah, S. Abdel Khalek, O. Abdinov, R. Aben, B. Abi, M. Abolins, O.S. AbouZeid, and et al. Evidence for the spin-0 nature of the higgs boson using atlas data. *Physics Letters B*, 726(1-3):120144, Oct 2013.

[9] John F. Gunion, Howard E. Haber, Gordon L. Kane, and Sally Dawson. *The Higgs Hunter's Guide*, volume 80. 2000.

[10] G.C. Branco, P.M. Ferreira, L. Lavoura, M.N. Rebelo, Marc Sher, and Joao P. Silva. Theory and phenomenology of two-Higgs-doublet models. *Phys. Rept.*, 516:1–102, 2012.

[11] Sally Dawson, Christoph Englert, and Tilman Plehn. Higgs Physics: It ain't over till it's over. *Phys. Rept.*, 816:1–85, 2019.

[12] A. Djouadi, W. Kilian, M. Mühlleitner, and P.M. Zerwas. Testing higgs self-couplings at e^+e^- linear colliders. *The European Physical Journal C*, 10(1):2743, Aug 1999.

[13] G. Cynolter, E. Lendvai, and G. Pocsik. Resonance production of three neutral supersymmetric Higgs bosons at LHC. *Acta Phys. Polon. B*, 31:1749–1757, 2000.

[14] Milada Margarete Mühlleitner. *Higgs particles in the standard model and supersymmetric theories*. PhD thesis, Hamburg U., 2000.

[15] E. Accomando et al. Physics at the CLIC multi-TeV linear collider. In *11th International Conference on Hadron Spectroscopy*, CERN Yellow Reports: Monographs, 6 2004.

[16] Tilman Plehn and Michael Rauch. Quartic higgs coupling at hadron colliders. *Physical Review D*, 72(5), Sep 2005.

[17] U. Baur, T. Plehn, and David L. Rainwater. Determining the Higgs Boson Selfcoupling at Hadron Colliders. *Phys. Rev. D*, 67:033003, 2003.

[18] Ulrich Baur, Tilman Plehn, and David L. Rainwater. Measuring the Higgs Boson Self Coupling at the LHC and Finite Top Mass Matrix Elements. *Phys. Rev. Lett.*, 89:151801, 2002.

[19] U. Baur, T. Plehn, and D. Rainwater. Examining the higgs boson potential at lepton and hadron colliders: A comparative analysis. *Physical Review D*, 68(3), Aug 2003.

[20] U. Baur, T. Plehn, and David L. Rainwater. Probing the Higgs selfcoupling at hadron colliders using rare decays. *Phys. Rev. D*, 69:053004, 2004.

[21] Matthew J. Dolan, Christoph Englert, and Michael Spannowsky. Higgs self-coupling measurements at the LHC. *JHEP*, 10:112, 2012.

[22] Vernon Barger, Lisa L. Everett, C.B. Jackson, and Gabe Shaughnessy. Higgs-Pair Production and Measurement of the Triscalar Coupling at LHC(8,14). *Phys. Lett. B*, 728:433–436, 2014.

[23] J. Baglio, A. Djouadi, R. Grber, M.M. Mühlleitner, J. Quevillon, and M. Spira. The measurement of the higgs self-coupling at the lhc: theoretical status. *Journal of High Energy Physics*, 2013(4), Apr 2013.

[24] F. Maltoni, E. Vryonidou, and M. Zaro. Top-quark mass effects in double and triple Higgs production in gluon-gluon fusion at NLO. *JHEP*, 11:079, 2014.

[25] Chih-Ting Lu, Jung Chang, Kingman Cheung, and Jae Sik Lee. An exploratory study of Higgs-boson pair production. *JHEP*, 08:133, 2015.

[26] Prospects for HH measurements at the HL-LHC. 12 2018.

[27] Philipp Roloff, Ulrike Schnoor, Rosa Simoniello, and Boruo Xu. Double Higgs boson production and Higgs self-coupling extraction at CLIC. 1 2019.

[28] Eleonora Rossi. Measurement of Higgs-boson self-coupling with single-Higgs and double-Higgs production channels. 10 2020.

[29] Biagio Di Micco, Maxime Gouzevitch, Javier Mazzitelli, and Caterina Vernieri. Higgs boson potential at colliders: status and perspectives. *Reviews in Physics*, page 100045, Aug 2020.

[30] D. de Florian et al. Handbook of LHC Higgs Cross Sections: 4. Deciphering the Nature of the Higgs Sector. 2/2017, 10 2016.

[31] Vernon Barger, Lisa L. Everett, C.B. Jackson, and Gabe Shaughnessy. Higgs-pair production and measurement of the triscalar coupling at lhc(8,14). *Physics Letters B*, 728:433436, Jan 2014.

[32] S. Dawson, S. Dittmaier, and M. Spira. Neutral higgs-boson pair production at hadron colliders: Qcd corrections. *Physical Review D*, 58(11), Nov 1998.

[33] R. Frederix, S. Frixione, V. Hirschi, F. Maltoni, O. Mattelaer, P. Torrielli, E. Vryonidou, and M. Zaro. Higgs pair production at the LHC with NLO and parton-shower effects. *Phys. Lett. B*, 732:142–149, 2014.

[34] Daniel de Florian and Javier Mazzitelli. Higgs Boson Pair Production at Next-to-Next-to-Leading Order in QCD. *Phys. Rev. Lett.*, 111:201801, 2013.

[35] Jonathan Grigo, Kirill Melnikov, and Matthias Steinhauser. Virtual corrections to higgs boson pair production in the large top quark mass limit. *Nuclear Physics B*, 888:1729, Nov 2014.

[36] Ding Yu Shao, Chong Sheng Li, Hai Tao Li, and Jian Wang. Threshold resummation effects in Higgs boson pair production at the LHC. *JHEP*, 07:169, 2013.

[37] Daniel de Florian and Javier Mazzitelli. Higgs pair production at next-to-next-to-leading logarithmic accuracy at the LHC. *JHEP*, 09:053, 2015.

[38] Long-Bin Chen, Hai Tao Li, Hua-Sheng Shao, and Jian Wang. Higgs boson pair production via gluon fusion at N^3LO in QCD. *Phys. Lett. B*, 803:135292, 2020.

[39] Jonathan Grigo, Jens Hoff, and Matthias Steinhauser. Higgs boson pair production: top quark mass effects at NLO and NNLO. *Nucl. Phys. B*, 900:412–430, 2015.

[40] Jonathan Grigo, Jens Hoff, Kirill Melnikov, and Matthias Steinhauser. On the Higgs boson pair production at the LHC. *Nucl. Phys. B*, 875:1–17, 2013.

[41] Jonathan Grigo, Jens Hoff, Kirill Melnikov, and Matthias Steinhauser. Higgs boson pair production at the LHC: top-quark mass effects at next-to-leading order. *PoS*, RADCOR2013:006, 2013.

[42] Ramona Grber, Andreas Maier, and Thomas Rauh. Reconstruction of top-quark mass effects in higgs pair production and other gluon-fusion processes. *Journal of High Energy Physics*, 2018(3), Mar 2018.

[43] Joshua Davies, Ramona Gröber, Andreas Maier, Thomas Rauh, and Matthias Steinhauser. Padé approach to top-quark mass effects in gluon fusion amplitudes. *PoS*, RADCOR2019:079, 2019.

[44] Joshua Davies, Go Mishima, Matthias Steinhauser, and David Wellmann. Double-higgs boson production in the high-energy limit: planar master integrals. *Journal of High Energy Physics*, 2018(3), Mar 2018.

[45] Joshua Davies, Go Mishima, Matthias Steinhauser, and David Wellmann. Double higgs boson production at nlo in the high-energy limit: complete analytic results. *Journal of High Energy Physics*, 2019(1), Jan 2019.

[46] Joshua Davies, Gudrun Heinrich, Stephen P. Jones, Matthias Kerner, Go Mishima, Matthias Steinhauser, and David Wellmann. Double Higgs boson production at NLO: combining the exact numerical result and high-energy expansion. *JHEP*, 11:024, 2019.

[47] S. Borowka, N. Greiner, G. Heinrich, S.P. Jones, M. Kerner, J. Schlenk, and T. Zirke. Full top quark mass dependence in Higgs boson pair production at NLO. *JHEP*, 10:107, 2016.

[48] K.G. Chetyrkin and F.V. Tkachov. Integration by parts: The algorithm to calculate -functions in 4 loops. *Nuclear Physics B*, 192(1):159 – 204, 1981.

[49] S. Laporta. High precision calculation of multiloop Feynman integrals by difference equations. *Int. J. Mod. Phys. A*, 15:5087–5159, 2000.

[50] Gudrun Heinrich. Sector Decomposition. *Int. J. Mod. Phys. A*, 23:1457–1486, 2008.

[51] S. Catani and M.H. Seymour. A general algorithm for calculating jet cross sections in nlo qcd. *Nuclear Physics B*, 485(1-2):291419, Feb 1997.

[52] S. Catani and M.H. Seymour. The dipole formalism for the calculation of qcd jet cross sections at next-to-leading order. *Physics Letters B*, 378(1):287 – 301, 1996.

[53] Julien Baglio, Francisco Campanario, Seraina Glaus, Margarete Mühlleitner, Michael Spira, and Juraj Streicher. Gluon fusion into Higgs pairs at NLO QCD and the top mass scheme. *Eur. Phys. J. C*, 79(6):459, 2019.

[54] J. Baglio, F. Campanario, S. Glaus, M. Mühlleitner, J. Ronca, M. Spira, and J. Streicher. Higgs-Pair Production via Gluon Fusion at Hadron Colliders: NLO QCD Corrections. *JHEP*, 04:181, 2020.

[55] J. Baglio, F. Campanario, S. Glaus, M. Mühlleitner, J. Ronca, and M. Spira. $gg \to HH$: Combined Uncertainties. 8 2020.

[56] Murray Gell-Mann. A Schematic Model of Baryons and Mesons. *Phys. Lett.*, 8:214–215, 1964.

[57] G. Zweig. *An SU(3) model for strong interaction symmetry and its breaking. Version 2*, pages 22–101. 2 1964.

[58] David J. Gross and Frank Wilczek. Ultraviolet behavior of non-abelian gauge theories. *Phys. Rev. Lett.*, 30:1343–1346, Jun 1973.

[59] H. David Politzer. Reliable perturbative results for strong interactions? *Phys. Rev. Lett.*, 30:1346–1349, Jun 1973.

[60] M.Y. Han and Yoichiro Nambu. Three Triplet Model with Double SU(3) Symmetry. *Phys. Rev.*, 139:B1006–B1010, 1965.

[61] H. Fritzsch, Murray Gell-Mann, and H. Leutwyler. Advantages of the Color Octet Gluon Picture. *Phys. Lett. B*, 47:365–368, 1973.

[62] D.J. Gross and Frank Wilczek. Asymptotically Free Gauge Theories - I. *Phys. Rev. D*, 8:3633–3652, 1973.

[63] H.David Politzer. Asymptotic Freedom: An Approach to Strong Interactions. *Phys. Rept.*, 14:129–180, 1974.

[64] S.L. Glashow. Partial Symmetries of Weak Interactions. *Nucl. Phys.*, 22:579–588, 1961.

[65] Abdus Salam and John Clive Ward. Electromagnetic and weak interactions. *Phys. Lett.*, 13:168–171, 1964.

[66] Steven Weinberg. A model of leptons. *Phys. Rev. Lett.*, 19:1264–1266, Nov 1967.

[67] Kazuhiko Nishijima. Charge Independence Theory of V Particles. *Prog. Theor. Phys.*, 13(3):285–304, 1955.

[68] M. Gell-Mann. The interpretation of the new particles as displaced charge multiplets. *Nuovo Cim.*, 4(S2):848–866, 1956.

[69] Gerard 't Hooft. Renormalizable Lagrangians for Massive Yang-Mills Fields. *Nucl. Phys. B*, 35:167–188, 1971.

[70] Gerard 't Hooft and M.J.G. Veltman. Regularization and Renormalization of Gauge Fields. *Nucl. Phys. B*, 44:189–213, 1972.

[71] Nicola Cabibbo. Unitary symmetry and leptonic decays. *Phys. Rev. Lett.*, 10:531–533, Jun 1963.

[72] Makoto Kobayashi and Toshihide Maskawa. CP Violation in the Renormalizable Theory of Weak Interaction. *Prog. Theor. Phys.*, 49:652–657, 1973.

[73] B. Pontecorvo. Inverse beta processes and nonconservation of lepton charge. *Sov. Phys. JETP*, 7:172–173, 1958.

[74] Ziro Maki, Masami Nakagawa, and Shoichi Sakata. Remarks on the Unified Model of Elementary Particles. *Progress of Theoretical Physics*, 28(5):870–880, 11 1962.

[75] P.A. Zyla et al. Review of Particle Physics. *PTEP*, 2020(8):083C01, 2020.

[76] Howard E. Haber and Gordon L. Kane. The Search for Supersymmetry: Probing Physics Beyond the Standard Model. *Phys. Rept.*, 117:75–263, 1985.

[77] Jihn E. Kim. Light Pseudoscalars, Particle Physics and Cosmology. *Phys. Rept.*, 150:1–177, 1987.

[78] R.D. Peccei and Helen R. Quinn. CP Conservation in the Presence of Instantons. *Phys. Rev. Lett.*, 38:1440–1443, 1977.

[79] Neil Turok and John Zadrozny. Electroweak baryogenesis in the two doublet model. *Nucl. Phys. B*, 358:471–493, 1991.

[80] James M. Cline, Kimmo Kainulainen, and Axel P. Vischer. Dynamics of two Higgs doublet CP violation and baryogenesis at the electroweak phase transition. *Phys. Rev. D*, 54:2451–2472, 1996.

[81] Lars Fromme, Stephan J Huber, and Michael Seniuch. Baryogenesis in the two-higgs doublet model. *Journal of High Energy Physics*, 2006(11):038038, Nov 2006.

[82] T.D. Lee. A Theory of Spontaneous T Violation. *Phys. Rev. D*, 8:1226–1239, 1973.

[83] Nilendra G. Deshpande and Ernest Ma. Pattern of Symmetry Breaking with Two Higgs Doublets. *Phys. Rev. D*, 18:2574, 1978.

[84] K.G. Klimenko. On Necessary and Sufficient Conditions for Some Higgs Potentials to Be Bounded From Below. *Theor. Math. Phys.*, 62:58–65, 1985.

[85] John F. Gunion and Howard E. Haber. The CP conserving two Higgs doublet model: The Approach to the decoupling limit. *Phys. Rev. D*, 67:075019, 2003.

[86] Felix Kling, Shufang Su, and Wei Su. 2hdm neutral scalars under the lhc. *Journal of High Energy Physics*, 2020(6), Jun 2020.

[87] Shinya Kanemura and Kei Yagyu. Unitarity bound in the most general two Higgs doublet model. *Phys. Lett. B*, 751:289–296, 2015.

[88] I.F. Ginzburg and I.P. Ivanov. Tree-level unitarity constraints in the most general 2HDM. *Phys. Rev. D*, 72:115010, 2005.

[89] Johan Bijnens, Jie Lu, and Johan Rathsman. Constraining General Two Higgs Doublet Models by the Evolution of Yukawa Couplings. *JHEP*, 05:118, 2012.

[90] Vernon D. Barger, J.L. Hewett, and R.J.N. Phillips. New Constraints on the Charged Higgs Sector in Two Higgs Doublet Models. *Phys. Rev. D*, 41:3421–3441, 1990.

[91] Benjamin W. Lee, C. Quigg, and H.B. Thacker. Weak Interactions at Very High-Energies: The Role of the Higgs Boson Mass. *Phys. Rev. D*, 16:1519, 1977.

[92] M. Carena and H.E. Haber. Higgs boson theory and phenomenology. *Progress in Particle and Nuclear Physics*, 50(1):63152, Jan 2003.

[93] Sheldon L. Glashow and Steven Weinberg. Natural Conservation Laws for Neutral Currents. *Phys. Rev. D*, 15:1958, 1977.

[94] Antonio Pich and Paula Tuzn. Yukawa alignment in the two-higgs-doublet model. *Physical Review D*, 80(9), Nov 2009.

[95] Antonio Pich and Paula Tuzon. The aligned two-higgs doublet model, 2010.

[96] H. Serdio. Yukawa alignment in a multi higgs doublet model: An effective approach. *Physics Letters B*, 700(2):133138, Jun 2011.

[97] Laura Lopez Honorez, Emmanuel Nezri, Josep F. Oliver, and Michel H.G. Tytgat. The Inert Doublet Model: An Archetype for Dark Matter. *JCAP*, 02:028, 2007.

[98] Ernest Ma. Verifiable radiative seesaw mechanism of neutrino mass and dark matter. *Physical Review D*, 73(7), Apr 2006.

[99] ERNEST MA. Common origin of neutrino mass, dark matter, and baryogenesis. *Modern Physics Letters A*, 21(23):17771781, Jul 2006.

[100] DEBASISH MAJUMDAR and AMBAR GHOSAL. Dark matter candidate in a heavy higgs model: Direct detection rates. *Modern Physics Letters A*, 23(24):20112022, Aug 2008.

[101] Alejandra Melfo, Miha Nemevek, Fabrizio Nesti, Goran Senjanovi, and Yue Zhang. Inert doublet dark matter and mirror/extra families after xenon100. *Physical Review D*, 84(3), Aug 2011.

[102] I. F. Ginzburg, K. A. Kanishev, M. Krawczyk, and D. Sokoowska. Evolution of the universe to the present inert phase. *Physical Review D*, 82(12), Dec 2010.

[103] Tommi Alanne, Kimmo Kainulainen, Kimmo Tuominen, and Ville Vaskonen. Baryogenesis in the two doublet and inert singlet extension of the Standard Model. *JCAP*, 08:057, 2016.

[104] Marcela Carena, David Garcia, Ulrich Nierste, and Carlos E.M. Wagner. Effective lagrangian for the interaction in the mssm and charged higgs phenomenology. *Nuclear Physics B*, 577(1-2):88120, Jun 2000.

[105] Sacha Davidson and Howard E. Haber. Basis-independent methods for the two-Higgs-doublet model. *Phys. Rev. D*, 72:035004, 2005. [Erratum: Phys.Rev.D 72, 099902 (2005)].

[106] Emanuele Bagnaschi, Felix Brümmer, Wilfried Buchmüller, Alexander Voigt, and Georg Weiglein. Vacuum stability and supersymmetry at high scales with two Higgs doublets. *JHEP*, 03:158, 2016.

[107] Kaustubh Agashe, Roberto Contino, and Alex Pomarol. The Minimal composite Higgs model. *Nucl. Phys. B*, 719:165–187, 2005.

[108] Martin Schmaltz and David Tucker-Smith. Little higgs theories. *Annual Review of Nuclear and Particle Science*, 55(1):229270, Dec 2005.

[109] Csaba Csaki, Christophe Grojean, and John Terning. Alternatives to an Elementary Higgs. *Rev. Mod. Phys.*, 88(4):045001, 2016.

[110] Indrani Chakraborty and Anirban Kundu. Two-higgs doublet models confront the naturalness problem. *Physical Review D*, 90(11), Dec 2014.

[111] Gustavo Burdman, Carlos E.F. Haluch, and Ricardo D. Matheus. Is the LHC Observing the Pseudo-scalar State of a Two-Higgs Doublet Model ? *Phys. Rev. D*, 85:095016, 2012.

[112] P. M. Ferreira, Rui Santos, Marc Sher, and Joo P. Silva. Could the lhc two-photon signal correspond to the heavier scalar in two-higgs-doublet models? *Physical Review D*, 85(3), Feb 2012.

[113] Georges Aad et al. Measurements of the Higgs boson production and decay rates and constraints on its couplings from a combined ATLAS and CMS analysis of the LHC pp collision data at $\sqrt{s} = 7$ and 8 TeV. *JHEP*, 08:045, 2016.

[114] Study of the double Higgs production channel $H(\to b\bar{b})H(\to \gamma\gamma)$ with the ATLAS experiment at the HL-LHC. 1 2017.

[115] E.W.Nigel Glover and J.J. van der Bij. HIGGS BOSON PAIR PRODUCTION VIA GLUON FUSION. *Nucl. Phys. B*, 309:282–294, 1988.

[116] T. Plehn, M. Spira, and P.M. Zerwas. Pair production of neutral higgs particles in gluon-gluon collisions. *Nuclear Physics B*, 479(1-2):4664, Nov 1996.

[117] O.J.P. boli, G.C. Marques, S.F. Novaes, and A.A. Natale. Twin higgs-boson production. *Physics Letters B*, 197(1):269 – 272, 1987.

[118] Duane A. Dicus, Chung Kao, and Scott S.D. Willenbrock. Higgs boson pair production from gluon fusion. *Physics Letters B*, 203(4):457 – 461, 1988.

[119] Wai-Yee Keung. Double Higgs From $W - W$ Fusion. *Mod. Phys. Lett. A*, 2:765, 1987.

[120] Kalpana J. Kallianpur. Pair-production of higgs bosons via heavy quark annihilation. *Physics Letters B*, 215(2):392 – 396, 1988.

[121] A. Dobrovolskaya and V. Novikov. On heavy Higgs boson production. *Z. Phys. C*, 52:427–436, 1991.

[122] Vernon D. Barger, Tao Han, and R.J.N. Phillips. Double Higgs Boson Bremsstrahlung From W and Z Bosons at Supercolliders. *Phys. Rev. D*, 38:2766, 1988.

[123] M. Moretti, S. Moretti, F. Piccinini, R. Pittau, and A.D. Polosa. Higgs boson self-couplings at the LHC as a probe of extended Higgs sectors. *JHEP*, 02:024, 2005.

[124] A. Djouadi, M. Spira, and P.M. Zerwas. Production of Higgs bosons in proton colliders: QCD corrections. *Phys. Lett. B*, 264:440–446, 1991.

[125] D. Graudenz, M. Spira, and P. M. Zerwas. Qcd corrections to higgs-boson production at proton-proton colliders. *Phys. Rev. Lett.*, 70:1372–1375, Mar 1993.

[126] M. Spira, A. Djouadi, D. Graudenz, and R.M. Zerwas. Higgs boson production at the lhc. *Nuclear Physics B*, 453(1-2):1782, Oct 1995.

[127] Charalampos Anastasiou, Stefan Bucherer, and Zoltan Kunszt. Hpro: A nlo monte-carlo for higgs production via gluon fusion with finite heavy quark masses. *Journal of High Energy Physics*, 2009(10):068068, Oct 2009.

[128] Daniel de Florian, Ignacio Fabre, and Javier Mazzitelli. Higgs boson pair production at nnlo in qcd including dimension 6 operators. *Journal of High Energy Physics*, 2017(10), Oct 2017.

[129] John C. Collins, Davison E. Soper, and George F. Sterman. Factorization of Hard Processes in QCD. *Adv. Ser. Direct. High Energy Phys.*, 5:1–91, 1989.

[130] Davison E. Soper. Parton distribution functions. *Nuclear Physics B - Proceedings Supplements*, 53(1-3):6980, Feb 1997.

[131] R. P. Feynman. Space-time approach to quantum electrodynamics. *Phys. Rev.*, 76:769–789, Sep 1949.

[132] T. Kinoshita. Mass singularities of Feynman amplitudes. *J. Math. Phys.*, 3:650–677, 1962.

[133] T. D. Lee and M. Nauenberg. Degenerate systems and mass singularities. *Phys. Rev.*, 133:B1549–B1562, Mar 1964.

[134] Stefano Catani, Stefan Dittmaier, Michael H. Seymour, and Zoltn Trcsnyi. The dipole formalism for next-to-leading order qcd calculations with massive partons. *Nuclear Physics B*, 627(1-2):189265, Apr 2002.

[135] S. Frixione, Z. Kunszt, and A. Signer. Three-jet cross sections to next-to-leading order. *Nuclear Physics B*, 467(3):399442, May 1996.

[136] David A. Kosower. Antenna factorization of gauge-theory amplitudes. *Physical Review D*, 57(9):54105416, May 1998.

[137] A. Gehrmann-De Ridder and M Ritzmann. Nlo antenna subtraction with massive fermions. *Journal of High Energy Physics*, 2009(07):041041, Jul 2009.

[138] Roberto Bonciani, Giuseppe Degrassi, Pier Paolo Giardino, and Ramona Gröber. Analytical Method for Next-to-Leading-Order QCD Corrections to Double-Higgs Production. *Phys. Rev. Lett.*, 121(16):162003, 2018.

[139] S. Borowka, N. Greiner, G. Heinrich, S.P. Jones, M. Kerner, J. Schlenk, U. Schubert, and T. Zirke. Higgs Boson Pair Production in Gluon Fusion at Next-to-Leading Order with Full Top-Quark Mass Dependence. *Phys. Rev. Lett.*, 117(1):012001, 2016. [Erratum: Phys.Rev.Lett. 117, 079901 (2016)].

[140] Christian Schubert. On the gamma(5) problem of dimensional renormalization. 12 1993.

[141] Stephen L. Adler. Axial vector vertex in spinor electrodynamics. *Phys. Rev.*, 177:2426–2438, 1969.

[142] J.S. Bell and R. Jackiw. A PCAC puzzle: $\pi^0 \to \gamma\gamma$ in the σ model. *Nuovo Cim. A*, 60:47–61, 1969.

[143] P. Breitenlohner and D. Maison. Dimensionally Renormalized Green's Functions for Theories with Massless Particles. 2. *Commun. Math. Phys.*, 52:55, 1977.

[144] G. Passarino and M. Veltman. One-loop corrections for e+e annihilation into + in the weinberg model. *Nuclear Physics B*, 160(1):151 – 207, 1979.

[145] Michael Spira. HIGLU: A program for the calculation of the total Higgs production cross-section at hadron colliders via gluon fusion including QCD corrections. 10 1995.

[146] T. Hahn. Generating and calculating one loop Feynman diagrams with FeynArts, FormCalc, and LoopTools. In *6th International Workshop on New Computing Techniques in Physics Research: Software Engineering, Artificial Intelligence Neural Nets, Genetic Algorithms, Symbolic Algebra, Automatic Calculation*, 4 1999.

[147] Vladyslav Shtabovenko, Rolf Mertig, and Frederik Orellana. FeynCalc 9.3: New features and improvements. *Comput. Phys. Commun.*, 256:107478, 2020.

[148] G Peter Lepage. A new algorithm for adaptive multidimensional integration. *Journal of Computational Physics*, 27(2):192 – 203, 1978.

[149] L. F. Richardson. The approximate arithmetical solution by finite differences of physical problems involving differential equations, with an application to the stresses in a masonry dam. *Philosophical Transactions of the Royal Society of London. Series A, Containing Papers of a Mathematical or Physical Character*, 210:307–357, 1911.

[150] Jon Butterworth, Stefano Carrazza, Amanda Cooper-Sarkar, Albert De Roeck, Jol Feltesse, Stefano Forte, Jun Gao, Sasha Glazov, Joey Huston, Zahari Kassabov, and et al. Pdf4lhc recommendations for lhc run ii. *Journal of Physics G: Nuclear and Particle Physics*, 43(2):023001, Jan 2016.

[151] L. A. Harland-Lang, A. D. Martin, P. Motylinski, and R. S. Thorne. Parton distributions in the lhc era: Mmht 2014 pdfs. *The European Physical Journal C*, 75(5), May 2015.

[152] S. Borowka, N. Greiner, G. Heinrich, S.P. Jones, M. Kerner, J. Schlenk, U. Schubert, and T. Zirke. Higgs boson pair production in gluon fusion at next-to-leading order with full top-quark mass dependence. *Physical Review Letters*, 117(1), Jun 2016.

[153] Massimiliano Grazzini, Gudrun Heinrich, Stephen Jones, Stefan Kallweit, Matthias Kerner, Jonas M. Lindert, and Javier Mazzitelli. Higgs boson pair production at NNLO with top quark mass effects. *JHEP*, 05:059, 2018.

[154] G. Degrassi, M. Fedele, and P.P. Giardino. Constraints on the trilinear higgs self coupling from precision observables. *Journal of High Energy Physics*, 2017(4), Apr 2017.

[155] R. Grber, M. Mühlleitner, M. Spira, and J. Streicher. Nlo qcd corrections to higgs pair production including dimension-6 operators. *Journal of High Energy Physics*, 2015(9), Sep 2015.

[156] G. Buchalla, M. Capozi, A. Celis, G. Heinrich, and L. Scyboz. Higgs boson pair production in non-linear effective field theory with full mt-dependence at nlo qcd. *Journal of High Energy Physics*, 2018(9), Sep 2018.

[157] A. Djouadi, W. Kilian, M. Mühlleitner, and P.M. Zerwas. Production of neutral higgs-boson pairs at lhc. *The European Physical Journal C*, 10(1):4549, Aug 1999.

[158] Xin Li and M.B. Voloshin. Remarks on double higgs boson production by gluon fusion at threshold. *Physical Review D*, 89(1), Jan 2014.

[159] N. Gray, David J. Broadhurst, W. Grafe, and K. Schilcher. Three Loop Relation of Quark (Modified) Ms and Pole Masses. *Z. Phys. C*, 48:673–680, 1990.

[160] K.G. Chetyrkin. Quark mass anomalous dimension to o (s4). *Physics Letters B*, 404(1-2):161165, Jul 1997.

[161] K. G. Chetyrkin and M. Steinhauser. Short-distance mass of a heavy quark at order α_s^3. *Physical Review Letters*, 83(20):40014004, Nov 1999.

[162] K.G. Chetyrkin and M. Steinhauser. The relation between the and the on-shell quark mass at order s3. *Nuclear Physics B*, 573(3):617651, May 2000.

[163] Kirill Melnikov and Timo van Ritbergen. The three-loop relation between the and the pole quark masses. *Physics Letters B*, 482(1-3):99108, Jun 2000.

[164] Michael Spira. Effective multi-higgs couplings to gluons. *Journal of High Energy Physics*, 2016(10), Oct 2016.

[165] Marvin Gerlach, Florian Herren, and Matthias Steinhauser. Wilson coefficients for higgs boson production and decoupling relations to os4$\mathcal{O}\left(\alpha_s^4\right)$. *Journal of High Energy Physics*, 2018(11), Nov 2018.

[166] Ansgar Denner and S. Dittmaier. Reduction schemes for one-loop tensor integrals. *Nucl. Phys. B*, 734:62–115, 2006.

[167] Francisco Campanario. Towards pp -> VVjj at NLO QCD: Bosonic contributions to triple vector boson production plus jet. *JHEP*, 10:070, 2011.

[168] G. Barucchi and G. Ponzano. Differential equations for oneloop generalized feynman integrals. *Journal of Mathematical Physics*, 14:396–401, 03 1973.

[169] A. V. Kotikov. Differential equations method: New technique for massive Feynman diagrams calculation. *Phys. Lett.*, B254:158–164, 1991.

[170] T. Gehrmann and E. Remiddi. Differential equations for two-loop four-point functions. *Nuclear Physics B*, 580(1-2):485518, Jul 2000.

[171] Ettore Remiddi. Differential equations for Feynman graph amplitudes. *Nuovo Cim.*, A110:1435–1452, 1997.

[172] Mario Argeri and Pierpaolo Mastrolia. Feynman diagrams and differential equations. *International Journal of Modern Physics A*, 22(24):43754436, Sep 2007.

[173] Mario Argeri, Stefano Di Vita, Pierpaolo Mastrolia, Edoardo Mirabella, Johannes Schlenk, Ulrich Schubert, and Lorenzo Tancredi. Magnus and Dyson Series for Master Integrals. *JHEP*, 03:082, 2014.

[174] John C. Collins. *Renormalization: An Introduction to Renormalization, The Renormalization Group, and the Operator Product Expansion*, volume 26 of *Cambridge Monographs on Mathematical Physics*. Cambridge University Press, Cambridge, 1986.

[175] J. Collins, F. Wilczek, and A. Zee. Low-energy manifestations of heavy particles: Application to the neutral current. *Phys. Rev. D*, 18:242–247, Jul 1978.

[176] William J. Marciano. Flavor thresholds and Λ in the modified minimal-subtraction scheme. *Phys. Rev. D*, 29:580–582, Feb 1984.

[177] P. Nason, S. Dawson, and R.K. Ellis. The total cross section for the production of heavy quarks in hadronic collisions. *Nuclear Physics B*, 303(4):607 – 633, 1988.

[178] K.G. Chetyrkin, Bernd A. Kniehl, and M. Steinhauser. Decoupling relations to O (alpha-s**3) and their connection to low-energy theorems. *Nucl. Phys. B*, 510:61–87, 1998.

Acknowledgements

It has been a long journey up here, a journey that I could never have ended without the precious help and support from many colleagues and friends.

First of all, I would like to thank my thesis director, Dr. Francisco Campanario for the immense patience, the fruitful discussions, for sharing his countless codes and knowledge with me, for all the hours spent into the debugging, but expecially for giving me the possibility of joining this project and of collaborating with many amazing physicists, allowing me to do this first priceless experience as a researcher. I also would like to thank all my collaborators Dr. Julien Baglio, Dr. Seraina Glaus, Prof. Dr. Margarete Müllheitner and Dr. Michael Spira: Dr. Julien Baglio for sharing with me the struggle of the cross-check of the real corrections (which is still currently uncomplete), for the hospitality at the CERN and for all the discussions; Dr. Seraina Glaus and Prof. Dr. Margarete Müllheitner for hosting me for the one-month stay at the KIT; Dr. Michael Spira for the explanations regarding all the theoretical background of this project in their tiniest details.

I thank also the colleagues of the MUonE collaboration for permitting me to contribute to this immense project that, for reasons of time, I did not included in this thesis. In particular I would like to thank Prof. Pierpaolo Mastrolia for being a guide and to push forward the calculation of the virtual corrections of the μe-scattering despite of all the issues. I would also thank Amedeo Primo and Ulrich Schubert for the help in the composition of all the parts of the calculation.

I would like to thank my collegue and friend William Torres for the irreplaceable support, discussions, trouble-shooting, for correcting my silly mistakes, for his help and discussions over AIDA, and for a lot of other things that I am definitely forgetting. But you know me Will. I would also thank Ivan Rosario, my office mate and colleague for his help, kindness, for the extremely interesting and not only physics-related discussions, and for the help with the abstract. I also thank Andres, Jesus and Selomit for the trying to teach me the castellano, without any actual success: I am not that good student after all. I also thank all my past office mates, colleagues and companions that accompanied me through this experience.

Last but not least, ringrazio i miei genitori Bruno e Lina per avermi supportato, spronato e creduto in me in ogni momento, senza se e senza ma. Senza di voi, oltre a non arrivare fino a qui, chissà se mai avrei avuto la forza di fare questa esperienza lontano da casa. Questo è un cammino che mi porterà spesso lontano da voi, ma per sempre considererò voi la mia "casa". Spero un giorno di rendervi davvero orgogliosi.

– Jonathan